

**Impact of CO₂ and pH on the distribution
and stable carbon isotopic composition of
microbial biomarker lipids**

Petra Larissa Schoon

Promotoren

Prof. dr. ir. S. Schouten, Utrecht University and Royal Netherlands
Institute for Sea Research, The Netherlands

Prof. dr. ir. J.S. Sinninghe Damsté, Utrecht University and Royal
Netherlands Institute for Sea Research, The Netherlands

Thesis committee

Prof. dr. H. de Baar, Royal Netherlands Institute for Sea Research,
The Netherlands

Dr. H. Brinkhuis, Royal Netherlands Institute for Sea Research, The
Netherlands

Dr. J.W. de Leeuw, Royal Netherlands Institute for Sea Research, The
Netherlands

Prof. dr. T. Wagner, School of Civil Engineering and Geosciences,
United Kingdom

The research presented in this thesis was funded by the Darwin Center
for Biogeosciences and the Royal Netherlands Institute for Sea Research
(NIOZ).

ISBN 978-94-6203-299-6

Cover design by Petra Schoon

Printed by Wöhrmann Print Service, Zutphen

Impact of CO₂ and pH on the distribution and stable carbon isotopic composition of microbial biomarker lipids

Invloed van CO₂ en pH op de distributiepatronen
en stabiele koolstofisotoopsamenstelling van
microbiële biomarkerlipiden

(met een samenvatting in het Nederlands)

Proefschrift

ter verkrijging van de graad van doctor aan de Universiteit Utrecht op
gezag van de rector magnificus, prof. dr. G.J. van der Zwaan, ingevolge het
besluit van het college voor promoties in het openbaar te verdedigen op
woensdag 3 april 2013 des middags te 2.30 uur

door

Petra Larissa Schoon

geboren op 5 september 1980 te Rotterdam

Promotoren: Prof. dr. ir. S. Schouten
Prof. dr. ir. J.S. Sinninghe Damsté

*“The presence of those seeking the truth is infinitely to be preferred to those
who think they’ve found it.”*

From: The Monstrous Regiment – A Discworld Novel by Terry Pratchett

Voor mijn ouders

TABLE OF CONTENTS

Chapter 1	9
General Introduction	

Part 1 Contemporary Systems

Chapter 2	23
Stable carbon isotopic fractionation associated with photosynthesis in <i>Phaeocystis antarctica</i> and <i>Proboscia alata</i> is mainly controlled by variations in aqueous CO₂ concentrations	

Petra L. Schoon, Astrid Hoogstraten, Jaap S. Sinninghe Damsté, and Stefan Schouten

Chapter 3	35
The influence of lake water pH and alkalinity on the distribution of core and intact polar lipid branched glycerol dialkyl glycerol tetraethers in lakes	

Petra L. Schoon, Anna de Kluijver, Jack J. Middelburg, John A. Downing, Jaap S. Sinninghe Damsté, and Stefan Schouten

Submitted to Organic Geochemistry

Chapter 4	57
Environmental controls on the distribution of intact polar lipids in oligotrophic and eutrophic lakes	

Ellen Hopmans, Petra L. Schoon, Anna de Kluijver, Jack J. Middelburg, John A. Downing, Jaap S. Sinninghe Damsté, and Stefan Schouten

Submitted to Limnology and Oceanography

Part II Ancient high CO₂ and low pH worlds: Eocene Hyperthermals

Chapter 5 81

Extreme warming and environmental change of the North Sea Basin across the Palaeocene-Eocene boundary as revealed by biomarker lipids

Petra L. Schoon, Claus Heilmann-Clausen, Bo Pagh Schultz, Jaap S. Sinninghe Damsté, and Stefan Schouten

Submitted to Organic Geochemistry

Chapter 6 99

Constraining the magnitude of Early Eocene global carbon isotope excursion using lipids of marine Thaumarchaeota

Petra L. Schoon, Claus Heilmann-Clausen, Bo Pagh Schultz, Appy Sluijs, Jaap S. Sinninghe Damsté, and Stefan Schouten

Submitted to Earth and Planetary Science Letters

Chapter 7 119

Stable carbon isotope patterns of marine biomarker lipids in the Arctic Ocean during Eocene Thermal Maximum 2

Petra L. Schoon, Appy Sluijs, Jaap S. Sinninghe Damsté, and Stefan Schouten

Published in: Paleoceanography 26: PA3215, 2011

References 143

Summary 172

Samenvatting 176

Acknowledgements / Dankwoord 182

Curriculum Vitæ 185

CHAPTER 1

General Introduction

“Carbon dioxide, that is, the aerial form of carbon ...: this gas which constitutes the raw material of life, the permanent store upon which all that grows draws, and the ultimate destiny of all flesh, is not one of the principal components of air but rather a ridiculous remnant, an ‘impurity’, thirty times less abundant than argon, which nobody even notices. ... This, on the human scale, is ironic acrobatics, a juggler’s trick, an incomprehensible display of omnipotence-arrogance, since from this ever renewed impurity of the air we come, we animals and we plants, and we the human species, with ... our millenniums of history, our wars and shames, nobility and pride.”

Fragment from: The Periodic Table by Primo Levi

1.1 OCEAN ACIDIFICATION: “THE OTHER CO₂ PROBLEM”

The ongoing emission of fossil fuels, in combination with deforestation, cement production and agricultural development, has led to an increase in the atmospheric carbon dioxide pressure ($p\text{CO}_2$) since the industrial revolution, which encompasses the last ~250 years (*IPCC* 2007). From the background pre-industrial level of about 280 ppmv, $p\text{CO}_2$ levels have increased rapidly and will most likely reach 400 ppmv in 2015 and will increase even further to 500-1000 ppmv at the end of this century (*IPCC* 2007). The main concern of this predicted rise in atmospheric CO₂ is a global warming of ca. 0.1 °C per decade (*IPCC* 2007). Other related climate responses likely to occur, are a reduction in Greenland and Antarctic ice sheet volumes, a global sea level rise, melting of the upper Arctic permafrost layer, high local variability in precipitation, enhanced strength of mid-latitude westerly winds, and an intensification of tropical cyclone activity (*IPCC* 2007).

Nevertheless, the actual CO₂ concentration could have been much higher, was it not that the world oceans act as a major sink of carbon dioxide. In fact, since the industrial revolution, about half of the emitted anthropogenic CO₂ has been taken up by the oceans (*Sabine et al.*, 2004), due to its high solubility in water. The addition of CO₂ in water leads to an array of chemical reactions (**Fig. 1.1**), and a shift in ocean chemistry. That is, the balance between the concentrations of carbon dioxide (CO₂), bicarbonate (HCO₃⁻) and carbonate (CO₃²⁻), which are the major carbon species that make up dissolved inorganic carbon (DIC). As illustrated in **figure 1.1**, dissolved CO₂ dissociates in carbonic acid (H₂CO₃). In turn, this weak acid dissociates almost immediately in HCO₃⁻ and a hydrogen ion (H⁺). Thus, it is this increase in the concentration of hydrogen ions, initiated by the absorption of atmospheric gaseous CO₂ by surface ocean waters, that in the end results in a decrease of the ocean water pH (*Zeebe et al.*, 2008; *Feely et al.*, 2004; *Cao et al.*, 2007), a process termed ocean acidification. Some of these excess H⁺ react with CO₃²⁻ to form an additional HCO₃⁻ ion (**Fig. 1.1**). This natural buffering mechanism of the ocean waters keeps the pH always slightly alkaline between 7.8 and 8.3. It also has moderated the actual magnitude of anthropogenic-induced ocean acidification. The average change in seawater pH in the world oceans for the period between 1900 to 1990 is approximately 0.1 unit (*Raven et al.*, 2005). This seems low, but, keeping in mind that pH is based on a log-scale, it still corresponds to a massive 30% increase in hydrogen ion concentration. When CO₂ emissions unabatedly continue, a further decrease of ~0.6 pH units is expected for the coming centuries (*Caldeira & Wickett*, 2003; *Orr et al.*, 2005; *Zeebe et al.*, 2008).

Due to the reduction in the carbonate saturation state of the oceans, the addition of anthropogenic carbon will also promote the dissolution of calcium carbonate (CaCO₃) (**Fig. 1.1**), thereby enhancing the carbonate buffering capacity of the ocean. It has been suggested from modelling and experimental studies that this will negatively affect the calcification rate of certain calcifying marine microorganisms

(Kleypas *et al.*, 1999; Riebesell *et al.*, 2000; Orr *et al.*, 2005; Raven *et al.*, 2005), and may cause major changes in ecosystem dynamics and biodiversity. Corals are believed to be especially vulnerable to changes in ocean chemistry, because of their aragonite skeletons. This in contrast to organisms which make their tests out of calcite (e.g. foraminifera and coccolithophores), the more stable and therefore less soluble form of calcium carbonate. However, the response of most marine microorganisms on elevated aqueous CO_2 conditions may not be that straightforward and have been shown to be highly dependent on morphological variations between species and environmental factors (Langer *et al.*, 2006; Fabry *et al.*, 2008; Iglesias-Rodriguez *et al.*, 2008). A decrease in seawater pH level is also shown to effect non-calcifying organisms, although the exact impact is less clear. For instance, Beman *et al.* (2010) showed that ocean acidification may lead to a considerable decrease in nitrification rates, and thus changes the availability of nitrogen in the ocean. Important groups of photosynthetic phytoplankton, such as diatoms and dinoflagellates, but also bacteria, archaea and viruses that stand at the basis of the marine food chain, are key contributors to biogeochemical processes. A clear understanding of the impact of ocean acidification on these organisms is, therefore, of paramount importance.

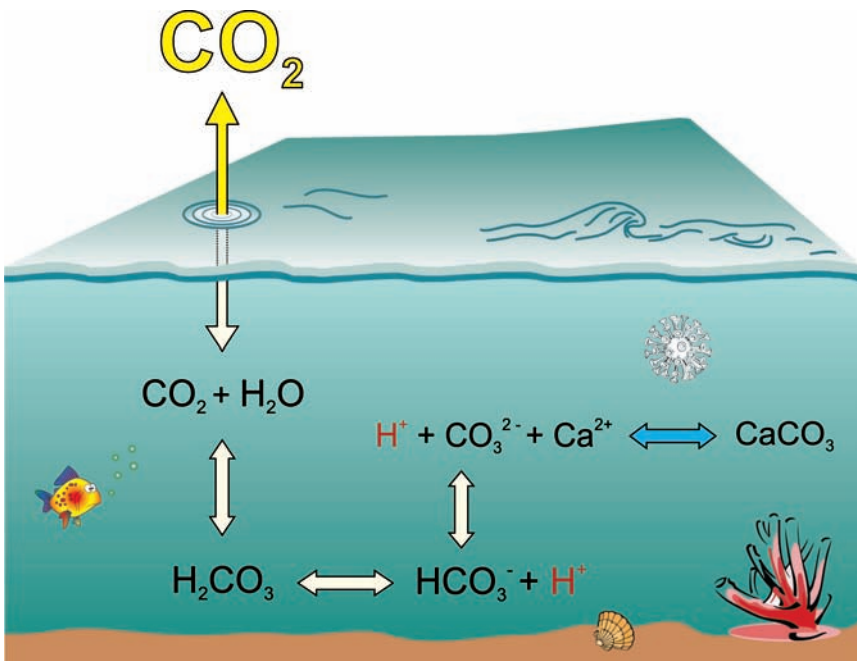


Figure 1.1 | Seawater carbonate reactions. The uptake of atmospheric CO_2 leads to an increase in hydrogen ion concentrations, and in turn, promotes the dissolution of calcium carbonates.

1.2 PAST CARBON CYCLE PERTURBATIONS

The current carbon cycle perturbation by human activity is not unique: the geologic record documents several prolonged periods of elevated levels of atmospheric carbon dioxide and concomitant global warming, and are in these cases mainly induced by enhanced tectonic activity. However, the main difference between present-day and past carbon cycle perturbations is the time scale at which the forcing mechanisms operate (Zeebe *et al.*, 2008; Zachos *et al.*, 2010). Current rates of atmospheric carbon release is on average 9 Pg per year (Le Quéré *et al.*, 2009), which is most likely higher than for any greenhouse period in the geological past (Hönisch *et al.*, 2012). Recently, Hönisch *et al.* (2012) performed a thorough evaluation of seven geological time intervals from the past ~300 million years which are characterized by enhanced CO₂ release to the atmosphere, lowering of seawater pH and/or a decrease in calcium carbonate saturation (**Fig. 1.2**). Palaeoclimate observations of these geologic intervals can therefore be put into perspective with contemporary ocean acidification.

The most recent and best documented episodes of past ocean acidification (**Fig. 1.2**), are several so-called hyperthermals that occurred superimposed on the long-term warming trend during the Late-Palaeocene and Early-Eocene (ca. 59-51 Ma; Zachos *et al.*, 2008). These short-lived intervals (<200 kyrs) of climate change, are recognized in various stable isotope records (e.g. Kennett & Stott, 1991; Röhl *et al.*, 2007; Lourens *et al.*, 2005). Although the temporal and spatial resolution of most of these hyperthermals still have to be resolved, they are all characterized by a global negative carbon isotope excursion and show signs of substantial ocean chemistry changes (e.g. Zachos *et al.*, 2005; Stap *et al.*, 2009). These recurring carbon isotope excursions can best be explained by a pulsed mode of carbon release into the ocean-atmosphere system (Dickens, 2000, 2003). Several sources of carbon have been proposed, such as the release of thermogenic methane due to contact metamorphism (Svensen *et al.*, 2004), rapid burning of terrestrial organic matter (Kurtz *et al.*, 2003), the release of carbon stored in permafrost soils at high latitudes triggered by orbital forcing (DeConto *et al.*, 2012), and the dissociation of methane hydrates from continental margins (Dickens, 1995).

In terms of magnitude and duration, the Palaeocene-Eocene Thermal Maximum (PETM; ~56 Ma) is considered as the most severe hyperthermal and documents a global warming of 5-8 °C in many marine and terrestrial sections worldwide (e.g. Sluijs *et al.*, 2006, 2007b, 2011; Weijers *et al.*, 2007a; Zachos *et al.*, 2003, 2006; Tripathi & Elderfield, 2005; Wing *et al.*, 2005; Thomas *et al.*, 2002; Kennett & Stott, 1991). The PETM is further characterized by a negative carbon isotope excursion of 2-7 ‰, depending on the carbon reservoir analyzed (Sluijs & Dickens, 2012), which lasted ~220 kyr (Röhl *et al.*, 2007; Abdul Aziz *et al.*, 2008; Murphy *et al.*, 2010). Evidence for severe ocean acidification during the PETM comes from the South Atlantic. Geochemical data from 5 deep sea sediment cores show severe carbonate

dissolution indicating a 2 km shoaling of the carbon compensation depth (*Zachos et al.*, 2005). Within the same sections, similar observations, although smaller in magnitude, have been made for the Eocene Thermal Maximum 2 (ETM2), that occurred 2 myr after the PETM (e.g. *Stap et al.*, 2009).

1.3 RECONSTRUCTION OF pH LEVELS AND ATMOSPHERIC CARBON DIOXIDE CONCENTRATIONS

An important requirement to use past geological records of ocean acidification as analogues for future carbon cycle changes, are the availability of accurate reconstructions of ocean carbonate chemistry. Direct measurements of the changes in ocean carbonate chemistry are only available for the last 50 years or so (*IPCC* 2007), and $p\text{CO}_2$ measurements from air bubbles in ice only go back ~ 650 ka (e.g. *Barnola et al.*, 1983, 1987; *Monnin et al.*, 2001; *Petit et al.*, 1999; *Siegenthaler et al.*, 2005). To gain information of this kind from the more distant geological past, one has to rely on the geochemical information that is locked within the sedimentary record. These so-called proxies form the foundation of palaeoclimate and -environmental reconstructions.

Four terrestrial-based proxies have been developed to reconstruct atmospheric CO_2 levels, i.e. leaf stomata density (*van den Burgh et al.*, 1993; *Retallack*, 2001; *Royer et al.*, 2001a,b), the stable carbon isotopic composition of pedogenic carbonates (*Cerling*, 1991; *Mora et al.*, 1991; *Eckart et al.*, 1999) and goethites (*Yapp*, 2004) in palaeosoils, the stable carbon isotope composition of fossil bryophytes (*Fletcher et al.*, 2005), and the differential speciation of sodium carbonate precipitates in lakes (*Lowenstein & Demicco*, 2006). They, however, do not provide any direct information on the chemical state of the oceans.

To date, there are three proxies that can be used to directly assess changes in ocean water carbonate chemistry. The use of boron isotopes and the B/Ca ratio are based on the differential partitioning of the trace element boron into the calcite tests of planktonic foraminifera, and have frequently been used to reconstruct past seawater pH (*Sanyal et al.*, 1995; *Pearson & Palmer*, 2000b, 2002; *Palmer & Pearson*, 2003; *Yu et al.*, 2007). However, a reduced carbonate saturation state of the ocean reduces the preservation potential of calcium carbonate, in the form of foraminiferal shells, complicating the use of these proxies. Furthermore, additional complications may arise when applying boron isotopes to periods older than ~ 20 Ma, due to the relatively short residence time of boron in the ocean (*Pagani et al.*, 2005a). Finally, the stable carbon isotopic composition of phytoplankton (e.g. *Freeman & Hayes*, 1992; *Jasper & Hayes*, 1990; *Jasper et al.*, 1994) offers a promising tool to reconstruct the CO_2 concentration in seawater, and has particularly great potential in environmental settings that are rich in organic matter and poor in carbonate. In section 1.4.2 this proxy will be discussed in more detail.









Period	Age	CO ₂ source	Magnitude of change in:			
			pCO ₂	pH	saturation	temp.
Anthropocene	present - future		↑	↓	↓	↑
Last deglaciation	17.8 - 11.6 ka		↑	↓	↓	↑
Oligocene-Pliocene	34.0 - 2.6 Ma		↑	—	↓	↑
Eocene hyperthermals	58 - 51 Ma		↑	↓	↓	↑
End Cretaceous	65 Ma		↑	?	↓	↑
Ocean anoxic events	~93, ~120, ~183 Ma		↑	?	?	↑
Triassic-Jurassic	199.6 Ma		↑	?	?	↑
Permian-Triassic	252.3 Ma		↑	?	?	↑

Figure 1.2 | Overview of future and past ocean acidification events, modified after *Hönisch et al.* (2012). Shown are the various different causes of carbon release and its impact on $p\text{CO}_2$, pH, carbonate saturation, and temperature. The size of the arrows correspond to the relative magnitude of each change based on direct and indirect geological and geochemical proxy data.

1.4 BIOMARKER LIPIDS AS TOOL FOR TRACING $\text{pH}/[\text{CO}_2(\text{aq})]$ CHANGES IN AQUATIC SYSTEMS

After death, a small fraction (<1%) of the organic material escapes heterotrophic recycling and is transported and buried within the sediments (*de Leeuw et al.*, 1995). The molecular remains of organisms preserved in the sedimentary record are called biomarkers. Of all organic molecules, lipids have the highest preservation potential. Even after long-term subjection to diagenetic and catagenetic processes, these compounds still possess traits from their precursors. Information on the environmental conditions of the original organism are locked within the structure of the carbon skeleton and its isotopic composition. Studying the distribution and stable carbon isotopic composition of microbial lipids may therefore contain valuable information on changes in environmental pH and $[\text{CO}_2(\text{aq})]$, as many organisms are known to alter their cell membrane composition to changing

environmental factors. They may therefore be a useful tool for studying the process of contemporary and past ocean acidification. Below we discuss some of the biomarker lipids which show some promise.

1.4.1 Branched glycerol dialkyl glycerol tetraethers

Branched glycerol dialkyl glycerol tetraethers (GDGTs; **Fig. 1.3a**) are bacterial membrane lipids found mainly in terrestrial environments, such as soils and lakes (*Sinninghe Damsté et al.*, 2000; *Weijers et al.*, 2006a, 2007; *Schouten et al.*, 2000b; *Hopmans et al.*, 2004; *Blaga et al.*, 2009; *Yang et al.*, 2011) and, to a lesser extent, also in continental margin sediments (*Schouten et al.*, 2000b; *Hopmans et al.*, 2004). The distribution of branched GDGTs in soils (*Weijers et al.*, 2007b) and lake sediments (*Tierney & Russell*, 2009; *Tierney et al.*, 2010, 2012; *Sun et al.*, 2011) have shown to relate strongly to pH. In soils this relationship was empirically established by *Weijers et al.* (2007b), and is founded on the degree of cyclization within the branched GDGT structure. That is, the relative abundance of branched GDGTs containing cyclopentane moieties increased with an increase in hydrogen ion concentration in soils (**Fig. 1.3b**). A linear negative relationship with pH was established with the introduction of the CBT index (**Fig. 1.3c**). A relationship also exists between the distribution of branched GDGTs and mean annual air temperatures (*Weijers et al.*, 2007b) and, as yet, most studies have focussed on the use of branched GDGTs as continental temperature proxy (e.g. *Peterse et al.*, 2009a, 2009b, 2009c, 2011; *Tierney & Russell*, 2009). Their potential to reconstruct pH has been less well constrained.

1.4.2 Stable carbon isotopic fractionation of marine algal lipids

Stable carbon isotopes of organic matter serve as a powerful tool to trace variations in the sources and sinks of carbon and are therefore important in understanding the biogeochemical processes within the carbon cycle. There is considerable variation in the carbon isotopic composition of biomass between organisms (*Schidlowski & Aharon*, 1992), and this is mainly determined by four aspects (*Hayes*, 1993, 2001): (1) the carbon isotopic composition of the source carbon, (2) the carbon-fixation mechanism of the organism, (3) carbon isotopic offsets during metabolism processes, and (4) the redistribution of carbon during each process. The difference between the final stable carbon isotopic composition of the organic matter and the initial carbon isotopic composition of the carbon source is referred to as carbon isotopic fractionation.

Carbon uptake by most marine phytoplankton is through the Calvin-Benson Cycle. In contrast to higher plants, the source carbon (aqueous CO₂) is mainly assimilated passively through diffusion over the cell membrane. The dependence of isotopic fractionation to the aqueous CO₂ concentration in marine phytoplankton was first observed by *Degens et al.* in 1968. Since that time, this concept has been used for the development of a method to reconstruct ancient pCO₂ levels (e.g. *Free-*

man & Hayes, 1992; Jasper & Hayes, 1990, 1994). Soon it became clear, however, that the relationship between the aqueous CO₂ concentration and isotopic fractionation was confounded by physiological and environmental factors, such as growth rates, cell geometry, and nutrient availability (e.g. Laws *et al.*, 1995; Bidigare *et al.*, 1997; Rau *et al.*, 1997; Popp *et al.*, 1998b). At present, these factors are only well-constrained for alkenones, long-chain C₃₇ di-unsaturated ketones derived from prymnesiophyte algae (e.g. Pagani, 2002). This has seriously limited the application of isotopic fractionation for the reconstruction of past *p*CO₂ levels to these biomarkers. Alkenones are, however, not always present in sediments, and it would therefore be valuable to expand the set of applicable biomarkers for *p*CO₂ reconstructions. For instance, Bice *et al.* (2006) and Sinninghe Damsté *et al.* (2008) have used biomarkers derived from other important phytoplankton groups, to reconstruct *p*CO₂ levels in the Cretaceous atmosphere.

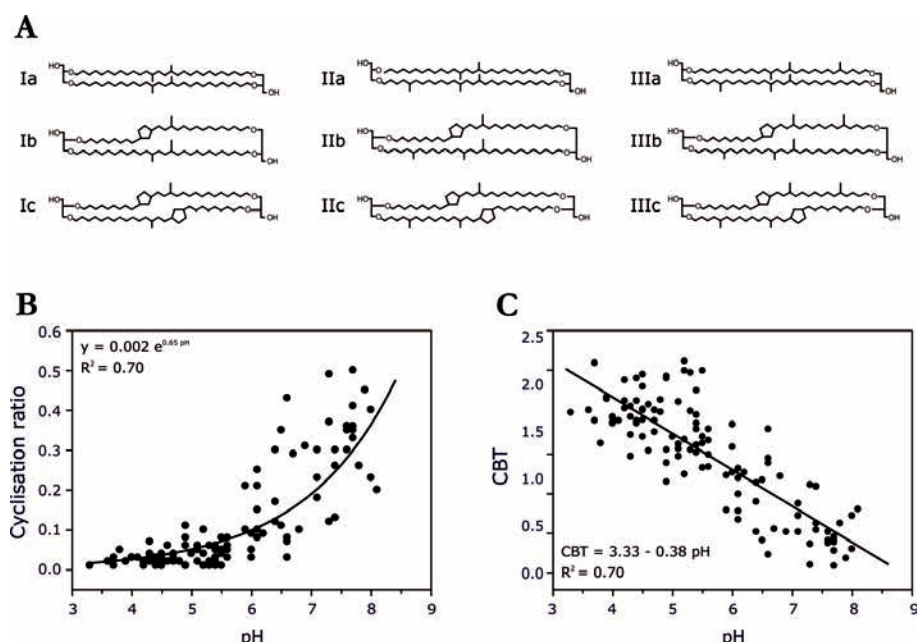


Figure 1.3 | (a) Molecular structures of branched glycerol dialkyl glycerol tetraethers; (b) regression plot showing the correlation between soil pH and the degree of cyclization of the branched GDGTs; (c) regression plot showing the correlation between soil pH and the CBT index, which is defined as: $\text{CBT} = -\text{LOG}_{10} [\text{Ib} + \text{IIb}] / [\text{Ia} + \text{Ib}]$.

1.5 OBJECTIVES AND OUTLINE OF THIS THESIS

The main aim of this thesis, is to gain a better understanding of the impact of ocean acidification, i.e. high atmospheric CO₂ concentrations and low pH conditions, on the distribution and stable carbon isotopic composition of (membrane) lipids of microbial organisms in present day and past environments. General research questions, inherent to this objective, would be: How do extant species of important phytoplankton groups that produce specific biomarkers respond to elevated *p*CO₂ levels? What is the impact of pH on important biomarker lipid groups, derived from algae, bacteria, and archaea? What are the changes in biomarker distribution and carbon isotopic composition during geological periods of rapid ocean acidification? To address such questions, this thesis is divided in two parts based on the approach of the different studies:

Part I Contemporary Systems

In **chapter 2** the results of experimental studies involving two different algal species (*Phaeocystis antarctica* and *Proboscia alata*) are discussed. These species are selected for their cosmopolitan distribution and their importance in carbon cycle dynamics. To understand their response in stable carbon isotopic fractionation to aqueous CO₂ concentrations, cultures were designed to mimic different environmental conditions by combining three different concentrations in atmospheric CO₂ with two different light intensities. The carbon isotopic fractionation factors were calculated from the stable carbon isotopic values of the cell material and [CO₂(aq)]. The results show that the observed variations in stable carbon isotopic fractionation for both species can be mainly ascribed to the concentrations of dissolved inorganic carbon and, thus, with *p*CO₂. Light intensity and specific growth rates did not have any effect. This increases the likelihood of finding algal biomarkers, such as long-chain diols, produced by *Proboscia* diatoms, suitable for the reconstruction of ancient atmospheric CO₂ concentrations.

Due to the strong buffering capacity of the ocean, processes that determine the carbonate chemistry are difficult to separate, keeping seawater pH within a strict range. In contrast, lakes exhibit a strong variability in pH, CO₂ content and DIC, which are not necessarily connected. This makes them excellent environments to investigate the effect of pH on the distribution of membrane lipids independent of carbonate chemistry. To this end, the suspended particulate matter sampled from 23 lakes in Minnesota and Iowa, USA, were studied. **Chapter 3** and **4** focuses on the distribution of branched GDGTs and IPLs, respectively. As expected, a strong relationship between the distribution of branched GDGTs and lake water pH was found, strengthening the hypothesis that branched GDGTs are not only transported to lakes by soil erosion, but are *in situ* produced in the lake water column, as well. Although not entirely understood, we further found a strong relationship with lake water alkalinity. This is strong evidence that branched

GDGTs record changes in water chemistry. The results presented in **Chapter 4** provide one of the first characterizations of IPLs in lakes. A high diversity of intact polar lipid classes was found in all of the USA lakes. Some significant differences were observed between Iowa and Minnesota, which are mainly related to differences in trophic level and could not be explained by the variation in lake pH. Hence, IPLs appear not very well suited for environmental pH reconstructions.

Part II Ancient high CO₂ and low pH worlds: Eocene Hyperthermals

Understanding the underlying mechanisms that drive PETM warming relies on a good latitudinal coverage of the various climate records. In **Chapter 5**, the distribution and stable carbon isotopic composition of specific marine and terrestrial biomarker lipids were analyzed, from two PETM sites located in the eastern North Sea Basin. Here, negative CIEs of ~ 7 ‰ in TOC and of ~ 5.5 ‰ in terrestrial long-chain *n*-alkanes were recorded. The PETM was further characterized by severe oxygen depletion and a warming of at least 8 °C of both continental and sea surface waters. Indications were, however, found that these changes may have been amplified by local influences in addition to the global climate changes that are in general associated with the PETM. This reconstruction of the North Sea Basin based on organic biomarker records, therefore, provide important insights into the regional magnitude of the CIE, warming and environmental changes in Northern Europe during the PETM.

Chapter 6 discusses the potential for the use of biphytanes derived from Thaumarchaeotal glycerol dialkyl glycerol tetraethers, as a proxy for the stable carbon isotopic composition of dissolved inorganic carbon. This was studied in sediments derived from Danish PETM and Arctic ETM2 sections. Due to the constant carbon isotopic fractionation of ~ 20 ‰ **between dissolved inorganic carbon** and the biphytanes, the variations in the stable carbon isotopic composition of this biomarker should reflect that of the ocean-atmosphere carbon reservoir. The reconstructed carbon isotope shifts recorded in crenarchaeol-derived biphytanes was ~ 3.6 ‰ and ~ 2.5 ‰ for the PETM and ETM2, respectively. This led to the conclusion, that the stable carbon isotopic composition of Thaumarchaeotal lipids is a promising tool to reconstruct stable carbon isotopic variations in ocean water dissolved inorganic carbon and may, therefore, be valuable in constraining the magnitude of the actual atmospheric carbon isotope excursions during Eocene hyperthermals.

The study presented in **Chapter 7**, involves the first quantification of the variations in atmospheric CO₂ concentration during Eocene Thermal Maximum 2. To this end, the carbon isotopic fractionation patterns were constructed of three independent organic biomarkers to obtain estimates of *p*CO₂. The three proxies yielded similar values and suggested an increase towards at least 4 times pre-industrial levels (~ 1100 ppmv) across Eocene Thermal Maximum 2. These results,

clearly shows the potential of the use of algal biomarkers other than alkenones, as palaeo- $p\text{CO}_2$ proxy.

In summary, the impact of present-day ocean acidification on the development of future climate change is still not entirely understood. Of key importance, in this matter, is the role of primary producers within the global carbon cycle and underlying feedback mechanisms. Studying past periods of ocean acidification that are characterized by low pH and high atmospheric CO_2 levels, are important in unravelling these issues. The results presented in this thesis demonstrates that the distribution and stable carbon isotopic composition of certain biomarker lipids have the potential to add considerable value in studying contemporary and past ocean acidification. More research is needed to demonstrate the robustness of these proxies and potential caveats in their applications. Once this has been achieved, studies of past ocean acidification events can reveal the response of primary producers to large shifts in ocean pH, and in turn, can be used to assess changes in ocean carbonate chemistry and the global carbon cycle.



Part I





Contemporary Systems



CHAPTER 2

Stable carbon isotopic fractionation associated with
photosynthesis in *Phaeocystis antarctica* and *Proboscia alata* is
mainly controlled by variations in aqueous CO₂ concentrations

Petra L. Schoon, Astrid Hoogstraten, Jaap S. Sinninghe Damsté, and Stefan
Schouten

ABSTRACT

The stable carbon isotopic fractionation in photosynthetic algae has been the subject of many studies, but the controlling factors are still not well understood. In this study we analysed the stable carbon isotopic ($\delta^{13}\text{C}$) composition of the cell material of the marine diatom *Proboscia alata* and the prymnesiophyte *Phaeocystis antarctica* cultured under varying $p\text{CO}_2$ concentrations, in order to study the effect of aqueous CO_2 concentrations ($[\text{CO}_2(\text{aq})]$) on the carbon isotopic fractionation (ϵ_p) of these important primary producers. In addition, the algae were subjected to low ($40 \mu\text{mol photons m}^{-2} \text{s}^{-1}$) and high ($240 \mu\text{mol photons m}^{-2} \text{s}^{-1}$) light intensities. Our results clearly show that for both marine algal species, $[\text{CO}_2(\text{aq})]$ is the main controlling factor on ϵ_p , while factors like growth rate, cell geometry and light intensity, were of subordinate importance. The results raises the possibility that certain algal biomarkers may be suitable to reconstruct ancient $p\text{CO}_2$ concentrations.

2.1 INTRODUCTION

Over the last decades a large number of studies have investigated the stable carbon isotopic fractionation (ϵ_p), defined as the difference between the stable carbon isotopic composition of the carbon substrate and the organic carbon, in photosynthetic organisms (Popp *et al.*, 1989, 1998b; Rau *et al.*, 1992; Freeman & Hayes, 1992; Lams *et al.*, 1995, 2002; Bidigare *et al.*, 1997; Benthien *et al.*, 2007; Hendriks & Pagani, 2007). In higher plants that utilize the Calvin-Benson Cycle, also known as the C_3 -pathway, to take up CO_2 during photosynthesis, ϵ_p can be described as follows (Farquhar *et al.*, 1994):

$$\epsilon_p = (\delta^{13}C_e - \delta^{13}C_{OM}) / (1 + \delta^{13}C_{OM}/1000) = \epsilon_f + (\epsilon_f - \epsilon_i) * (C_i/C_e) \quad (\text{Eq. 2.1})$$

In this model, which operates on the assumption that CO_2 is transported over the cell membrane by passive diffusion, $\delta^{13}C_e$ is the stable carbon isotopic composition of inorganic carbon, $\delta^{13}C_{OM}$ the stable carbon isotopic composition of organic carbon, ϵ_i the fractionation associated with transport, ϵ_f the fractionation due to carbon fixation of the RubisCO enzyme, and C_e and C_i , the concentrations of external CO_2 and internal CO_2 , respectively. A similar model was initially also applied for marine photoautotrophs using the $\delta^{13}C$ value of specific compounds of marine algae and assuming a constant offset between the $\delta^{13}C$ of biomarker and biomass (Freeman & Hayes, 1992; Jasper & Hayes, 1990, 1994). Using this method, estimates of ancient atmospheric CO_2 levels can in principle be obtained, which is one of the main parameters which needs to be constrained for past climates.

Subsequent empirical and theoretical studies have shown, however, that the relationship between ϵ_p and the aqueous CO_2 concentration ($[CO_2(aq)]$) is not that straightforward for marine photoautotrophs and depends on a number of environmental and physiological parameters (e.g. Lams *et al.*, 1995; Bidigare *et al.*, 1997; Rau *et al.*, 1997; Popp *et al.*, 1998b). In general, the importance of C_e on determining the magnitude of ϵ_p , as evident from equation 2.1, depends mainly on the carbon demand of the cell (Rau *et al.*, 1992; Francois *et al.*, 1993), which is defined as the CO_2 gradient over the cell (i.e. $C_e - C_i$). When this CO_2 gradient is constant, then $[CO_2(aq)]$ is the main controlling factor of ϵ_p . However, there are several physiological factors that influence the carbon demand of the cell, thereby changing the size of C_i . For example, several culture experiments and field studies showed that variations in growth rate can be equally or even more important than variations in $[CO_2(aq)]$ (Lams *et al.*, 1995, 1997; Bidigare *et al.*, 1997; Burkhardt *et al.*, 1999). In turn, growth rates are controlled by environmental factors, such as light intensity and nutrient availability, while carbon demand is also impacted by cell geometry (Popp *et al.*, 1998b; Cassar *et al.*, 2006; Lams *et al.*, 1995, 2002; Rost *et al.*, 2002). Popp *et al.* (1998b) modelled the impact of growth rate and cell size as follows:

$$\epsilon_p = \epsilon_f + (\epsilon_f - \epsilon_i) * (1 - \mu/KC_e), \quad (\text{Eq. 2.2})$$

in which μ is the specific growth rate and K relates to the cell carbon-to-surface area ratio of the algal cell. Thus, to reconstruct ancient atmospheric CO_2 levels using preserved organic carbon of marine photoautotrophs, growth rate, as well as cell dimensions, need to be constrained (Pagani, 2002). Growth rate constraints can be in part achieved by assuming certain nutrient concentrations such as phosphate (Bidigare *et al.*, 1997; Pagani, 2002), or nitrogen isotopes (Andersen *et al.*, 1999), while constraints on cell size can be achieved by using specific biomarker lipids or measuring cell remains, such as coccolithophorid shells (Henderiks & Pagani, 2007). However, these assumptions lead to relatively great uncertainty in reconstructing ancient $p\text{CO}_2$ levels (e.g. Schoon *et al.*, 2011).

Another aspect that has to be addressed is the magnitude of ϵ_p , the maximum fractionation associated with RubisCO, the enzyme that facilitates the carboxylation of CO_2 during photosynthesis. This is a biochemical reaction with a kinetic isotopic fractionation and is associated with a relatively high carbon isotopic discrimination against ^{13}C . Although ϵ_f is accepted to range between 25–27 ‰ for most marine algae (cf. Goericke *et al.*, 1994; Popp *et al.*, 1998b), Boller *et al.* (2011) recently showed that this strongly depends on the type of RubisCO used. For the coccolithophore *Emiliania huxleyi* they found an isotope fractionation by the RubisCO enzyme of only ~ 11 ‰, much smaller than previously assumed. Furthermore, many marine algae have various transport mechanisms to actively concentrate CO_2 to compensate for the increase in carbon demand under CO_2 -limiting conditions, or even use bicarbonate directly (e.g. Giordano *et al.*, 2005). Finally, light intensity may also have a direct effect on ϵ_p . In culture studies, *Emiliania huxleyi* was observed to increase the carbon isotope fractionation with increasing light intensity, while $[\text{CO}_2(\text{aq})]$ was found to be of negligible influence on ϵ_p (Rost *et al.*, 2002). This observation was theoretically explained by increased activity of a carbonate concentration mechanism (CCM) in the algal cell with increasing light intensity (Cassar *et al.*, 2006).

Thus, the relationship between photoautotrophic organic carbon and external CO_2 concentrations are complex and seemingly depend on many factors that may implicate the use of $\delta^{13}\text{C}$ of phytoplankton as a $p\text{CO}_2$ proxy. However, the number of algae investigated for their stable carbon isotopic fractionations under varying CO_2 concentrations and light conditions is still limited.

In this study, we determined the stable carbon isotopic fractionation of two marine algae, i.e. the diatom *Proboscia alata* and the prymnesiophyte *Phaeocystis antarctica*, which are important primary producers and contribute significantly to the carbon cycle in present day oceans (Schoemann *et al.*, 2005 and references therein; Hasle & Syvertsen, 1996). The algae were cultured under different $p\text{CO}_2$ and light intensities to investigate the combined effect of these parameters on the carbon isotopic fractionation during photosynthesis. During our experiments we also monitored other factors such as growth rates and nutrients. The results shed light on the controlling factors of stable carbon isotopic fractionation in these two algal species.

2.2 MATERIALS & METHODS

The experimental setup for *P. alata* is described in detail by Hoogstraten *et al.* (2012) and are identical for *P. antarctica*. In short, *P. antarctica* and *P. alata* were cultured semi-continuously, i.e. 16:8 h light:dark cycle, and at constant temperatures of 4 °C and 3 °C, respectively. The cultures were continuously aerated with pCO₂ mixtures of 190, 380 and 750 ppmv, which resulted in differences in the aqueous CO₂ concentrations. This was combined with two different light intensities (high: 240 μmol photons m⁻² s⁻¹ and low: 40 μmol photons m⁻² s⁻¹), thus for each algal species, 6 experiments were carried out. The cultures were diluted regularly to maintain exponential cell growth (Hoogstraten *et al.*, 2012). Before and after each dilution during the experiment, water samples were taken to determine dissolved inorganic carbon (DIC), total alkalinity and nutrient levels (nitrogen and phosphate). Measurements and calculations of the nutrient levels and carbonate system are described by Hoogstraten *et al.* (2012) (**Table 2.1**). Total alkalinity and DIC were determined using a VINDTA 3C according to Dickson & Goyet (1994) and Dickson *et al.* (2007), and subsequently [CO₂(aq)] was determined using the CO₂ system calculations of Lewis & Wallace (1998). Nutrient concentrations were determined according to Grasshoff *et al.* (1983).

Sampling of biomass and for the stable carbon isotopic composition of DIC ($\delta^{13}\text{C}_{\text{DIC}}$) analysis was done at the end of the experiments in the late exponential phase. To obtain cell material, the culture medium was filtered over pre-combusted Whatman 0.7 μm GF/F filters (Ø 47 mm). Directly after filtration, the filters were stored frozen at -20 °C until further analysis. In addition, samples for $\delta^{13}\text{C}_{\text{DIC}}$ were taken in 100 mL glas bottles and sealed with air-tight caps. Subsequently, mercury chloride was added for preservation. For the analyses of $\delta^{13}\text{C}_{\text{DIC}}$, a helium headspace was created and the samples were subsequently acidified with 100 % H₃PO₄, which was added 1 h prior to analysis at room temperature to achieve complete reaction. The headspace was then analyzed on a ThermoFinnigan Gas Bench II coupled to a ThermoFisher Delta^{plus} mass spectrometer. Stable carbon isotope ratios were calibrated against NBS-19 carbonate (IAEA). Standard deviations for $\delta^{13}\text{C}_{\text{DIC}}$ were on average 0.2 ‰. Prior to the analysis of the stable carbon isotope composition of the organic matter ($\delta^{13}\text{C}_{\text{OM}}$), the filters were freeze-dried. With a special punching device (Ø 6 mm) about 6 circles were punched out of the filters and folded into tin cups. Values of $\delta^{13}\text{C}_{\text{OM}}$ were determined on a Flash elemental analyzer coupled to a ThermoFisher Delta^{plus} mass spectrometer (EA/irm-MS) and blank corrected for the contribution of filter material. Stable carbon isotope ratios were calibrated against the lab standard benzoic acid which was calibrated against NBS-22. When sufficient material was available, $\delta^{13}\text{C}_{\text{OM}}$ was analyzed in duplicate.

Table 2.1 | Background data of the *Phaeocystis antarctica* and *Proboscia alata* cultures

Culture	Photon flux $\mu\text{mol m}^{-2} \text{s}^{-1}$	DIC $\mu\text{mol kg}^{-1}$	$\delta^{13}\text{C}_{\text{DIC}}$ ‰	$[\text{CO}_2(\text{aq})]$ $\mu\text{mol kg}^{-1}$	$\delta^{13}\text{C}_c$ ‰	NO_3^- $\mu\text{mol L}^{-1}$	PO_4^{3-} $\mu\text{mol L}^{-1}$	μ d^{-1}	μ/C_c $\mu\text{mol kg}^{-1} \text{d}^{-1}$	V/A μm	$\delta^{13}\text{C}_{\text{org}}$ ‰	σ_p ‰
<i>Phaeocystis antarctica</i>												
Low C_c , HL	240	1600*	2.2	2.3*	-9.2	0.29	0.10	1.2	0.54	n.d.	-14.5	4.3
Intermediate C_c , HL	240	2090	-4.7	5.3	-16.1	6.8	0.20	1.2	0.22	n.d.	-23.8	6.7
High C_c , HL	240	2120	-8.0	5.8	-19.4	0	0.25	0.2	0.04	n.d.	-29.7	9.4
Low C_c , LL	40	2120	-0.3	6.9	-11.7	49.3	2.5	0.5	0.08	n.d.	-25.6	13.1
Intermediate C_c , LL	40	2190	-0.8	9.2	-12.1	48.9	2.3	0.8	0.09	n.d.	-28.6	15.8
High C_c , LL	40	2350	-5.0	19.4	-16.4	32.1	1.1	1.0	0.05	n.d.	-36.6	19.7
<i>Proboscia alata</i>												
Low C_c , HL	240	2130	-0.4	7.1	-11.9	42.6	2.2	0.2	0.03	6.8	-32.5	21.1
Intermediate C_c , HL	240	2240	-1.7	11.6	-13.2	41.9	2.1	0.4	0.03	6.7	-36.1	23.5
High C_c , HL	240	2420	-11.9	29.8	-23.4	42.9	1.9	0.4	0.02	6.6	-47.1	23.7
Low C_c , LL	40	2160	-2.6	8.0	-14.1	46.2	2.4	0.4	0.06	6.9	-36.0	21.5
Intermediate C_c , LL	40	2270	-5.6	13.5	-17.1	45.8	2.4	0.5	0.03	6.9	-39.4	22.0

n.d. = not determined
* average value over whole experiment

2.2.1 Branched glycerol dialkyl glycerol tetraethers

We calculated ϵ_p according to:

$$\epsilon_p = 10^3 [(\delta^{13}\text{C}_{\text{OM}} + 1000) / (\delta^{13}\text{C}_e + 1000) - 1] \quad (\text{Eq. 2.3})$$

in which $\delta^{13}\text{C}_e$ is the stable carbon isotopic composition of the external aqueous CO_2 concentrations. The latter was estimated using the equation of *Mook et al.*, 1974:

$$\delta^{13}\text{C}_e \approx \delta^{13}\text{C}_{\text{DIC}} - 1 + (24.12 - 9866/\text{T}) \quad (\text{Eq. 2.4})$$

with T representing the temperature of the water in degrees Kelvin. Values for $\delta^{13}\text{C}_{\text{OM}}$, $\delta^{13}\text{C}_e$ and ϵ_p are given in **Table 2.1**.

2.2.2 Statistical analysis

All statistical analyses were performed using 12.0 SigmaPlot (Systat Software, Inc.). Correlation coefficients between ϵ_p and important environmental parameters of *P. antarctica* (n=6) and *P. alata* (n=5) were calculated using a Pearson Product Moment Correlation (**Table 2.2**).

2.3 RESULTS

The continuous aeration with air containing $p\text{CO}_2$ values of 190, 280 and 750 ppmv for the LL and HL cultures resulted in $[\text{CO}_2(\text{aq})]$ values that varied from 2.6 to 19.4 $\mu\text{mol kg}^{-1}$ and from 7.1 to 29.8 $\mu\text{mol kg}^{-1}$ for *P. antarctica* and *P. alata*, respectively (**Table 2.1**). We were not able to recover sufficient biomass from the LL culture grown at the highest $p\text{CO}_2$ value of *P. alata* due to the very

Table 2.2 | Pearson Product Moment Correlation between ϵ_p and environmental and physiological variables. Correlations in *italic* have P-values <0.05

	<i>P. alata</i> ϵ_p (‰)	<i>P. antarctica</i> ϵ_p (‰)
DIC	0.843	<i>0.830</i>
C_e	0.763	<i>0.900</i>
$1/\text{C}_e$	-0.853	<i>-0.856</i>
μ	0.666	<i>-0.214</i>
μ/C_e	-0.568	<i>-0.740</i>
V/A	-0.777	
NO_3^-	-0.486	0.763
PO_4^{3-}	-0.738	0.671

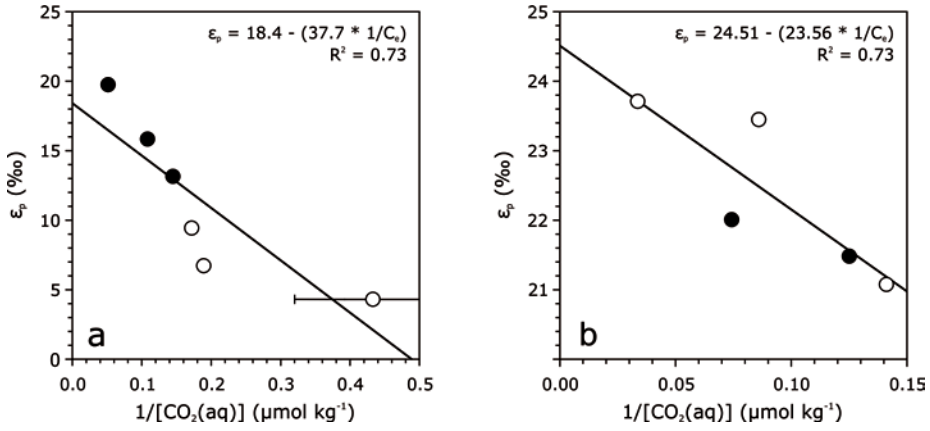


Figure 2.1 | Correlations between ϵ_p and $1/[\text{CO}_2(\text{aq})]$ for (a) *Phaeocystis antarctica* and (b), *Proboscia alata*. High light cultures are indicated with open circles, and low light cultures are indicated with filled circles.

low growth rates during this treatment (Hoogstraten *et al.*, 2012). The growth rates of *P. alata* at the time of harvesting show little variation between the cultures and range between 0.2 d^{-1} in the low C_e HL culture and 0.5 d^{-1} in the high C_e HL culture. Growth rates of *P. antarctica* varied from 0.2 to 1.2 d^{-1} and was lowest in the high C_e HL culture and highest in the low C_e HL culture. For *P. antarctica*, nitrate and phosphate concentrations varied considerably among the two light treatments (0 – $49.3 \mu\text{mol L}^{-1}$ and 0.1 – $2.46 \mu\text{mol L}^{-1}$, respectively), mainly due to the high nutrient uptake in the HL cultures. In contrast, nutrient concentrations remained in a narrow range for *P. alata* (41.9 – $46.2 \mu\text{mol L}^{-1}$ and 1.9 – $2.4 \mu\text{mol L}^{-1}$ for nitrate and phosphate, respectively). The $\delta^{13}\text{C}_{\text{DIC}}$ values ranged between -8.0 to 2.2 ‰ and -11.9 to -0.4 ‰ for *P. antarctica* and *P. alata*, respectively. The range in $\delta^{13}\text{C}_{\text{OM}}$ values for *P. antarctica* is -44.5 to -36.6 ‰ and -47.1 to -32.5 ‰ for *P. alata*. Calculated values for ϵ_p for *P. antarctica* varied widely from 4.3 to 19.7 ‰ , while those for *P. alata* varied in a relatively narrow range from 21.1 to 23.7 ‰ .

2.4 DISCUSSION

Following previous studies (Freeman & Hayes, 1992; Francois *et al.*, 1993; Rau *et al.*, 1997) and equation 2.1, a linear relationship is predicted between ϵ_p and $1/C_e$, and can be simplified (Jasper *et al.*, 1994) into:

$$\epsilon_p = \epsilon_f - b / [\text{CO}_2(\text{aq})] \quad (\text{Eq. 2.5})$$

in which b is a representation of physiological factors that may influence the $\epsilon_p - 1/[\text{CO}_2(\text{aq})]$ relationship. When plotting ϵ_p as a function of $1/[\text{CO}_2(\text{aq})]$, we find

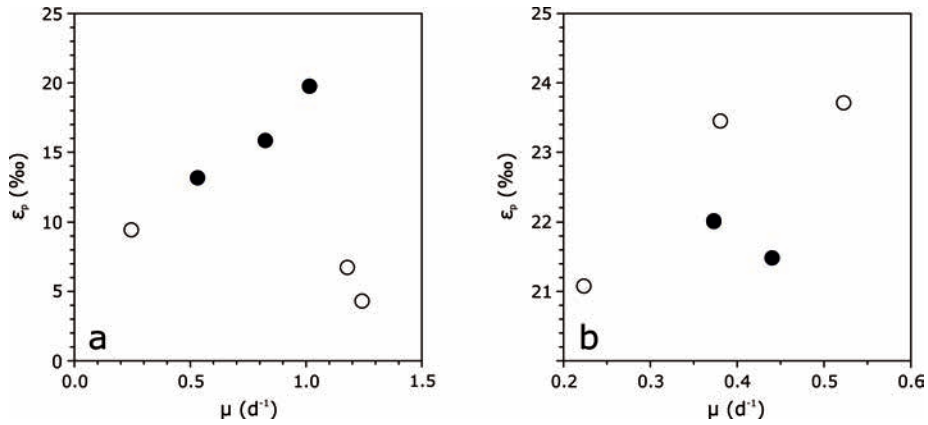


Figure 2.2 | Correlations between ϵ_p and μ for (a) *Phaeocystis antarctica* and (b), *Proboscia alata*. High light cultures are indicated with open circles, and low light cultures are indicated with filled circles.

strong significant negative linear relationships for both cultured marine algal species (**Figs. 2.1a and b; Table 2.2**). Interestingly, all data seem to plot around the correlation line, i.e. there is no apparent difference in behaviour of the low and high light intensity experiments. This suggests that light intensity does not appear to exhibit a large effect on the $\epsilon_p - 1/[\text{CO}_2(\text{aq})]$ relationships. This is in contrast with previous observations of, e.g. *Rost et al.* (2002) who observed a major effect of light intensity on ϵ_p , whereas effects caused by variations in C_e were only minor. *Cassar et al.* (2002) attributed this to the operation of a CCM in *E. huxleyi*. Species that belong to the genus *Phaeocystis*, as well as diatoms, also seem to possess a CCM, and thus it would be expected that *P. antarctica* would also show a substantial effect of light on the ϵ_p . This is, however, not the case. It has been observed that the CCM of *Phaeocystis* is more efficient than that of *E. huxleyi* (*Reinfelder, 2011*, and references cited therein), but it is unclear why this would impact the effect of light intensity on carbon isotopic fractionation.

One of the most important physiological factors that has been shown to impact the stable carbon isotopic fractionation in marine algae is growth rate (*Laws et al., 1995; Bidigare et al., 1997; Popp et al., 1998b*). A direct correlation of μ with ϵ_p does not result in a significant relationship for both *P. antarctica* and *P. alata* (**Figs. 2.2a and b; Table 2.2**), which suggests that for these species, specific growth rate does not exert a major influence on their carbon isotopic fractionation under the given culture conditions. We examined whether a relationship exists between μ , $[\text{CO}_2(\text{aq})]$ and ϵ_p . When plotting ϵ_p against $\mu/[\text{CO}_2(\text{aq})]$, we do not observe any significant improvement in the correlations, but actually a decrease for both *P. antarctica* (from $R^2 = 0.73$ to $R^2 = 0.55$) and *P. alata*, (from $R^2 = 0.73$ to $R^2 = 0.32$)

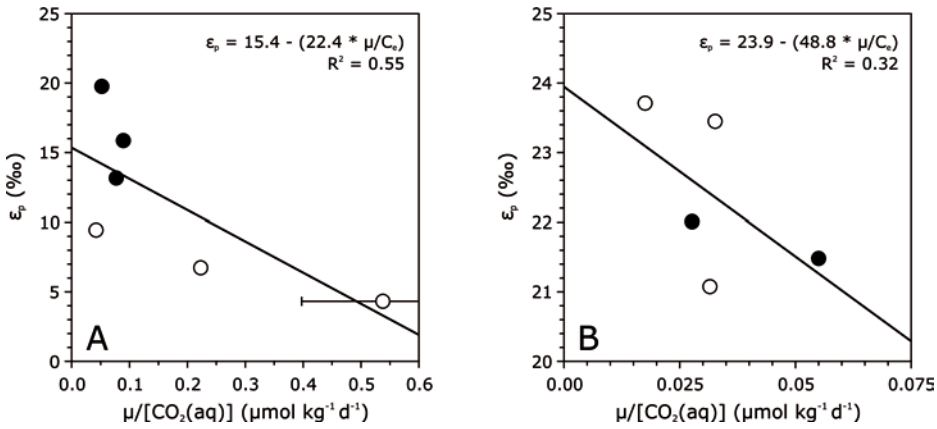


Figure 2.3 | Correlations between ϵ_p and $\mu/[CO_2(aq)]$ for (a) *Phaeocystis antarctica* and (b), *Proboscia alata*. High light cultures are indicated with open circles, and low light cultures are indicated with filled circles.

(Figs. 2.3a and b; Table 2.2). This clearly implies that for these species specific growth rate does not contribute to the observed variation in ϵ_p .

Interestingly, the two marine algae respond differently in isotopic fractionations with respect to $1/[CO_2(aq)]$, i.e. the slope is higher for *P. antarctica* compared to *P. alata* ($-37.7\ \text{‰}\ \mu mol\ d\ kg^{-1}$ versus $-23.6\ \text{‰}\ \mu mol\ d\ kg^{-1}$), while the intercept is higher for *P. alata* compared to *P. antarctica* ($24.3\ \text{‰}$ versus $19.7\ \text{‰}$; Figs. 2.1a and b). In general, it has been shown that the slope and intercept of the relationship described in equation 2.5 is highly species-specific (Bidigare *et al.*, 1997; Laws *et al.*, 1995; Popp *et al.*, 1998b). The intercept is expected to represent the maximum isotope effect (ϵ_i) associated with the enzyme RubisCO (Eq. 2.5; Popp *et al.*, 1998b). The ϵ_i -value for *P. alata* lies close to the range found for marine algae (i.e. 25-27 ‰, Goericke *et al.*, 1994) and is also consistent with that of the marine diatom *P. tricornutum* grown under chemostat conditions (Laws *et al.*, 1995; Popp *et al.*, 1998b). However, the ϵ_i -value of *P. antarctica* is lower than inferred for most marine algae. This may be due to a different RubisCO type for this species as has been observed for the prymnesiophyte algae *E. huxleyi* (Boller *et al.*, 2011). It is, therefore, possible that, in general, prymnesiophyte algae contain Rubisco enzymes that fractionate less compared to other algae. A low intercept ($\epsilon_i \sim 17\ \text{‰}$) was also observed for the cyanobacterium *Synochococcus* sp. (Popp *et al.*, 1998b), but for this bacterium no relationship with $1/C_e$ was found, in contrast to *P. antarctica*.

The differences in the slopes may be explained by variations in the species-specific factor K (Eq. 2.2). Popp *et al.* (1998b) have shown that this factor K relates to cell geometry, i.e. the ratio between cell volume and surface area (V/A), which in turn directly relates to the carbon demand of the cell (Francois *et al.*, 1993; Popp

et al., 1998b). If so, then the higher K-value of *P. antarctica* compared to *P. alata* would suggest a much higher V/A ratio. During the experiment of *P. alata*, Hoogstraten *et al.* (2012) determined the geometry of the cells, and observed a significant decrease in cell volume with increasing $[\text{CO}_2(\text{aq})]$. Assuming a cylindrical form of the cells of *P. alata* (Popp *et al.*, 1998b), V/A ratios are estimated to range between 6.6 to 6.9 μm and are not significantly correlated with ϵ_p values ($R^2 = 0.6$; $P = 0.122$; **Table 2.2**). Unfortunately, morphological parameters for *P. antarctica* were not determined, and a direct comparison of V/A ratios is therefore not possible. Mathot *et al.* (2000) found an average cell diameter of $3.1 \pm 0.6 \mu\text{m}$ for *P. antarctica*, which, since it is a roughly spherical cell, translates into a V/A ratio of ca. 1.9 μm . This value is considerably lower than the V/A ratios estimated for *P. alata* which is inconsistent with the idea that K decreases with increasing V/A. The difference in the slopes of the $\epsilon_p - 1/[\text{CO}_2(\text{aq})]$ relationships between *P. antarctica* and *P. alata* can therefore not be explained by a variation in cell geometry alone.

2.5 CONCLUSIONS

Our results suggests that the carbon isotopic fraction of the two common marine algal species *Phaeocystis antarctica* and *Proboscia alata* are mainly controlled by aqueous CO_2 concentrations, and that light intensity, as well as specific growth rates, did not exert considerable influence. The ϵ_p vs. $1/[\text{CO}_2(\text{aq})]$ relationships between the two species were significantly different, suggesting that the mechanisms that underlie the variation in carbon isotopic fractionation are highly species-dependent conforming previous studies. It is clear, that further studies are required to resolve these underlying mechanisms. Nevertheless, the results from our study raises perspective for the application of stable carbon isotopic composition of organic carbon of certain marine algae, and their specific biomarker lipids, to estimate past atmospheric CO_2 concentrations.

ACKNOWLEDGMENTS

We thank Jort Ossebaar, Michiel Kienhuis, Marianne Baas, Daphne Rekers and Angela Pitcher for their laboratory assistance. Financial support for this research was provided by the Darwin Center for Biogeosciences and a VICI grant from the Netherlands Organisation for Scientific Research to Stefan Schouten.

CHAPTER 3

The influence of lake water pH and alkalinity on the
distribution of core and intact polar branched glycerol dialkyl
glycerol tetraethers

Petra L. Schoon, Anna de Kluijver, Jack J. Middelburg, John A. Downing,
Jaap S. Sinninghe Damsté, and Stefan Schouten

Submitted to Organic Geochemistry

ABSTRACT

Branched glycerol dialkyl glycerol tetraethers (GDGTs) are bacterial membrane lipids, ubiquitously present in soils and peat bogs, but also in rivers, lakes, and lake sediments. The distribution of branched GDGTs in soils is mainly controlled by pH and mean annual air temperature, but the controls on the distribution of branched GDGTs present in lake sediments are less well understood. Several studies have found a relationship between the distribution of branched GDGTs in lake sediments and average lake water pH, suggesting an aquatic source of branched GDGTs besides that of soils transported towards the lakes by means of erosion. In this study, we sampled the surface water suspended particulate matter (SPM) from 23 lakes in Minnesota and Iowa, USA, that widely vary in pH, alkalinity and trophic state. The SPM was analysed for concentrations and distributions of core lipid (presumed of fossil origin) and intact polar lipid (IPL, presumed to derive from living cells) branched GDGTs. The presence of substantial amounts (18-48 %) of IPL-derived branched GDGTs suggests that branched GDGTs are likely of autochthonous origin. Importantly, a strong correlation between the distribution of branched GDGTs and lake water pH was found, confirming a predominant *in situ* production. An even more significant correlation was found with lake water alkalinity, although the underlying mechanism that controls this relationship is not well understood. Our results raise the potential to reconstruct pH/alkalinity of past lake environments, which would provide important knowledge on past developments of lake water chemistry.

3.1 INTRODUCTION

Lakes are relatively small aquatic systems that cover only 3% of the total Earth's continental surface (Downing *et al.*, 2006). Despite this relative small fraction, they play a major role as contributors to the total global carbon budget (Dean & Gorham, 1998; Cole *et al.*, 2007; Battin *et al.*, 2008) and are important regulators of the carbon cycle due to the many feedbacks they provide, either as CO₂ emitters or as carbon sinks (Downing *et al.*, 2008; Tranvik *et al.*, 2009). In addition, lakes are sensitive to variations in chemical, physical and biological parameters, making them susceptible to climate change and have high sediment accumulation rates and great organic carbon preservation potential (Meyers *et al.*, 1993, 1997). They are thus excellent recorders of the continental response to climate change (e.g. Adrian *et al.*, 2009). Lake sediment records of specific aquatic organisms (e.g. diatoms, chironomids, and chrysophyte cysts) can provide information on past variability in a number of lake parameters, such as water level, topography, catchment, mean annual air temperatures, and lake water chemistry (Lotter *et al.*, 1997; Castañeda & Schouten, 2011 and references cited therein). Lakes are complex systems, however, and nonlinear responses due to confounding factors make it difficult to separate regional variability from global climate variability (Adrian *et al.*, 2009; Wagner & Adrian, 2009a). To improve continental climate reconstructions, it is therefore important to develop new lacustrine proxies, making independent comparisons possible.

Recently, branched glycerol dialkyl glycerol tetraethers (GDGTs; see **Fig. 3.1** for structures), preserved in lake sediments, have gained attention as potential proxies for continental climate reconstructions (Blaga *et al.*, 2010; Tyler *et al.*, 2010; Tierney *et al.*, 2010; Tierney & Russell, 2009; Zink *et al.*, 2010). Branched GDGTs are membrane lipids containing branched alkanes ether-linked to a glycerol moiety and occur ubiquitously in continental environmental settings (e.g. Schouten *et al.*, 2000b). Although first detected and identified in peats (Sinninghe Damsté *et al.*, 2000), they are found to be ubiquitously occurring in soils as well (Weijers *et al.*, 2006b). They are also detected in coastal sediments (Schouten *et al.*, 2000b; Hopmans *et al.*, 2004), in stalagmites (Yang *et al.*, 2011), and in lake sediments (e.g. Schouten *et al.*, 2000b; Hopmans *et al.*, 2004; Blaga *et al.*, 2009). Due to their non-isoprenoid carbon skeleton structures and specific stereoisomer configuration, they were proposed to be produced by soil bacteria (Weijers *et al.*, 2006a). This has recently been confirmed by the identification of one branched GDGT in members of the phylum Acidobacteria (Sinninghe Damsté *et al.*, 2011).

At present, nine branched GDGT structures have been identified with varying amounts of methyl branches and cyclopentyl moieties (**Fig. 3.1**). Weijers *et al.* (2007b) found that the branched GDGT distribution in soils is controlled by specific environmental parameters. Through an empirical study based on >100 globally distributed soils these authors found a significant positive correlation between the number of cyclopentyl moieties, expressed as the cyclization index of branched

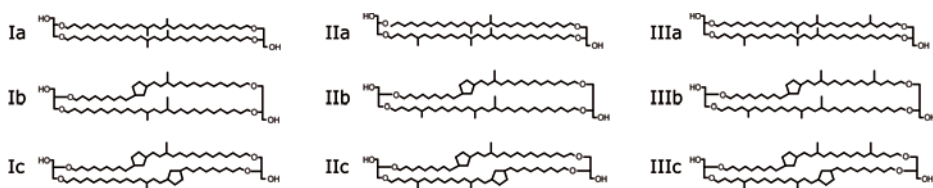


Figure 3.1 | Molecular structures of the branched GDGT membrane lipids analysed in this study

tetraethers (CBT index), with soil pH. Likewise, they found a correlation between the number of methyl branches, expressed as the methyl index of branched tetraethers (MBT index), with mean annual air temperatures (MAAT) and with soil pH. Several studies have confirmed these relationships between soil pH and temperature with the distribution of branched GDGTs in soils, providing support for the use of the MBT and CBT proxies (e.g. *Peterse et al.*, 2009c, 2010).

Soil-derived branched GDGTs are transported to aquatic systems by means of soil erosion through terrestrial runoff (e.g. *Hopmans et al.*, 2004). As shown from a sediment-trap record from the East-African Lake Challa, this influx is mainly governed by variations in rainfall intensity (*Verschuren et al.*, 2009). There is increasing evidence that branched GDGTs are produced *in situ* as well, either at the sediment-water interface or within the water column of the lake itself (*Sinninghe Damsté et al.*, 2009; *Tierney & Russell*, 2009; *Tierney et al.*, 2010, 2012; *Tyler et al.*, 2010; *Zink et al.*, 2010; *Bechtel et al.*, 2010; *Sun et al.*, 2011), which hampers the application of the MBT and CBT proxies using lake sediments. A partially aquatic origin of branched GDGTs is supported by the difference in branched GDGT distribution in lake sediments and the corresponding catchment soils (*Sinninghe Damsté et al.*, 2009; *Tierney & Russell*, 2009; *Loomis et al.*, 2011). Furthermore, a relationship was found between the distribution of branched GDGTs present in lake surface sediments with water-column pH (*Tierney & Russell*, 2009; *Tierney et al.*, 2010, 2012; *Sun et al.*, 2011). As yet, however, this relationship has not been tested for suspended particulate matter (SPM) in lakes.

Here, we investigated the distribution and concentrations of branched GDGTs in the surface water SPM of 23 lakes in Iowa and Minnesota, USA (**Fig. 3.2**). The lakes in Iowa were (hyper)eutrophic and relatively high in pH (7.8 to 9.8) and alkalinity (1950 to 4750 $\mu\text{eq L}^{-1}$). In contrast, nearly all of the lakes in Minnesota were meso-oligotrophic and show a range in pH and alkalinity from 6.7 to 8.4 and 150 to 3686 $\mu\text{eq L}^{-1}$, respectively. The wide range in pH and alkalinity values makes it possible to study the effect of lake chemistry parameters on the distribution of the branched GDGTs. We analysed both core branched GDGTs, representing dead, non-living ("fossil") matter, and intact polar lipid (IPL)-derived branched GDGTs, representing living cells (e.g. *White et al.*, 1979; *Harvey et al.*,

1986) and compared the impact of lake pH and alkalinity on the distribution of the branched GDGTs from these two pools (i.e. “fossil” vs. “living”). This allows us to study the sources of branched GDGTs present in the water column of these lakes and gives more insight on the factors controlling their distribution.

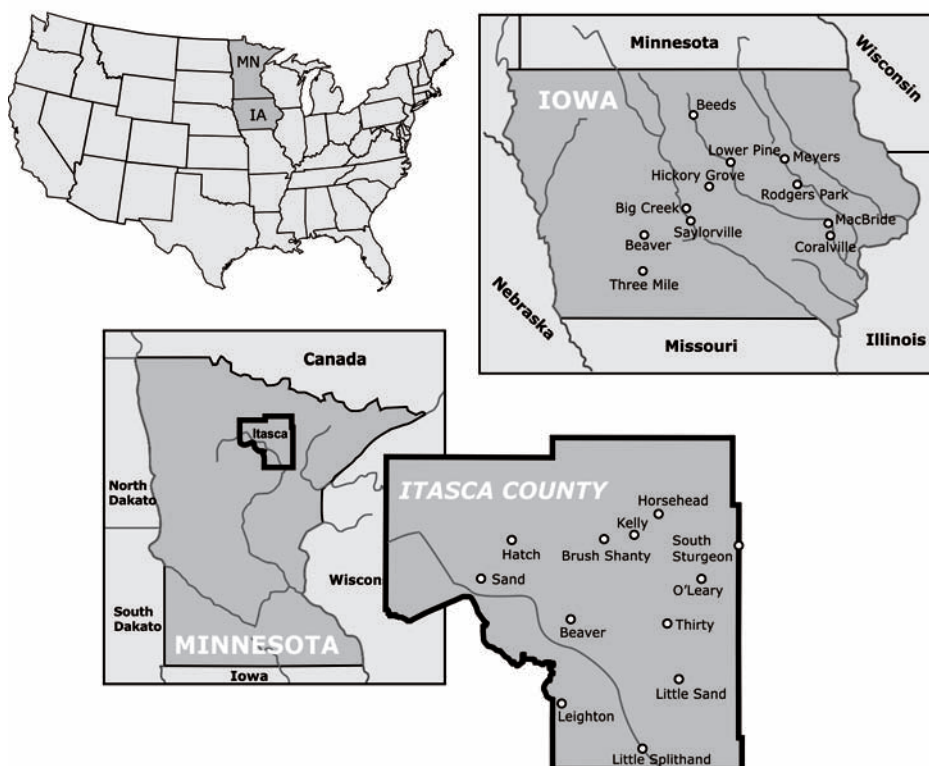


Figure 3.2 | Map showing the locations of the lakes sampled in this study. IA = Iowa, MN = Minnesota

3.2 LAKE LIMNOLOGY

The lakes investigated in this study were selected based on average pH and alkalinity values of previous sampling campaigns performed by the Iowa State University annually in the summer months, which were part of an assessment of the quality of lake water in Iowa and Minnesota. Full lake reports can be found at <http://limnology.eeob.iastate.edu/lakereport> and <http://limnoweb.eeob.iastate.edu/itascalakes>.

Most lakes in Iowa are manmade and are mainly for recreational purposes, drinking water supplies, and flood control. On average, the studied lakes (**Fig. 3.2; Table 3.1**) were relatively shallow (4.4–14.6 m) and small in terms of relative surface area (0.09 to 3.60 km²). Exceptions are the lakes at Coralville and Saylorville (21 and 24 km²), which are reservoirs with an emergency spillway to control floods of the Iowa and Des Moines Rivers, respectively. Most of the lakes are longer than they are wide and have a dendritic shape. This kind of bathymetry is typical for manmade lakes as they are often located in drowned river valleys at the end of a drainage basin (Kalff, 2003). Inflow and outflow of water occurs mainly at one point and is manually controlled, resulting in a unidirectional through-flow of the water (Kalff, 2003). The deepest point of the lakes is most often located near the dam.

All studied lakes in Iowa are eutrophic and had total phosphorous (TP) values above 20 µg L⁻¹ (**Table 3.1**; see also *de Kluijver*, 2012). Land use in Iowa State is highly demanding in terms of nutrient cycling and belongs to one of the most intensive agricultural areas in the world (*Arbuckle & Downing*, 2001). More than 90% of the land area of Iowa State is in use for the production of maize and soy beans (row crops). This particular type of agriculture has a high influence on the nutrient loads of the lake watershed (*Arbuckle & Downing*, 2001) and is reflected in the overall high N:P stoichiometry of the lakes (19 to 290; **Table 3.1**) and leads to very high biological productivity. In summer, many lakes develop a thermocline and become thermally stratified. Due to the high oxygen demand, bottom waters may become hypoxic (O₂ concentrations of < 2 mg L⁻¹).

The lakes studied in the North of Minnesota are distributed across the south-east and central part of Itasca County (**Fig. 3.2; Table 3.1**). In Itasca County alone there are over 1000 lakes, which all have a natural origin. The catchment areas of these lakes developed since the last glaciation about 12,000 years ago and consist of carbonate-poor glacial deposits (till). The area is highly forested and consists of a mixture of evergreens, such as pine and spruce, and deciduous trees. The average surface area of the lakes is 1.7 km² and ranges between 0.2 and 14 km². The maximum lake depth ranges between 4.3 to 26.8 m with an average of 12.2 m. The lakes have TP values ranging between 2–30 µg L⁻¹ (**Table 3.1**) and the trophic states are meso-oligotrophic, except for Little Splithand Lake which can be classified as eutrophic (*de Kluijver*, 2012).

3.3 METHODOLOGY

3.3.1 Sampling

Suspended particulate matter (SPM) of 23 lakes (11 in Iowa and 12 in Minnesota) was collected in the Summer (July–August) of 2009 (**Fig. 3.2**). Sampling of lake water for SPM collection was performed at the deepest part of the lake, determined by sonar and Geographical Positioning System (GPS), within the mixed-layer about

Table 3.1 | Locations and general properties of the sampled lakes.

Lake name	State	County	Coordinates	Max depth (m)	Area (km ²)	Temperature (°C)	O ₂ (μmol L ⁻¹)	pH	ALK (μeq L ⁻¹)	DIC (μmol kg ⁻¹)	ΣN (μmol L ⁻¹)	ΣP (μg L ⁻¹)	N/P
Hickory Grove	Iowa	Story	41°N59'25" 93°W21'49.5"	10.2	0.406	22.8	12.2	8.6	3540	2498	4940	54	91
Coralville Reservoir	Iowa	Johnson	41°N43'36.3" 91°W31'46"	9.7	21.367	24.2	6.3	7.8	4750	4554	6500	207	31
Lake MacBride	Iowa	Johnson	41°N47'36.4" 91°W34'23.4"	13.3	3.598	22.0	6.5	8.8	2350	1977	1270	68	19
Meysers Lake	Iowa	Black Hawk	42°N27'42.2" 92°W17'21.9"	6.1	0.109	27.1	145	9.8	2150	1492	2140	209	10
Rodgers Park Lake	Iowa	Benton	42°N12'4.4" 92°W4'32.6"	4.4	0.089	24.6	7.6	8.4	3600	3337	6810	51	135
Lower Pine Lake	Iowa	Hardin	42°N22'1" 93°W4'41"	5.0	0.250	24.1	7.9	8.6	2900	2500	4150	128	32
Beeds Lake	Iowa	Franklin	42°N46'13.5" 93°W14'11.6"	6.9	0.365	23.8	9.7	8.5	4550	4186	9320	36	258
Beaver Lake	Iowa	Dallas	41°N31'56.5" 94°W12'45.3"	11.5	0.133	24.1	104	9.5	2050	1696	1690	153	11
Three Mile Lake	Iowa	Union	41°N41'19.2" 94°W12'48.7"	12.0	3.279	21.3	3.2	9.1	1950	1695	1000	45	22
Big Creek Lake	Iowa	Polk	41°N47'38.8" 93°W43'54.6"	14.6	3.298	25.0	8.2	8.5	3950	3888	6120	21	287
Saylorville Reservoir	Iowa	Polk	41°N43'37" 93°W41'59"	10.5	24.098	25.3	9.7	8.5	4100	4033	4900	116	42
Leighton	Minnesota	Itasca	47°N11'48.5" 93°W45'12.2"	19.2	0.927	19.4	8.1	8.4	3700	2992	490	8	61
Little Splithand	Minnesota	Itasca	47°N 59' 25" 93°W 21' 49.5"	7.6	0.902	19.2	7.8	8.2	2050	1687	150	30	5
Sand	Minnesota	Itasca	47°N35'8.2" 93°W58'26"	11.0	13.726	19.9	6.8	7.7	2350	606	150	14	11
Beaver Lake	Minnesota	Itasca	47°N26'39.1" 93°W39'20.5"	9.1	0.190	19.7	7.9	6.9	200	88	150	16	9
South Sturgeon	Minnesota	Itasca	47°N37'57.5" 93°W4'12"	13.1	0.777	18.6	8.3	6.1	450	197	150	14	11
O'Leary	Minnesota	Itasca	47°N34'39.4" 93°W11'15.4"	4.3	0.530	19.2	8.7	6.7	200	80	440	14	31
Kelly	Minnesota	Itasca	47°N39'37.4" 93°W23'1"	11.9	0.279	20.2	8.7	6.9	150	52	150	9	17
Horsehead	Minnesota	Itasca	47°N41'30.1" 93°W18'51.5"	4.9	0.308	19.9	7.0	6.7	150	55	150	7	21
Brush Shanty	Minnesota	Itasca	47°N39'0.4" 93°W27'49.7"	10.7	0.607	20.3	8.2	7.4	550	290	345	10	35
Little Sand	Minnesota	Itasca	47°N15'13.7" 93°W16'47.3"	13.4	0.862	22.8	8.5	8.2	1500	1880	840	15	56
Hatch	Minnesota	Itasca	47°N39'33.8" 93°W44'53.5"	26.8	0.983	20.3	9.0	8.4	3600	3038	546	2	273
Thirty	Minnesota	Itasca	47°N28'28.6" 93°W18'29.9"	4.3	0.441	22.0	8.9	7.1	250	123	150	16	9

2 meters below the lake surface (epilimnion) and transferred in pre-cleaned 1 L bottles. SPM was obtained by filtering the lake water over a pre-combusted 0.7 μm GF/F filter (47 mm) using a multi-valve filtration device attached to a vacuum pump. The SPM samples were transported on dry ice and then stored at -20°C . At the time of SPM sampling, water-column profile measurements, such as pH, dissolved oxygen, temperature, and thermocline depth, were taken using a YSI 6600 multi-parameter probe. Nutrient levels were measured in discrete samples. Measurement of TP was performed following the ascorbic acid method with persulfate digestion (APHA, 1998). Both TP and TN were analysed using a HP 8453 Spectrophotometer at the ISU Limnology Laboratory. Additional water samples were taken for laboratory pH and alkalinity analyses, that were determined by ISU using a potentiometric titration method (to a pH of 4.5). The alkalinity is given in terms of the equivalent concentrations of titratable base ($\mu\text{eq L}^{-1}$) and is a measure of the capacity of solutes to neutralize acid. Lake water characteristics important for this study are listed in **Table 3.1**.

3.3.2 Extraction and separation of IPL- and CL-derived branched GDGTs

All filters containing SPM were freeze-dried and then cut in small pieces with scissors. The filters were extracted ultrasonically (3x) in a methanol (MeOH):dichloromethane (DCM):phosphorous (P)-buffer in the ratio 2:1:0.8 (v:v:v) according to a modified Bligh and Dyer method (Bligh & Dyer, 1959; Rütters *et al.*, 2002). The sonicated samples were centrifuged to separate the supernatant from the residue. To achieve complete separation of the different solvent layers, DCM and P-buffer were added to the supernatant in a new volume ratio of 1:1:0.9 / DCM:MeOH:P-buffer. The DCM layer containing the intact polar lipid fraction was transferred to a round-bottom flask. The remaining layer was washed twice with DCM. The combined DCM-layers were subsequently evaporated to near-dryness using a rotary evaporator. The extract was then transferred to a pre-weighed vial using a mixture of DCM:MeOH (v:v, 1:1) and dried under N_2 . An aliquot of the Bligh and Dyer extracts were transferred over an activated silica gel column to separate the CL-GDGTs from the IPL-GDGTs, modified from Oba *et al.* (2006) and Pitcher *et al.* (2009), using hexane/ethyl acetate (1:1, v:v) and methanol as eluents, respectively. The IPL fraction was then subjected to acid hydrolysis by refluxing for 2 h in 2 ml of 1.5 N HCl/MeOH. During this chemical degradation process, the polar head groups are cleaved thereby releasing the core lipids. After cooling to room temperature, the pH of the mixture was then adjusted to a pH of 4-5 with a 2N KOH:MeOH (1:1, v:v) solution and then bi-distilled water and DCM was added to obtain separation of the different layers. After retrieving the DCM layer, the mixture was additionally washed three times with DCM. The combined DCM layers were then dried over a column containing sodium sulfate.

The fractions containing the CL- and IPL-derived GDGTs were filtered through a 0.45 μm PTFE filter and subsequently dissolved in a hexane:isopropanol mixture (99:1, v:v) at a concentration of 10 mg mL^{-1} .

3.3.3 HPLC/MS analysis

The fractions containing the CL- and IPL-derived GDGTs were analysed according to *Schouten et al.* (2007a), using high performance liquid chromatography/atmospheric pressure chemical ionization-mass spectrometry (HPLC/APCI-MS) on a Agilent 1100 series. Detection of the branched GDGTs was through single ion monitoring (SIM) of the different $M+H^+$ ions. The IPL- and CL-derived branched GDGTs were quantified by comparing the integrated areas of the $[M+H]^+$ molecular ion peaks with a C_{46} GDGT internal standard (added prior to analysis) according to *Huguet et al.* (2006).

The CBT and MBT indices were calculated using the equations given by *Weijers et al.* (2007b):

$$CBT = -\text{LOG}_{10} ([Ib + IIb] / [Ia + IIa]) \quad (\text{Eq. 3.1})$$

$$MBT = [Ia+Ib+Ic] / [Ia+Ib+Ic+IIa+IIb+IIc+IIIa+IIIb+IIIc] \quad (\text{Eq. 3.2})$$

Roman numerals refer to GDGT structures in **Figure 3.1**.

3.3.4 Statistical analysis

All statistical analyses were performed using 12.0 SigmaPlot (Systat Software, Inc.). Correlation coefficients and the significance of the correlations ($P < 0.05$) were calculated using a Pearson Product Moment Correlation. We performed a student t-test to assess the differences in branched GDGT distributions between the Iowa and Minnesota lakes.

3.4 RESULTS

3.4.1 Lake pH and alkalinity

Differences in pH and alkalinity among lakes are consistent with expectations for eutrophic vs. oligotrophic systems. The Iowa lakes studied have overall high pH values ranging between 7.8 and 9.8 (**Fig. 3.3 and Table 3.1**). These high pH values are most likely a result of the high primary productivity in these lakes, mainly due to the high nutrient inputs, causing a drawdown in aqueous CO_2 concentrations (*de Kluijver*, 2012). The lakes in Minnesota are generally lower in pH than the lakes in Iowa (6.7 to 8.4; **Fig. 3.3 and Table 3.1**). Differences in the range and magnitude of alkalinity are also quite large between Iowa and Minnesota lakes, from 1950 to 4750 $\mu\text{eq L}^{-1}$ in Iowa and 150 to 3700 $\mu\text{eq L}^{-1}$ in Minnesota (**Table 3.1 and Fig. 3.3**).

3.4.2 GDGT concentrations and distribution patterns

3.4.2.1 Concentrations of CL and IPL derived branched GDGTs

The SPM of the sampled lakes all contained branched GDGTs, although absolute concentrations varied substantially among the lakes (**Figs. 3.4a and b; Table 3.2**

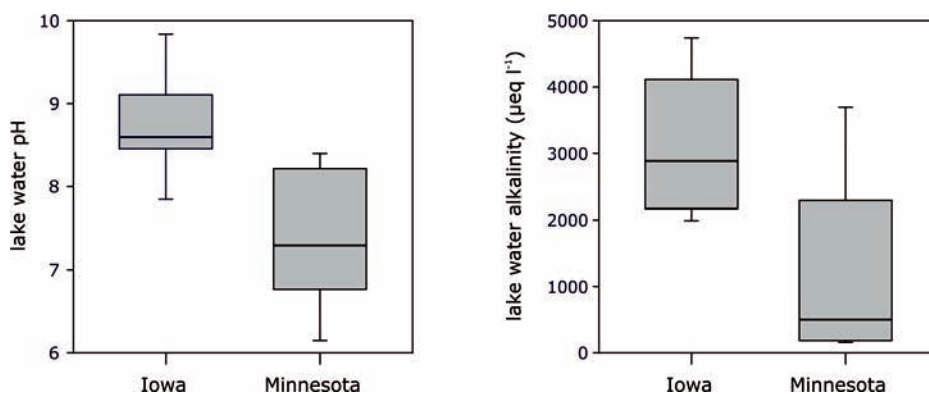


Figure 3.3 | Box plots showing the range in (a) lake water pH and (b) lake water alkalinity of the time of sampling.

and 3.3). Concentrations in Minnesota lakes range from 1.9 to 58 ng L^{-1} and in Iowa lakes from 1.6 to 23 ng L^{-1} . In all lakes, the amount of CL-derived branched GDGTs are higher than the IPL-derived branched GDGTs. In the Iowa lakes $40 \pm 4\%$ of the total pool of branched GDGTs is IPL-derived, whereas in the Minnesota lakes this ranges between 18 and 45 % (**Fig. 3.4c and d**). Branched GDGTs IIa-c are most abundant ($\sim 55\%$ of the CL-derived and 18 % of the IPL-derived total branched GDGTs) followed by GDGTs Ia-c ($\sim 22\%$ CL-derived and $\sim 15\%$ of IPL derived total branched GDGTs).

There is a considerable variation in branched GDGT distribution between the Iowa and Minnesota lakes (**Fig. 3.5**). The most striking is the variation in the relative abundance of branched GDGTs with cyclopentane moieties, especially those with one cyclopentane moiety (Ib, IIb, IIIb) (**Figs. 3.4a and b; Fig. 3.5**), which comprise $27 \pm 3\%$ and $12 \pm 6\%$ of total branched GDGTs in the Iowa and Minnesota lakes, respectively.

3.4.2.2 CL- and IPL-derived CBT and MBT indices

The higher abundance of branched GDGTs with one cyclopentane moiety in Iowa lakes is reflected in the lower CBT values (0.38 ± 0.06) compared to the lakes in Minnesota (0.86 ± 0.26), both in the IPL-derived as well as CL fractions (**Figs. 3.4e and f; Table 3.1**). For both the CL and IPL fractions, there is a significant difference between the CBT indices of the Iowa and Minnesota lakes ($P < 0.001$). In contrast, MBT values for both the CL- and IPL-derived branched GDGTs, are not significantly different between the Iowa and Minnesota lakes ($P > 0.05$). Moreover, the IPL-derived MBT values for the Iowa lakes, are significantly ($P < 0.001$) higher, 0.43 ± 0.04 than the CL-derived MBT values, 0.35 ± 0.03 . The CL- and IPL-derived MBT values (0.34 ± 0.07 and 0.39 ± 0.07 , respectively) for the Minnesota lakes do not show a significant difference ($P = 0.1$) compared to each other.

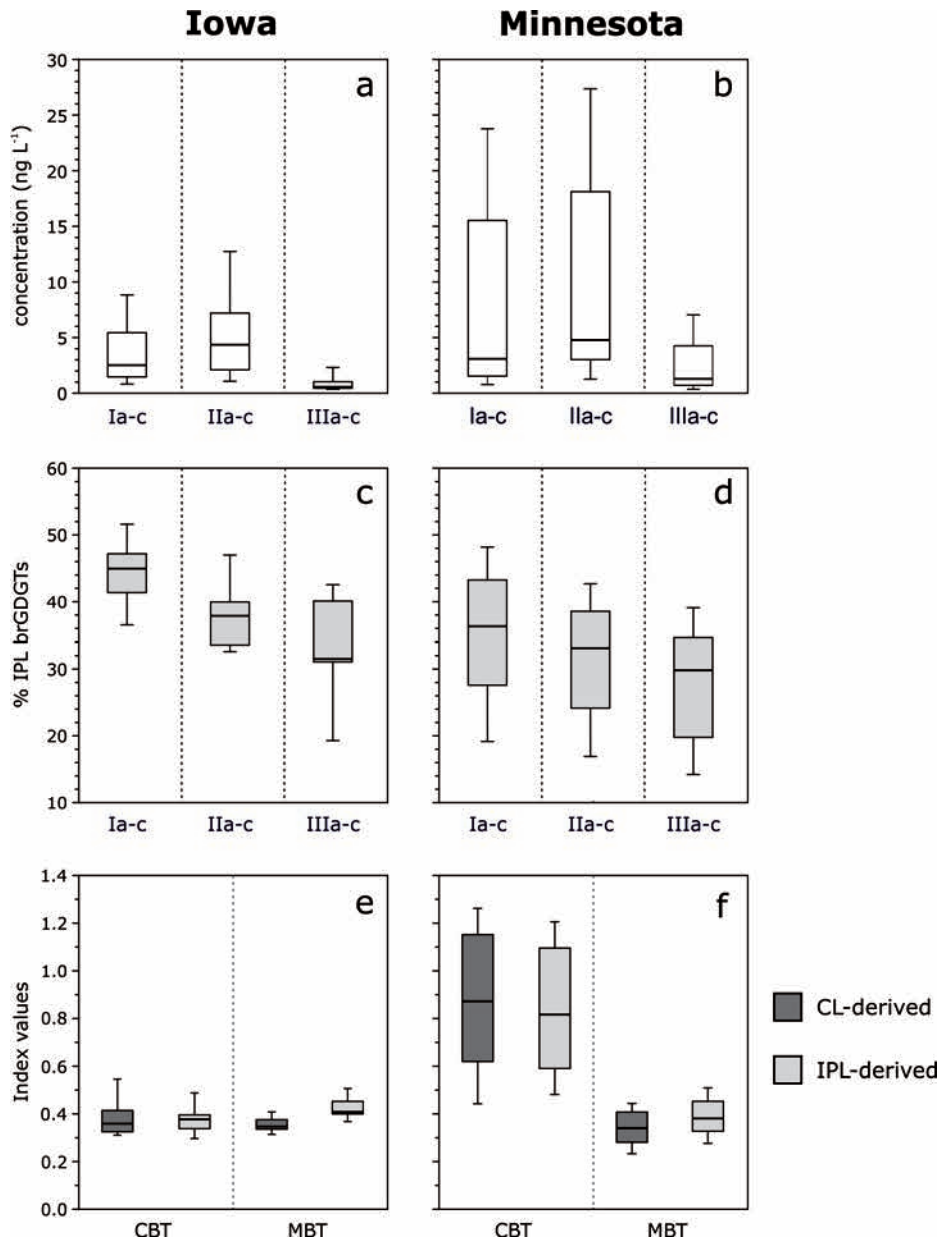


Figure 3.4 | Box plots showing the differences in **(a and b)** the concentrations of branched GDGTs Ia-c, IIa-c, and IIIa-c for both the CL- and the IPL-derived pools, **(c and d)** the relative concentrations of the IPL-derived branched GDGTs Ia-c, IIa-c, and IIIa-c, and **(e and f)** the range of the CL- and IPL-derived CBT and MBT index values, between the Iowa **(a, c and e)** and Minnesota **(b, d and f)** lakes.

Table 3.2 | Concentrations of the branched GDGTs present in the core lipid fractions of the Iowa and Minnesota lakes and inferred MBT and CBT indices. Roman numerals refer to structures shown in **Fig. 3.1**.

Lake name	Branched GDGTs (ng L ⁻¹)										Indices	
	Ia	Ib	Ic	IIa	IIb	IIc	IIIa	IIIb	IIIc	Total	MBT	CBT
<i>Iowa</i>												
Hickory Grove	1.0	0.5	0.1	1.9	0.6	n.d.	0.3	n.d.	n.d.	4.4	0.35	0.41
Coralville Reservoir	2.5	1.4	0.3	4.6	1.9	0.2	1.1	0.2	n.d.	12.2	0.34	0.33
Lake MacBride	0.6	0.3	n.d.	0.9	0.3	n.d.	0.2	n.d.	n.d.	2.4	0.38	0.42
Meyers Lake	0.8	0.4	0.0	1.7	0.7	0.0	0.1	0.1	n.d.	4.0	0.31	0.36
Rodgers Park Lake	0.5	0.3	0.0	1.0	0.4	0.0	0.2	0.0	n.d.	2.5	0.34	0.37
Lower Pine Lake	1.7	0.9	0.1	3.1	1.3	0.1	0.5	0.1	0.1	7.9	0.35	0.34
Beeds Lake	0.2	0.1	0.0	0.4	0.2	n.d.	0.1	n.d.	n.d.	1.0	0.33	0.32
Beaver Lake	2.1	1.1	0.2	3.5	1.2	n.d.	0.5	n.d.	n.d.	8.5	0.39	0.39
Three Mile Lake	1.8	0.6	0.1	2.3	0.6	n.d.	0.7	n.d.	n.d.	6.0	0.41	0.55
Big Creek Lake	0.4	0.3	0.0	0.8	0.4	0.0	0.1	0.1	n.d.	2.1	0.35	0.31
Saylorville Reservoir	0.3	0.2	0.0	0.6	0.3	0.0	0.1	n.d.	n.d.	1.5	0.34	0.33
<i>Minnesota</i>												
Leighton	0.7	0.2	0.0	1.9	0.5	0.0	0.3	0.1	n.d.	3.7	0.24	0.60
Little Splithand	0.9	0.3	0.0	2.6	0.8	0.1	0.9	0.1	n.d.	5.7	0.23	0.50
Sand	0.7	0.1	n.d.	1.5	0.3	n.d.	0.4	n.d.	n.d.	3.0	0.28	0.68
Beaver Lake	7.8	0.6	0.1	8.1	0.4	0.2	2.0	n.d.	n.d.	19.2	0.44	1.20
South Sturgeon	0.9	0.1	0.0	1.6	0.1	0.0	0.6	n.d.	n.d.	3.3	0.32	1.06
O'Leary	14.6	1.2	0.3	17.9	1.1	0.4	5.0	0.1	0.1	40.6	0.40	1.16
Kelly	3.4	0.2	0.1	3.6	0.2	0.1	0.9	0.0	0.0	8.4	0.43	1.26
Horsehead	16.0	1.4	0.3	18.1	1.2	0.5	5.3	0.1	n.d.	42.8	0.41	1.12
Brush Shanty	1.2	0.2	0.0	1.8	0.2	0.1	0.5	n.d.	n.d.	3.9	0.35	0.89
Little Sand	1.7	0.2	0.1	2.6	0.4	0.1	0.8	0.0	n.d.	5.8	0.35	0.86
Hatch	0.2	0.1	0.0	0.5	0.2	0.0	0.1	0.0	n.d.	1.1	0.29	0.44
Thirty	6.3	1.0	0.3	10.2	1.8	0.3	2.9	0.2	n.d.	22.9	0.33	0.77

n.d. = not detected

Table 3.3 | Concentrations of the branched GDGTs present in the intact polar lipid fractions of the Iowa and Minnesota lakes and inferred MBT and CBT indices. Roman numerals refer to structures shown in **Fig. 3.1**.

Lake name	Branched GDGTs (ng L ⁻¹)										Indices	
	Ia	Ib	Ic	IIa	IIb	IIc	IIIa	IIIb	IIIc	Total	MBT	CBT
<i>Iowa</i>												
Hickory Grove	0.9	0.4	n.d.	1.2	0.5	n.d.	0.2	n.d.	n.d.	3.1	0.41	0.39
Coraville Reservoir	2.6	1.6	0.3	4.0	1.7	0.2	0.8	n.d.	n.d.	11.2	0.40	0.30
Lake MacBride	0.3	0.2	n.d.	0.4	0.2	n.d.	0.1	n.d.	n.d.	1.2	0.42	0.36
Meyers Lake	0.7	0.3	n.d.	1.1	0.6	n.d.	0.1	n.d.	n.d.	2.8	0.37	0.30
Rodgers Park Lake	0.4	0.2	0.0	0.6	0.2	0.0	0.1	n.d.	n.d.	1.7	0.40	0.38
Lower Pine Lake	1.8	0.7	n.d.	2.0	0.6	n.d.	0.4	n.d.	n.d.	5.5	0.45	0.46
Beeds Lake	0.2	0.1	n.d.	0.2	0.1	n.d.	0.0	n.d.	n.d.	0.6	0.45	0.40
Beaver Lake	1.8	0.9	0.1	2.1	0.8	n.d.	0.2	n.d.	n.d.	5.8	0.48	0.38
Three Mile Lake	1.1	0.4	0.1	1.1	0.3	n.d.	0.2	n.d.	n.d.	3.2	0.51	0.49
Big Creek Lake	0.3	0.2	0.0	0.5	0.2	0.0	0.1	n.d.	n.d.	1.3	0.41	0.34
Saylorville Reservoir	0.3	0.1	n.d.	0.4	0.2	n.d.	0.1	n.d.	n.d.	1.1	0.40	0.34
<i>Minnesota</i>												
Leighton	0.2	0.1	0.0	0.5	0.1	n.d.	0.1	n.d.	n.d.	1.0	0.31	0.56
Little Spilthand	0.4	0.2	0.0	1.0	0.3	n.d.	0.3	n.d.	n.d.	2.1	0.28	0.48
Sand	0.3	0.1	n.d.	0.6	0.1	0.0	0.1	0.0	n.d.	1.3	0.30	0.68
Beaver Lake	7.2	0.6	0.2	6.0	0.4	0.1	1.2	n.d.	n.d.	15.5	0.51	1.14
South Sturgeon	0.7	0.1	0.0	1.0	0.1	0.0	0.3	n.d.	n.d.	2.2	0.37	0.98
O'Leary	6.7	0.6	0.2	7.3	0.5	0.2	1.8	n.d.	n.d.	17.2	0.43	1.12
Kelly	0.8	0.1	n.d.	0.7	0.0	n.d.	0.2	n.d.	n.d.	1.8	0.48	1.20
Horsehead	5.4	0.6	0.1	5.4	0.4	0.2	1.3	n.d.	n.d.	13.3	0.46	1.03
Brush Shanty	0.8	0.1	0.0	1.1	0.2	0.0	0.2	n.d.	n.d.	2.5	0.40	0.81
Little Sand	1.3	0.2	0.1	1.7	0.3	0.1	0.4	n.d.	n.d.	4.1	0.38	0.83
Hatch	0.2	0.1	n.d.	0.3	0.1	n.d.	0.1	n.d.	n.d.	0.8	0.37	0.55
Thirty	4.1	0.7	0.2	5.6	1.0	0.2	1.4	n.d.	n.d.	13.3	0.38	0.76

n.d. = not detected

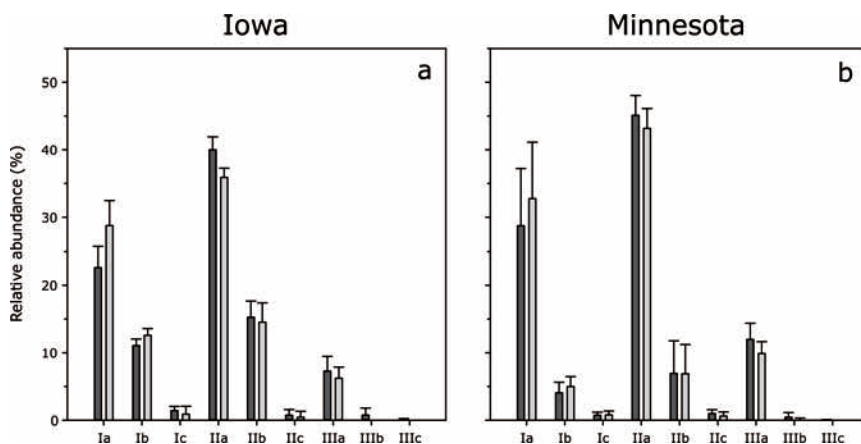


Figure 3.5 | Average relative distribution of the CL- (dark grey) and IPL-derived (light grey) branched GDGTs of the Iowa and Minnesota lakes

3.5 DISCUSSION

3.5.1 Assessing *in situ* production

The fact that there is a substantial amount of IPL-derived branched GDGTs (18 to 45 % compared to core lipids) in the SPM, likely indicates substantial amount of *in situ* production of branched GDGTs in both the Iowa and Minnesota lakes. This is substantiated by the identical distributions between the CL- and IPL-derived branched GDGTs as shown in **figure 3.5**. Furthermore, for both the MBT and CBT indices, there is a strong correlation between the CL- and IPL-derived fractions (**Fig. 3.6**). The relationship between CL- and IPL-derived CBT values is similar to the 1:1 line (**Fig. 3.6b**), which suggests that the majority of the CL-derived branched GDGTs have a similar source as the IPL-derived branched GDGTs and are thus most likely autochthonous.

Interestingly, the relationship between CL- and IPL-derived MBT values (**Fig. 3.6a**) deviates from the 1:1 line, i.e. IPL-derived MBT values are higher than the CL-derived MBT values. Core lipid branched GDGTs likely represent an average signal of several months to years, whereas the IPL-derived branched GDGTs are likely representing a time period of days to months. The MBT index has been found to be impacted by temperature, whereas the CBT index mainly relates to pH. The geographical area of our lake dataset is characterized by a continental climate with warm to hot summers and cold winters, and temperatures can fluctuate considerably. Therefore, the IPL-derived MBT values likely reflect the warm summer temperatures at time of sampling, while the CL-derived MBT values represent a longer-term signal including colder months. In contrast, lake pH levels are likely less variable over periods of weeks to months, and therefore the CL- and IPL-derived CBT values are more similar.

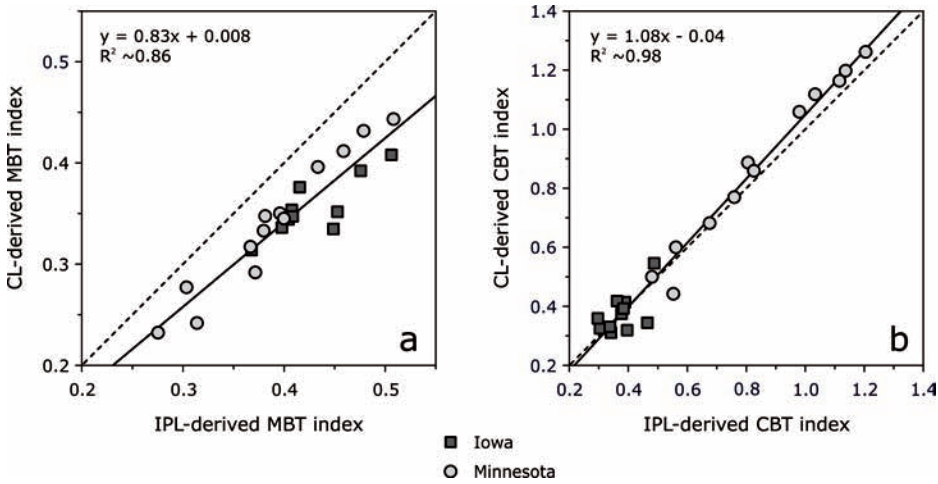


Figure 3.6 | Scatter plot showing the relationships between (a) the CL- and IPL-derived MBT indices and (b) the CL- and IPL-derived CBT indices.

3.5.2 Temperature

Mean annual and summer air temperatures (MAAT and MSAT, respectively) are on average 5–6 °C higher in Iowa (~9 °C and 24 °C) than in Minnesota (~4 °C and 18 °C) (data from <http://www.ncdc.noaa.gov>). However, air temperatures during July/August 2009, collected from nearby weather stations, were somewhat lower than yearly averages, 22 ± 2 °C and 17 ± 2 °C for Iowa and Minnesota, respectively, and are also a few degrees lower than lake surface temperatures measured at the time of sampling, i.e. 24 ± 2 °C (Iowa lakes) and 20 ± 1 °C (Minnesota lakes). We compared the MAAT/MSAT estimates with those derived from the MBT/CBT temperature calibrations (**Table 3.4**). In previous studies, the MBT/CBT calibration for soils (Weijers *et al.*, 2007b) did not hold when applied to lake sediments, and reconstructed MAAT values underestimated by 5 to 10 °C. This effect has been ascribed to an aquatic source of branched GDGTs preserved in the lake sediments, in addition to the ones transported to the lake through soil erosion (Sinninghe Damsté *et al.*, 2009; Tierney & Russel, 2009). Since we find strong evidence for aquatic *in situ* production, a large underestimation of temperature using the soil calibration would be expected. Indeed, the soil calibration of Weijers *et al.* (2007b) substantially underestimates MSAT, and measured lake temperatures (**Table 3.4**) are in agreement with previous studies (Sinninghe Damsté *et al.*, 2009; Tierney & Russel, 2009; Tierney *et al.*, 2009, 2010; Tyler *et al.*, 2010; Sun *et al.*, 2011; Pearson *et al.*, 2011; Bechtel *et al.*, 2010). In contrast, all calibrations based on lake sediments (Pearson *et al.*, 2011; Sun *et al.*, 2011; Tierney *et al.*, 2010) result in more or less the same temperature estimates using IPL-derived CBT/MBT values, yielding temperatures that closely resemble

Table 3.4 | Observed temperatures, including the lake water (in situ) temperature, mean annual air temperature (MAAT) and mean summer air temperature (MSAT), and estimated CL- and IPL-derived MAAT using the soil calibration of *Weijers et al.* (2007) and lake calibration of *Tierney et al.* (2010), and estimated CL- and IPL-derived MSAT using the lake calibrations of *Sun et al.* (2011) and *Pearson et al.* (2011). Data for the observed MAAT and MSAT are derived from www.noaa.gov.

	Iowa		Minnesota	
<i>Observed temperatures</i>				
MAAT‡	9		4	
MSAT‡	24		18	
Air temperatures July/August 2009	22 ± 2		17 ± 2	
<i>In situ</i> temperature	24 ± 2		20 ± 1	
<i>Estimated temperatures</i>				
Global soil calibration ^a	8 ± 1	12 ± 2	3 ± 2	5 ± 2
Tropical lake sediment calibration ^b	20 ± 1	22 ± 1	15 ± 1	17 ± 1
Asian lake sediment calibration ^c	20 ± 0	22 ± 1	16 ± 1	17 ± 1
Global lake sediment calibration ^d	24 ± 1	25 ± 1	18 ± 2	19 ± 1

[‡]Data from www.noaa.gov

^aMAAT = -6.1 + 50 * MBT - 9.35 * CBT (*Weijers et al.*, 2010)

^bMAAT = 11.84 + 32.54 * MBT - 9.32 * CBT (*Tierney et al.*, 2010)

^cMSAT = 13.116 - 7.998 * CBT + 27.752 * MBT (*Sun et al.*, 2010)

^dMSAT = 47.4 + (20.9 * Ia) - (37.1 * IIa) - (53.5 * IIIa) (*Pearson et al.*, 2010)

the MSAT of the two states (**Table 3.4**). Temperatures from CL-derived MBT/CBT values are consistently a few degrees lower, which agrees with the “colder” signal of core lipids (see previous section). They are, however, substantially higher than MAAT, suggesting that the core lipids still predominantly contain a summer temperature signal.

3.5.3 Lake water pH

Correlation of lake pH with MBT and CBT shows that there is no significant relation between MBT and lake pH, for both the CL- and IPL-derived fractions ($R^2 = 0.06$ and $R^2 = 0$, respectively). This is in agreement with observations for soils where MBT is only weakly correlated with soil pH (*Weijers et al.*, 2007b). We do obtain a significant negative correlation, when we plot CBT values against lake water pH values (**Fig. 3.7a and b**):

$$\text{CL-derived CBT} = 2.97 - 0.29 * \text{pH} \quad (R^2 = 0.69) \quad (\text{Eq. 3.3})$$

$$\text{IPL-derived CBT} = 2.78 - 0.27 * \text{pH} \quad (R^2 = 0.72) \quad (\text{Eq. 3.4})$$

The fact that we find a strong correlation between CBT and lake water pH, as well as a good correlation between both pools of branched GDGTs, strongly suggests an *in situ* production of the branched GDGTs within the lake water col-

umn. The correlation between CL-derived CBT and pH closely resembles those based on tropical lake sediments from Africa (Tierney *et al.*, 2010), but differs from the soil calibration of Weijers *et al.* (2007b) and, surprisingly, also from the lake sediment calibration of Sun *et al.* (2011) (**Fig. 3.7a**). At pH values above or near 8.5, CBT values are not increasing with pH and are rather constant at ~ 0.4 . Sun *et al.* (2011) observed a similar pattern for high pH lakes ($\text{pH} > 8.5$) in their Chinese lake sediment dataset and suggested that a certain threshold is reached at $\text{pH} > 8.5$, i.e. the bacteria reach their limit in making adaptations to their membrane lipids at these high pH levels. At pH levels of < 7.5 , bacteria regulate their intracellular pH (which is higher than that of their surroundings) by creating a proton gradient to drive energy reactions over the cell membrane (e.g. Booth, 1985). To accommodate growth at higher pH levels it is important for the organism to maintain the internal pH within the cell constant. To optimize the proton gradient and maintain pH homeostasis at increasing external pH levels, the permeability of the cell membrane is regulated by making the membrane lipids more rigid (Haines, 2001; Konings *et al.*, 2002, 2006). In bacteria that produce branched GDGTs, this is most likely done by adjusting the amount of cyclopentyl moieties in their cell membrane (Weijers *et al.*, 2007b). Under more alkaline conditions, however, microorganisms have a reversed pH gradient over their cell membrane, i.e., their internal pH is lower than that of their surroundings (e.g. Booth, 1985). Most neutrophiles and alkaliphiles are able to perform energy transduction by establishing a sodium-gradient in combination with an H^+ -gradient, and are able to switch between H^+ and Na^+ as coupling ions (Speelmans *et al.*, 1995). The advantage of Na^+ as coupling ion is that the permeability of the cell membrane for Na ions is much lower compared with H^+ (Mulkidjanian *et al.*, 2008 and references therein). In theory, this would imply that further adaptation of the cell membrane is not needed to overcome H^+ leakage. Thus, if the bacteria that produce branched GDGTs indeed use sodium for energy transduction at alkaline pH, this could possibly explain the apparent constant CBT values of ~ 0.4 at pH values > 8.5 (**Figs. 3.7a and b**).

3.5.4 Lake water alkalinity

Aside from a large gradient in pH, our lake dataset also exhibits a large gradient in alkalinity (**Fig. 3.3**). The alkalinity in lakes is mainly determined by the interplay of climatic and geologic factors (Gorham *et al.*, 1983), controlling the type and amount of ions that are transported from the drainage basin. The relatively low alkalinity of the lakes in Minnesota is mainly due to the carbonate-poor glacial till in the watershed, whereas the high alkalinity in the manmade lakes of Iowa, results most likely from anthropogenic influences (Jones & Bachmann, 1978). To moderate field pH levels, farmers tend to add substantial amounts of lime. Furthermore, the inflow of agricultural derived base ions, mainly in the form of hydrogen phosphates and sodium nitrates enhances biologically mediated processes such as nitrate as-

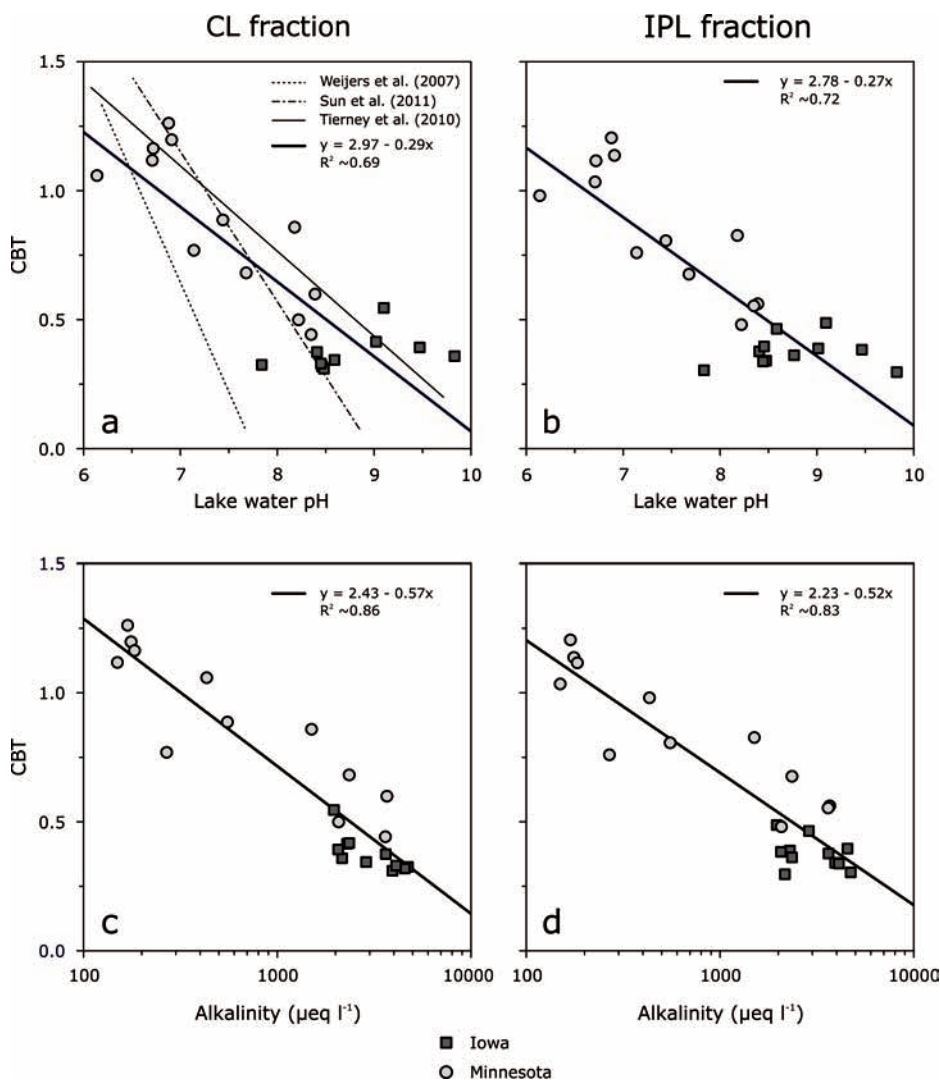


Figure 3.7 | Scatter plots showing the relationship between lake water pH and (a) the CL-derived CBT index values and (b) the IPL-derived CBT index values and, scatter plots showing the relationships between lake water alkalinity and (c) the CL-derived CBT index values and (d) the IPL-derived CBT index values. The thick solid lines are the correlations obtained for the SPM lake dataset in this study. Shown in plot a are the soil calibration of *Weijers et al.* (2007) and the lake sediment calibrations of *Sun et al.* (2011) and *Tieney et al.* (2010).

simulation and denitrification, which can substantially increase the alkalinity of the lake water (*Schindler*, 1985).

Strikingly, a stronger correlation is obtained when plotting the CL- and IPL-derived CBT values against the common logarithm of lake water alkalinity (**Figs. 3.7c and d**) than with pH:

$$\text{CBT} = 2.43 - 0.57 * \text{LOG}_{10}(\text{alkalinity}) \quad (R^2 = 0.86) \quad (\text{Eq. 3.5})$$

$$\text{CBT} = 2.23 - 0.52 * \text{LOG}_{10}(\text{alkalinity}) \quad (R^2 = 0.83) \quad (\text{Eq. 3.6})$$

Thus, higher alkalinity corresponds to an increase in the relative abundance of branched GDGTs that possess one or more cyclopentyl moieties. In Iowa lakes, the pH is decoupled from alkalinity for lakes with pH values above 8.5, which have more or less similar alkalinity values ($\sim 2500 \mu\text{eq L}^{-1}$; **Fig. 3.8**). Since CL- and IPL-derived CBT values in these lakes are more or less constant and do not seem to vary with pH (**Figs. 3.7a and b**), it may explain the stronger correlations with alkalinity. Possibly, this may be related to the use of different ion transfer mechanisms (H^+ vs. Na^+) within the branched GDGT-producing lake bacteria as discussed above. Although sodium is an important contributor to alkalinity in natural waters, the underlying mechanism remains unclear because attribution is complicated due to the covariance between alkalinity, total nitrogen and other variables.

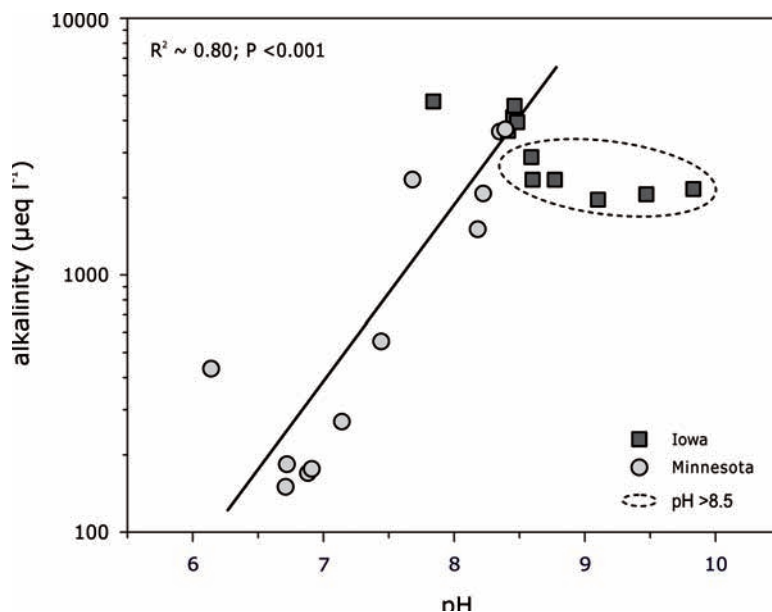


Figure 3.8 | Relationship between pH and alkalinity for the lakes that have pH values below 8.5. Lakes with pH values above 8.5 are within the dotted circle.

3.6 CONCLUSIONS

The strong correlations of the core lipid and intact polar lipid branched GDGT distributions in lake water SPM indicates that the majority of the branched GDGTs are produced *in situ*. Furthermore, temperature estimates based on IPL-derived MBT/CBT correspond well with *in situ* lake and summer air temperatures while those of core lipids yield colder temperature estimates as the latter represent a longer time interval (months to years) compared to the intact polar lipids (weeks or months). The good correlation we find between CL- and IPL-derived CBT values and pH shows that the distribution of branched GDGTs present in Iowa and Minnesota lakes is largely controlled by the buffering capacity of the lake water. This substantiates the evidence that the branched GDGT are autochthonous and that core lipids and intact polar lipids derive from the same source. Furthermore, the CBT-pH correlation compares well with that found in a tropical lake sediment study. This suggests that the CBT index inferred from the distribution in lake sediments can be used for the reconstruction of lake water pH as an alternative for or in addition to pH reconstructions using diatom transfer functions. Caution is needed with lakes that have alkaline pH levels (> 8.5), e.g. lakes that are located in dense populated and agricultural areas. Our study further shows an excellent relationship between the CBT values and the logarithm of alkalinity. The exact mechanism behind the alkalinity-CBT relationship remains as yet unclear, but may be related to the difference in ionic composition, besides H^+ , among the lakes.

ACKNOWLEDGMENTS

We thank Kelly Poole, Amber Erickson, Dan Kendall, and Jingyang Li, from the ISU Limnology Laboratory, and Joshua McGinnis from the lake survey in Grand Rapids, Itasca (MN), for their technical support during our collaboration. Parts of this manuscript are based upon work supported by the Iowa Department of Natural Resources and the National Science Foundation under Grant No. 005309844. From the Royal NIOZ Texel we thank Annelieke Mets, Jort Ossebaer, Marianne Baas, Michiel Kienhuis, Jan van Ooijen and Karel Bakker for their laboratory and analytical support. Partial funding for this project came from the Darwin Center of Biogeosciences (publication number xxx). Financial support came also from a VICI grant from the Netherlands Organisation for Scientific Research to Stefan Schouten.

CHAPTER 4

Environmental controls on the distribution of intact polar lipids in oligotrophic and eutrophic lakes

Ellen C. Hopmans, Petra L. Schoon, Anna de Kluijver, Jack J. Middelburg,
John A. Downing, Jaap S. Sinninghe Damsté, and Stefan Schouten

Submitted to Limnology and Oceanography

ABSTRACT

We characterized the intact polar lipid (IPL) composition of suspended particulate matter in the surface waters of 23 oligotrophic lakes and eutrophic lakes in Minnesota and Iowa (USA). A high diversity of IPL classes was detected and comprised amongst others the glycerophospholipids phosphatidylcholine, phosphatidylglycerol, phosphatidylethanolamine, the sulfur-containing glycerolipid sulfoquinovosyldiacylglycerol, and the betaine lipids diacylglyceryl-trimethylhomoserine, diacylglyceryl-hydroxymethyltrimethylalanine, and diacylglyceryl-carboxyhydroxymethylcholine. Most IPL classes were detected in all lakes, but eutrophic Iowa lakes contained a relatively high abundance of lyso-IPLs, which were generally not detected in oligotrophic Minnesota lakes, possibly as a consequence of the high ion content in Iowa lakes. Using selected reaction monitoring we detected a variety of glycolipids derived from N_2 -fixing heterocystous cyanobacteria in all lakes, suggesting their presence in both oligotrophic as well as eutrophic lakes. Correlation of glycolipid abundance with environmental parameters showed that high productivity lakes have high glycolipid abundances, suggesting that an increased activity of heterocystous cyanobacteria is needed to supply bioavailable nitrogen for sustaining primary productivity. We also observed distributional differences in glycolipids likely due to differences in cyanobacterial species. Finally, we detected only low amounts of IPLs with a crenarchaeol moiety, the characteristic lipid for ammonia-oxidizing Thaumarchaeota, primarily with a monohexose headgroup and only in some eutrophic Iowa lakes. Indirect analysis of IPL crenarchaeol showed that its abundance was generally low in oligotrophic Minnesota lakes and higher in the eutrophic Iowa lakes. Possibly they were inhibited by the high dissolved organic carbon concentrations in Minnesota lakes as suggested previously for other lakes.

4.1 INTRODUCTION

Intact polar lipids (IPLs) occur ubiquitously in the natural environment as they are the main building blocks of membranes of cellular microorganisms. They are generally composed of a glycerol backbone with ester-linked fatty acids attached to the *sn*-1 and *sn*-2 positions and a polar head group at the *sn*-3 position (e.g. *Fahy et al.* 2005; e.g. **Fig. 4.1**). Some IPL classes, or fatty acids derived thereof, are synthesized predominately by specific microbial groups and can thus potentially be used as chemotaxonomic markers (e.g. *Shan*, 1974; *Lechevalier & Lechevalier*, 1989; *Sturt et al.*, 2004). Furthermore, IPL molecules are thought to degrade rapidly upon cell death and therefore predominately derive from living (microbial) cells (*White et al.*, 1979; *Harvey et al.*, 1986). Thus, IPL analysis has the potential to provide valuable information on living microbes complementary to that obtained by microbiological and molecular techniques. Furthermore, IPL compositions are known to be sensitive to environmental conditions such as nutrient limitation (e.g. *Benning et al.*, 1995), thus potentially yielding information on the physiology of microbes. For example, marine cyanobacteria have been shown to replace phospholipids with sulfur-containing IPLs under P-limiting conditions (*van Mooy et al.*, 2009).

Up to now, most environmental IPL analysis has been indirect in the form of fatty acids derived from phospholipids ('PLFA'). The development of methods for the direct analysis of IPLs (e.g. *Fang & Barcelona*, 1998; *Rütters et al.*, 2002a; *Sturt et al.*, 2004) now allows the rapid assessment of the full structural diversity of IPLs, including headgroup composition. This analytical advancement has increased our knowledge on the sources and diversity of IPLs in natural environments, in particular in sediments (e.g. *Zink et al.*, 2003; *Biddle et al.*, 2006; *Lipp & Hinrichs*, 2009), in suspended particulate matter from marine waters (e.g. *van Mooy et al.*, 2006, 2009; *Schubotz et al.*, 2009; *Popendorf et al.*, 2011; *Brandsma et al.*, 2012a) and sediments and microbial mats from extreme environments (e.g. *Bradley et al.*, 2009; *Borin et al.*, 2010; *Bühning et al.*, 2011). Studies of the IPL composition of suspended particulate matter in lakes have been relatively limited, however. *Ertefai et al.* (2008) examined a polluted meromictic lake and found a range of phospholipids and some glycolipids with a predominance of betaine lipids in the epilimnion and dialkylglycerol-phosphatidylethanolamine lipids in the hypolimnion. *Bühning et al.* (2009) analysed a microbial mat from a hypersaline lake and found a predominance of ornithine and betaine lipids. *Wormer et al.* (2012) analysed glycolipids specific for heterocystous cyanobacteria in a number of Spanish lakes and found their distribution to relate to different taxonomic groups within the heterocystous cyanobacteria.

Here we analysed the IPL composition of particulate matter in surface waters from two contrasting sets of lakes: Twelve highly eutrophic lakes in Iowa and Minnesota and eleven meso-oligotrophic lakes in Minnesota (**Fig. 4.2**; see also *de Kluijver*, 2012). We determined the general structural diversity of IPLs and compared this with the trophic nature of the lakes. In addition, we performed targeted

analysis of IPLs derived from N₂-fixing heterocystous Cyanobacteria (glycolipids; *Bauersachs et al.*, 2009a) and ammonia-oxidizing Thaumarchaeota (crenarchaeol; *Pitcher et al.*, 2011a, and references cited therein), both crucial microbes involved in nitrogen cycling. The results shed light on the potential of IPLs to track specific microbes in contrasting lake environments.

4.2 MATERIALS AND METHODS

4.2.1 Sampling

All samples for this study were taken during Summer 2009 (see *de Kluijver*, 2012). Water samples were collected from the deepest part of the lake within the mixed-zone layer (~2 m below surface) and transferred in pre-cleaned 1 L bottles and subsequently transported on ice to the Limnology Laboratory of Iowa State University. Here, the lake water was filtered through 0.7 μm GF/F filters (47 mm diameter, precombusted at 450 °C for 12 h; Whatman) using a multi-valve vacuum filtration unit to obtain particulate matter for IPL analysis. All filters were stored frozen at -20 °C for the duration of the sampling and until extraction in the lab.

4.2.2 Environmental parameters

Background data are available as part of a long-term lake monitoring program and can be found at <http://limnology.eeob.iastate.edu/lakereport> and <http://limnoweb.eeob.iastate.edu/itascalakes> as well as in *de Kluijver* (2012). Briefly, total phosphorus (TP) was analyzed with an HP 8453 Spectrophotometer using the ascorbic acid method in Standard Methods (*American Public Health Association*, 1998). Total nitrogen (TN) was analyzed as described by *Crumpton et al.* (1992) using the method of persulfate digestion and second derivative ultraviolet spectroscopy. Dissolved organic carbon was determined with a Shimadzu TOC-V Analyzer using the high-temperature combustion method in Standard Methods (*American Public Health Association*, 1998). POC were analyzed for carbon content on a Thermo Electron Flash EA 1112 analyzer (EA) coupled to a Delta V isotope ratio mass spectrometer (IRMS). For chlorophyll *a*, water was filtered through a 0.45 μm filter that was subsequently extracted in 100% acetone using a probe sonicator (*Jeffrey et al.*, 1997). Chlorophyll *a* was measured with a TD-700 Fluorometer using the non-acidified fluorometry EPA method 445.0 (*Arar & Collins*, 1997). Total alkalinity and pH were analyzed at 25 °C through a probe measurement and titration to a pH of 4.5 (*American Public Health Association*, 1998). The alkalinity is given in terms of the equivalent concentrations of titratable base ($\mu\text{eq L}^{-1}$) and is a measure of the acid neutralizing capacity (ANC).

4.2.3 Extraction

The GF/F filters were freeze-dried before the IPLs were extracted using a modi-

Environmental controls on IPL-distribution in lakes

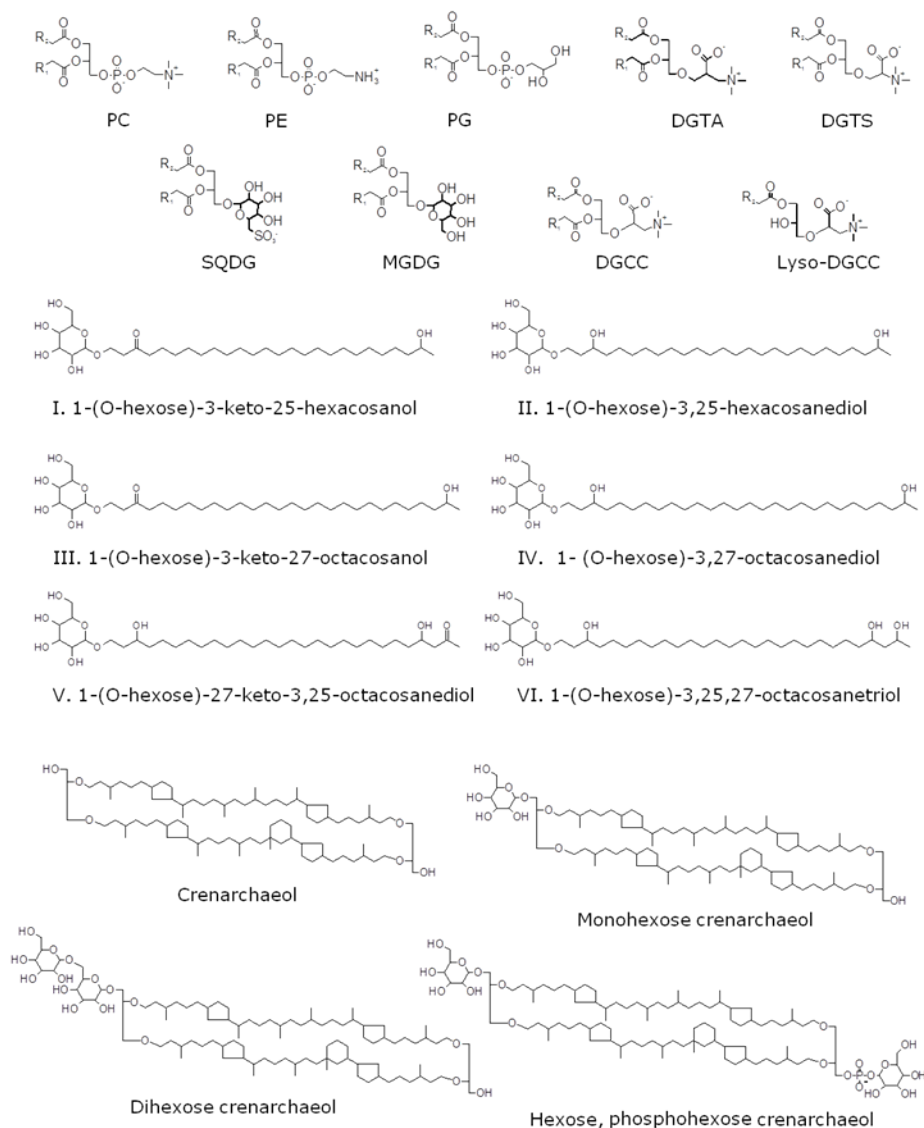


Figure 4.1 Structures of IPLs investigated in this study. PC = phosphatidylcholine, PG = phosphatidylglycerol, PE = phosphatidylethanolamine, SQDG = sulfoquinovosyldiacylglycerol, DGTS = diacylglyceryltrimethylhomoserine, DGTa = diacylglycerylhydroxymethyltrimethylalanine, DGCC = diacylglycerylcarboxyhydroxymethylcholine, MGDG = monogalactosyldiacylglycerol, DGDG = digalactosyldiacylglycerol. R1 and R2 = fatty acid tails.

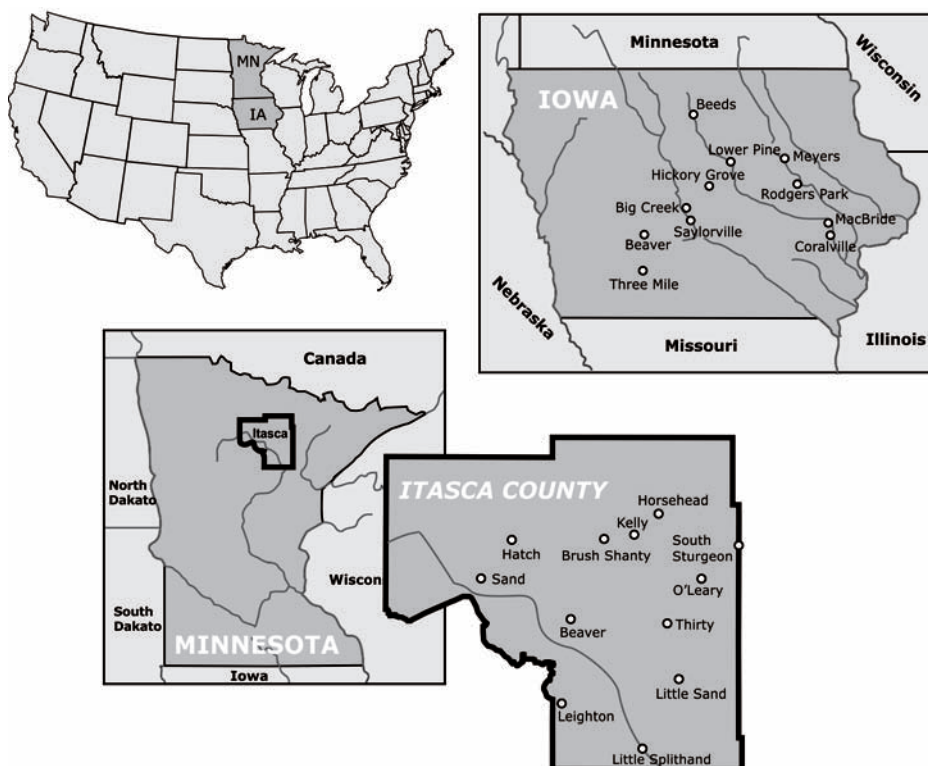


Figure 4.2 | Area map with lakes examined in this study

fied Bligh-Dyer procedure (Bligh & Dyer, 1959). Briefly, the filters were extracted ultrasonically three times for 10 min in a solvent mixture of methanol, dichloromethane and phosphate buffer (2:1:0.8, v:v). After sonication, the combined supernatants were phase-separated by adding additional dichloromethane and buffer to a final solvent ratio of 1:1:0.9 (v:v). The organic phase containing the IPLs was collected and the aqueous phase re-extracted three times with dichloromethane. Finally, the combined extract was dried under a stream of nitrogen gas. Before analysis, the extract was redissolved in a mixture of hexane:2-propanol:water (72:27:1, v:v) at a concentration of 10 mg mL⁻¹, and aliquots were filtered through 0.45 μ m regenerated cellulose syringe filters (4 mm diameter; Grace Alltech, Deerfield, IL).

4.2.4 General IPL analysis

For general IPL screening, the Bligh Dyer extracts were analyzed according to Sturt et al. (2004) with some modifications. High performance liquid chromatography/mass spectrometry (HPLC/MS) was performed on an Agilent 1200 series LC (Agi-

lent, San Jose, CA), equipped with thermostatted auto-injector and column oven, coupled to a LTQ XL linear ion trap with Ion Max source with electrospray ionization (ESI) probe (Thermo Scientific, Waltham, MA). Separation was achieved on an Lichrosphere diol column (250 x 2.1 μm , 5 μm particles; Grace Alltech, Deerfield, IL) maintained at 30 °C. The following elution program was used with a flow rate of 0.2 mL min⁻¹: 100% A for 1 min, followed by a linear gradient to 66% A: 34% B in 17 min, maintained for 12 min, followed by a linear gradient to 35% A: 65% B in 15 min, where A = hexane/2-propanol/formic acid/14.8 M NH_{3aq} (79:20:0.12:0.04 [volume in volume in volume in volume, v/v/v/v]) and B = 2-propanol/water/formic acid/ 14.8 M NH_{3aq} (88:10:0.12:0.04 [v/v/v/v]). Total run time was 60 min with a re-equilibration period of 20 min between runs. ESI settings were as follows: capillary temperature 275 °C, sheath gas (N₂) pressure 25 (arbitrary units), auxiliary gas (N₂) pressure 15 (arbitrary units), sweep gas (N₂) pressure 20 (arbitrary units), spray voltage 4.5 kV (positive ion ESI). The lipid extract was analyzed by an MS routine where a positive ion scan (m/z 400-2000) was followed by a data dependent MS² experiment where the base peak of the mass spectrum was fragmented (normalized collision energy (NCE) 25, isolation width 5.0, activation Q 0.175). This was followed by a data-dependent MS³ experiment where the base peak of the MS² spectrum was fragmented under identical fragmentation conditions. This process was repeated on the 2nd to 4th most abundant ions of the initial mass spectrum.

4.2.5 Glycolipid analysis

Glycolipids were analysed using HPLC/ESI-MS² as previously reported by *Bauersachs et al.* (2009a). HPLC analysis of total lipid extracts was performed using an Agilent 1100 series LC (Agilent, San Jose, CA) coupled to a Thermo TSQ Quantum ultra EM triple quadrupole mass spectrometer with an Ion Max Source with ESI probe (Thermo Electron Corporation, Waltham, MA) operated in positive ion mode. Separation was achieved on a LiChrosphere DIOL column (250 mm x 2.1 mm i.d., 5 μm ; Alltech, Deerfield, IL) maintained at 30 °C. HPLC/MS² analysis was performed in selective reaction monitoring (SRM) mode using transitions specific for glycolipids I-VI (**Fig. 4.1**) following *Bauersachs et al.* (2010). Since we do not have any glycolipid standard available, we report the abundances as peak area L⁻¹ or in % abundance of total glycolipids.

4.2.6 Crenarchaeol IPL analysis

In order to detect the specific crenarchaeol IPLs with high sensitivity we used the SRM method of *Pitcher et al.* (2011b) using HPLC-ESI-triple quadrupole MS². This method allows the detection of IPLs with crenarchaeol as a core lipid and five different head groups, i.e., a monohexose, a dihexose, a hexose and phosphohexose head groups (**Fig. 4.1**). Separation was achieved on a LiChrospher diol column

(250 × 2.1 mm, 5 µm particles, Alltech) maintained at 30°C. The following linear gradient was used with a flow rate of 0.2 mL min⁻¹: 100% A:0% B to 35% A: 65% B over 45 min, maintained for 20 min, then back to 100% A for 20 min to re-equilibrate the column. Detection of crenarchaeol-based IPLs was achieved by using conditions, and monitoring the transitions as described by *Pitcher et al.* (2011b).

To quantify IPL-derived crenarchaeol, one aliquot of the Bligh-Dyer extract was separated into a IPL and core lipid fraction according to *Oba et al.* (2006) and *Pitcher et al.* (2009), except that a hexane:ethyl acetate (EtOAc) (1:1, v/v) mixture was used to obtain the core lipid fractions, and that IPL fractions were retrieved by flushing the silica column with MeOH. A C₄₆ GDGT internal standard was added to both CL and IPL fractions according to *Huguet et al.* (2006). The IPL fractions were subjected to acid hydrolysis (3 h reflux with 1N HCl/MeOH solution) to cleave off the head groups, thereby releasing the GDGTs as core lipids (IPL-derived GDGTs). The IPL-derived fraction was dissolved in hexane:isopropanol (99:1, v/v), filtered over a 0.45 µm PTFE filter, and concentrated to about 3 mg/ml prior to analysis using HPLC/ atmospheric pressure chemical ionization (APCI)–MS on an Agilent 1100 series LC/MSD SL according to *Schouten et al.* (2007a).

4.3 RESULTS

4.3.1 Environmental context of the studied lakes

The environmental conditions of the Minnesota and Iowa lakes, respectively, are distinctly different (**Table 4.1**). The Iowa lakes are all eutrophic to hypereutrophic due to high nutrient loads from agricultural run-off (*Arbuckle & Downing*, 2001), while those in Minnesota are all, but one, meso- to oligotrophic and relatively pristine in nature. This results in relative high total P and N concentrations, low DOC, and high pH for the Iowa lakes and low P and N concentrations, low pH and high DOC for the Minnesota lakes (**Table 4.1**). Total P concentrations ranged from 21 to 209 µg L⁻¹ for Iowa lakes and 2 to 30 µg L⁻¹ for Minnesota lakes, while total N concentrations ranged from 1.0 to 9.3 mg L⁻¹ for Iowa lakes and 0.2 to 0.8 mg L⁻¹ for Minnesota lakes. Due to the high nutrient concentrations, POC and chlorophyll *a* concentrations were high in Iowa lakes, ranging from 0.7 to 9.9 mg L⁻¹ and 5.9 to 63.6 µg L⁻¹, respectively, and substantially lower at Minnesota lakes, ranging from 0.3 to 3.0 mg L⁻¹ and 0.9 to 18.7 µg L⁻¹, respectively (**Table 4.1**). Thus, primary productivity was generally high in Iowa lakes and lower in Minnesota lakes during the sampling period.

4.3.2 General IPL screening

The IPLs detected in the SPM of surface waters of the Minnesota and Iowa lakes contain a large variety of head groups. This included, amongst others, the glycerophospholipids phosphatidylcholine (PC), phosphatidylglycerol (PG), and phospho-

Table 4.1 | Location and background data on Iowa and Minnesota lakes (from *de Kluijver, 2012*).

Lake name	Latitude	Longitude	Temperature (C)	pH	ALK $\mu\text{eq L}^{-1}$	DOC mg L^{-1}	POC mg L^{-1}	Chlorophyll a $\mu\text{g L}^{-1}$	Total N mg L^{-1}	Total P $\mu\text{g L}^{-1}$	N:P
Iowa Lakes											
Hickory Grove	41°N59'25"	93°W21'49.5"	22.8	8.6	3540	n.d.	n.d.	12.0	7.9	54	91
Coralville Reservoir	41°N43'36.3"	91°W31'46"	24.2	7.8	4750	3.0	1.9	14.9	6.5	207	31
Lake MacBride	41°N47'36.4"	91°W34'23.4"	22.0	8.8	2350	3.7	2.8	9.9	1.3	68	19
Meyers Lake	42°N27'42.2"	92°W17'21.9"	27.1	9.8	2150	7.2	9.9	63.6	2.1	209	10
Rodgers Park Lake	42°N12'4.4"	92°W4'32.6"	24.6	8.4	3600	3.0	0.7	5.9	6.8	51	135
Lower Pine Lake	42°N2.21"	93°W4'41"	24.1	8.6	2900	3.5	4.0	21.0	4.2	128	32
Beets Lake	42°N46'13.5"	93°W1'411.6"	23.8	8.5	4550	3.2	0.9	8.0	9.3	36	258
Beaver Lake	41°N31'56.5"	94°W12'45.3"	24.1	9.5	2050	5.7	5.1	38.7	1.7	153	11
Three Mile Lake	41°N4'19.2"	94°W12'48.7"	21.3	9.1	1950	5.8	2.7	17.7	1.0	45	22
Big Creek Lake	41°N47'38.8"	93°W43'54.6"	25.0	8.5	3950	2.8	1.3	14.2	6.1	21	287
Saylorville Reservoir	41°N43'37"	93°W41'59"	25.3	8.5	4100	3.9	1.3	12.3	4.9	116	42
Minnesota Lakes											
Leighton	47°N11'48.5"	93°W45'12.2"	19.4	8.4	3700	9.9	0.7	2.2	0.5	8	61
Little Splithand	47°N 59'25"	93°W21'49.5"	19.2	8.2	2050	13.2	2.1	18.7	0.2	30	5
Sand	47°N35'8.2"	93°W58'26"	19.9	7.7	2350	16.3	0.9	4.5	0.2	14	11
Beaver Lake	47°N26'39.1"	93°W39'20.5"	19.7	6.9	200	9.4	1.5	4.5	0.2	16	9
South Sturgeon	47°N37'57.5"	93°W4'12"	18.6	6.1	450	24.7	0.6	5.4	0.2	14	11
O'Leary	47°N34'39.4"	93°W11'15.4"	19.2	6.7	200	8.5	2.3	4.8	0.4	14	31
Kelly	47°N39'37.4"	93°W23'1"	20.2	6.9	150	9.9	1.2	1.1	0.2	9	17
Horsehead	47°N41'30.1"	93°W18'51.5"	19.9	6.7	150	9.2	2.1	1.2	0.2	7	21
Brush Shanty	47°N39'0.4"	93°W27'49.7"	20.3	7.4	550	12.4	0.6	1.8	0.3	10	35
Little Sand	47°N15'13.7"	93°W16'47.3"	22.8	8.2	1500	12.1	1.2	1.9	0.8	15	56
Hatch	47°N39'33.8"	93°W44'53.5"	20.3	8.4	3600	10.5	0.3	0.9	0.5	2	273
Thirty	47°N28'28.6"	93°W18'29.9"	22.0	7.1	250	14.4	3.0	4.1	0.2	16	9

n.d. = not determined

tidylethanolamine (PE), the sulfur-containing glycerolipid sulfoquinovosyldiacylglycerol (SQDG), the betaine lipids diacylglyceryl-trimethylhomoserine (DGTS), diacylglyceryl-hydroxymethyltrimethylalanine (DGTA), and diacylglyceryl-carboxyhydroxymethylcholine (DGCC), and the glycerolipids mono- and digalactosyldiacylglycerol (MGDG and DGDG) (e.g. **Fig. 4.3**). In addition, we detected sometimes high abundances of ethoxylated surfactants (identification based on MS fragmentation (cf. *Frömel & Knepper*, 2008), likely of anthropogenic origin, which were present in the SPM of the lake water itself as these compounds were absent in some lakes and did not show up in lab blanks. Ether lipids could not be detected using this general screening method. Each of the main IPL classes contained a large variety of IPL species with different fatty acid compositions. The main fatty acid constituents were C14:0, C16:0, C16:1, C18:1, C18:2 and C18:3 with more minor amounts of C16:2, C20:5 and C22:6. No particular trends could be detected with the different lakes. The fatty acid composition inferred from the IPLs compares well with the polar lipid fatty acid (PLFA) composition determined separately for the same lake SPM samples (*de Kluijver*, 2012). The PLFA showed a dominance of C16:0 (~30% on average of total PLFA), C16:1 ω 7c (14%), C18:3 ω 3 (11%), C18:1 ω 9c (9%), C20:5 ω 3 (8%), C18:2 ω 6 (6%), and C22:6 ω 4 (5%) (*de Kluijver*, 2012). Due to the high IPL diversity, lack of suitable standards, and large differences in ionization efficiency between IPLs, it was not possible to quantify the IPLs and perform a quantitative comparison of the IPL distribution. Nearly all IPL classes were detected in the SPM of both Minnesota as well as Iowa lakes, however. The main difference observed was an unusual high abundance of lyso-IPLs, i.e., IPLs in which one of the fatty acid chains is not present, in the Iowa lakes, while SPM of Minnesota lakes generally lacked lyso-IPLs (e.g. **Fig. 4.3**). Furthermore, in Minnesota lakes, DGTA/DGTS was generally the most abundant IPL class in the HPLC base peak chromatogram while DGCC was more common in the SPM of Iowa lakes (e.g. **Fig. 4.3**).

4.3.3 Heterocyst glycolipids

To assess the structural diversity in heterocyst glycolipids we performed a targeted essay using HPLC/MS² following *Bauersachs et al.* (2009a). We found all targeted glycolipids in all lakes (e.g. **Fig. 4.4**) though with varying abundance and distribution (**Table 4.2**). In general, 1-(O-hexose)-3,25-hexacosanediol (glycolipid **II**; **Fig. 4.1**) dominated and comprised between 48 to 96% of the targeted glycolipids. The other glycolipids varied in abundance between 1 and 29 % with 1-(O-hexose)-3-keto-27-octacosanol (glycolipid **III**) generally always in lowest abundance, never reaching more than 7% of total targeted glycolipids (**Table 4.2**).

4.3.4 Thaumarchaeotal lipids

General IPL screening, as discussed above, did not reveal the presence of ether

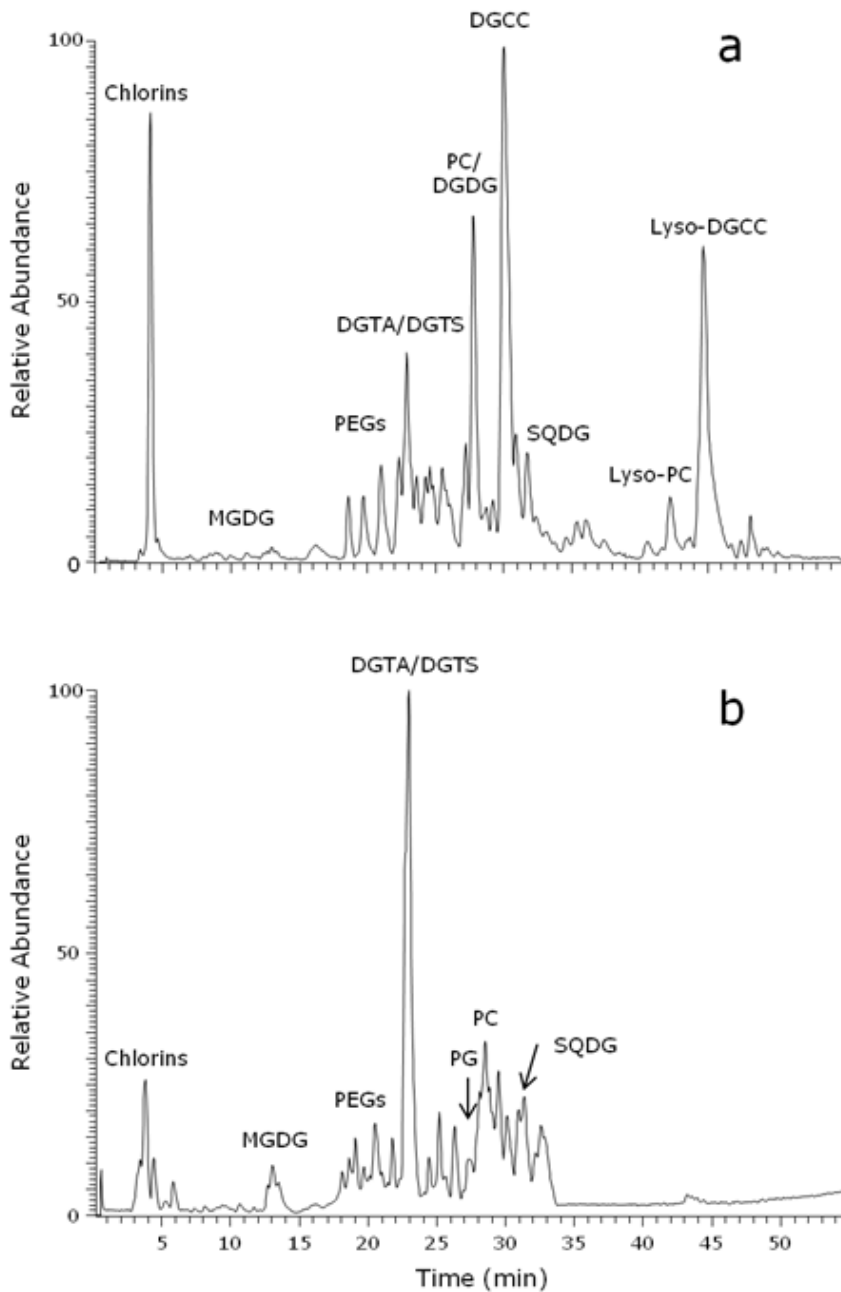


Figure 4.3 | Partial base peak chromatogram (Gaussian smoothed) of the HPLC/ESI-MS analysis of IPLs in the particulate matter sampled at (a) Lake MacBride, Iowa and (b) Lake Thirty, Minnesota. For structures and acronyms of IPLs see **Fig. 4.1**. ES = ethoxylated surfactants.

IPLs. To assess the presence of archaeal IPLs we, therefore, performed a more sensitive assay using HPLC/MS² following *Pitcher et al.* (2011b), where IPLs with a crenarchaeol core lipid (**Fig. 4.1**) are targeted. In most lakes we could not detect crenarchaeol IPLs, i.e., those analyzed by our SRM method. Only in a few lakes from Iowa weak signals of the hexose, dihexose, and hexose, phosphohexose crenarchaeol (**Fig. 4.1**) could be detected. We, therefore, used an alternative method, i.e., isolation of an IPL fraction using column chromatography and subsequent hydrolysis yielding the core GDGT lipids (*Pitcher et al.*, 2009). The IPL-derived crenarchaeol concentrations were higher in Iowa lakes, where concentrations ranged from 0.12 to 1.2 ng L⁻¹, than in Minnesota lakes where they ranged from 16 to 180 pg L⁻¹ (**Table 4.2**).

Table 4.2 | Abundance and distribution of heterocyst glycolipids and IPL-derived crenarchaeol in Iowa and Minnesota lakes.

Lake name	Glycolipids (area L ⁻¹)	I ^a (%)	II (%)	III (%)	IV (%)	V (%)	VI (%)	'Calothrix' ^b (%)	Hg ₂₅	IPL-derived crenarchaeol (pg L ⁻¹)
Iowa Lakes										
Hickory Grove	4.7E+09	1.1	68	8.6	4.3	6.0	19	26	0.02	1220
Coralville Reservoir	2.4E+08	17	56	7.8	14	1.7	6.3	8.0	0.24	1060
Lake MacBride	1.0E+09	3.8	60	8.8	18	1.6	12	14	0.06	220
Meyers Lake	2.1E+11	7.0	49	9.8	3.2	29.3	11	41	0.12	200
Rodgers Park Lake	4.7E+08	5.7	52	8.4	2.7	28.1	11	39	0.10	160
Lower Pine Lake	2.6E+09	1.3	96	8.6	1.3	0.1	0.8	0.9	0.01	1120
Beeds Lake	1.1E+08	23	50	8.5	6.7	6.5	10.7	17	0.31	120
Beaver Lake	5.1E+10	4.6	48	9.5	27	2.2	10.7	13	0.09	300
Three Mile Lake	3.6E+09	5.0	74	9.1	5.0	2.1	12.8	15	0.06	320
Big Creek Lake	3.0E+08	4.8	73	8.5	5.0	2.3	14.6	17	0.06	180
Saylorville Reservoir	9.1E+07	3.6	68	8.5	18	0.7	6.7	7.4	0.05	120
Minnesota Lakes										
Leighton	4.1E+08	14	77	8.4	5.1	0.0	1.9	1.9	0.15	18
Little Splithand	1.3E+10	12	61	8.2	3.5	6.2	16	22	0.17	21
Sand	2.2E+09	10	62	7.7	4.3	5.1	17	22	0.14	21
Beaver Lake	4.2E+08	10	70	6.9	4.1	4.0	11	15	0.12	48
South Sturgeon	3.0E+07	5.7	65	6.1	5.1	4.7	19	23	0.08	16
O'Leary	8.8E+07	9.5	72	6.7	5.1	3.5	8.0	11	0.12	95
Kelly	1.3E+09	17	60	6.9	2.2	7.1	13	20	0.22	39
Horsehead	1.9E+08	8.5	77	6.7	2.1	1.7	10	12	0.10	82
Brush Shanty	4.5E+08	8.0	67	7.4	6.2	5.0	11	16	0.11	26
Little Sand	1.8E+09	10	64	8.2	3.9	6.3	14	20	0.14	45
Hatch	4.3E+08	9.4	61	8.4	2.7	6.4	20	26	0.13	37
Thirty	1.4E+09	9.5	58	7.1	3.9	7.3	20	27	0.14	180

^a Percentage of glycolipid as part of total glycolipids. For structure number see **Fig. 4.1**.

^b Percentage of glycolipids V+VI, potentially derived from *Calothrix* species.

4.4 DISCUSSION

4.4.1 Influence of trophic state on general IPL distributions

Our lake data set comprises eleven lakes from Minnesota which can be characterized as meso- to oligotrophic, based on the relatively low concentrations in TP and chlorophyll *a*, while the eleven lakes from Iowa and one from Minnesota can be characterized as eutrophic to hyper-eutrophic (**Table 4.1**). This difference in trophic state has not led to large differences in IPL head group diversity, i.e., most IPL head groups are found in SPM of both the Iowa as well as Minnesota lakes. A somewhat similar phenomenon has been observed in marine environments; both in coastal seas as well as open ocean sites, or oligotrophic as well as eutrophic oceanic provinces, similar types of IPLs are found (e.g. *Schubotz et al.*, 2009; *van Mooy et al.*, 2006, 2010; *Brandsma et al.*, 2012a). Indeed, the IPL classes found in our lake data set are also found in SPM of marine waters, suggesting there is no particular striking difference in IPL head group diversity between lakes and marine waters, as perhaps could be expected because of the often distinct genetic differences between marine and freshwater phytoplankton. Interestingly, a large part of IPLs detected is dominated by non-phospholipids, i.e., the N-containing betaine lipids (DGTS/DGTA, DGCC), the sulfur-containing SQDGs and MGDG and DGDG. A similar phenomenon has been observed in marine environments (e.g. *Schubotz et al.*, 2009; *van Mooy et al.*, 2006; *van Mooy & Fredericks*, 2010; *Popendorf et al.*, 2011; *Brandsma et al.*, 2012a). Culture studies have suggested that some phospholipids are replaced by non-P containing lipids under P-limiting conditions (e.g. *Minnikin et al.*, 1974; *Benning et al.*, 1995). Phospholipids were generally not dominating, however, irrespective of the P-concentrations or TN:TP ratio, suggesting that nutrients were not substantially affecting the IPL composition. Indeed, *van Mooy & Fredericks* (2010) suggested that this process only occurs at P concentrations below 30 nmol L⁻¹ and concentrations in the here studied lakes are higher (**Table 4.1**).

One pronounced difference between the IPL composition in Iowa lakes versus Minnesota lakes is the relatively higher abundance of lyso-IPLs, in particular lyso-PC and lyso-DGCC (**Fig. 4.1**), in Iowa lakes (**Fig. 4.1**). This does not seem an artifact of our sample work-up or storage conditions as SPM from both Iowa and Minnesota lakes were treated identically. Lyso-lipids are intermediates in the metabolism and turnover of intact polar lipids, but lyso-(phospho)lipids also function as secondary messenger and appear to influence lipid-protein interactions in the lipid membrane (*Meijer & Munnik*, 2003 and references therein; *Ishii et al.*, 2004 and references therein; *Fuller & Rand*, 2001). Recently, lyso-lipids were shown to stimulate channels that protect bacterial cells from osmotic pressure (*Nomura et al.*, 2012). A relatively higher abundance of lyso-lipids might therefore be an environmental adaptation to pH or ionic strength of the lake waters. Although the lyso-lipids were mostly observed in Iowa lakes and the pH of these lakes is generally higher than the pH of the Minnesota lakes, a clear relation was not observed within the

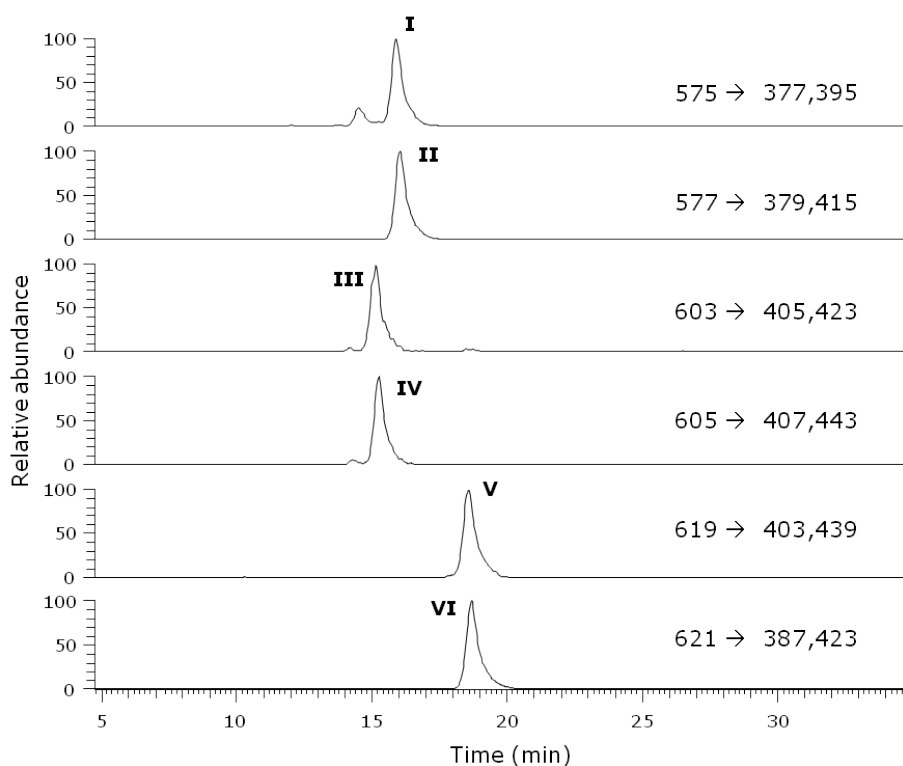


Figure 4.4 | Partial base peak chromatogram (Gaussian smoothed) of the HPLC/ESI-MS² analysis of heterocyst glycolipids in the particulate matter sampled at Hickory Grove Lake, Iowa. Roman numerals refer to structures in Fig. 4.1.

set of Iowa lakes. However, ion concentrations are generally higher in Iowa lakes than in Minnesota lakes, due to a combination of geological and anthropogenic factors (Jones & Bachman, 1978; Gorham *et al.*, 1983). Therefore, the reason for the high relative abundance of lyso-lipids in the Iowa lake IPLs may be the high ion concentrations.

There are a large variety of sources for each of the different IPL classes. For example, SQDGs are found in thylakoid membranes of phototrophic organisms (e.g. Frenzén, 2004). PEs are generally found in bacteria, while PCs are mostly found in eukaryotes (e.g. Sohlenkamp *et al.*, 2003 and references cited therein). Betaine lipids such as DGTA/DGTS and DGCC are found in a variety of eukaryotes and bacteria (e.g. Dembitsky, 1996). No specific IPL class could be detected which could be unambiguously related to specific groups of microbes, however, i.e., at the genera/family level. Thus, it seems, as with marine environments (Brandsma *et al.*, 2012a, 2012b), that general IPL screening does not reveal substantial details on the

Table 4.3 | Pearson Product Moment correlations between environmental parameters and IPL abundances. Correlations in *italic* have P-values <0.05, those in **bold** have P-values <0.01.

Parameter	Glycolipid abundance	Calothrix (%)	IPL-derived crenarchaeol	Hg ₂₆
Temperature	<i>0.488</i>	0.186	0.404	-0.113
pH	<i>0.498</i>	0.113	0.281	-0.190
Alkalinity	-0.013	-0.089	0.399	0.091
DOC	-0.081	0.247	<i>-0.476</i>	0.031
DIC	-0.063	-0.147	0.370	0.109
POC	0.888	0.248	0.288	-0.190
Chlorophyll <i>a</i>	0.882	0.247	0.245	-0.155
Total N	-0.033	0.012	0.459	0.154
Total P	0.598	-0.034	0.547	-0.058
N:P	-0.176	0.152	-0.049	0.175

microbial composition of lake environments. Therefore, it is recommended to perform more targeted screening of IPLs known to be derived from specific microbes as done here for glycolipids from heterocystous cyanobacterial and crenarchaeol IPLs derived from Thaumarchaeota.

4.4.2 Influence of N and P on heterocyst glycolipid distribution and abundance

Heterocyst glycolipids are unique tracers for heterocystous cyanobacteria and are only found when these cyanobacteria form heterocyst cells and perform N₂ fixation (Walsby, 1985; Murry & Wolk, 1989; Bauersachs *et al.*, 2009b). Thus, the presence of glycolipids unambiguously indicate the presence of N₂-fixing heterocystous cyanobacteria. Many studies have been performed examining the controlling factors on the distribution of cyanobacteria in lakes and a frequently cited hypothesis is that they particularly dominate at low N:P ratio's due to their ability of N₂ fixation (Schindler, 1977; Smith, 1983). Other studies have shown, however, that this hypothesis cannot fully explain their occurrence and that this is correlated to other factors such as total nutrient concentrations, CO₂ concentrations, light, temperature, and stratification conditions (Downing *et al.*, 2001; Wagner & Adrian, 2009). Furthermore, these studies rarely considered whether the cyanobacteria were actually performing N₂-fixation or were mainly using available nutrients (Ferber *et al.*, 2004).

The fact that we find heterocyst glycolipids in all lakes strongly suggests that cyanobacterial N₂-fixation is ongoing in both oligotrophic as well as eutrophic lakes. To investigate the factors controlling their abundance, we compared the abundance of total glycolipids with environmental parameters, in particular TN, TP and N:P as they are thought to substantially affect the abundance of cyanobacteria (Table 4.3; Fig. 4.4). We did not find a correlation with N:P (Fig. 4.4a;

Table 4.3). A significant relation is found with total P, and especially chlorophyll *a* concentrations and POC (**Table 4.3**) where higher abundance of glycolipids is correlated with higher POC and chlorophyll *a* concentrations (**Fig 4.4b**). *Ferber et al.* (2004) also noted a correlation of heterocyst cell concentrations with chlorophyll *a* concentrations for a hypertrophic lake. Possibly, an increased activity of heterocystous cyanobacteria is needed to supply bioavailable nitrogen for sustaining the higher primary productivity in, e.g. the Iowa lakes. We should, however, note that most environmental parameters in our lake data set are also significantly correlated which each other (data not shown) making it difficult to constrain the relation of individual environmental parameters with glycolipid abundance.

There are also some strong differences in the distribution of glycolipids. One likely cause is that different glycolipids occur in different genera, i.e., glycolipids I-IV occur in genera of the family Nostocaceae, while glycolipids V-VI occur in *Calothrix* species of the family Rivulariaceae (*Bauersachs et al.*, 2009b). Surveys of Iowa lakes using microscopy have shown that the major species of cyanobacteria in Iowa lakes are composed of *Microcystis* and *Oscillatoria* (<http://limnology.ecob.iastate.edu>), both non-heterocystous cyanobacteria. The most frequently encountered heterocystous cyanobacteria are *Anabaena* and *Aphanizomenon*, both belonging to the family Nostocaceae and known producers of glycolipids I-IV (*Bauersachs et al.*, 2009b). However, *Calothrix* species have rarely been reported in Iowa lakes, although we did not analyse the cyanobacterial species composition of the lake at the time of sampling. Thus, it might be possible that heterocystous cyanobacterial species other than *Calothrix* were the source for glycolipids V-VI. Nevertheless, if we assume that glycolipids V-VI are derived from species other than those belonging to the family Nostocaceae, then their relative abundance among N_2 -fixing heterocystous cyanobacteria varies between 1 and 40%, assuming that the glycolipid abundance reflects the abundance of heterocystous cyanobacterial biomass (**Table 4.2**). The varying contributions of these glycolipids did not correlate with any of the measured environmental parameters (**Table 4.3**). *Bauersachs et al.* (2009b) found a correlation between incubation temperature and the distribution of glycolipids I and II in cultivated heterocystous cyanobacteria and quantified this in the so-called HG_{26} index:

$$HG_{26} = (\text{glycolipid I}) / (\text{glycolipid I} + \text{glycolipid II}) \quad (\text{Eq. 4.1})$$

Indeed, *Wormer et al.* (2012) found a strong sigmoidal relation of the HG_{26} with lake water temperature in their Spanish lakes. However, no significant correlation of the HG_{26} with temperature, as well as other parameters, was observed in our data set (**Table 4.3**). Thus it is uncertain what the mechanism is behind the diversity changes in the glycolipid distributions of the heterocystous cyanobacteria.

4.4.3 Influence of trophic state on Thaumarchaeota abundance

Thaumarchaeota have been relatively well studied in the marine environment but to a lesser extent in freshwater environments, with most studies focused on one or a few lakes (e.g. *Auguet et al.*, 2008, 2011; *Woltering et al.*, 2012). These studies generally found that the abundance of Thaumarchaeota, or the *amoA* functional gene involved in ammonia oxidation, correlated with ammonia or nitrite concentration, suggesting an important role for these microbes in the nitrogen cycling in lakes. Only a few studies have focused on the impact of other environmental parameters on the abundance of Thaumarchaeota in oligotrophic *versus* eutrophic lakes. *Wu et al.* (2010) examined ammonia-oxidizing Thaumarchaeota in sediments from the eutrophic lake Taihu (China) and found a negative relation between Thaumarchaeota abundance and TOC, TN, and chlorophyll *a* concentration which was explained by a physiological inhibition by organic compounds and high ammonia levels (*Könneke et al.*, 2005). *Hermann et al.* (2009) examined ammonia-oxidizing Thaumarchaeota in sediments of oligotrophic to mesotrophic lakes and found that their abundance was negatively correlated with ammonia levels but also with pH. They explained this by the higher affinity of Thaumarchaeota for low levels of ammonia compared to ammonia-oxidizing bacteria (*Martens-Habbena et al.*, 2009) and the observation that ammonia-oxidizing Thaumarchaeota are more abundant and active at lower pH in soils (*Nicol et al.*, 2008).

Before discussing our results, an important methodological issue with the crenarchaeol IPL results has to be considered, i.e., filtration efficiency. Thaumarchaeota generally have small cell sizes ($<1\ \mu\text{m}$; *Könneke et al.*, 2005) and it has been reported that a large part of the active cells pass through $0.7\ \mu\text{m}$ filters as used here (*Pitcher et al.*, 2011a; *Ingalls et al.*, 2012). Thus, we may have missed a large portion of the Thaumarchaeotal population. *Herfort et al.* (2006) recovered 95% of GDGT concentrations in the North Sea with filters of $0.7\ \mu\text{m}$ pore size, however, likely due to the higher turbidity in this coastal sea, where particulate matter can rapidly clog filters, effectively reducing the nominal pore size. Furthermore, *Ingalls et al.* (2012) still recovered 20-70% of intact polar GDGTs from Puget Sound on $0.7\ \mu\text{m}$ pore size filters. The lakes investigated are likely more comparable to these coastal systems than to the deep water column of the Arabian Sea and thus the effective filtration efficiency, and thus recovery of the Thaumarchaeotal population, may be still have been relatively high. However, there is a weak correlation ($r=0.50$, $p=0.016$) between the concentration of IPL-derived crenarchaeol and the amount of SPM collected with each filter, suggesting that filtration efficiency might be of importance.

We examined the potential controlling factors on Thaumarchaeotal abundance suggested previously for lakes, in particular nitrogen levels and pH, by correlating them with the abundance of IPL-derived crenarchaeol (**Fig. 4.6; Table 4.3**). Remarkably, we find significant positive relations between IPL-derived crenarchaeol and total N and total P, and a negative relation with DOC (**Table 4.3**;

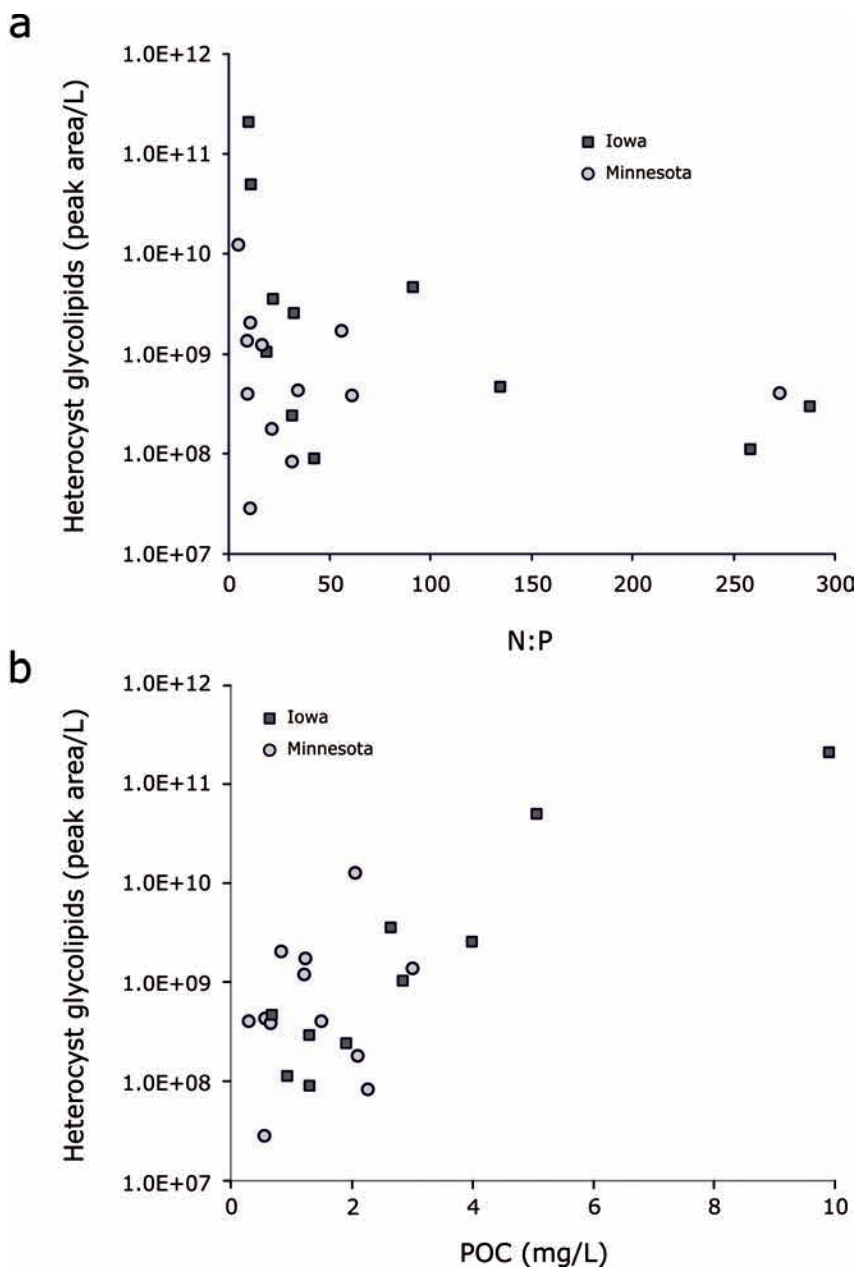


Figure 4.5 | Correlation of heterocyst glycolipid abundance with (a) N:P ratio and (b) particulate organic carbon (POC) concentrations. Note the log-scale for the glycolipid abundance.

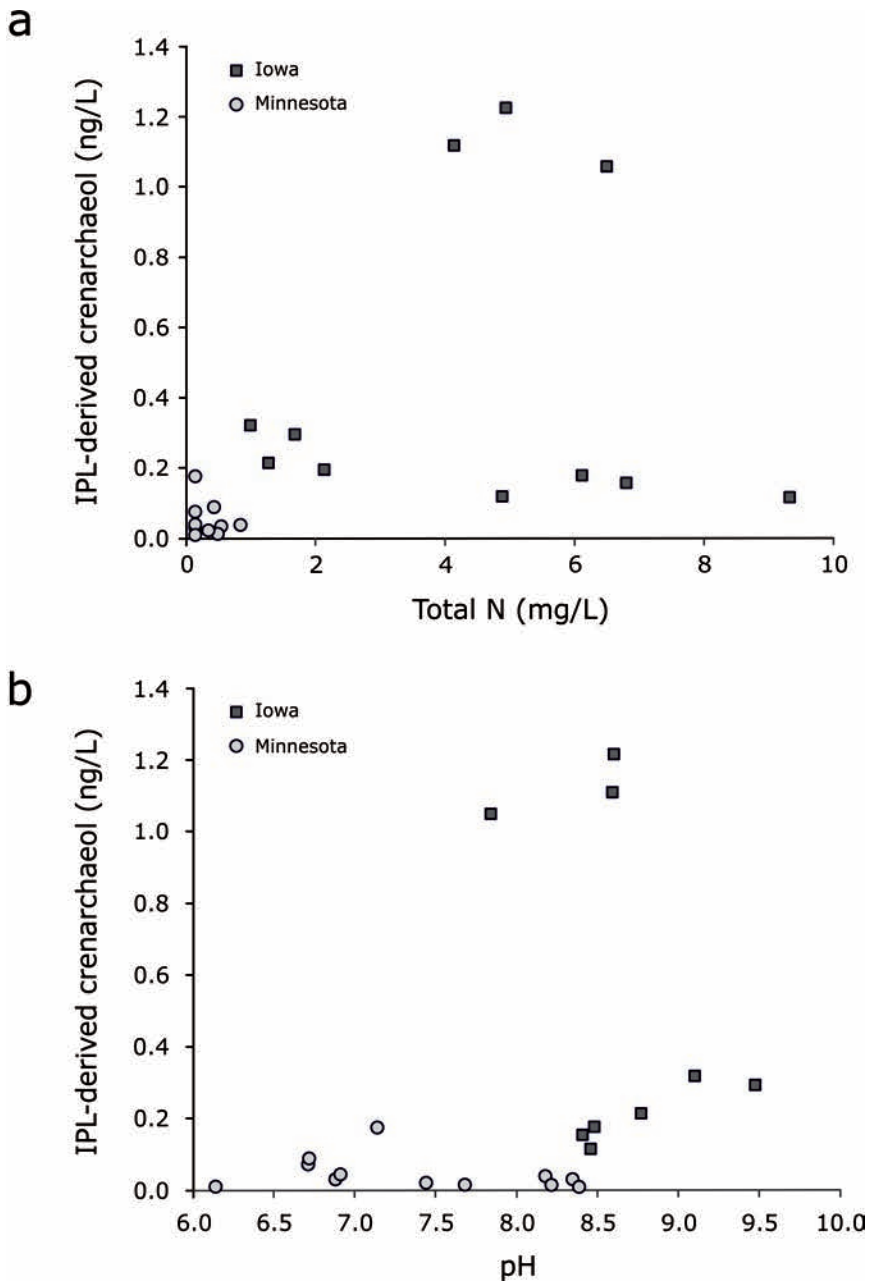


Figure 4.6 | Correlation of IPL-derived crenarchaeol concentrations with (a) Total Nitrogen (TN) and (b) pH.

e.g. **Fig. 4.5a**). This contrasts the idea that Thaumarchaeota are more competitive at low levels of ammonia (*Martins Habbena et al.*, 2009) but supports the idea that they can be inhibited by high organic compound concentrations as suggested for other lakes (*Herrmann et al.*, 2009; *Wu et al.*, 2010). Interestingly, there is no significant correlation with pH (**Table 4.3**), but plotting IPL-derived crenarchaeol against pH shows that it is generally more abundant at pH >8.5 (**Fig. 4.6b**), which disagrees with the observation that ammonia-oxidizing Thaumarchaeota are decreasing in abundance and activity with increasing pH in soil (*Nicol et al.*, 2008) and in lakes (*Herrmann et al.*, 2009). It is in agreement with the observation of *Wu et al.* (2010) for the eutrophic lake Taihu, however, who found a positive correlation of Thaumarchaeota abundance with pH. Furthermore, *Beman et al.* (2010) found that marine nitrification rates substantially decrease when pH is lower while *Rudd et al.* (1988) observed substantially lower nitrification rates in acidified lakes. *Beman et al.* (2010) attributed this to the shifting equilibrium from NH_3 , the substrate for nitrifiers, to NH_4^+ . Possibly, this could partly explain the lower abundance of ammonia-oxidizing Thaumarchaeota in lakes with pH <8.5, i.e. the lower availability of NH_3 .

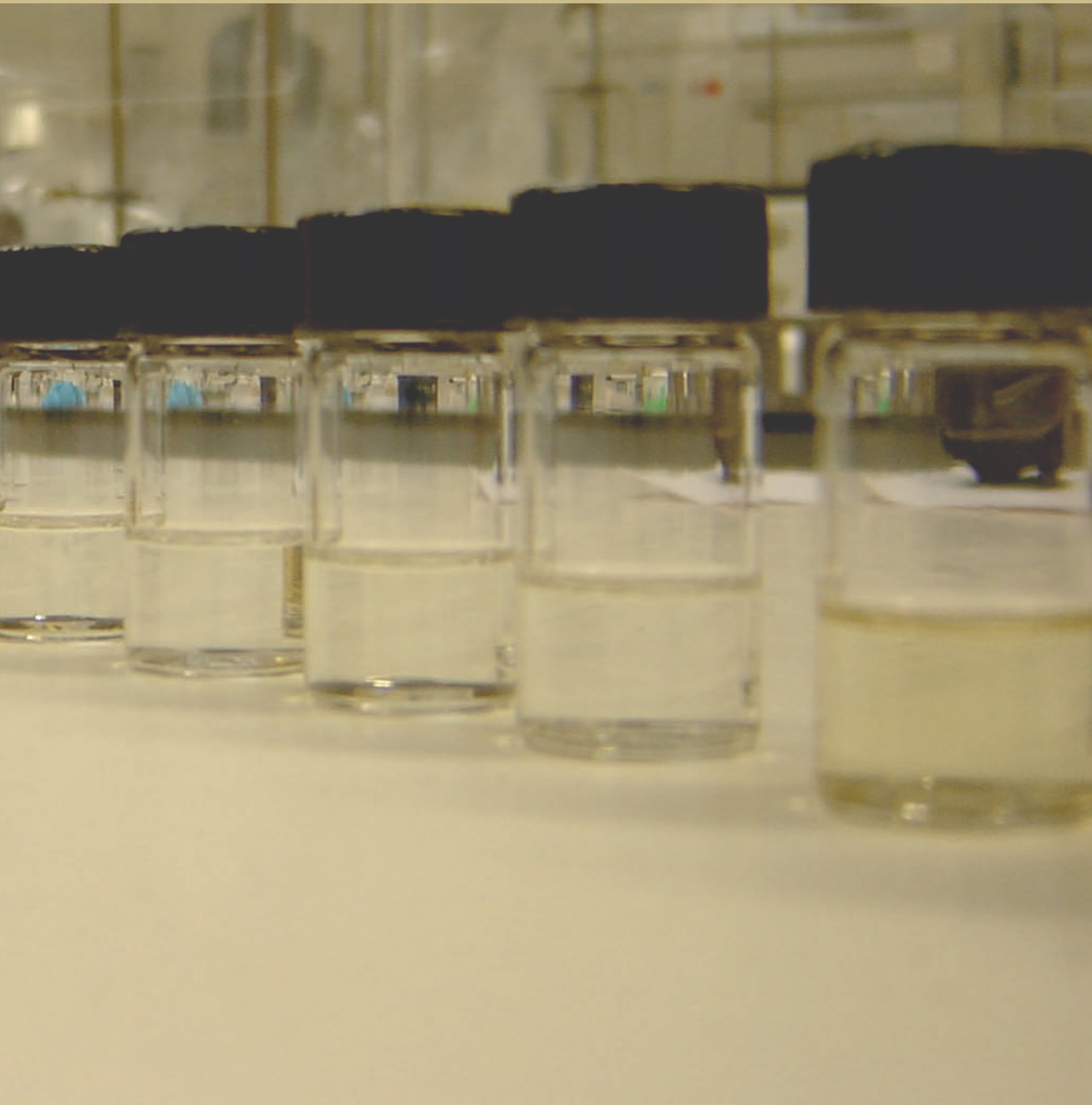
ACKNOWLEDGMENTS

We thank Kelly Poole, Amber Erickson, Dan Kendall, and Jingyang Li, from the ISU Limnology Laboratory, and Joshua McGinnis from the Water Quality Lab of Itasca Community College, Grand Rapids, MN, for technical support. Financial support for this study was obtained from the Darwin Center for Biogeosciences with financial aid from the NIOZ, the Iowa Department of Natural Resources, the Itasca Water Legacy Partnership, and the Minnesota Pollution Control Agency.

Part II



*High CO₂/low pH worlds:
Eocene Hyperthermals*



CHAPTER 5

**Extreme warming and environmental change of the North Sea
Basin across the Palaeocene-Eocene boundary**

Petra L. Schoon, Claus Heilmann-Clausen, Bo Pagh Schultz, Jaap S.
Sinninghe Damsté, and Stefan Schouten

Submitted to Organic Geochemistry

ABSTRACT

The profound warming and associated environmental changes during the Palaeocene-Eocene Thermal Maximum (PETM; ~56 Ma) have been documented at several sites from different latitudes around the world. However, climate records from Northern Europe are still lacking. In this study we analyzed the distribution patterns and stable carbon isotopes of marine and terrestrial biomarker lipids in two PETM sections in Denmark situated within the epicontinental North Sea Basin. The negative carbon isotope excursion (CIE) of 4-7 ‰ recorded in land plant-derived *n*-alkanes is similar to what has been observed at other locations, although variations between these two proximal sites suggests that local factors, such as regional vegetation patterns and sources of *n*-alkanes, also influenced the CIE. Sulfur-bound isorenieratane, a biomarker for green sulfur bacteria indicating photic zone euxinia, was only detected in sediments from the PETM interval with an elevated organic carbon content. This reflects a distinct shift in depositional environment at the onset of the PETM from well-oxygenated to anoxic and sulfidic. These euxinic conditions are comparable with those during the PETM in the Arctic Ocean, which suggests that restricted water column ventilation and enhanced carbon burial occurs on a wide scale. Sea surface and continental air temperatures, based on the TEX₈₆ and CBT/MBT proxies, rise simultaneously towards peak temperatures of 31 °C and 29 °C, respectively. Although TEX₈₆ temperatures are potentially biased by soil organic matter input, the similarity between these two independent proxy records, suggests a warming of 8-10 °C, much larger than recorded elsewhere. This may be due to regional conditions amplifying the warming at this mid-latitude site.

5.1 INTRODUCTION

The Palaeocene-Eocene Thermal Maximum (PETM, ~56 Ma) has been documented in sediments all over the world, recording extreme warming and environmental changes, and is associated with a massive release of ^{13}C -depleted carbon to the oceans and atmosphere as reflected by a negative carbon isotope excursion (CIE) of $>2.5\text{‰}$ (Kennett & Stott, 1991; Schouten *et al.*, 2007b; Sluijs *et al.*, 2007a). Deep sea sediments have recorded a surface ocean warming of 4 to 8 °C (Fig. 5.1), based on the Mg/Ca ratio and $\delta^{18}\text{O}$ composition of planktonic foraminifera (Kennett and Stott, 1991; Schouten *et al.*, 2007b; Thomas *et al.*, 2002; Tripathi & Elderfield, 2005; Zachos *et al.*, 2003). Unfortunately, these records are often affected by redeposition of secondary calcite during early diagenesis (Pearson *et al.*, 2001b; Schrag, 1999) and carbonate dissolution due to the vertical progradation of the lysocline (Stap *et al.*, 2009; Zachos *et al.*, 2005; Zeebe & Zachos, 2007). Furthermore, the decrease in seawater pH may have increased $\delta^{18}\text{O}$ values causing a potential underestimation of PETM warming (Uchikawa & Zeebe, 2010).

The distribution of archaeal and bacterial glycerol dialkyl glycerol tetraethers (GDGTs) can also be used to infer sea surface temperature (SST), using the TEX_{86} proxy (Schouten *et al.*, 2002), and mean annual air temperature (MAT), using the MBT/CBT proxy (Weijers *et al.*, 2007b). So far, TEX_{86} palaeothermometry has been applied to four PETM sections (Sluijs *et al.*, 2006, 2007, 2011; Zachos *et al.*, 2006), whereas a PETM MAT record based on the MBT/CBT proxy is only available for the Arctic region (Weijers *et al.*, 2007a). The temperature records based on TEX_{86} show similar warming as those recorded by Mg/Ca and $\delta^{18}\text{O}$ of foraminifera, i.e. 5-8 °C (Fig. 5.1). Arctic continental air temperatures inferred from MBT/CBT values increased by about 8 °C (Weijers *et al.*, 2007a), which is somewhat larger than recorded for high latitude sea surface waters but similar to mid-latitude sites (Fig. 5.1). The temperature records generated up to now thus show that the warming during the PETM is fairly uniform (i.e. 4-6 °C), but that the warming of the New Jersey continental margin, as well as of southern high latitudes, is slightly larger (Fig. 5.1). However, global coverage of the existing PETM temperature records is still relatively poor, limiting the understanding of the underlying mechanisms of heat transport that drive greenhouse climates, such as during the PETM (cf. Huber and Caballero, 2011). Also, most records are based on a single location which prohibits an assessment of local variability compared to imposed global changes.

Previously, the PETM has been identified in two sections in Denmark, situated in the eastern part of the North Sea Basin (Fig. 5.1), and is based on dinoflagellate stratigraphy and a 6-8 ‰ CIE in organic carbon (Heilmann-Clausen & Schmitz, 2000; Schmitz *et al.*, 2004). Due to the close proximity to coastal areas it is likely that the sedimentary organic carbon contains large amounts of terrestrial organic matter, which may have a different stable carbon isotopic composition than marine organic matter (Bowen *et al.*, 2004; Schouten *et al.*, 2007b; Smith *et al.*, 2007). The rela-

tively large CIE in organic carbon may therefore be attributed to variations in the ratio of terrestrial to marine organic carbon. On the other hand, such a large CIE is also observed in land plant-derived *n*-alkanes at different PETM sites around the world (e.g. *Handley et al.*, 2008; *Pagani et al.*, 2006b; *Schouten et al.*, 2007b), and has led to the suggestion that the atmospheric CIE may have been larger than the generally accepted 2–3 ‰ recorded by marine calcite (*Handley et al.*, 2008, 2011; *Pagani et al.*, 2006b). To gain insight in the regional response of marine and terrestrial carbon reservoirs to the carbon cycle perturbations during the PETM in Northern Europe, we analyzed the distribution and stable carbon isotopic composition of specific marine and terrestrial biomarker lipids from two PETM sites in Denmark. In addition, we analyzed the distribution of GDGTs to determine TEX₈₆-derived sea water and MBT/CBT-derived continental air temperatures. Our results provide insights into the regional magnitude of the CIE, warming and environmental changes in Northern Europe during the PETM.

5.2 SITE DESCRIPTION AND DEPOSITIONAL SETTING

In this study, we used sediments from two sections in Denmark covering the Palaeocene-Eocene transition (**Fig. 5.1**). The study area is situated in the Norwegian-Danish Basin, a sub-basin of the larger, almost land-locked, epicontinental North Sea Basin. Water depths at the study sites during the late Palaeocene-early Eocene probably varied between upper bathyal and outer neritic (*Heilmann-Clausen*, 2006; *Knox et al.*, 2010). Nearest coastlines were situated in southern Norway, northern Germany and in Sweden (*Knox et al.*, 2010). Sea level changes in the basin were probably caused mainly by phases of thermal subsidence and uplift due to varying activity of the Iceland mantle plume, and the onset of sea-floor spreading between Greenland and the British Isles-Norway (*Knox*, 1996a; *Knox et al.*, 2010). The sedimentary succession of the late Palaeocene-early Eocene in Denmark consists of mainly hemipelagic mudstones and a local diatomite. A lithostratigraphic subdivision and mapping is given by *Heilmann-Clausen et al.* (1985). A prominent series of volcanic ash layers is present in the earliest Eocene sediments. The ashes are subdivided into a lower series given negative numbers, and an upper positive series (*Bøggild*, 1918).

One of the sampled Palaeocene-Eocene sections was recovered in a core obtained from a borehole (D.G.I. 83101) drilled in 1983 in Store Bælt, the strait between the Danish islands Sjælland and Fyn. The position of the borehole is 55°N 21°N – 11° 05'E (**Fig. 5.2**). The section is one of the most continuous Palaeocene-Eocene records in Denmark (*Nielsen et al.*, 1986). In this study, we analysed sediments of this core from 142.57 to 123.60 mbsf (meters below sea floor) covering 5 different lithological units. The late Palaeocene succession includes, in ascending order, the Holmehus Formation, the informal Østerrende Clay and the informal Glauconitic Silt unit (*Nielsen et al.*, 1986). Above the latter unit follows the Ølst

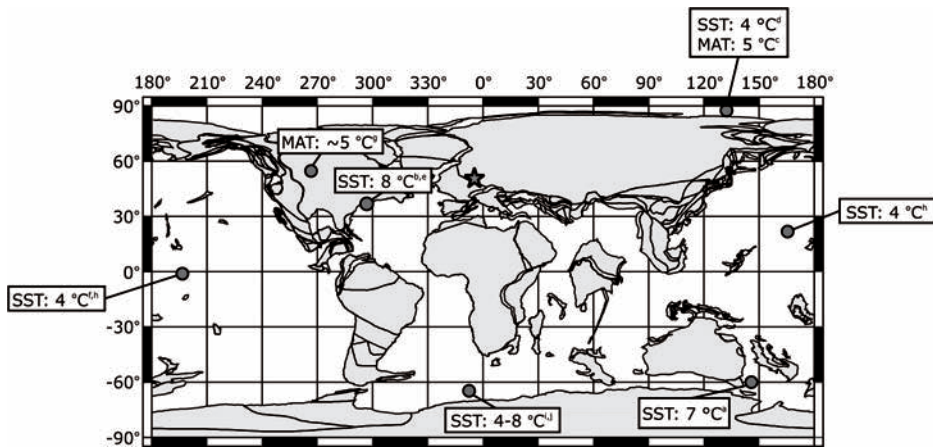


Figure 5.1 | Plate tectonic reconstruction of 55 Ma (www.ods.de/ods) and reconstructed warming during the PETM. The dots show locations where PETM SST and MAT warming have been reconstructed: ^aSluijs *et al.*, 2011 (TEX₈₆), ^bSluijs *et al.*, 2007 (TEX₈₆), ^cWeijers *et al.*, 2007 (CBT/MBT), ^dSluijs *et al.*, 2006 (TEX₈₆), ^eZachos *et al.*, 2006 (TEX₈₆), ^fTripati & Elderfield, 2005 (Mg/Ca and $\delta^{18}\text{O}$ of planktonic foraminifera), ^gWing *et al.*, 2005 (leaf margin analysis), ^hZachos *et al.*, 2003 (Mg/Ca and $\delta^{18}\text{O}$ of planktonic foraminifera), ⁱThomas *et al.*, 2002 ($\delta^{18}\text{O}$ of planktonic foraminifera), ^jKennett & Stott, 1991 ($\delta^{18}\text{O}$ of planktonic foraminifera). The star indicates the location of this study.

Formation, which belongs to the early Eocene (Heilmann-Clausen & Schmitz, 2000), and of which we only studied the lower part, i.e. the Haslund Member which corresponds to the negative numbered ash series of Bøggild (1918). The basal part of this member is referred to the informal Stolleklint Clay (Heilmann-Clausen, 1995). Our uppermost sample is from a level above the Stolleklint Clay (Fig. 5.3A). The Holmehus Formation consists of hemipelagic non-calcareous mudstones, with an overall high degree of bioturbation (Nielsen *et al.*, 1996). The common *Zoophycos* burrows suggest an upper bathyal depositional environment (Bottjer & Droser, 1992). The Holmehus Formation is gradually overlain by the informal Østerrende Clay, which was deposited in a more proximal setting, probably in somewhat shallower waters (Heilmann-Clausen, 1995, 2006). The Østerrende Clay is sharply overlain by the Glauconitic Silt of latest Palaeocene age. This unit is characterized as a clayey, sandy silt; the silt and sand mainly consist of biogenic and authigenic grains (Nielsen *et al.*, 1986). The Glauconitic Silt includes a fauna with primitive forms of agglutinated foraminifers (Laurson & King, 1999) and is most likely deposited under low sedimentation rates in an upper bathyal or outer neritic environment. There is a distinct transition between the Glauconitic Silt and the lowermost Eocene Stolleklint Clay which consists of finely laminated, non-calcareous clay. The lower boundary of the Stolleklint Clay is marked by a sharp negative isotope shift in total organic carbon (TOC) of ~6 ‰ at the base of the Stolleklint Clay between 133.24

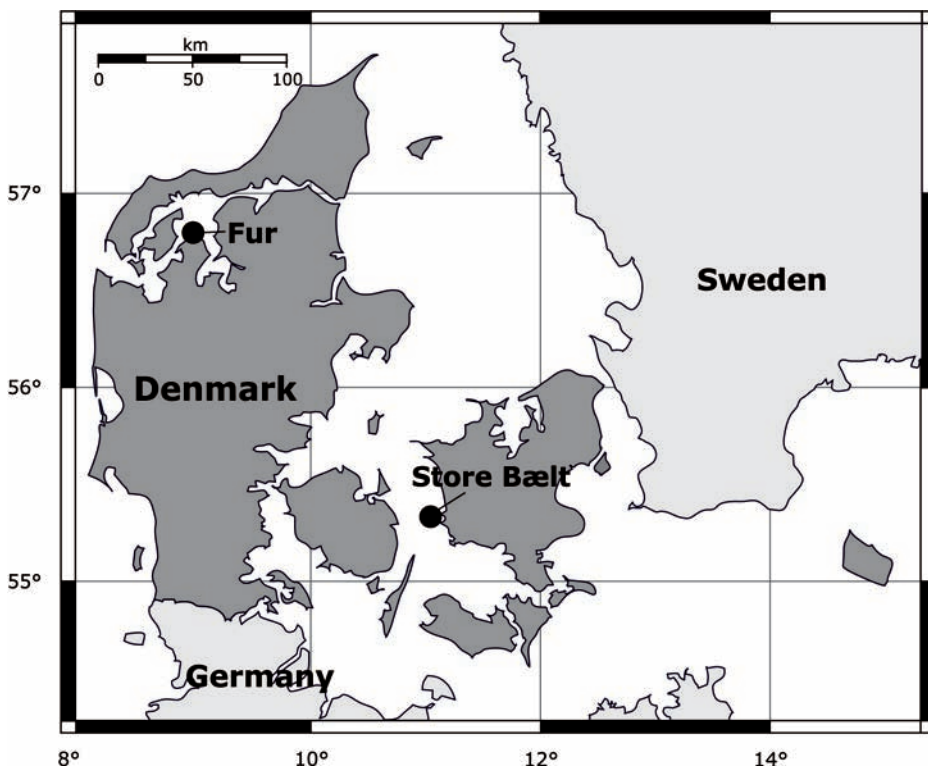


Figure 5.2 | Map of Denmark showing the location of the two study sites at Fur Island and Store Bælt.

and 132.53 mbsf (Heilmann-Clausen & Schmitz, 2000; Schmitz *et al.*, 2004), concomitant with a sudden dominance of the dinocyst genus *Apectodinium* (Nielsen *et al.*, 1986) marking the onset PETM.

The other studied section is a beach and cliff section at Stolleklint on the island Fur located in western Limfjorden, NW Denmark (**Fig. 5.2**; 56° 50' 28"N – 8° 59' 29"E). The lower part of this PETM section became exposed after a storm in 2005 and gave an opportunity for sampling across the Palaeocene/Eocene transition, which is placed at the base of the Stolleklint Clay. The Stolleklint Clay overlies a succession which can be correlated with the Østerrende Clay-Glauconitic Silt found in Store Bælt (**Fig. 5.3b**). Like in Store Bælt, a sudden dominance of the dinocyst *Apectodinium* begins at the base of the Stolleklint Clay. Unfortunately, from ~2.5 m above the base of the Stolleklint Clay an interval with an estimated thickness of 10-20 meters is partly unexposed and has been disturbed by the last glaciation. Above this interval follow undisturbed sediments representing the top-most ~3 m of the Stolleklint Clay, which are again overlain by the Fur Formation

(Fig. 5.3b). The latter is a clayey diatomite intercalated with volcanic ash layers (Pedersen, 1981; Pedersen & Surlyk, 1983; Pedersen *et al.*, 2004). The boundary between the Stolleklint Clay and the Fur Formation is placed at the thick white ash layer -33 (Heilmann-Clausen *et al.*, 1985). The dominance of *Apectodinium* spp. continues a short distance above ash -33, i.e., into the basal few meters of the Fur Formation (Heilmann-Clausen, 1994). Previous results from two other sections in Denmark (Heilmann-Clausen & Schmitz, 2000; Schmitz *et al.*, 2004) show that the dominance of *Apectodinium* closely corresponds to the CIE. The maximum of the CIE is therefore expected to be present in the glacially-disturbed interval. The top of the section here studied is at ash layer -17 in the lower part of the Fur Formation. Ash -17 is well above the zone with abundant *Apectodinium* (Heilmann-Clausen, 1994). Ash layer -17 is radiometrically dated at 55.12 ± 0.12 Ma (Storey *et al.*, 2007). Dating the onset of the PETM is based on the extrapolation of the absolute age of this particular ash layer (Hilgen *et al.*, 2010; Westerhold *et al.*, 2009).

5.3 METHODS

5.3.1 Bulk preparation

Prior to analysis, sediment samples from Store Bælt and Fur were freeze-dried and grounded to a fine powder, partially using pestle and mortar and partially by means of a bowl mill. For the analyses of the TOC content and stable carbon isotopes of TOC ($\delta^{13}\text{C}_{\text{TOC}}$), powdered sediment samples were acidified with 1M HCl for the removal of all carbonates from the sediment matrix. Ca. 1.0 mg of decalcified sediment was weighed into a tinfoil cup and subsequently analyzed on a Flash elemental analyzer coupled to a ThermoFisher Delta^{plus} mass spectrometer. The instruments were calibrated against in-house standards and are the means of duplicate runs with a reproducibility of 0.1 % for TOC content and 0.1 ‰ for $\delta^{13}\text{C}_{\text{TOC}}$.

5.3.2 Extraction and fractionation

Total lipid extracts were obtained by extracting each sample with a Dionex Accelerated Solvent Extractor (ASE) using a 9:1 (v:v) mixture of dichloromethane (DCM) and methanol (MeOH), at high temperature (100 °C) and pressure (7.6×10^6 Pa). The extracts were then separated into an apolar and a polar fraction by means of column chromatography using an Al_2O_3 column and solvent mixtures of 9:1 (v:v) hexane:DCM, and 1:1 (v:v) DCM:MeOH, respectively. The apolar fractions were analyzed for the distribution and stable carbon isotopic composition of land plant-derived *n*-alkanes. Prior to compound specific isotope analysis of the *n*-alkanes, the unsaturated hydrocarbons were removed from the apolar fraction using a small column filled with Ag^+ -impregnated silica and hexane as eluent. The polar fractions were analyzed for GDGTs. Finally, sulfur-bound isorenieratane was analyzed by desulfurization of an aliquot of the total extract using Raney Nickel as described previously by Schoon *et al.* (2011). The desulfurized extract was sepa-

rated into an apolar and polar fraction as described above. The apolar fraction was analyzed for the concentration and stable carbon isotopic composition of S-bound isorenieratane.

5.3.3 GC, GC-MS and GC-irmMS analysis

Apolar fractions were analyzed on a HP 6890 gas chromatograph (GC) and on a Thermofinnigan TRACE GC coupled to a Thermofinnigan DSQ quadrupole mass spectrometer (GC/MS) for biomarker lipid identification. Compound specific carbon isotope analysis was done on a Finnigan Delta V isotope ratio mass spectrometer (IRMS) coupled to an Agilent 6890 GC. All GC, GC-MS, and GC-IRMS conditions are the same as described in *Schoon et al.* (2011). All stable carbon isotope values are reported in the $\delta^{13}\text{C}$ notation relative to the VPDB ^{13}C standard.

5.3.4 GDGT analysis

Polar fractions were dissolved in a hexane:propanol (99:1, v:v) solution and filtered over a 0.45 μm PTFE filter prior to analysis. Samples were analyzed using high performance liquid chromatography/atmospheric pressure chemical ionization- mass spectrometry (HPLC/APCI-MS) according to *Schouten et al.* (2007a). To assess SST and MAT, we calculated the TEX_{86} (*Schouten et al.*, 2002) and the MBT/CBT indices (*Weijers et al.*, 2007b), respectively. To convert TEX_{86} values into SSTs we used the recently redefined calibration of *Kim et al.* (2010) ($\text{TEX}_{86}^{\text{H}}$), which is recommended for palaeothermometry of greenhouse worlds with SST $>15^\circ\text{C}$. The MBT/CBT index is based on the relative distribution of soil-derived branched GDGTs (*Weijers et al.*, 2007b). MAT estimates were calculated using the global soil calibration of *Weijers et al.* (2007b), based on a dataset of 134 soils. Additionally, we calculated the BIT index (*Hopmans et al.*, 2004), which is the ratio between soil derived branched GDGTs and aquatic crenarchaeol, and is a measure for the relative input of soil organic matter.

5.4 RESULTS AND DISCUSSION

5.4.1 Magnitude of CIE during the PETM

At the Store Bælt borehole we recorded a prominent decrease of $\sim 6\text{‰}$ in $\delta^{13}\text{C}_{\text{TOC}}$ between 132.53 and 133.24 mbsf (**Fig. 5.3a**), whereas the $\delta^{13}\text{C}_{\text{TOC}}$ record at Fur Island shows an abrupt decrease of $\sim 5\text{‰}$ (**Fig. 5.3b**). The $\delta^{13}\text{C}$ profile of TOC at Store Bælt clearly mimics the general shape that is often found in many marine and continental PETM sections (*Sluijs et al.*, 2007a and references cited therein), i.e. a rapid onset followed by a plateau and a gradual decrease, although the glacially disturbed interval in the PETM section at Fur (**Fig. 5.3b**) probably masks the maximum of the CIE.

The distribution and stable carbon isotope values of long chain *n*-alkanes

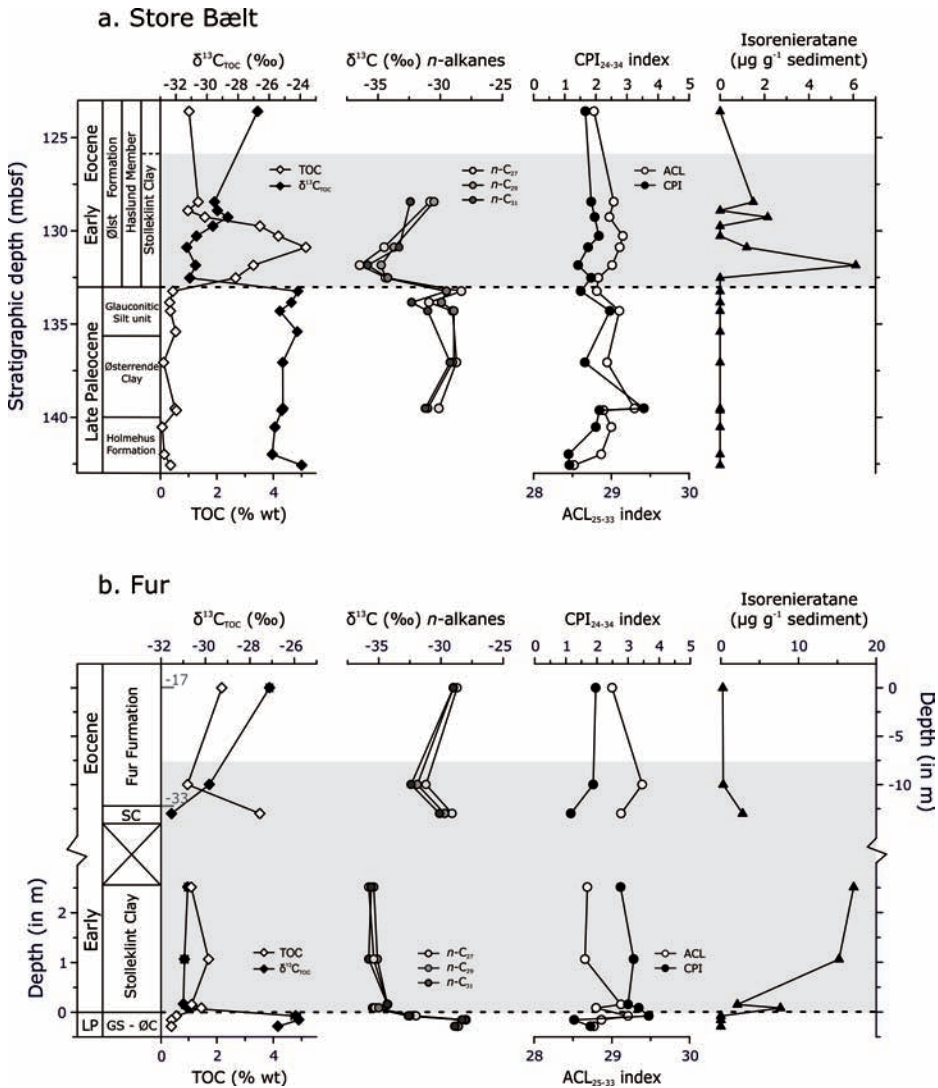


Figure 5.3 | Profiles of the PETM section at (a) Store Bælt and (b) Fur Island, showing the TOC content and the stable carbon isotopic composition of TOC, the stable carbon isotopic compositions of the C_{27} (light grey), C_{29} (middle grey), C_{32} (dark grey) n -alkanes, the Carbon Preference Index (CPI) and Average Chain Length (ACL) index of the odd-carbon-number $C_{25-C_{35}}$ n -alkanes, and the abundance of S-bound isorenieratane. The dotted line indicates the onset of the CIE of the PETM and the grey area indicates the entire PETM interval. Note the different depth scale below and above the glacially-disturbed interval described in the text. The ash layers -33 and -17 of *Bøgild* (1918) are shown. Abbreviations: LP= Late Palaeocene, GS = Glauconitic Silt unit, OC = Østerrende Clay, SC = Stolleklint Clay.

were also studied. Odd carbon numbered *n*-alkanes, generally in the range of 25 to 35 carbon atoms, are typically derived from epicuticular leaf waxes of higher land plants (Eglinton & Hamilton, 1967). The carbon preference index (CPI) is a measurement to express the relative predominance of these odd-numbered *n*-alkanes (Bray & Evans, 1961; Marzì *et al.*, 1993). The CPI values for both Danish sections are mostly well above 1 (up to 3.5; **Figs. 5.3a and b**), suggesting a substantial contribution of terrestrial-derived *n*-alkanes to the sediments, though marine-derived *n*-alkanes likely contribute as well. Of the odd-carbon numbered *n*-alkanes the C_{29} *n*-alkane is the most dominant in all sediments, followed by either the C_{27} or the C_{31} *n*-alkane. This is reflected in the Average Chain Length (ACL_{25-35}) of odd-numbered long-chain *n*-alkanes in the range of 25 to 35 carbon atoms, which at both sites varies around 29 (**Figs. 5.3a and b**). The $\delta^{13}C$ values fluctuate around -29.5 ‰ for the *n*- C_{27} and *n*- C_{29} alkanes and around -30.5 ‰ for the *n*- C_{31} alkane during the latest Palaeocene for both sites (**Figs. 5.3a and b**). At Store Bælt, the $\delta^{13}C$ values of the *n*- C_{27} , *n*- C_{29} , and *n*- C_{31} alkanes decrease coincident with the CIE in TOC, with ~5.7 ‰, 4.6 ‰, and 3.8 ‰, respectively (**Fig. 5.3a**). At Fur, the magnitude of the CIE in the *n*-alkanes is higher, ranging from 6.2 ‰ for the *n*- C_{27} and *n*- C_{31} alkanes to 6.7 ‰ for the *n*- C_{29} alkane (**Fig. 5.3b**). In this section, the decrease in $\delta^{13}C$ appears to slightly precede the CIE in TOC, but this pattern is only recorded in one data point and is not apparent at Store Bælt.

Most PETM sites record terrestrial CIE's in the range of 4-6 ‰ (e.g. Handley *et al.*, 2008, 2011; Pagani *et al.*, 2006b; Smith *et al.*, 2007), similar to that recorded for TOC and *n*-alkanes at Store Bælt. The *n*-alkane isotopic shifts at Fur are 1-2 ‰ larger and correspond to those reported for a PETM section in Tanzania where terrestrial *n*-alkanes record a CIE of 6-7 ‰ (Handley *et al.*, 2008). The most important amplification mechanisms that have been postulated to explain the larger terrestrial CIE in comparison to the marine CIE, include an increase in humidity (Bowen *et al.*, 2004; Pagani *et al.*, 2006b), or a change in vegetational patterns (Schouten *et al.*, 2007b; Smith *et al.*, 2007). Alternatively, the actual amplitude of the atmospheric CIE is much larger than the ~3-3.5 ‰ inferred from marine calcite (cf. Diefendorf *et al.*, 2011; Handley *et al.*, 2008; Pagani *et al.*, 2006b).

For both the Danish sites we only observe minor fluctuations in ACL during the PETM, suggesting no clear evidence for large changes in vegetational patterns. However, the CPI values around the CIE at Fur (2-3) are substantial higher compared to those at Store Bælt (~1.8). The more reduced CIE in the *n*-alkanes observed at Store Bælt may thus be due to a larger imprint of marine-derived *n*-alkanes which have a smaller CIE compared to terrestrial *n*-alkanes.

5.4.2 Stratification and photic zone anoxia

At the onset of the PETM substantial changes in TOC levels are recorded. The sediments of the late Palaeocene at Store Bælt are overall low in TOC (<1 %) but

at the onset of the CIE the TOC levels abruptly increases, towards peak values of 5 % at 130.89 m depth (**Fig. 5.3a**). A similar pattern is visible in the TOC record at Fur with values increasing from <1 to up to 3.5 %. (**Fig. 5.3b**). The low organic carbon content, the ample evidence of bioturbation in the sediments and the high glauconitic content in the clayey and sandy silt deposits just before the onset of the PETM are all indicative for a well-oxygenated water column. Both Danish sections show an abrupt lithological transition at the Palaeocene/Eocene boundary. The relative amount of organic carbon increases rapidly in concert with the CIE and remains high throughout the PETM interval (**Figs. 5.3a and b**). This implies, together with the fine-laminated clays devoid of benthos and high sulfur (pyrite) content, the development of anoxic and sulfidic bottom waters (*Nielsen et al.*, 1986; *Pedersen*, 1981).

That intense euxinic conditions existed during the PETM is further evident by the presence of sulfur-bound isorenieratane at both Danish locations. S-bound isorenieratane is a diagenetic product of isorenieratene, a characteristic pigment that is used by green sulfur bacteria during photosynthesis. Besides light (*Overmann et al.*, 1992), these phototrophic bacteria further need free sulfide (H_2S) and anoxic conditions to thrive (*Sinninghe Damsté et al.*, 1993; *Summons & Powell*, 1986). The presence of these lipids in the Danish PETM sediments, therefore, indicate a specific palaeoenvironment, i.e. photic zone euxinia (PZE). At Fur, S-bound isorenieratane is detected in the entire PETM interval with the highest abundance ($\sim 17 \mu\text{g g}^{-1}$ TOC) occurring 2.51 m after the onset of the CIE (**Fig. 5.3b**). Outside the PETM interval this biomarker is below detection limit. The isorenieratane distribution profile at Store Bælt shows a slightly different pattern. At this site, isorenieratane is not always present throughout the PETM interval and the first detection, which corresponds to the highest abundance ($\sim 6 \mu\text{g g}^{-1}$ TOC), occurs after the onset of the PETM (**Fig. 5.3a**). Nevertheless, evidence for PZE at these two locations suggests that a large part of the eastern North Sea basin became stratified and had euxinic waters reaching into the photic zone. The development of photic zone euxinia in the North Sea basin could have been triggered by multiple causes, such as substantial increases in primary productivity, possibly due to higher nutrient loads by adjacent rivers (*Knox*, 1996b). In addition, due to the increased warming during the PETM, intermediate waters became depleted in oxygen, resulting from enhanced microbial recycling and lower solubility of oxygen in warmer waters (*Chun et al.*, 2010; *Nicolo et al.*, 2010). According to modelling studies (e.g. *Bice & Marotzke*, 2002; *Zeebe & Zachos*, 2007) and reconstructions of deep sea circulation patterns (*Tripathi & Elderfield*, 2005), deep water formation was distorted during the PETM causing a worldwide reorganization of the ocean currents. This may explain the stratification of the water column in the eastern part of the North Sea Basin, which suggests a limited exchange with adjacent water masses, potentially linked with regional tectonic uplift (*Bice & Marotzke*, 2002; *Knox*, 1998; *Tripathi & Elderfield*, 2005).

Episodes of photic zone euxinia, coincident with bottom water anoxia, and increased sedimentary organic matter contents have also been reported for the Lomonosov Ridge in the Arctic Ocean during the PETM (*Sluijs et al.*, 2006). The increase in fresh water input due to an enhanced hydrological cycle (*Pagani et al.*, 2006b), in combination with an increase in primary productivity, has been invoked to explain the stagnant water masses in this enclosed high latitude basin. The fact that two basins at different latitudes became anoxic suggests that restricted water column ventilation was a common feature during the PETM. Such a widespread anoxia in shelf seas is reminiscent of the black shale deposits of the early Toarcian. During this period biomarkers of green sulfur bacteria have also been found (*Schouten et al.*, 2000c; *Sinninghe Damsté & Schouten*, 2006; *van Breugel et al.*, 2006), suggesting the development of photic zone euxinia over large areas in the European epicontinental seas and Tethys continental margin. This suggests that the stratification of epicontinental seas may have been a common phenomenon in a greenhouse climate mode (cf. *Jenkyns*, 2010). Furthermore, a prominent negative carbon isotope excursion is also measured in both inorganic and organic carbon during the early Toarcian (*Jenkyns & Clayton*, 1997; *Jiménez et al.*, 1996; *Kemp et al.*, 2005; *Schouten et al.*, 2000c). The parallels between the early Toarcian black shales and several PETM sites therefore suggest that the underlying mechanisms may be the same. The potentially globally enhanced stratification during the PETM, possibly in combination with elevated productivity, could thus have led to enhanced carbon burial providing a negative feedback to the release of carbon during the PETM (*Bowen & Zachos*, 2010).

5.4.3 Sea surface and air temperature records

The TEX₈₆ reconstructed SST records at both studied Danish locations show a marked increase parallel to the negative excursion in $\delta^{13}\text{C}_{\text{TOC}}$, although the record at Store Bælt exhibits more scatter than the record at Fur (**Fig. 5.4a**). For the latest Palaeocene, the TEX₈₆ shows a cooling trend from 24 to 17 °C, followed by a sharp increase at the onset of the PETM. Estimated peak SSTs for the sections at Store Bælt and Fur are 29.5 °C and 31 °C, respectively. These peak SST values agree well with other temperature records from mid-latitude sites (**Fig. 5.1**), and may represent summer temperatures (cf. *Sluijs et al.*, 2006, 2011). The total magnitude of the temperature anomaly would then be 12–14 °C, much larger than observed elsewhere (**Fig. 5.1**). However, when the unusually large cooling phase prior to the PETM is not considered then the change in temperature is ca. 8–10 °C, only slightly higher than that observed at other mid-latitude sites. The strong cooling of ca. 7 °C before the onset of the PETM observed in the Danish records has not been observed elsewhere. On the contrary, most PETM sites show either relatively stable background SST values (*Sluijs et al.*, 2011; *Zachos et al.*, 2003), or even a warming that preceded the negative CIE (*Sluijs et al.*, 2007; *Tripathi & Elderfield*, 2004).

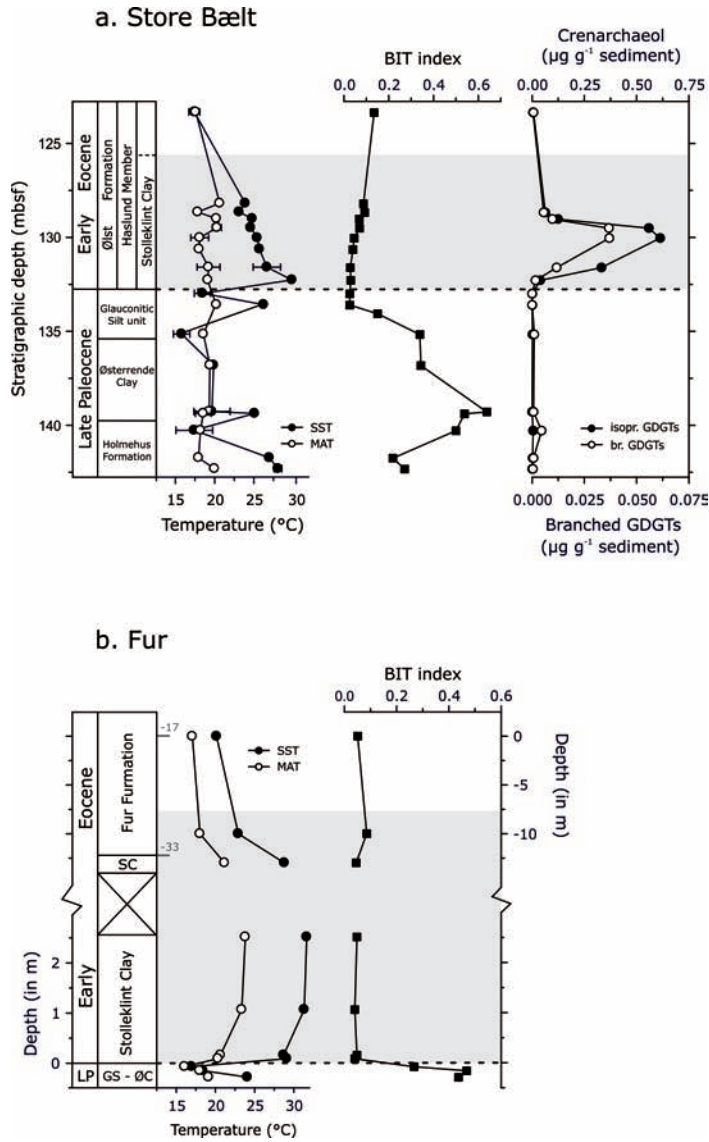


Figure 5.4 | Profiles of the PETM section at (a) Store Bælt and (b) Fur Island showing the sea surface temperatures derived from TEX_{86} and mean annual air temperatures derived from the CBT/MBT proxy, the BIT index, and absolute concentrations of crenarchaeol and branched GDGTs in $\mu\text{g g}^{-1}$ sediment. Note the difference in scale for both, which differs by a factor of ten. The dotted line indicates the onset of the CIE of the PETM and the grey area indicates the entire PETM interval. Note the different depth scale below and above the glacially-disturbed interval described in the text. The ash layers -33 and -17 of *Boggild* (1918) are shown. Abbreviations: LP = Late Palaeocene, GS = Glaucinitic Silt unit, ØC = Østerrende Clay, SC = Stolleklint Clay.

It is possible that the TEX_{86} records at our sites are biased. For instance, the TEX_{86} values can be affected by the input of soil-derived isoprenoid GDGTs (*Weijers et al.*, 2006b). The BIT index is a proxy for the relative input of soil organic matter (*Hopmans et al.*, 2004). Before the PETM, BIT values are generally high between 0.3 to 0.7 at both sites, indicative for a substantial input of soil-derived OM (**Figs. 5.4a and b**). These high values suggest that the TEX_{86} values are likely affected by soil organic matter input and thus the SST estimates for the latest Palaeocene can be biased. Before the onset of the CIE, BIT values gradually decrease to <0.1 and remain low during the PETM (**Figs. 5.4a and b**). Thus, these TEX_{86} values are unlikely to be substantially affected by terrestrial input at that time, suggesting that the magnitude of warming may indeed be 8–10 °C. Another possibility is that the TEX_{86} values in the late Palaeocene are affected by oxic degradation. The TOC values for late Palaeocene sediments at both sites are low ($<1\%$) and the depositional environment was oxic prior to the PETM and thus organic matter, including GDGTs, will have been exposed substantially to oxygen and likely be severely degraded. This is supported by palynological observations of organic particles in the Holmehus Formation, which are generally degraded and corroded (*Heilmann-Clausen et al.*, 1985). *Huguet et al.* (2009) have shown in turbidites that upon prolonged exposure to oxic conditions, crenarchaeol is more prone to oxic degradation during early diagenesis than branched GDGTs, leading to higher BIT values. Indeed, before the PETM, concentrations of the branched GDGTs and crenarchaeol are low (**Fig. 5.4a**) and concomitant with the onset of the CIE and the development of photic zone euxinia, there is a substantial increase in the concentration of crenarchaeol towards peak values of $\sim 0.6\ \mu\text{g g}^{-1}$ sediment (**Fig. 5.4a**). In contrast, the branched GDGT concentration during that same interval increases considerably less (**Fig. 5.4a**). Thus, the high BIT values prior to the PETM may have been caused by severe oxic degradation. By association, this selective degradation of the marine signal may then have also biased TEX_{86} temperature estimates, although it is still uncertain to what degree it affects the temperature estimates (*Huguet et al.*, 2009).

Interestingly, reconstructed MATs based on the MBT/CBT proxy from Fur Island shows a similar pattern as the TEX_{86} record: a cooling from 22 to 17 °C for the latest Palaeocene followed by an increase of 12 °C across the P/E boundary (**Fig. 5.4b**). These almost identical patterns between two independently calibrated temperature proxies suggest that potential biases on the TEX_{86} temperature records prior to the PETM, as discussed above, may have not been severe. Like with the TEX_{86} record, the CBT/MBT record of Store Bælt exhibits considerably more scatter and warming trends are less evident. Despite this, the continental temperatures still show roughly the same pattern compared to the TEX_{86} temperature record of this site, with background values of ca. 22 °C and a cooling trend to low values ($\sim 17\text{ °C}$) just before the onset of the PETM. Peak MAT values occur later than for TEX_{86} but are of similar magnitude ($\sim 24.5\text{ °C}$) at this depth

(129.75-129.27 mcd). The only other MBT/CBT record of the PETM shows a $\sim 8^\circ\text{C}$ warming of the continents around the Arctic region (Weijers *et al.*, 2007a) (Fig. 5.1). In contrast, the continental temperature increase in the Bighorn Basin (Fig. 5.1), based on leaf margin analysis, is substantially lower (5°C), although this increase is possibly underestimated (Wing *et al.*, 2005). Except for the 8°C temperature increase recorded in $\delta^{18}\text{O}$ of planktonic foraminifera and TEX_{86} at the mid-latitude sites from the New Jersey shelf (Fig. 5.1), the $8\text{-}10^\circ\text{C}$ warming of the surface waters is the largest temperature anomaly so far recorded for the PETM. As suggested by Zachos *et al.* (2006), it is possible that shallow marine sites are affected by variations in regional and seasonal parameters, causing a larger warming at continental margins in comparison with open marine records.

5.5 CONCLUSIONS

We studied two PETM sections from the eastern part of the North Sea Basin, which both are marked by a negative CIE in TOC of 5-6 ‰. Analyses of the stable carbon isotopes of higher plant-derived long-chain *n*-alkanes reveal a terrestrial CIE of 4-6 ‰ at Store Bælt, but at Fur the terrestrial CIE magnitude is 1-2 ‰ higher and seems to precede the CIE in TOC. These variations in the $\delta^{13}\text{C}$ profiles between the two sites likely reflect regional rather than global changes. The large differences in CPI values between the two sites suggest different sources of the *n*-alkanes (marine- vs. terrestrial-derived). This complicates the interpretation of the onset and magnitude of the CIE recorded in the *n*-alkanes in sediment records.

The onset of the CIE is accompanied by a marked change in lithology, increasing organic matter content and the presence of sulfur-bound isorenieratane, indicating a substantial change in depositional environment from well-oxygenated to anoxic and sulfidic, likely due to a combination of diminished oxygen supply by intermediate waters and increased primary productivity. These euxinic conditions are similar to those previously reported for the Lomonosov Ridge in the Arctic Ocean, suggesting that restricted water column ventilation was common in semi-enclosed basins during the PETM. This is reminiscent of the early Toarcian where a negative CIE is also accompanied by photic zone euxinia in shelf seas and organic matter deposition.

TEX_{86} SST records show a warming of $8\text{-}10^\circ\text{C}$ towards peak temperatures of 31°C . This warming is, however, preceded by a remarkable cooling of several degrees. Potentially, the reconstructed TEX_{86} values are biased by oxic degradation and selective preservation of soil organic matter during the latest Palaeocene. However, continental air temperatures reconstructed using the MBT/CBT index show a similar warming, and also include a cooling prior to the PETM. It is possible that these temperature records reflect additional local conditions besides the global changes associated with the PETM. This may also explain the extraordinary warming of at least 8°C recorded by the two independent temperature proxies.

Our study thus suggests that it is important to study climate records from multiple locations within a region to separate the regional from the global climate variability.

ACKNOWLEDGMENTS

We thank Jort Ossebaar, Anhelique Mets, Michiel Kienhuis, Marianne Baas, and Daphne Rekers for their laboratory assistance. We also thank Katarzyna Śliwińska for useful discussions. Financial support for this research was provided by the Darwin Center for Biogeosciences and a VICI grant from the Netherlands Organisation for Scientific Research to Stefan Schouten.

CHAPTER 6

Constraining the magnitude of Early Eocene global carbon isotope excursions using lipids of marine Thaumarchaeota

Petra L. Schoon, Claus Heilmann-Clausen, Bo Pagh Schultz, Appy Sluijs,
Jaap S. Sinninghe Damsté, and Stefan Schouten

Submitted to Earth and Planetary Science Letters

ABSTRACT

The Palaeocene-Eocene Thermal Maximum (PETM; ~56 Ma) and Eocene Thermal Maximum 2 (ETM2; ~53 Ma) are geological short episodes of extreme global warming and environmental change. Both the PETM and ETM2 are associated with the injection of ^{13}C -depleted carbon into the ocean-atmosphere system as revealed through a globally recognized carbon isotope excursion (CIE) and massive dissolution of deep sea carbonate. However, the magnitude of these CIEs vary with the type of fossil matter, i.e. carbonates, bulk organic matter, and terrestrial and marine biomarker lipids, making it difficult to constrain the actual CIE in atmospheric and oceanic carbon pools. Here we analyzed the stable carbon isotopic composition ($\delta^{13}\text{C}$) of glycerol dibiphytanyl glycerol tetraether lipids (GDGT) derived from marine Thaumarchaeota in sediments deposited during the PETM in the North Sea Basin and ETM2 in the Arctic Ocean. The $\delta^{13}\text{C}$ values of these lipids are potentially directly recording variations in $\delta^{13}\text{C}$ dissolved inorganic carbon (DIC) and can thus provide a record of marine $\delta^{13}\text{C}$ DIC across both these Eocene hyperthermals. Reconstructed pre-CIE $\delta^{13}\text{C}_{\text{DIC}}$ values are slightly lower (0.5-1 ‰) than modern day values and decrease with ~3.6 ‰ and ~2.5 ‰ for the PETM and ETM2, respectively. The CIE in crenarchaeol for ETM2 is higher than that in marine calcite from other locations, possibly because of the admixture of deep water ^{13}C -depleted CO_2 generated by the euxinic conditions that developed occasionally during ETM2. However, the reconstructed PETM CIE lies close to the CIE inferred from marine calcite, suggesting that the $\delta^{13}\text{C}$ record of crenarchaeol may document the actual magnitude of the CIE in marine DIC during the PETM in the North Sea Basin. The $\delta^{13}\text{C}$ of thaumarchaeotal lipids is thus a promising novel tool to reconstruct the $\delta^{13}\text{C}$ of DIC in sediments that are devoid of carbonates, but relatively rich in organic matter, such as shallow marine coastal settings.

6.1 INTRODUCTION

Late Palaeocene to Early Eocene climate conditions were the warmest of the Cenozoic Era as evidenced by deep sea temperature records (e.g. *Zachos et al.*, 2001, 2008). During this interval, temperatures increased gradually, especially at mid and high latitudes, resulting in a reduced latitudinal temperature gradient (e.g. *Bijl et al.*, 2009; *Huber & Caballero*, 2011 and references cited therein). The cause of this warming remains unclear, but is most likely the result of a combination of enhanced tectonism leading to elevated atmospheric CO₂ levels (*Hancock et al.*, 2007; *Leon-Rodriguez & Dickens*, 2010) and reorganization of ocean circulation patterns (*Dickens et al.*, 1997; *Thomas & Shackleton*, 1996). A superimposed warming peak marks the Palaeocene-Eocene boundary at ~56 Ma, and is known as the Palaeocene-Eocene Thermal Maximum (PETM) (e.g. *Zachos et al.*, 2001). Proxy temperature records using Mg/Ca ratios and oxygen isotopes of planktonic foraminifera (*Kennett & Stott*, 1991; *Pearson et al.*, 2001b; *Tripathi & Elderfield*, 2005; *Zachos et al.*, 2003), or TEX₈₆ palaeothermometry (e.g. *Sluijs et al.*, 2006, 2011; *Zachos et al.*, 2006) show a 5–8 °C global warming of deep and surface ocean waters. Additionally, a rapid large decrease in stable carbon isotope ratios ($\delta^{13}\text{C}$) in marine and terrestrial carbonates and organic matter and massive dissolution of seafloor carbonates provide evidence for the massive and rapid injection of ¹³C-depleted carbon in the oceans and atmosphere (*Dickens et al.*, 1997; *Zachos et al.*, 2005; *McInerney & Wing*, 2011).

Several mechanisms have been proposed to explain this global negative carbon isotope excursion (CIE), amongst others the release of thermogenic methane due to contact metamorphism (*Svensen et al.*, 2004), rapid burning of terrestrial organic matter (*Kurtz et al.*, 2003), the release of carbon stored in permafrost soils at high latitudes triggered by orbital forcing (*DeConto et al.*, 2012), and the dissociation of methane hydrates (*Dickens*, 1995). These hypotheses provide mechanisms that not only explain the CIE of the PETM, but also offers an explanation for the several smaller CIEs that have occurred after the PETM, such as the Eocene Thermal Maximum 2 (ETM2) and H2 event (*Lourens et al.*, 2005; *Nicolo et al.*, 2007; *Sluijs et al.*, 2009; *Stap et al.*, 2010; *Westerhold et al.*, 2009). However, the methane hydrate hypothesis is especially appealing since the carbon stored in this reservoir has relatively low $\delta^{13}\text{C}$ values (<60 ‰; *Kvenvolden*, 1993) and thus relatively low amounts of carbon are needed to explain the large (~3 ‰) CIE in the global exogenic carbon pool. However, authentication of the sources of the ¹³C-depleted carbon strongly depends on the magnitude of the actual CIE recorded in the PETM sediments (e.g. *Pagani et al.*, 2006a). Unfortunately, the reported magnitude of the CIEs vary widely between different marine and terrestrial carbon records, such as carbonate shells, bulk organic matter and specific terrestrial and marine biomarkers (see Table 1 in *McInerney & Wing*, 2011). These variations in shape and magnitude of individual carbon isotope records are often caused through changes in: (1) the rela-

tive abundance of mixed components with different $\delta^{13}\text{C}$ values within a measured substrate, (2) change in isotope fractionation through physiological change, (3) the isotope composition of the carbon source (*Sluijs & Dickens*, 2012). Although the magnitude of the biases generated by these factors is relatively well known, assessing the magnitude of these biases for any individual $\delta^{13}\text{C}$ record is difficult (*Sluijs & Dickens*, 2012).

In this study, we investigate the potential use of the stable carbon isotopic composition ($\delta^{13}\text{C}$) of the biomarker lipid crenarchaeol, which exclusively occurs in ammonia-oxidizing Thaumarchaeota (*Pitcher et al.*, 2011a and references cited therein), to reconstruct the variations in $\delta^{13}\text{C}$ of marine dissolved inorganic carbon (DIC) during the Eocene hyperthermals. Several studies using ^{13}C -labeling experiments and cultivation studies showed that Thaumarchaeota have a chemoautotrophic lifestyle (*Jung et al.*, 2011; *Park et al.*, 2010; *Wuchter et al.*, 2003), using ammonium as electron donor, which is oxidized to nitrite (*Hallam et al.*, 2006; *Könneke et al.*, 2005; *Wuchter et al.*, 2006). Based on the relatively ^{13}C enriched isotopic composition of crenarchaeol, and the isoprenoidal ether-bound lipids (biphytanes) derived thereof, compared to algal biomarkers, it was suggested that Thaumarchaeota take up bicarbonate as a carbon source (*Hoefs et al.*, 1997; *Pearson et al.*, 2001a; *Kuypers et al.*, 2001). Furthermore, *Kuypers et al.* (2001) found that the ^{13}C of the crenarchaeol was enriched by 3 ‰ compared to modern values during the mid-Cretaceous oceanic anoxic event 1b and attributed this to the 2–3 ‰ $\delta^{13}\text{C}$ offset between modern and mid-Cretaceous DIC. Confirmation came from *Berg et al.* (2007), showing that Thaumarchaeota assimilate carbon through the 3-hydroxypropionate/4-hydroxybutyrate biochemical pathway, which involves the direct utilization of bicarbonate.

The active uptake of HCO_3^- by Thaumarchaeota suggests that the $\delta^{13}\text{C}$ composition of Thaumarchaeal lipids may be independent to variations in CO_2 concentrations, unlike phytoplankton (e.g. *Laws et al.*, 1995), and predominantly depend on the $\delta^{13}\text{C}$ of HCO_3^- . This is supported by labelling studies with enrichment cultures of marine Thaumarchaeota, which showed no limitation on growth rates of the Thaumarchaeota in response to increased aqueous HCO_3^- -levels (*Park et al.*, 2010). Importantly, *Könneke et al.* (2012) found that the $\delta^{13}\text{C}$ compositions of both biomass as well as crenarchaeol of the Thaumarchaeote *Nitrosopumilus maritimus* was indeed independent of DIC concentrations, and the carbon isotopic fractionation between crenarchaeol and DIC was a consistent -19.7 ± 0.5 ‰. Interestingly, reported $\delta^{13}\text{C}$ values of crenarchaeol in modern marine sediments range from -18 to -23 ‰, averaging around -21 ± 1 ‰ (*Schouten et al.*, 2013). Assuming that DIC of marine surface waters at these sites is roughly between -1 to 1.5 ‰ (*Kroopnick*, 1985), the $\delta^{13}\text{C}$ values of crenarchaeol are thus fairly consistent with a fractionation of ~ 20 ‰ as observed in *N. maritimus*. Thus, the $\delta^{13}\text{C}$ composition of biphytanes derived from GDGTs produced by Thaumarchaeota may thus be a new tool to reconstruct past $\delta^{13}\text{C}$ values of marine DIC. This is a major advantage compared to other biomarker proxies reconstructing the CIE because bicarbonate comprises

the largest carbon reservoir in the global exogenic carbon cycle. Furthermore, since crenarchaeol is a unique biomarker lipid for marine Thaumarchaeota, the CIE in crenarchaeol should not be affected by mixing of different components with different $\delta^{13}\text{C}$ values as with e.g. TOC.

To test this hypothesis, we analyzed the $\delta^{13}\text{C}$ compositions of the biphytane moieties derived of archaeal GDGTs, obtained after ether-bond cleavage with HI/LiAlH_4 , from sediment records spanning the PETM and ETM2 in the North Sea Basin and Arctic Ocean, respectively. We compare the $\delta^{13}\text{C}$ values of the biphytanes with each other, in order to constrain sources of GDGTs and utilize the $\delta^{13}\text{C}$ value of the biphytane specifically derived from crenarchaeol to reconstruct $\delta^{13}\text{C}_{\text{DIC}}$ across the Eocene hyperthermals.

6.2 MATERIALS AND METHODS

6.2.1 Samples and sampling sites

In this study, we used sediment samples that were previously used for other palynological and (organic) geochemical studies of the North Sea Basin PETM (Nielsen *et al.*, 1986; Schmitz *et al.*, 2004; Schoon *et al.*, 2013) and Arctic Ocean ETM2 (Schoon *et al.*, 2011; Sluijs *et al.*, 2009) (**Table 6.1**). Sediments that cover the Palaeocene – Eocene transition are derived from three sites located in Denmark (**Fig. 6.1**). At time of deposition, Denmark was situated in the eastern part of the semi-enclosed, epicontinental, North Sea Basin. Two of the study sites are outcrops of which one is located in the western Limfjorden area on the island Fur and the other is the Ølst-Hinge clay pit located in central Jutland. The third study site is an offshore section located in the sea strait Store Bælt cored in 1983 (borehole no. 83101 carried out by the Danish Geotechnical Institute) in between the Danish islands Sjælland and Fyn (Nielsen *et al.*, 1986). The PETM has been recognized at these sites on the basis of a 6–8 ‰ CIE in total organic carbon (TOC) and on the concomitant abundance peaks of dinocysts that belong to the organic-walled dinoflagellate cyst genus *Apectodinium*, including the species *Apectodinium angustum*, which is diagnostic of the PETM (Heilmann-Clausen & Schmitz, 2000; Schmitz *et al.*, 2004). The continuous section at Store Bælt records the entire CIE of the PETM. The Fur section, however, is interrupted by a glacially-disturbed interval of 10–20 m and possibly the maximum of the CIE of the PETM is missing (Schoon *et al.*, 2013). The part of the Ølst-Hinge section studied here, is a record of the earliest Eocene and includes the recovery phase of the CIE of the PETM.

Samples from ETM2 are derived from the Integrated Ocean Drilling Project (IODP) Hole 302-4A, which was retrieved in 2004 (Backman *et al.*, 2006). The site is located on the Lomonosov Ridge at ~85 °N palaeolatitude in the Central Arctic Ocean (O'Regan *et al.*, 2008) (**Fig. 6.1**). This marine sedimentary sequence contains the ETM2 interval between 368.9 and 368.2 meters composite depth (mcd) based

Table 6.1 | Stable carbon isotope values of TOC and biphytanes for three PETM sections in Denmark and for a ETM2 section (IODP 302) from the Lomonosov Ridge, Arctic Ocean.

Sample code	Location	Age	Depth (m)	Stable carbon isotopic composition ($\delta^{13}\text{C}$) in ‰ VDPB				
				TOC	BP-0	BP-1	BP-2	BP-3
PS090785	Fur, Denmark	CIE PETM	30.51	-27.1 \pm 0.1	-22.7 \pm 0.1	-22.9 \pm 0.3	-21.9 \pm 0.3	-21.3 \pm 0.4
PS090784	Fur, Denmark	CIE PETM	20.51	-29.8 \pm 0.1	-25.2 \pm 0.1	-24.4 \pm 0.2	-22.8 \pm 0.5	-22.5 \pm 0.4
PS090783	Fur, Denmark	CIE PETM	17.51	-31.5 \pm 0.0	-27.1 \pm 0.1	-26.2 \pm 0.3	-24.0 \pm 0.0	-23.8 \pm 0.1
PS090782	Fur, Denmark	CIE PETM	2.51	-30.8 \pm 0.1	-28.3 \pm 0.3	-25.9 \pm 0.2	-25.5 \pm 0.2	-25.1 \pm 0.2
PS090781	Fur, Denmark	CIE PETM	1.06	-30.9 \pm 0.2	-27.2 \pm 0.6	-24.3 \pm 0.1	-23.7 \pm 0.2	-23.8 \pm 0.3
PS090751	Fur, Denmark	CIE, PETM	0.15	-31.0 \pm 0.1	-27.2 \pm 0.5	-24.5 \pm 0.2	-23.5 \pm 0.2	-23.4 \pm 0.1
PS090750	Fur, Denmark	CIE, PETM	0.08	-30.8 \pm 0.0	-25.3 \pm 0.2	-24.5 \pm 0.3	-23.2 \pm 0.2	-23.2 \pm 0.1
PS090749	Fur, Denmark	latest Palaeocene	-0.08	-25.9 \pm 0.2	-25.7 \pm 0.2	-31.5 \pm 0.1	-22.1 \pm 0.3	-21.1 \pm 0.3
PS090748	Fur, Denmark	latest Palaeocene	-0.16	-25.8 \pm 0.0	-30.4 \pm 0.2	-31.4 \pm 0.4	-22.5 \pm 0.1	-21.7 \pm 0.4
PS090747	Fur, Denmark	latest Palaeocene	-0.29	-26.7 \pm 0.0	-26.2 \pm 0.1	-26.6 \pm 0.2	-22.4 \pm 0.3	-21.6 \pm 0.2
PS090790	Ølst-Hinge, Denmark	earliest Eocene	9.27	-2604 \pm 0.0	-23.1 \pm 0.2	-24.7 \pm 0.5	-22.5 \pm 0.3	-22.9 \pm 0.5
PS090788	Ølst-Hinge, Denmark	earliest Eocene	6.84	-27.2 \pm 0.0	-22.3 \pm 0.3	-22.6	-21.7 \pm 0.2	-21.5 \pm 0.3
PS090787	Ølst-Hinge, Denmark	earliest Eocene	4.52	-26.5 \pm 0.0	-24.0 \pm 0.3	-22.5 \pm 0.2	-22.9 \pm 0.1	-22.5 \pm 0.2
PS090786	Ølst-Hinge, Denmark	earliest Eocene	0.02	-27.0 \pm 0.0	-24.3 \pm 0.3	-20.0 \pm 0.2	-21.0 \pm 0.1	-20.4 \pm 0.2
PS090789	Ølst-Hinge, Denmark	CIE PETM	-1.20	-31.0 \pm 0.1	-27.4 \pm 0.0	-25.6 \pm 0.2	-24.3 \pm 0.1	-24.3 \pm 0.2
PS090746	Store Belt, Denmark	CIE PETM	128.45	-29.5 \pm 0.1	-27.8 \pm 0.4	-24.0 \pm 0.3	-22.7 \pm 0.2	-22.5 \pm 0.1
PS105882	Store Belt, Denmark	CIE PETM	129.27	-28.6 \pm 0.1	-26.3 \pm 0.0	-25.7 \pm 0.3	-23.2 \pm 0.0	-22.5 \pm 0.2
PS090745	Store Belt, Denmark	CIE PETM	130.89	-31.3 \pm 0.1	-26.8 \pm 0.3	-24.2 \pm 0.1	-23.2 \pm 0.5	-23.1 \pm 0.4
PS103458	Store Belt, Denmark	CIE PETM	131.85	-30.7 \pm 0.1	-26.1 \pm 0.3	-24.6 \pm 0.2	-23.8 \pm 0.3	-23.7 \pm 0.2
302-4-27X1-59-60	Lomonosov Ridge, Arctic Ocean	Post-ETM2	367.99	-29.1	-25.7 \pm 0.1	-28.3 \pm 0.8	-23.8 \pm 0.2	-22.7 \pm 0.1
302-4-27X1-118-120	Lomonosov Ridge, Arctic Ocean	CIE ETM2	368.58	-29.3	-26.1 \pm 0.1	-27.3 \pm 1.4	-25.4 \pm 0.9	-22.7 \pm 0.0
302-4-27X1-122-124	Lomonosov Ridge, Arctic Ocean	CIE ETM2	368.62	-29.8	-25.6 \pm 0.1	nd.	nd.	-22.7 \pm 0.2
302-4-27X1-132-134	Lomonosov Ridge, Arctic Ocean	CIE ETM2	368.72	-0.8	-24.7 \pm 0.0	-25.5	-24.9 \pm 0.0	-23.0 \pm 0.4
302-4-27X1-139-141	Lomonosov Ridge, Arctic Ocean	CIE ETM2	368.79	-31.2	-22.6 \pm 0.3	-20.8 \pm 0.2	-21.3 \pm 0.0	-20.2 \pm 0.1
302-4-27X1-12-14	Lomonosov Ridge, Arctic Ocean	CIE ETM2	369.00	-27.5	-23.3 \pm 0.2	-19.0 \pm 0.2	-21.4 \pm 0.3	-20.9 \pm 0.1
302-4-27X1-31-32	Lomonosov Ridge, Arctic Ocean	Pre-ETM2	369.21	-27.5	-23.0 \pm 0.4	-21.0 \pm 0.1	-20.4 \pm 0.2	-19.5 \pm 0.3

nd. = not detected

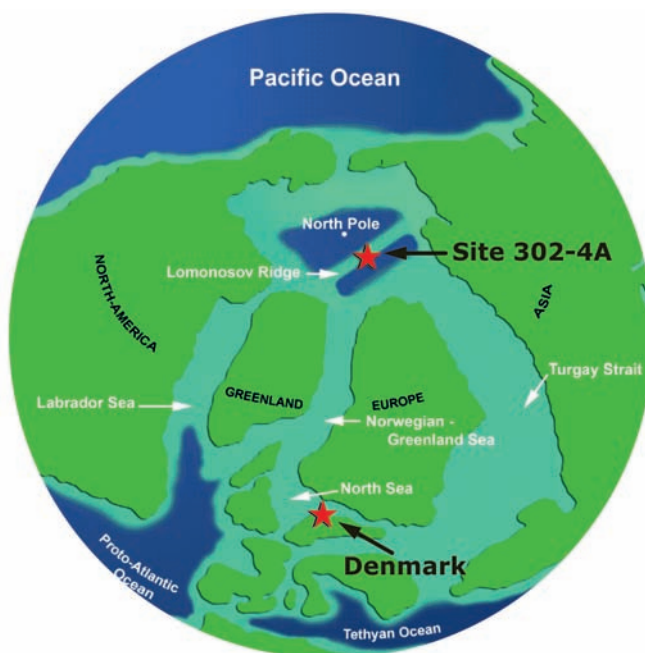


Figure 6.1 Palaeogeographical map of the Late Palaeocene and Early Eocene showing the study locations of the PETM (Denmark) and ETM2 (Lomonosov Ridge). Adapted from *Sluijs et al. (2009)*

on the 3.5 ‰ CIE in TOC and the presence of the dinocyst species *Cerodinium wardenese* and *Hystriochosphaeridium tubiferum* (*Sluijs et al., 2009*). During the early Eocene this location was warm and strongly influenced by freshwater input and high nutrient concentrations (*Sluijs et al., 2009*).

6.2.2 $\delta^{13}\text{C}$ analyses of GDGT-derived biphytanes

All sediment samples were extracted by means of a Dionex Accelerated Solvent Extractor (ASE) using a 9:1 (v:v) mixture of dichloromethane (DCM) and methanol (MeOH), at high pressure (7.6×10^6 Pa) and temperature (100 °C). An aliquot of the total extract was separated into an apolar and a polar fraction using a small column with activated alumina (Al_2O_3) using *n*-hexane/DCM (9:1, v:v) and MeOH/DCM (1:1, v:v) as eluents, respectively. The GDGTs, present in the polar fraction, were analyzed by high pressure liquid chromatography-mass spectrometry (HPLC-MS) as previously described by *Sluijs et al. (2009)* for Arctic Ocean ETM2, and *Schoon et al. (2013)* for the North Sea Basin PETM, to determine their relative abundances.

To be able to analyze the stable carbon isotopic composition of these lipids, the polar fractions were refluxed with 56 wt% HI (in H₂O) for 1 h, which cleaves the ether bonds of GDGTs and releases their isoprenoid carbon skeletons (*Schouten et al.*, 1998b). Subsequently, the alkyl iodides formed were isolated by column chromatography over a Al₂O₃ column and reduced to hydrocarbons by refluxing with LiAlH₄ for 1 h in 1,4-dioxane. Prior to analysis by gas chromatography (GC), gas chromatography/mass spectrometry (GC/MS) and isotope ratio monitoring-GC/MS, a cleaning step was performed using Ag⁺-impregnated silica to isolate the released saturated hydrocarbons. GC analyses were performed on a Hewlett-Packard instrument 6890 equipped with an on-column injector and a flame ionization detector (FID). A fused silica capillary column (25 m x 0.32 mm) coated with CP-Sil 5 (film thickness 0.12 µm) was used with He as carrier gas. Samples were dissolved in *n*-hexane and injected at 70 °C and subsequently the temperature increased to 130 °C at a rate of 20 °C/min and then at a rate of 4 °C/min the temperature was raised to 320 °C for 20 min. GC/MS analyses were performed on a ThermoFinnigan TRACE GC. The chromatographic conditions were similar as described above. The GC was coupled with a ThermoFinnigan DSQ quadrupole mass spectrometer with ionization energy of 70 eV. The hydrocarbon fractions were analyzed in full scan mode with a mass range of *m/z* 50-800 at 3 scans s⁻¹. Identification of the acyclic and cyclic biphytanes was based on comparison with previously reported retention times and mass spectra (*Schouten et al.*, 1998b).

The stable carbon isotopic composition of the biphytanes was analyzed using a Finnigan DELTA-V irm-GC/MS coupled to an Agilent 6890 GC. The GC conditions are similar to those described above. The δ¹³C were calculated by integrating the 44, 45 and 46 mass ion currents of the individual peaks and that of the CO₂ reference peaks. The performance of the irm-GC/MS was monitored by regular injection of two predeuterated standards with known isotopic compositions. All carbon isotopic values were determined at least in duplicate and are averaged to obtain a mean and a standard deviation (σ), which are reported in the δ¹³C notation relative to the VPDB standard.

6.3 RESULTS

6.3.1 Variation in GDGT distribution

HPLC-MS analysis of the North Sea Basin PETM sediments showed that crenarchaeol is the most dominant GDGT throughout the entire Fur section (**Figs. 6.2a and 6.3**). Before and after the CIE, crenarchaeol is only slightly higher in relative abundance than GDGT-0, but during the entire PETM interval the abundance of crenarchaeol increases up to 75 % of total GDGTs (**Fig. 6.3**). The relative abundance of GDGTs in sediments deposited in the Arctic Basin do not show substantial variations across ETM2 with crenarchaeol being generally more abundant than GDGT-0 (**Fig. 6.4**). In both the PETM and ETM2 sediments, GDGT-1, -2, and

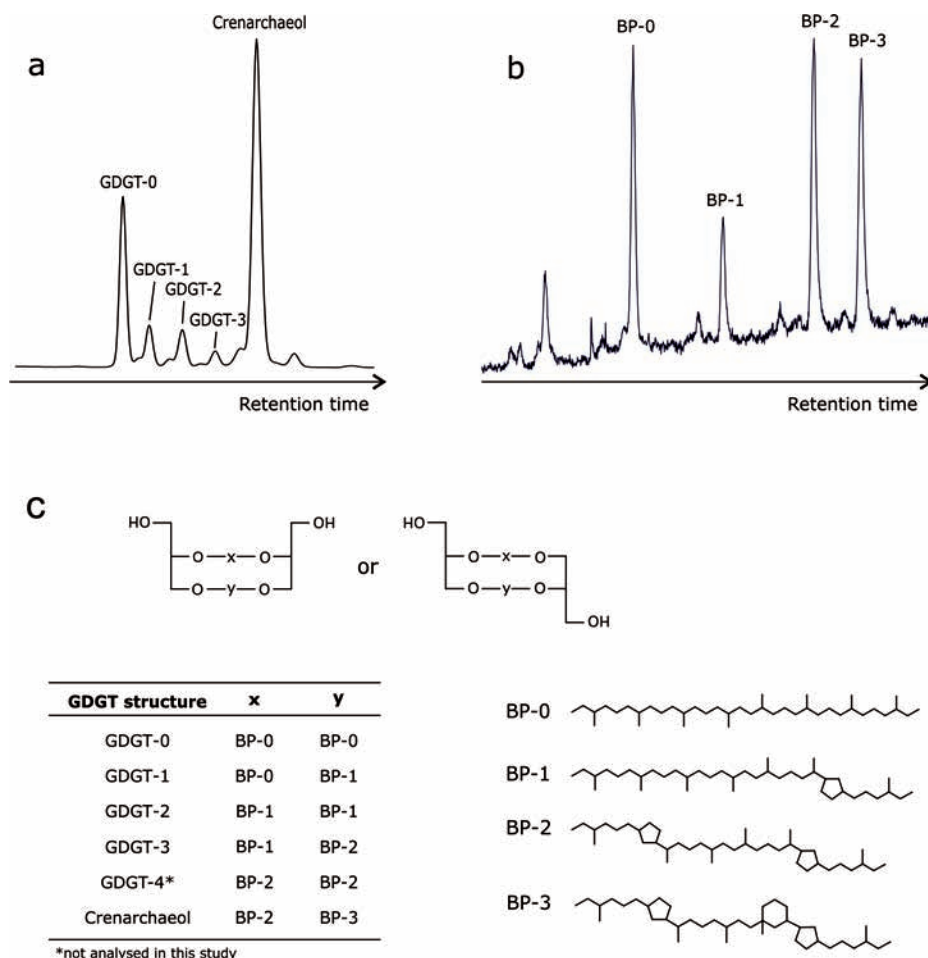


Figure 6.2 | (a) HPLC-MS base peak chromatogram and (b) partial GC-MS chromatogram of hydrocarbons released from HI/LiAlH₄ treatment of a sediment extract from the CIE of the PETM (130.89 m at Store Bält; **Table 6.1**), (c) Structures of the GDGTs and associated biphytanes.

-3 are only minor components (combined ranging from 0 to 20 % of all GDGTs) (**Figs. 6.3 and 6.4**).

Upon chemical degradation of the GDGTs with HI/LiAlH₄, four biphytanes, i.e., an acyclic (BP-0), a monocyclic (BP-1), a bicyclic (BP-2) and a tricyclic (BP-3) biphytane (e.g. **Fig. 6.2a and b**), were generated. The latter structure contains, besides two cyclopentane moieties, also a cyclohexane moiety and has been shown to exclusively derive from crenarchaeol (*Schouten et al.*, 2000b; *Sinninghe Damsté et al.*, 2002). Theoretically, the abundance of the released biphytanes depends on the rel-

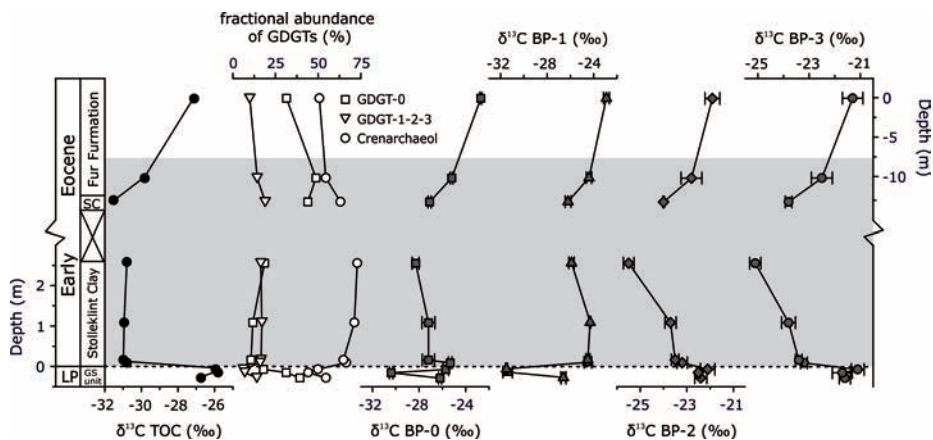


Figure 6.3 | Fractional abundance of GDGTs (percentage of total isoprenoid GDGTs) and $\delta^{13}\text{C}$ records of the TOC, and the acyclic (BP-0), monocyclic (BP-1), bicyclic (BP-2) and tricyclic (BP-3) biphytanes of the section at Fur, Denmark across the PETM. The dashed line indicates the onset of the CIE, whereas the grey area indicates the entire PETM interval. Abbreviations: LP = Late Palaeocene, GS = Glauconitic Silt, SC = Stolleklint Clay.

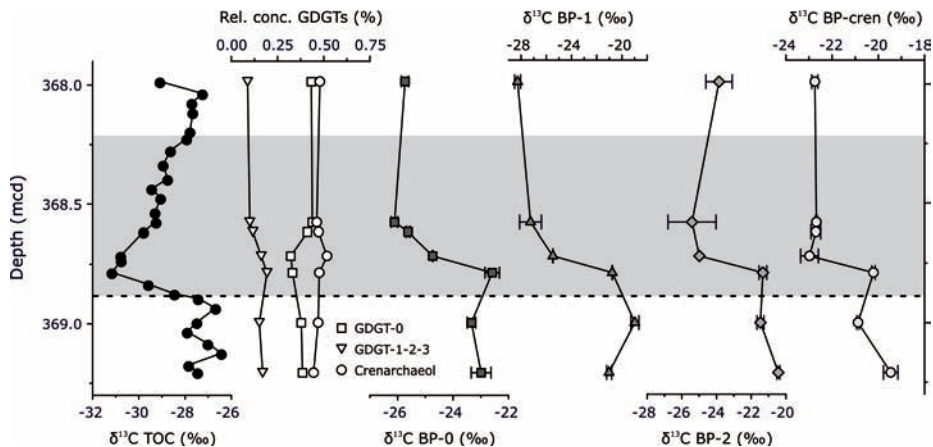


Figure 6.4 | Fractional abundance of GDGTs (percentage of total isoprenoid GDGTs) and $\delta^{13}\text{C}$ records of the TOC, and the acyclic (BP-0), monocyclic (BP-1), bicyclic (BP-2) and tricyclic (BP-3) biphytanes from sediments deposited during ETM2 in the Arctic Basin. The dashed line indicates the onset of the CIE, whereas the grey area indicates the entire ETM2 interval.

active concentration of the GDGTs and on the type of GDGT. For instance, both GDGT-0 and GDGT-1 contribute to the total pool of BP-0. However, GDGT-1 is only a minor contributor to the total pool of GDGTs and contains only one BP-0 moiety. This is in contrast to GDGT-0, which is a dominant GDGT in all samples and contains two BP-0 moieties (**Fig. 6.2c**). Therefore, GDGT-0 contributes substantially more to the total BP-0 pool than GDGT-1. Thus, if we assume that GDGT-4 does not contribute to the total pool of GDGTs in the PETM and ETM2 sediments and that GDGT-2 consists of two BP-1 moieties, it is possible to predict the distribution of the biphytanes from the distribution of the GDGTs. The relative amount of the biphytanes can then be calculated using the following formulas:

$$f_{BP-0} = f_{GDGT-0} + \frac{1}{2} * f_{GDGT-1} \quad (\text{eq. 6.1})$$

$$f_{BP-1} = \frac{1}{2} * f_{GDGT-1} + f_{GDGT-2} + \frac{1}{2} * f_{GDGT-3} \quad (\text{eq. 6.2})$$

$$f_{BP-2} = \frac{1}{2} * f_{\text{cren}} + \frac{1}{2} * f_{GDGT-3} \quad (\text{eq. 6.3})$$

$$f_{BP-3} = \frac{1}{2} * f_{\text{cren}} \quad (\text{eq. 6.4})$$

in which f stands for the fraction of the component. This calculated distribution fits well with the actual biphytane distribution observed after HI-LiAlH_4 degradation (**Figs. 6.2a and b and Fig. 6.5**), although, in general, the measured abundance of BP-0 and BP-1 is slightly higher than the expected fractional abundance calculated from the GDGT distribution, whereas the abundance of both BP-2 and -3 are slightly lower than the expected fractional abundance. At the onset of the CIE of the PETM, the ratio of BP-2 and BP-3 with respect to BP-0 increased substantially, in agreement with the dominance of crenarchaeol in these sediments (**Fig. 6.5**). After the PETM, the biphytane abundance equals those from prior to the PETM (**Fig. 6.5**). We further observe no substantial variation in biphytane distribution in the sediments from the Arctic Basin from before, during or after ETM2 (**Fig. 6.5**). That is, BP-0 is the most abundant, followed by BP-2 and BP-3. In all samples BP-1 is lowest in abundance (**Fig. 6.5**).

6.3.2 Stable carbon isotopic compositions of acyclic and cyclic biphytanes

Despite that GDGTs were detected in all sediments by HPLC-MS, it was not always possible to obtain $\delta^{13}\text{C}$ values of the biphytanes. For example, in most Late Palaeocene sediments, with TOC contents $<1\%$, biphytanes were below detection limit or only present in trace amounts. This corresponds well with the fact that absolute GDGT concentrations in these sediments are low ($<0.1\ \mu\text{g g}^{-1}$; Schoon *et al.*, 2013). Therefore, we could only obtain relatively complete (i.e. covering the CIE) biphytane $\delta^{13}\text{C}$ records for the PETM of the Fur section and ETM2 of the Arctic Basin, whereas for the other two Danish PETM sections we only obtained CIE and post CIE $\delta^{13}\text{C}$ values.

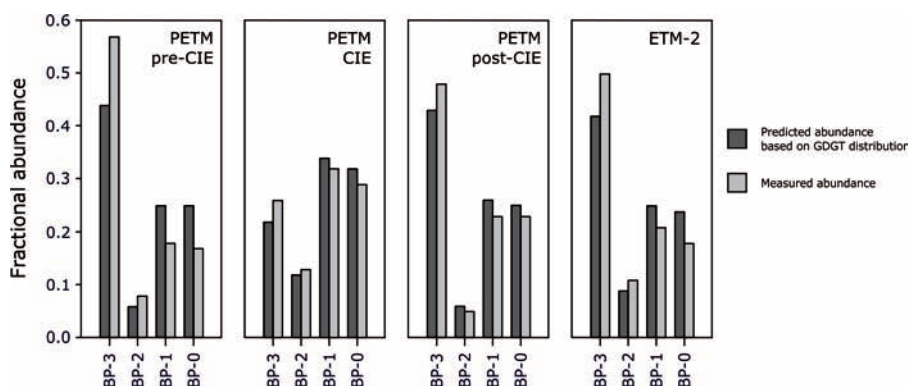


Figure 6.5 | Predicted (from measured GDGT distributions) and measured average fractional abundances of the four biphytanes released from the GDGTs present in the sediments representing intervals of the pre-CIE, CIE, post-CIE PETM and in the interval representing the entire ETM2.

6.3.2.1 PETM – North Sea

In general, BP-3 is most enriched in ^{13}C , with $\delta^{13}\text{C}$ values varying from -20 ‰ to -25 ‰, whereas BP-0 is generally the most ^{13}C -depleted from -22 ‰ down to values of -31 ‰ (Table 6.1). Intermediate $\delta^{13}\text{C}$ values are recorded for the other biphytanes. At the Fur section, BP-2 and BP-3 have $\delta^{13}\text{C}$ values of around -22 ‰ and -21 ‰, respectively, prior to the CIE of the PETM (Fig. 6.3). Both biphytanes show an initial shift of 1.5-2.0 ‰ coincident with the onset of the CIE in TOC (Fig. 6.3) and peak $\delta^{13}\text{C}$ values are reached just before the glacially-disturbed interval with a maximum negative shift of 3.2 ‰ in BP-2 and 3.6 ‰ in BP-3, respectively. Subsequently, the $\delta^{13}\text{C}$ values of these biphytanes increase, towards values slightly more negative than pre-excursion values. We observe a different $\delta^{13}\text{C}$ pattern for BP-0 and BP-1. Prior to the CIE in TOC both biphytanes show a distinct negative shift to depleted values of ~ -31 ‰ after which they return to initial $\delta^{13}\text{C}$ values of around -25 ‰ at and just after the onset of the CIE. Subsequently, both BP-0 and BP-1 $\delta^{13}\text{C}$ values show a gradual negative shift towards peak values of around -28 ‰ and -26 ‰, respectively. The $\delta^{13}\text{C}$ biphytane values of the CIE and post-CIE sections at Store Bælt and Ølst-Hinge, compare well with those in the equivalent sections at Fur (Table 6.1).

6.3.2.2 ETM2 – Arctic Ocean

Biphytane values range from -19 to -28 ‰ for the Arctic Basin sediments (Table 6.1). As for the PETM in the North Sea, BP-3 is the most enriched in ^{13}C , whereas BP-0 is in general the most ^{13}C -depleted. Prior to the CIE of ETM2, BP-2 and BP-3 have similar $\delta^{13}\text{C}$ values of around -21 ‰ and -20 ‰, respectively. All biphytanes shifts towards more negative $\delta^{13}\text{C}$ values during the CIE, though these shifts

occur slightly after the CIE in TOC, i.e. at 368.79 mcd versus 368.72 mcd, respectively (**Fig. 6.4**). The negative shift recorded in BP-3 is ~ 2.5 ‰ (**Fig. 6.4**), whereas the negative shift in BP-2 is larger, ~ 4.2 ‰.

6.4 DISCUSSION

6.4.1 Sources of the ether-bound biphytanes

The tricyclic biphytane (BP-3), which consists of two cyclopentyl moieties and one cyclohexyl moiety (**Fig. 6.2c**), derives exclusively from crenarchaeol, a specific membrane lipid of Thaumarchaeota (*Pitcher et al.*, 2011a and references cited therein). The bicyclic biphytane (BP-2) is also part of the carbon skeleton within crenarchaeol but can also be sourced from other GDGTs, such as GDGT-3 or GDGT-4 (**Fig. 6.2c**). This latter GDGT was not analysed in this study. It is likely that BP-0 predominantly derives from GDGT-0, while BP-1 is mainly sourced from GDGTs-1 and -2, which only have minor contributions to the GDGT-pool in the PETM and ETM2 sediments (**Figs. 6.3 and 6.4**).

Könneke et al. (2012) showed in their culture study of *N. maritimus* that all biphytanes derived of its GDGT membrane lipids have identical $\delta^{13}\text{C}$ values. Therefore, to examine whether the individual biphytanes are all derived from Thaumarchaeota, we compared the $\delta^{13}\text{C}$ compositions of BP-0, predominantly derived from GDGT-0, BP-1 and BP-2, which can originate from multiple GDGTs, with that of BP-3, which derives solely from thaumarchaeotal-derived crenarchaeol (**Fig. 6.6a**). The most significant relationship observed is that between BP-3 and BP-2, which generally have similar $\delta^{13}\text{C}$ values and lie close to the 1:1 line. This strongly suggests that BP-2 is also predominantly derived from crenarchaeol (cf. *Schouten et al.*, 1998b). The correlation between the $\delta^{13}\text{C}$ values of BP-3 and the other two biphytanes (BP-0 and BP-1) is considerably less and frequently they have substantially different $\delta^{13}\text{C}$ values. The $\delta^{13}\text{C}$ values of both BP-0 and BP-1 are nearly always depleted in ^{13}C compared to the $\delta^{13}\text{C}$ values of BP-3, i.e. on average by 3 ‰ for BP-0 and 1.5 ‰ for BP-1 (**Fig. 6.6a**). These ^{13}C -depleted values relative to those of BP-2 and BP-3, suggests they may have additional sources other than Thaumarchaeota, such as methanotrophs and methanogens, which are known to synthesize lipids with more depleted $\delta^{13}\text{C}$ values (e.g. *Summons et al.*, 1998). *Schouten et al.* (1998b) showed that in marine sediments the isotopic difference between BP-3 and BP-0 is larger with higher concentrations of BP-0 (i.e. GDGT-0) compared to that of BP-3 (i.e., crenarchaeol). They attributed this trend to an additional ^{13}C -depleted source of GDGT-0, likely through a contribution of methanogens. However, we do not observe such a trend in our data (**Fig. 6.6b**). Instead, we find a consistent isotopic offset of ~ 3.5 ‰ between BP-0 and BP-3 for the CIE of the PETM and ETM2, independent of the relative amount of crenarchaeol. This is, however, not the case for the post-PETM samples from the North Sea, which exhibit no significant isotopic difference.

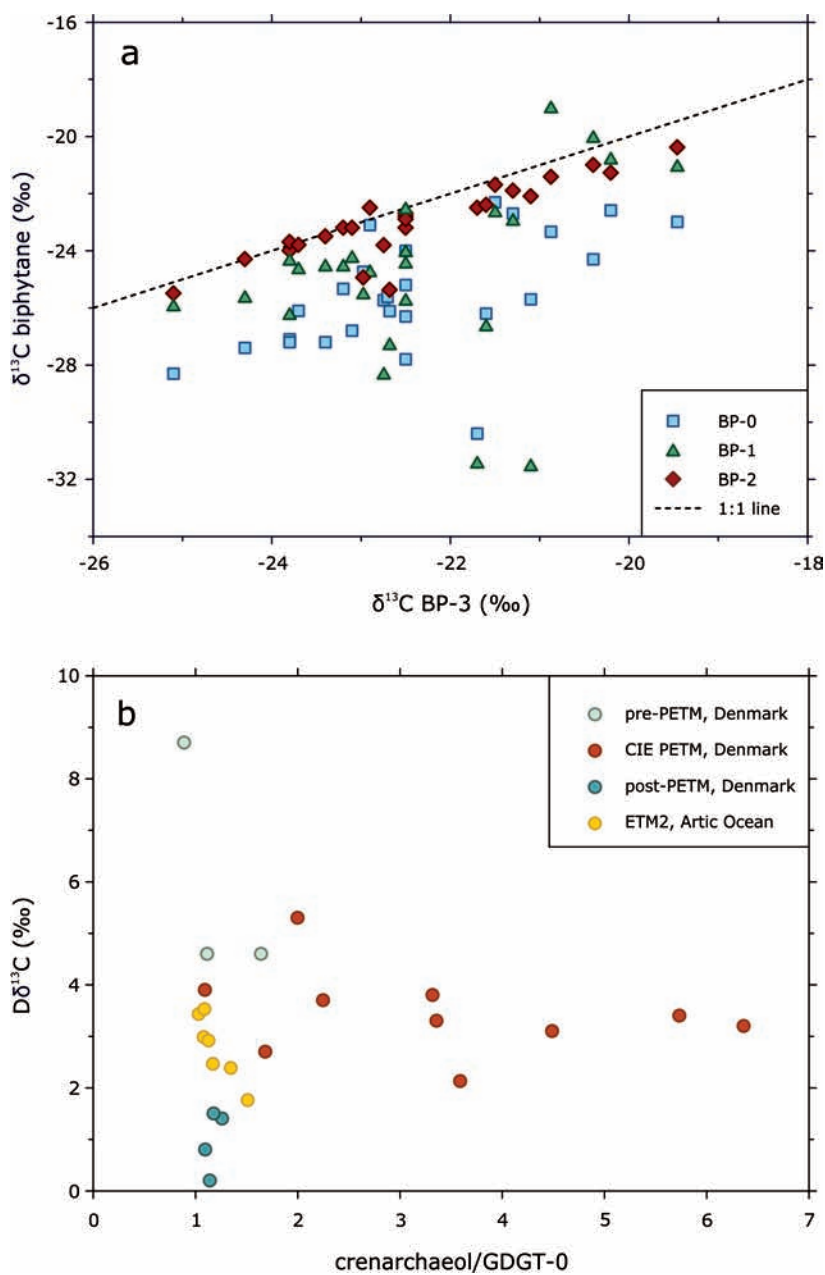


Figure 6.6 | (a) Cross-correlations of the stable carbon isotope composition of BP-3 with those of BP-0, BP-1 and BP-2. The dotted line indicates the 1:1 line. (b) Difference in stable carbon isotope composition ($\Delta\delta^{13}\text{C}$) of BP-3 and BP-0 as a function of the ratio of crenarchaeol and GDGT-0.

An input of GDGTs from sources other than Thaumarchaeota could potentially bias TEX_{86} records as this index includes GDGTs-1 and -2 and assumes they are solely derived from Thaumarchaeota. Indeed, the relatively negative $\delta^{13}\text{C}$ values of BP-0 and BP-1 before the onset of the PETM in sediments from the Danish section at Store Bælt coincide with relatively cool temperatures (*Schoon et al.*, 2013). A higher input of non-Thaumarchaeotal sourced GDGT-1 could indeed bias the GDGT distribution and lead to lower TEX_{86} values. However, reconstructed continental air temperatures using the distribution of branched GDGTs, derived from soil bacteria, showed similar low temperatures in the same interval, suggesting that this bias in the TEX_{86} record is relatively minor (*Schoon et al.*, 2013).

In any case, the similar isotopic composition and behaviour between BP-3 and BP-2 (**Fig. 6.6b**) confirms that both biphytanes derive from crenarchaeol and therefore their $\delta^{13}\text{C}$ values reflect that of crenarchaeol.

6.4.2 Magnitude and timing of the CIE in Thaumarchaeota

The magnitude of the carbon isotope excursion for BP-2 and BP-3 at the Danish PETM section at Fur, where we have a complete isotope record, is 3.6 ± 0.3 ‰ (**Fig. 6.3**). This is considerably less than measured in TOC (5-6 ‰) and *n*-alkanes (6-7 ‰) at this location (*Schoon et al.*, 2013), but is similar to the ~ 3 ‰ CIE measured in marine calcite elsewhere (*McInerney & Wing*, 2011 and references cited therein; *Dickens*, 2011 and references cited therein; *Sluijs & Dickens*, 2013). Possibly, peak values are masked by the glacially-disturbed interval at Fur (*Schoon et al.*, 2013) and, therefore, the CIE in crenarchaeol may be underestimated. However, the $\delta^{13}\text{C}$ values of BP-3 at the CIE sections of Store Bælt and Ølst-Hinge are nearly identical to that of Fur (**Table 6.1**), suggesting that the maximum ^{13}C -depletion of crenarchaeol is reached at Fur, and thus the CIE in crenarchaeol is unlikely to be higher than 3.6 ‰.

The magnitude of the CIE recorded in BP-3 at ETM2 is ~ 2.5 ‰. This is slightly lower than that measured for TOC (3.1 ‰; **Table 6.1**), but similar when corrected for terrestrial organic matter contributions (2.5 ‰; *Sluijs & Dickens*, 2013). It is smaller than excursions found for marine biomarkers, which ranged from 3.2 to 4.5 ‰ (*Schoon et al.*, 2011), but larger than the 1.4 ‰ excursion of deep marine calcite measured at Walvis Ridge (*Stap et al.*, 2010). These differences between CIEs in marine OM and crenarchaeol versus marine calcite potentially reflect local variations in the magnitude of the different CIEs in the DIC of the semi-restricted Arctic Basin and South Atlantic Ocean, respectively.

Intriguingly, the timing of the CIE of crenarchaeol apparently differs to that of TOC and marine biomarkers for ETM2. Where the marine biomarker CIEs all track the negative shift in $\delta^{13}\text{C}_{\text{TOC}}$ at 368.90 mcd marking the onset of ETM2 (*Sluijs et al.*, 2009; *Schoon et al.*, 2011), the $\delta^{13}\text{C}$ negative shift in BP-3 occurs later, i.e. between 368.79 and 368.72 mcd (**Fig. 6.4**). It is unclear why the sediment at 368.79

mcd does not show a more negative $\delta^{13}\text{C}$ compared to pre-CIE values. Although it is a single point in the record (attempts to obtain isotope data for other depth intervals were not successful), the other marine biomarkers in the same sediment interval already show a negative shift of $\sim 1\text{--}2\text{‰}$ (Schoon *et al.*, 2013). One possibility to explain the apparent delayed onset of the CIE of crenarchaeol, as well as the relatively large CIE compared to deep marine calcite, is that euxinic conditions developed in the deeper part of the photic zone during ETM2, as evidenced by the presence of derivatives of the biomarker isorenieratene derived from anoxygenic phototrophic green sulphur bacteria (Sluijs *et al.*, 2009). In the contemporary euxinic Black Sea, Thaumarchaeota reside at the deeper and colder chemocline (Coolen *et al.*, 2007), where $\delta^{13}\text{C}_{\text{DIC}}$ values are always substantially more negative than at the surface (e.g. $\sim -4.5\text{‰}$ for the Black Sea chemocline; Freeman & Wakeham, 1991) due to the production of depleted CO_2 by mineralization of descending particles rich in ^{13}C -depleted organic matter (Fry *et al.*, 1991; Freeman & Wakeham, 1991). It is therefore possible that the $\delta^{13}\text{C}$ of crenarchaeol may be more negative due to the migration of the Thaumarchaeota to deeper waters. Indeed, the $\delta^{13}\text{C}$ negative shift of the biphytanes at ETM2 coincides with peak concentrations of derivatives of the specific biomarker isorenieratene and with a sharp cooling of temperatures inferred from TEX_{86} (Sluijs *et al.*, 2009). This may imply that the Thaumarchaeota responded to the arising euxinic conditions at this location by migrating down towards the chemocline, thereby yielding lower TEX_{86} temperatures (cf. Menzies *et al.*, 2006) and depleted ^{13}C -values. At 368.79 mcd, where a CIE of crenarchaeol is not yet exhibited, no isorenieratane was detected (Schoon *et al.*, 2013) and thus euxinic conditions, which likely already developed in the bottom waters, did not reach the photic zone at this depth interval. Possibly, the Thaumarchaeota migrated initially upwards during the first stages of the CIE such that the CIE was partly offset by the more enriched $\delta^{13}\text{C}_{\text{DIC}}$ in the surface waters compared to deeper waters.

The observations at ETM2 do not seem to apply for the eastern North Sea Basin during the PETM. Schoon *et al.* (2013) also found isorenieratene derivatives in the sediments at the Fur section, suggesting that photic zone euxinia existed throughout the CIE. However, the TEX_{86} temperature records from all three Danish sites do not show any cooling events during the CIE of the PETM but rather a warming trend, as observed globally in PETM sections (Schoon *et al.*, 2013). This suggests that the niche of the Thaumarchaeota remained relatively constant there and possibly at shallower depths than in the Arctic Basin, with no apparent migration to deeper waters.

Thus, the $\delta^{13}\text{C}$ values of BP-3 suggest that the CIE recorded by Thaumarchaeota for ETM2 is possibly less than 2.5‰ and perhaps similar to the 1.4‰ recorded in marine calcite. Similar to the PETM, the CIE of crenarchaeol at ETM2 in the Arctic Basin is smaller than that recorded in other biomarkers such as sulfur-bound phytane and C_{25} HBI, which showed CIEs of 3.2‰ and 4.5‰ , respectively (Schoon *et al.*, 2011). Schoon *et al.* (2011) attributed the large magnitude of the CIE in these

algal biomarkers to enhanced CO₂ concentrations. In contrast, the $\delta^{13}\text{C}$ compositions of Thaumarchaeal lipids are independent to variations in DIC concentration, at least in culture experiments, and may predominantly depend on $\delta^{13}\text{C}$ of DIC only (Könneke *et al.*, 2012).

The $\delta^{13}\text{C}$ values of BP-3 not only allow to reconstruct variations in $\delta^{13}\text{C}_{\text{DIC}}$ but possibly also absolute $\delta^{13}\text{C}_{\text{DIC}}$ values, assuming the constant fractionation between biphytanes and DIC of ca. 20 ‰ observed in cultures (Könneke *et al.*, 2012) and modern sediments (Schouten *et al.*, 2013). Pre-PETM $\delta^{13}\text{C}_{\text{DIC}}$ estimates range between -1 to -2 ‰, more negative than contemporary $\delta^{13}\text{C}_{\text{DIC}}$ surface sea water values observed in the North Sea (~1 ‰; Mook & Tan, 1991). Pre-ETM2 $\delta^{13}\text{C}_{\text{DIC}}$ estimates are ~0 ‰, also lower than those observed in present-day Greenland Sea (~1.5 ‰; Kroopnick *et al.*, 1985) and the estimated surface water $\delta^{13}\text{C}_{\text{DIC}}$ value of ~1 ‰ in the Nansen Basin in the Arctic Ocean inferred from planktonic foraminifera (Bauch *et al.*, 2000). This is in contrast with planktonic and benthic foraminifera records, which suggests that late Palaeocene $\delta^{13}\text{C}_{\text{DIC}}$ is likely to have been slightly more enriched in ¹³C compared to present day (Hayes, 1999; Zachos *et al.*, 2001). One explanation could be that at present both the North Sea and the Arctic Ocean are relatively open systems with inflow of well oxygenated waters, whereas in the Early Palaeogene they were likely semi-enclosed basins with restricted inflow from the Atlantic or Tethys Ocean (Moran *et al.*, 2006; Brinkhuis *et al.*, 2006; Stein *et al.*, 2006; Kender *et al.*, 2012). This is comparable to estuarine circulation conditions of the Black Sea, where, due to intense recycling of CO₂, surface water $\delta^{13}\text{C}_{\text{DIC}}$ values in the Black Sea are in general lower than those of open waters (e.g. Fry *et al.*, 1991). Thus, local $\delta^{13}\text{C}_{\text{DIC}}$ values in the North Sea and Arctic Basins may have been more negative, due to restricted circulation, compared to the open ocean.

All together, our results suggest that the $\delta^{13}\text{C}$ values of Thaumarchaeotal biphytanes have the potential to record variations in $\delta^{13}\text{C}_{\text{DIC}}$ and can give insight in the magnitude of the carbon isotope excursions of the exogenic carbon pool during hyperthermals. The similar CIE of crenarchaeol compared to that of marine calcite during the PETM suggests that the marine DIC pool shifted with a maximum of 3.6 ‰, which is consistent with that found by Sluijs & Dickens (2012) in marine organic matter from the Lomonosov Ridge after correcting the TOC record for terrestrial contributions. However, to precisely constrain the CIE in marine DIC, $\delta^{13}\text{C}_{\text{DIC}}$ records, reconstructed by using the $\delta^{13}\text{C}$ values of crenarchaeol, from other PETM sites should be compared, as CIEs in $\delta^{13}\text{C}_{\text{DIC}}$ may have not been uniform across semi-enclosed basins, coastal seas and open oceans. Furthermore, potential factors influencing the magnitude of isotopic fractionation by Thaumarchaeota, such as temperature, growth rate and mixotrophy, should also be tested using culture experiments, although the relative consistent $\delta^{13}\text{C}$ values of crenarchaeol in modern sediments (Hoefs *et al.*, 1997; Schouten *et al.*, 2013) suggest these factors may be of relative minor importance.

6.5 CONCLUSIONS

We examined the potential use of stable carbon isotopes of Thaumarchaeotal GDGTs as a proxy for $\delta^{13}\text{C}_{\text{DIC}}$ in order to reconstruct the CIE of marine dissolved inorganic carbon during Eocene hyperthermals. The similar $\delta^{13}\text{C}$ composition of the tricyclic and bicyclic biphytanes in PETM and ETM2 sediments suggest they are both derived from the Thaumarchaeotal biomarker crenarchaeol, while other GDGTs have a more ^{13}C -depleted signature suggesting additional sources. The constant carbon isotopic fractionation ($\sim 20\text{‰}$) between the biphytanes and DIC, allowed us to reconstruct $\delta^{13}\text{C}_{\text{DIC}}$ records across two Eocene hyperthermals. We record $\delta^{13}\text{C}_{\text{DIC}}$ shifts of $\sim 3.6\text{‰}$ (from 0.5‰ to $\sim 4.6\text{‰}$) and $\sim 2.5\text{‰}$ (from ~ 0.5 to $\sim 3\text{‰}$) in the $\delta^{13}\text{C}$ of crenarchaeol for PETM and ETM2, respectively, which are similar and slightly higher than that of marine calcite. This suggests that the negative carbon isotope shifts recorded in crenarchaeol may represent the actual CIE of marine DIC at these sites during these Eocene hyperthermals.

ACKNOWLEDGMENTS

We thank C. Heeren, M. Kienhuis, J. Ossebaar, A. Mets and M. Baas for their laboratory and technical support. This is publication number 2013-xxx of the Darwin Center for Biogeosciences, which partially funded this project. Financial support also came from a VICI grant from the Netherlands Organisation for Scientific Research to Stefan Schouten. Appy Sluijs thanks the European Research Council under the European Community's Seventh Framework Program for ERC Starting Grant #259627.

CHAPTER 7

**Stable carbon isotope patterns of marine biomarker lipids in
the Arctic Ocean during Eocene Thermal Maximum 2**

Petra L. Schoon, Appy Sluijs, Jaap S. Sinninghe Damsté, and Stefan
Schouten

Published in: Paleocceanography 26: PA3215, 2011

ABSTRACT

The middle Palaeocene through early Eocene long-term gradual warming was superimposed by several transient warming events, such as the Paleocene-Eocene Thermal Maximum (PETM) and Eocene Thermal Maximum 2 (ETM2). Both events show evidence for extreme global warming associated with a major injection of carbon into the ocean-atmosphere system, but the mechanisms of carbon injection and many aspects of the environmental response are still poorly understood. In this study, we analyzed the concentration and stable carbon isotopic ($\delta^{13}\text{C}$) composition of several sulfur-bound biomarkers derived from marine photoautotrophs, deposited in the Arctic Ocean at $\sim 85^\circ\text{N}$, during ETM2. The presence of sulfur-bound biomarkers across this event points toward high primary productivity and anoxic bottom water conditions. The previously reported presence of isorenieratene derivatives indicates euxinic conditions in the photic zone, likely caused by a combination of enhanced primary productivity and salinity stratification. The negative carbon isotope excursion measured at the onset of ETM2 for several biomarkers, ranges between 3–4.5 ‰, much larger than the ~ 1.4 ‰ recorded in marine carbonates elsewhere, suggesting substantial enhanced isotopic fractionation by the primary producers likely due to a significant rise in $p\text{CO}_2$. In the absence of biogenic carbonates in the ETM2 section of our core we use coeval planktonic $\delta^{13}\text{C}$ from elsewhere to estimate surface water $\delta^{13}\text{C}$ in the Arctic Ocean and then apply the relation between isotopic fractionation and $p\text{CO}_2$, originally calibrated for haptophyte alkenones, to three selected organic biomarkers (i.e., S-bound phytane, C_{35} hopane and a C_{25} highly branched isoprenoid). This yields $p\text{CO}_2$ values potentially in the range of 4 times preindustrial levels. However, these estimates are uncertain due to a lack of knowledge on the importance of $p\text{CO}_2$ on photosynthetic isotopic fractionation.

7.1 INTRODUCTION

One of the most prominent features of Cenozoic climate is a global warming trend that started in the mid-Palaeocene (~59 Ma) and culminated during the Early Eocene Climatic Optimum (EECO; 52-50 Ma). During this time, several transient and geologically rapid episodes of extreme warming, or 'hyperthermals', occurred (e.g. *Zachos et al.*, 2008; *Lourens et al.*, 2005). These hyperthermals are characterized by a pronounced negative carbon isotope excursion (CIE) recorded in both organic and inorganic carbon reservoirs, and widespread, though variable, dissolution of deep sea carbonates (*Lourens et al.*, 2005; *Sluijs et al.*, 2007a; *Stap et al.*, 2010; *Leon-Rodriguez & Dickens*, 2010). These negative CIEs are generally thought to reflect the release of large amounts of ^{13}C -depleted carbon into the exogenic carbon pool (*Dickens et al.*, 2003). The extensively studied Paleocene-Eocene Thermal Maximum (PETM, ~56 Ma), was further characterized by ~4-9 °C warming of the continents and deep and surface ocean waters (e.g. *Kennett & Stott*, 1991; *Tripathi & Elderfield*, 2005; *Wing et al.*, 2005; *Sluijs et al.*, 2006; *Weijers et al.*, 2007). Approximately two million years later, the PETM was followed by Eocene Thermal Maximum 2 (ETM2) and the H2 hyperthermal events, characterized by similar climatic and geochemical changes as the PETM but of smaller magnitude (*Lourens et al.*, 2005; *Nicolo et al.*, 2007; *Sluijs et al.*, 2009; *Stap et al.*, 2009, 2010).

Critically, the magnitude of the CIE of the global exogenic carbon pool across the PETM remains contentious (*Dickens et al.*, 2011). Generally, calcium carbonate precipitated by benthic foraminifera in the deep ocean or outer shelf are considered to reliably reflect the global average magnitude of the CIE. However, the magnitude of the CIE may differ by up to 2 ‰ between such records (e.g. *John et al.*, 2008; *McCarren et al.*, 2008). In part, this likely reflects regional or local climate-driven deviations in the stable carbon isotopic composition ($\delta^{13}\text{C}$) of dissolved inorganic carbon from mean ocean values, which may regionally increase or decrease the magnitude of the CIE. In addition, part of the marine CIE signal may regionally be truncated in the deep sea due to severe dissolution and temporal absence of the critical foraminifera species during the early stages of the event (e.g. *Thomas et al.*, 2002; *McCarren et al.*, 2008). Finally, the magnitude of the CIE as recorded in foraminifera may have been dampened due to a decrease in seawater pH (*Uchikawa & Zeebe*, 2010). The terrestrial CIE signal as recorded in paleosol carbonates is on average ~1-2 ‰ larger than the marine signal (*Bowen et al.*, 2001). Although, in theory, the terrestrial carbonates should record the atmospheric CIE more directly, they may have been affected by diagenesis, and increased relative humidity and soil moisture (e.g. *Bowen et al.*, 2004). A large (4.5 ‰) CIE was also recorded in organic dinoflagellate cysts in two marginal marine sections (*Sluijs et al.*, 2007a), but, as yet, it remains uncertain if local factors other than the stable carbon isotopic composition ($\delta^{13}\text{C}$) of dissolved inorganic carbon influenced these records. Recent studies based on higher plant leaf wax *n*-alkanes (*Handley et al.*, 2008; *Pagani et al.*, 2006b; *Smith et al.*, 2007) suggest a large magnitude of the PETM-CIE.

However, biomarker analysis showed that angiosperms and gymnosperms have a different response to the environmental changes that took place during the PETM, resulting in different isotopic fractionation, causing an overestimation of the CIE (Schouten *et al.*, 2007a). The large CIE signal of $\sim 6\text{‰}$ generally recorded in terrestrial *n*-alkanes can therefore be explained by a shift in vegetation patterns from gymnosperm dominated to angiosperm dominated (Schouten *et al.*, 2007a; Smith *et al.*, 2007). Indeed, a recent tropical *n*-alkane record that should not be affected by such biases suggests a magnitude closer to 3‰ (Jaramillo *et al.*, 2010).

Molecular isotopic investigations on aquatic biomarkers have been limited to the $\delta^{13}\text{C}$ record of the C_{17} *n*-alkanes, possibly derived from algae and photosynthetic bacteria, which showed a lower CIE ($\sim 3.5\text{‰}$) compared to that of the terrestrial *n*-alkanes ($5\text{--}6\text{‰}$) (Pagani *et al.*, 2006b). However, it was suggested that the CIE recorded in the *n*- C_{17} alkanes was affected by increased paleoproductivity (Pagani *et al.*, 2006b). The isotopic response of marine primary producers during the PETM remains, therefore, poorly constrained.

In contrast to the PETM, $\delta^{13}\text{C}$ records of the CIE across ETM2 are relatively sparse (Lourens *et al.*, 2005; Nicolo *et al.*, 2007; Sluijs *et al.*, 2009; Stap *et al.*, 2010; Leon-Rodriguez & Dickens, 2010). At Walvis Ridge, the magnitudes of warming ($\sim 3\text{°C}$), carbonate dissolution and the CIE in benthic foraminifera ($\sim 1.4\text{‰}$) are smaller than those at the PETM (Lourens *et al.*, 2005; Stap *et al.*, 2009, 2010). ETM2 has recently been recognized in sediments deposited in the Central Arctic Ocean (Sluijs *et al.*, 2009; Stein *et al.*, 2006). In a recent study, Sluijs *et al.* (2009) found cysts of freshwater tolerant dinoflagellate species to dominate assemblages during ETM2, suggesting a freshening, stratification, and eutrophication of the Arctic Ocean surface waters. Bottom water anoxia was inferred from the presence of laminated sediments and the absence of organic linings of benthic foraminifera (Sluijs *et al.*, 2009). Furthermore, at some occasions anoxic conditions even reached into the photic zone, based on the presence of isorenieratene derivatives. The sea surface temperature proxy TEX_{86} (Sluijs *et al.*, 2006) indicated that Arctic Ocean surface waters warmed by $\sim 4\text{°C}$ during ETM2 (Sluijs *et al.*, 2009) though these estimates have some uncertainties (see detailed discussion in the Supplementary of Sluijs *et al.*, 2009). In addition, the presence of palm pollen in the interval of peak warmth implies that the mean temperature of the coldest month was above 8°C , constraining the lower temperature limit of the Arctic region during this Eocene hyperthermal event. This minimum temperature estimate is inferred from the habitats of modern biota. Paleobotanical inspection suggests that the stem structures of Paleogene palms is very similar to modern relatives which renders it highly unlikely that the palms were more resilient than at present (e.g. Royer *et al.*, 2002; Greenwood & Wing, 1995). The CIE in total organic carbon (TOC) is $\sim 3.5\text{‰}$ (Sluijs *et al.*, 2009), much larger than recorded in carbonates deposited elsewhere (Cramer *et al.*, 2003; Lourens *et al.*, 2005; Nicolo *et al.*, 2007; Stap *et al.*, 2009). However, this bulk organic carbon isotope record may have been biased due to changes in the source

(i.e. terrestrial vs. marine) of the bulk organic carbon.

To investigate the response of marine organisms across ETM2, we analyzed the concentrations and carbon isotopic composition of sulfur-bound biomarkers derived from marine phytoplankton in the Arctic Ocean record. Furthermore, we made a first attempt to roughly estimate changes in $p\text{CO}_2$ across ETM2, using reconstructed carbon isotope fractionations of three independent groups of marine microorganisms. Such $p\text{CO}_2$ estimates would considerably improve the insight in feedback mechanisms and climate sensitivity during past episodes of abrupt warming.

7.2 METHODS AND MATERIALS

7.2.1 Sample and site description

In 2004, Integrated Ocean Drilling Program (IODP) Expedition 302, also known as the Arctic Coring Expedition (ACEX), recovered lengthy portions of a 428 m marginal marine sedimentary sequence, at the crest of the Lomonosov Ridge in the Central Arctic Ocean ($\sim 85^\circ\text{N}$ paleolatitude) (**Fig. 7.1**; O'Regan *et al.*, 2008). Uppermost Paleocene and lower Eocene sediments deposited between 56 and 50 Ma consist of siliciclastic mudstones, barren of siliceous and calcium carbonate microfossils, but containing ample immature organic matter with a TOC content of up to 8 % (Stein *et al.*, 2006; O'Regan *et al.*, 2008). As suggested by the regular occurrence of dark laminated silty clays (O'Regan *et al.*, 2008), the high content of total sulfur (Ogawa *et al.*, 2009), the general absence of remains of benthic organisms (O'Regan *et al.*, 2008; Sluijs *et al.*, 2006, 2008), and trace metal information (Sluijs *et al.*, 2008), Arctic bottom waters were low in oxygen content throughout the studied interval covering ETM2 (Sluijs *et al.*, 2009), creating optimal conditions for biomarker preservation.

We studied the sediments from before to after the carbon isotope excursion (CIE) associated with ETM2, which are located ~ 20 m above the PETM. We used the same samples of Sluijs *et al.* (2009). The identification of the ETM2 interval is based on the presence of the dinoflagellates *Cerodinium wardenese* and *Hystriochosphaeridium tubiferum* (Sluijs *et al.*, 2008). The onset of ETM2 is placed at ~ 368.9 m composite depth below sea floor (mcd) according to the $\delta^{13}\text{C}$ composition of TOC (Sluijs *et al.*, 2009).

7.2.2 Biomarker analysis

Powdered and freeze-dried sediments (~ 5 g dry mass) were extracted with a Dionex Accelerated Solvent Extractor using a 9:1 (v:v) mixture of dichloromethane (DCM) and methanol (MeOH). An aliquot of the total extract was desulfurized to release sulfur-bound hydrocarbons using Raney Nickel, as previously described by Sinninghe Damsté *et al.* (1988). Prior to desulfurization an internal standard [2,3-di-

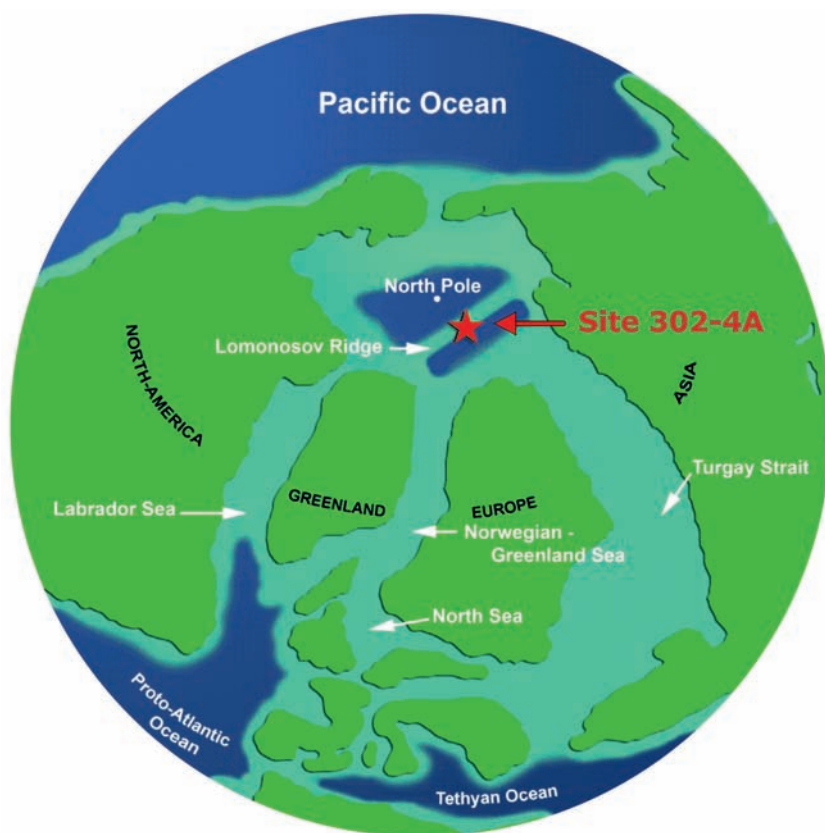


Figure 7.1 | Paleogeographical map of the Late Palaeocene - Early Eocene Central Arctic Basin, showing the position of IODP Hole 302-4A (modified from *Sluijs et al. (2009)*)

methyl-5-(1,1-d₂-hexadecyl)thiophene] was added to the total extract aliquots for quantitative analyses. Subsequently, the desulfurized total extracts were separated into polar and apolar fractions using a small column with activated alumina using hexane/DCM (9:1 v/v) and MeOH/DCM (1:1 v/v) as eluents, respectively. The apolar desulfurized fractions containing the released hydrocarbons, were hydrogenated using PtO₂/H₂ and analyzed by gas chromatography (GC) and GC/mass spectrometry (MS). GC analyses were performed using a Hewlett-Packard 6890 instrument equipped with a flame ionization detector (FID), a Flame Photometric Detector (FPD), and an on-column injector. A fused silica capillary column (25 m x 0.32 mm) coated with CP-Sil 5 (film thickness 0.12 µm) was used with helium as carrier gas. The oven was programmed at a starting (injection) temperature of 70 °C, which rose to 130 °C at 20 °C/min and then to 320 °C at 4 °C/min, at which it was maintained for 20 min. GC/MS analysis was done using a ThermoFinnigan

TRACE gas chromatograph using similar GC conditions as described above. The gas chromatograph was coupled with a Thermofinnigan DSQ quadrupole mass spectrometer with ionization energy of 70 eV and fractions were analyzed in full scan mode with a mass range of m/z 50-800 at three scans per second.

To prevent co-elution, *n*-alkanes were removed from the apolar fraction using a small column containing silicalite and cyclohexane as eluent (West *et al.*, 1990), before biomarker $\delta^{13}\text{C}$ analyses. The samples were analyzed on a Finnigan Delta V isotope ratio monitoring mass spectrometer coupled to an Agilent 6890 GC. Samples, dissolved in *n*-hexane, were analyzed using GC under conditions as described above. All carbon isotope compositions for the individual components are reported relative to the Vienna Pee Dee Belemnite (VDPB) standard and are average values of at least two runs.

7.3 RESULTS

7.3.1 Biomarker composition

Analysis of selected apolar fractions of sediments in the studied ETM2 interval showed a relatively high abundance of organic sulfur compounds (OSCs), such as C_{25} HBI thiolanes (Kohnen *et al.*, 1990) and a C_{35} hopanoid thiophene (Valisoulas *et al.*, 1984). The presence of these low molecular weight organic sulfur compounds suggests that sulfur has reacted with functionalized labile lipids and likely indicates the presence of more complex, higher molecular weight, organic sulfur compounds (Sinninghe Damsté & de Leeuw, 1990), which can potentially bias the distribution of biomarkers in apolar fractions (Kohnen *et al.*, 1991). Therefore, to release all S-bound carbon skeletons we desulfurized the total extracts using Raney Nickel (Sinninghe Damsté *et al.*, 1988). Apolar fractions of the desulfurized extracts contain mostly S-bound hydrocarbons, including $5\alpha\text{-C}_{27}\text{-C}_{29}$ steranes, $\text{C}_{30}\text{-C}_{35}$ hopanes, a C_{25} HBI and isorenieratane, predominantly with the $17\beta,21\beta(\text{H})$ configuration, and some free hydrocarbons, i.e. *n*-alkanes with a slight odd-over-even carbon number predominance (see **figure 7.2** for a typical gas chromatogram of one of the samples). We focused on five biomarkers for quantification and isotopic study (**Figs. 7.2 and 7.3**). S-bound phytane is an early diagenetic product of S-bound phytol (Brassell *et al.*, 1986). Whereas phytol is part of the chlorophyll *a* molecule, and consequently characteristic for all primary producers using photosynthesis, including cyanobacteria. It is unlikely that this sulfur-bound phytane derives from terrestrial chlorophyll as sulfur-incorporation occurs during early diagenesis, i.e. almost immediately after burial (e.g. Sinninghe Damsté & de Leeuw, 1990). Furthermore, S-bound phytane has a different isotopic composition than that of 'free' phytane showing its different origin (Kohnen *et al.*, 1992; Koopmans *et al.*, 1999). S-bound C_{25} HBI is derived from unsaturated C_{25} HBIs, which are synthesized by diatoms (Volkman *et al.*, 1994) and serves as a biomarker for four specific diatom

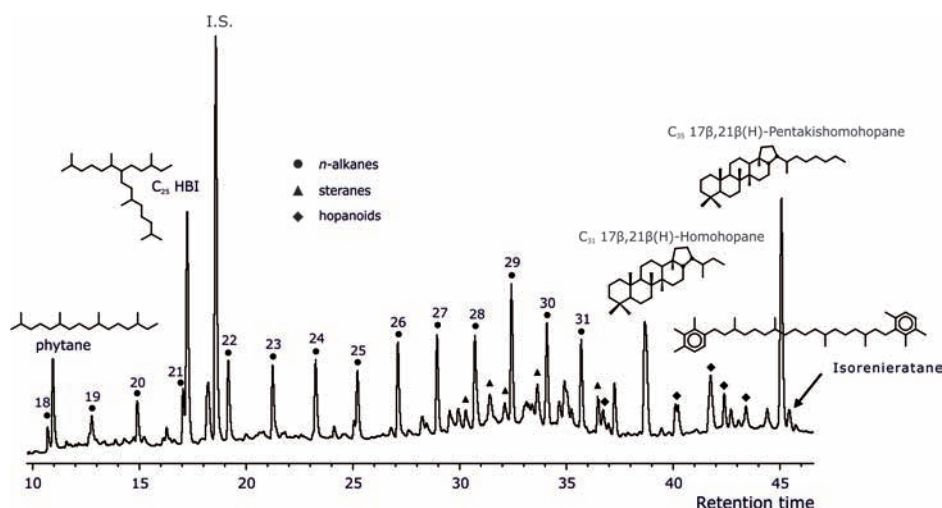


Figure 7.2 Gas chromatogram of the desulfurized apolar fraction of sample 302-4A-27X-1, 118-120. Indicated are the *n*-alkanes (circles), C_{27} - C_{29} steranes (triangles) and C_{30} - C_{35} hopanes (diamonds). Indicated at the corresponding peaks are the chemical structures of the S-bound of which the concentrations and $\delta^{13}C$ values are analysed.

genera (*Rhizosolenia*, *Haslea*, *Navicula*, and *Pleurosigma*) (Sinninghe Damsté *et al.*, 2004a and references therein). S-bound C_{31} 17 β ,21 β (H)-homohopane and S-bound C_{35} 17 β ,21 β (H)-pentakishomohopane derive from derivatives of the membrane lipid bacteriohopanepolyol. These compounds are produced by a large number of aerobic bacteria, including cyanobacteria (Rohmer *et al.*, 1992; Talbot *et al.*, 2008 and references therein), but have also been found in some strictly anaerobic bacterial groups (Fischer *et al.*, 2005; Sinninghe Damsté *et al.*, 2004b). The source of these compounds is therefore uncertain. We did not detect any 2-methyl hopanoids, which are considered to be specific for most, although not all, cyanobacteria (Summons *et al.*, 1999) and therefore a cyanobacterial origin for S-bound C_{35} hopane cannot be confirmed. However, it is often presumed, based on isotopic studies, that C_{35} hopane in marine sediments is mainly derived from cyanobacteria (Schoell *et al.*, 1994; Sinninghe Damsté *et al.*, 2008). Previously, we reported the presence of low amounts of S-bound isorenieratane in sediments between 368.9 and 367.9 mcd (Sluijs *et al.*, 2009). The precursor of S-bound isorenieratane is the diaromatic carotenoid isorenieratene. This pigment is produced by the brown strain of green sulfur bacteria, which are anaerobic photoautotrophs that thrive under euxinic (high free sulfide and low oxygen) conditions within the photic zone (Sinninghe Damsté *et al.*, 1993). In summary, it is likely that the selected biomarkers, except for S-bound isorenieratane, are all derived from marine primary producers, particularly as they are sulfur-bound and thus derived from labile precursors. Hence, they can provide insight into the response of these groups of organisms during ETM2 in the Arctic Ocean.

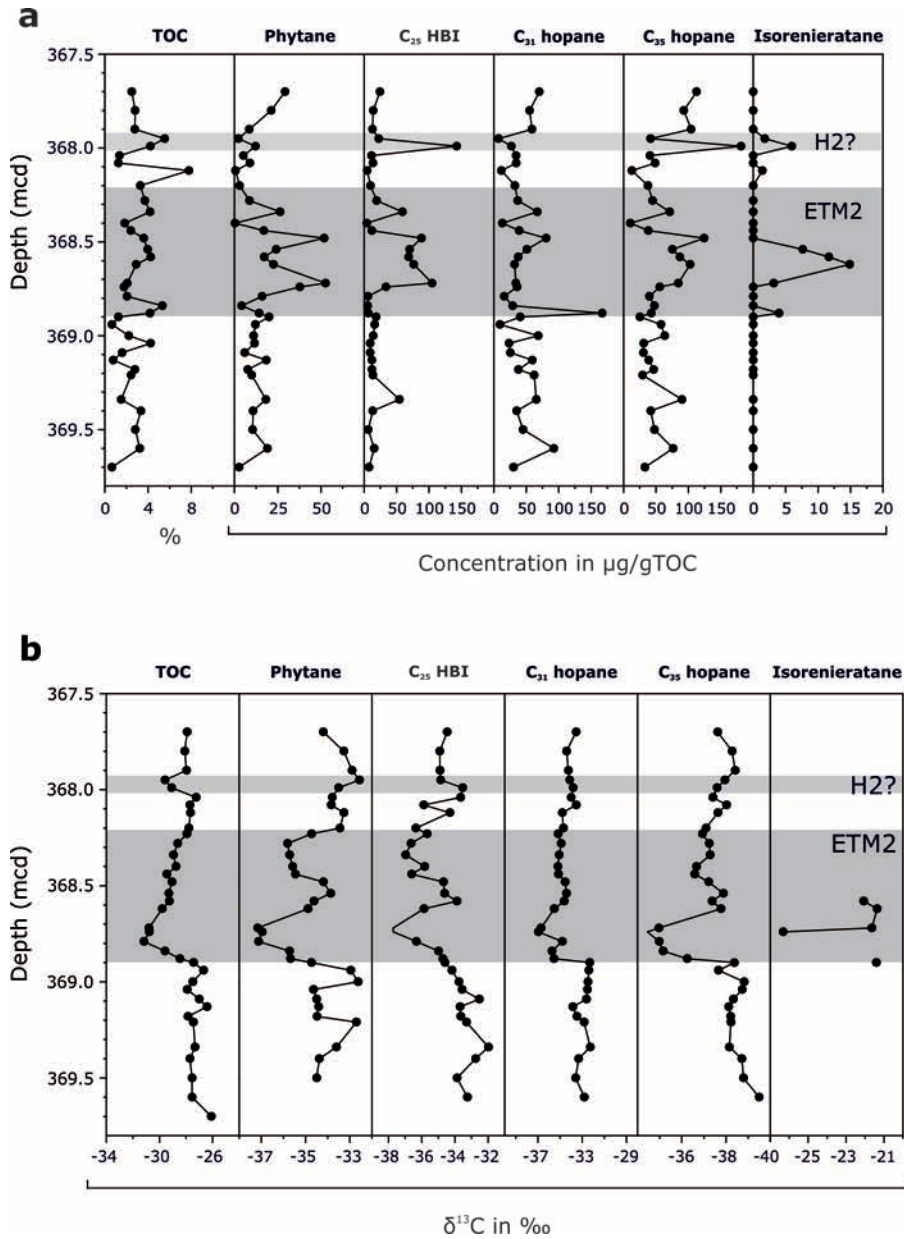


Figure 7.3 | Concentration profiles (a) and stable carbon isotope profiles (b) of TOC (Shuijs *et al.*, 2009) and the specific S-bound biomarkers phytane, C_{25} HBI, C_{31} hopane, C_{35} hopane and isorenieratane. The concentrations are given in $\mu\text{g/g C}$ and $\delta^{13}\text{C}$ values are in ‰ VPDB.

Table 7.1 | Relative abundances of TOC (in %) and S-bound biomarkers (in $\mu\text{g/g C}$).

Sample	Depth (m)	TOC (%)	Phytane	C_{25} HBI	C_{31} hopane	C_{35} hopane	isorenieratane
			$\mu\text{g/gC}$				
302-4-27X1-30-31	367.70	2.5	29.3	24.4	70.2	112.8	n.d.
302-4-27X1-40-41	367.80	2.8	21.3	14.2	55.2	93.2	n.d.
302-4-27X1-50-51	367.90	2.8	8.6	12.8	58.9	104.2	n.d.
302-4-27X1-55-57	367.95	5.6	2.3	22.5	7.4	41.8	1.8
302-4-27X1-59-61	367.99	4.2	12.2	142.9	27.1	181.2	6.0
302-4-27X1-64-66	368.04	1.4	5.2	11.3	34.5	40.8	n.d.
302-4-27X1-68-70	368.48	1.3	9.0	13.8	34.6	48.8	n.d.
302-4-27X1-72-74	368.12	7.8	0.7	4.7	11.8	12.9	1.4
302-4-27X1-80-82	368.20	3.3	3.0	9.8	32.6	37.7	n.d.
302-4-27X1-88-90	368.28	3.7	8.7	19.3	37.0	44.8	n.d.
302-4-27X1-94-96	368.34	4.2	26.4	59.1	67.1	71.2	n.d.
302-4-27X1-100-102	368.40	1.9	0.3	4.3	13.2	10.6	n.d.
302-4-27X1-104-106	368.44	2.4	17.0	12.0	39.3	38.3	n.d.
302-4-27X1-108-110	368.48	3.6	51.9	88.4	80.8	124.4	n.d.
302-4-27X1-114-116	368.54	4.0	24.2	70.3	51.0	75.4	7.6
302-4-27X1-118-120	368.58	4.3	17.2	68.7	37.8	87.1	11.7
302-4-27X1-122-124	368.62	2.9	22.6	76.5	32.1	102.8	14.9
302-4-27X1-132-134	368.72	2.1	52.7	104.9	34.2	84.5	3.2
302-4-27X1-134-136	368.74	1.8	37.8	33.8	35.8	56.0	n.d.
302-4-27X1-139-141	368.79	2.1	16.0	5.9	16.0	39.9	n.d.
302-4-27X1-144-146	368.84	5.3	4.2	5.5	29.1	47.7	n.d.
302-4-27X1-148-150	368.88	4.2	14.3	6.6	167.0	42.9	4.0
302-4-27X2-0-2	368.90	1.3	20.1	18.4	40.7	25.3	n.d.
302-4-27X2-4-6	368.94	0.7	12.2	16.2	9.5	58.0	n.d.
302-4-27X2-12-14	369.00	2.2	11.1	14.1	68.6	63.5	n.d.
302-4-27X2-14-16	369.04	4.3	11.7	9.5	23.5	31.3	n.d.
302-4-27X2-19-21	369.09	1.6	6.0	9.4	25.6	30.7	n.d.
302-4-27X2-23-25	369.13	0.8	18.4	12.1	59.5	38.9	n.d.
302-4-27X2-28-30	369.18	2.8	7.7	12.0	38.0	46.7	n.d.
302-4-27X2-31-33	369.21	2.4	10.0	13.6	62.3	29.6	n.d.
302-4-27X2-44-45	369.34	1.5	18.1	54.4	65.6	90.3	n.d.
302-4-27X2-50-51	369.40	3.4	10.8	13.3	35.2	42.0	n.d.
302-4-27X2-60-61	369.50	2.8	10.6	6.4	45.1	47.8	n.d.
302-4-27X2-70-72	369.60	3.2	19.1	15.5	92.6	76.7	n.d.
302-4-27X2-80-81	369.70	0.7	2.7	7.5	30.3	33.0	n.d.

^apreviously published in *Shajir et al. (2009)*

In the interval just below the CIE, concentrations of phytane and C_{25} HBI, both indicators for marine phytoplankton, are low ($<15 \mu\text{g/g TOC}$; **Table 7.1** and **Fig. 7.3a**). In contrast, both bacterial biomarkers, the C_{31} and C_{35} hopane, are relatively abundant ($>45 \mu\text{g/g TOC}$), while isorenieratane is below detection limit. Across the onset of the CIE, all biomarker concentrations remain relatively low, except for a short-lived increase in C_{31} hopane concentrations (up to $\sim 170 \mu\text{g/g TOC}$) at ~ 368.88 mcd. This coincides with the first detection of isorenieratane ($\sim 4 \mu\text{g/g TOC}$). Immediately after the peak of the CIE, at ~ 368.72 mcd, phytane, C_{35} hopane and the C_{25} HBI concentrations sharply increase, with peak values of

Table 7.2 | Stable carbon isotopic composition (in ‰ VPDB) of TOC and S-bound biomarkers.

Sample	Depth (m)	TOC (%)	Phytane	C ₂₅ HBI	C ₃₁ hopane	C ₃₅ hopane	isorenieratane
			$\delta^{13}\text{C}$ (‰)				
302-4-27X1-30-31	367.70	-27.9	-34.2	-34.5	-33.5	-32.4	
302-4-27X1-40-41	367.80	-28.1	-33.3 ± 0.1	-34.9 ± 0.0	-34.4 ± 0.2	-31.7 ± 0.1	
302-4-27X1-50-51	367.90	-28.0	-32.9	-34.9	-34.2 ± 0.5	-31.6 ± 0.2	
302-4-27X1-55-57	367.95	-29.6	-32.6 ± 0.1	-34.9 ± 0.2	-34.1 ± 0.3	-32.0 ± 0.6	
302-4-27X1-59-61	367.99	-29.1	-33.5 ± 0.1	-33.5 ± 0.1	-33.8 ± 0.4	-32.4 ± 0.3	
302-4-27X1-64-66	368.04	-27.2	-33.8 ± 0.1	-33.7 ± 0.1	-34.0 ± 0.3	-32.6 ± 0.2	
302-4-27X1-68-70	368.48	-27.7	-33.8 ± 0.0	-35.9	-33.5 ± 0.8	-32.0 ± 0.5	
302-4-27X1-72-74	368.12	-27.7	-33.3	-34.3 ± 0.3	-34.8 ± 0.5	-32.4 ± 0.0	
302-4-27X1-80-82	368.20	-27.8	-33.4 ± 0.5	-36.3 ± 0.3	-34.7 ± 0.1	-32.9 ± 0.3	
302-4-27X1-88-90	368.28	-27.9	-34.7 ± 0.3	-35.7 ± 0.2	-35.2 ± 0.2	-33.1 ± 0.1	
302-4-27X1-94-96	368.34	-28.6	-35.8 ± 0.1	-36.6 ± 0.0	-34.9 ± 0.0	-32.8 ± 0.1	
302-4-27X1-100-102	368.40	-28.9	-35.7 ± 0.1	-37.0 ± 0.4	-35.1 ± 0.2	-32.7 ± 0.3	
302-4-27X1-104-106	368.44	-28.8	-35.6	-35.8 ± 0.0	-35.2	-33.3 ± 0.4	
302-4-27X1-108-110	368.48	-29.4	-35.5 ± 0.1	-36.6 ± 0.1	-35.1 ± 0.3	-33.4 ± 0.2	
302-4-27X1-114-116	368.54	-29.1	-34.2 ± 0.3	-34.7 ± 0.4	-34.5 ± 0.1	-32.8 ± 0.2	
302-4-27X1-118-120	368.58	-29.3	-33.9 ± 0.1	-34.6 ± 0.1	-34.4 ± 0.2	-32.1 ± 0.3	-22.1 ± 0.5
302-4-27X1-122-124	368.62	-29.3	-34.6 ± 0.1	-33.9 ± 1.2	-34.6 ± 0.3	-32.6 ± 0.3	-21.4 ± 1.2
302-4-27X1-132-134	368.72	-29.8	-34.9 ± 0.0	-35.9 ± 0.0	-35.5 ± 0.1	-32.2 ± 0.0	-21.6 ± 0.3
302-4-27X1-134-136	368.74	-30.8	-37.2 ± 0.1	-37.7 ± 0.0	-36.7 ± 0.3	-35.0 ± 0.1	-26.3
302-4-27X1-139-141	368.79	-30.8	-37.0 ± 0.1	-37.7 ± 0.1	-37.0 ± 0.3	-35.5 ± 0.2	
302-4-27X1-144-146	368.84	-31.2	-37.1 ± 0.3	-36.3 ± 0.1	-34.8 ± 0.1	-35.0 ± 0.0	
302-4-27X1-148-150	368.88	-29.6	-35.7 ± 1.0	-35.0 ± 0.6	-35.7 ± 0.3	-34.8 ± 0.3	
302-4-27X2-0-2	368.90	-28.5	-35.7 ± 0.4	-34.7 ± 0.3	-35.5 ± 0.1	-33.8 ± 0.2	-21.4 ± 0.1
302-4-27X2-4-6	368.94	-27.4	-34.7 ± 0.0	-34.6 ± 0.4	-32.3 ± 0.1	-31.6 ± 0.1	
302-4-27X2-12-14	369.00	-26.7	-33.0 ± 0.7	-34.2	-32.4	-32.3 ± 0.1	
302-4-27X2-14-16	369.04	-27.5	-32.6 ± 0.5	-33.8 ± 0.4	-32.5 ± 0.2	-31.2 ± 0.1	
302-4-27X2-19-21	369.09	-27.9	-34.6 ± 0.2	-33.7 ± 0.1	-32.5 ± 0.1	-31.3 ± 0.1	
302-4-27X2-23-25	369.13	-27.0	-34.5	-32.5	-32.6 ± 0.4	-31.7 ± 0.6	
302-4-27X2-28-30	369.18	-26.4	-34.4 ± 0.2	-33.7	-33.8 ± 0.2	-31.9 ± 0.2	
302-4-27X2-31-33	369.21	-27.8	-34.5 ± 0.8	-33.6 ± 0.5	-33.5 ± 0.3	-31.8 ± 0.1	
302-4-27X2-44-45	369.34	-27.5	-32.7 ± 0.3	-33.3 ± 0.1	-32.8 ± 0.1	-31.8 ± 0.1	
302-4-27X2-50-51	369.40	-27.3	-33.6	-32.0 ± 0.2	-32.3 ± 0.9	-31.8 ± 0.2	
302-4-27X2-60-61	369.50	-27.7	-34.4 ± 0.1	-32.8 ± 0.4	-33.3 ± 0.3	-31.3 ± 0.3	
302-4-27X2-70-72	369.60	-27.6	-34.5 ± 0.6	-33.9 ± 0.3	-33.6 ± 0.0	-31.2 ± 0.1	
302-4-27X2-80-81	369.70	-27.5		-33.2 ± 0.3	-32.8 ± 0.4	-30.5 ± 0.3	

~50, ~100, and ~120 µg/g TOC, respectively. Isorenieratane is detected between 368.74 and 368.48 mcd, with peak concentrations of ~15 µg/g C at 368.62 mcd (*Sluijs et al.*, 2009).

Concentrations of phytane, the C₂₅ HBI and C₃₅ hopane are relatively high during this interval, but are relatively low at ~368.62 mcd where the isorenieratane concentration reaches its maximum. The C₃₁ hopane abundance remains relatively constant across the interval of detectable isorenieratane. Above 368.48 mcd, all biomarker concentrations return towards the “background” pre-ETM2 values. However, elevated isorenieratane, C₂₅ HBI and C₃₅ hopane concentrations reoccur

between 367.99 and 367.90 mcd. This interval also exhibits a negative excursion in $\delta^{13}\text{C}_{\text{TOC}}$ (**Fig. 7.3b**) and was therefore suggested by *Sluijs et al.* (2009) as a potential candidate for the H2 event (*Cramer et al.*, 2003), which has recently been shown to also reflect a hyperthermal (*Stap et al.*, 2010).

7.3.3 Compound-specific stable carbon isotope analysis

Stable carbon isotope analyses were performed, where possible, on phytane and C_{25} HBI as biomarkers for marine photosynthetic algae, and on C_{31} hopane and C_{35} hopane as biomarkers for (cyano)bacteria (**Fig. 7.3b** and **Table 7.2**). We were able to determine the $\delta^{13}\text{C}$ composition of isorenieratane for the sediments at 368.88 and 368.72–368.54 mcd (**Table 7.2**). Isorenieratane $\delta^{13}\text{C}$ values are 11–14 ‰ enriched relative to phytane in the same samples. Green sulfur bacteria use the reversed tricarboxylic acid cycle that discriminates much less against ^{13}C than the Calvin cycle, which is used by most photoautotrophic organisms (*Quandt et al.*, 1977). An enrichment of this magnitude for isorenieratane can therefore be expected and is consistent with previous observations (*Koopmans et al.*, 1996; *van der Meer et al.*, 1998).

Prior to the CIE of ETM2, the carbon isotope values are relatively stable, i.e. -27.3 ± 0.6 ‰ for TOC, -33.9 ± 0.8 ‰ for phytane, -33.2 ± 0.7 ‰ for C_{25} HBI, -32.9 ± 0.5 ‰ for C_{31} hopane and -31.5 ± 0.5 ‰ for C_{35} hopane. The drop in $\delta^{13}\text{C}$ of the analyzed specific biomarkers is essentially synchronous with the onset of the CIE in TOC (*Sluijs et al.*, 2009), confirming the initiation of the CIE at ~ 368.9 mcd. This drop is ~ 3.2 and ~ 4.5 ‰ for the algal biomarkers phytane and C_{25} HBI respectively, and ~ 4.1 ‰ for both the C_{31} and C_{35} hopane. Except for phytane, the magnitudes of the shifts are slightly higher than the ~ 3.5 ‰ shift in TOC.

Between 368.72 and 368.23 mcd, the $\delta^{13}\text{C}_{\text{TOC}}$ record shows a gradual recovery towards ‘background’ pre-ETM2 values. Interestingly, the biomarker $\delta^{13}\text{C}$ records show a more complex pattern (**Fig. 7.3b**). An initial increase in $\delta^{13}\text{C}$ values at ~ 368.7 mcd, is followed by a second drop in $\delta^{13}\text{C}$ between 368.48 and 368.23 mcd for phytane and C_{25} HBI. At 368.2 mcd all biomarkers have returned to their ‘background’, i.e. pre-ETM2 values. The potential presence of H2, based on the $\delta^{13}\text{C}_{\text{TOC}}$ record, is not apparent in the $\delta^{13}\text{C}$ records of any of the analyzed biomarkers.

7.4 DISCUSSION

7.4.1 Climatic and environmental changes across ETM2 in the Arctic Ocean

Prior to the onset of ETM2, both the biomarker concentrations and $\delta^{13}\text{C}$ values show only minor variations, suggesting that environmental conditions were relatively stable (**Figs. 7.3a and b**). Furthermore, no isorenieratane is detected in these sediments implying that the water column was not euxinic within the photic zone. This is also supported by relatively stable assemblages of typical open marine

dinoflagellate cysts in this interval (*Sluijs et al.*, 2009). Relatively high TOC concentrations and the presence of “sulfur-bound” organic molecules in these sediments points towards a relatively productive palaeoenvironment and low bottom water oxygen concentrations, which is in agreement with previous observations (*Sluijs et al.*, 2008; *Stein et al.*, 2006).

The synchronous drop in $\delta^{13}\text{C}$ at ~ 368.9 mcd of both the specific biomarkers and TOC confirms that the CIE in TOC is not caused by changes in the composition of the bulk organic matter, but is linked to the injection of ^{13}C -depleted carbon into the global exogenic carbon pool. During the recovery of ETM2, the $\delta^{13}\text{C}$ of the biomarkers no longer track the $\delta^{13}\text{C}_{\text{TOC}}$ profile. The $\delta^{13}\text{C}_{\text{TOC}}$ record shows a smooth return to background $\delta^{13}\text{C}$ values from 368.8 mcd, while the $\delta^{13}\text{C}$ profiles of the biomarkers abruptly move towards more positive values at 368.6 mcd (**Fig. 7.3b**). Additionally, directly after the CIE, at ~ 368.7 mcd, there is a sharp increase in concentrations of phytane, C_{25} HBI and C_{35} hopane, which is followed by the development of photic zone euxinia (PZE) as indicated by the presence of isorenieratene derivatives. Possibly, enhanced productivity contributed to the development of PZE conditions in this interval, as was suggested for ETM2 and the PETM in the Arctic Ocean (*Sluijs et al.*, 2006, 2009; *Stein et al.*, 2006). The increase in biomarker concentrations may also be explained by an increase in export production. However, *Knies et al.* (2008) investigated the response of marine productivity to variations in nutrient supply to the Cenozoic Arctic Ocean using nitrogen isotopes. For ETM2 they found evidence for an increase in primary production rates even after correcting for the higher burial efficiency caused by the euxinic conditions. Furthermore, abundances of the freshwater tolerant dinoflagellate species that peak synchronously with isorenieratane concentrations are also regarded as indicators for nutrient-rich conditions (*Sluijs et al.*, 2005, 2009). Although the timing with these dinoflagellate peaks is not perfectly synchronous, an increase in primary productivity could explain the increase in biomarker concentrations and the positive isotope shift in the specific biomarkers at 368.6 mcd, as an increase in primary productivity can lead to increased growth rates and decreased isotopic fractionation (*Jasper & Hayes*, 1990; *Laws et al.*, 1995; *Bidigare et al.*, 1997; *Popp et al.*, 1998b). Therefore, although the lipids obviously had to be exported from the surface ocean to settle on the seafloor, the increase in concentrations in our view was at least partially related to increased productivity. This would imply that during this interval regional effects control the biomarker records, whereas TOC in this case more accurately tracks the $\delta^{13}\text{C}$ evolution of the exogenic carbon pool.

At ~ 368.48 mcd, biomarker concentrations decrease and isorenieratane is below detection limit (**Fig. 7.3a**), suggesting that the PZE conditions ended. Subsequently, all biomarker isotope values return to ‘background’ pre-ETM2 values and continue to track the $\delta^{13}\text{C}_{\text{TOC}}$ signal (**Fig. 7.3b**).

7.4.2 H2-event

At ~368.0 mcd the TOC record exhibits a second negative CIE of ~2 ‰ (Fig. 7.3b). This interval was previously interpreted to possibly reflect the H2 event, although a potential hiatus and the absence of a biostratigraphic framework with sufficient detail complicates exact identification (Sluijs *et al.*, 2009). Indeed, the presence of isorenieratane coincident with the dominance of low-salinity-tolerant dinoflagellate species (Sluijs *et al.*, 2009), points to similar conditions as for ETM2. Remarkably, however, there is no negative carbon isotope shift in the biomarker $\delta^{13}\text{C}$ records. There are two possible explanations for this apparent discrepancy: (1) The negative $\delta^{13}\text{C}$ shift in TOC records an isotope excursion of the global exogenic carbon pool, but is obscured in the $\delta^{13}\text{C}$ records of the biomarkers because of an increase in productivity, although this likely should have affected $\delta^{13}\text{C}_{\text{TOC}}$ as well. (2) The shift in the $\delta^{13}\text{C}_{\text{TOC}}$ record is not recording a CIE but is caused by a change in source material transported towards the Arctic Basin. None of these explanations can be completely excluded and, thus, the nature of this interval cannot be further elucidated based on the $\delta^{13}\text{C}$ profiles of these marine biomarkers.

7.4.3 Estimating isotopic fractionation across ETM2

Based on the measured stable isotopic composition of S-bound phytane, C_{25} HBI and C_{35} hopane, we estimated the average carbon isotopic fractionation of photoautotrophs, and changes therein. Averaged $\delta^{13}\text{C}$ values were calculated for three time intervals: the pre-ETM2 interval (369.60-368.94 mcd), the CIE of ETM2 (368.84-368.72 mcd), and the post-ETM2 interval (368.20-368.04 mcd). Average biomarker $\delta^{13}\text{C}$ values for these three periods were used to estimate the isotopic fractionation (ϵ_p):

$$\epsilon_p = 10^3 [(\delta_d + 1000)/(\delta_p + 1000) - 1] \quad (\text{eq. 7.1})$$

where δ_p is the $\delta^{13}\text{C}$ value of the total organic carbon of the organism and δ_d is the $\delta^{13}\text{C}$ value of the carbon substrate. To obtain δ_p , a correction must be made for the isotopic offset between the biomarker lipid and cell biomass. Schouten *et al.* (1998a) and Oakes *et al.* (2005) reported, based on culture experiments and literature study of a range of different algae, that phytol is ~6 ‰ depleted relative to the total algal biomass. For C_{25} HBIs a depletion of 6.6 ‰ relative to biomass was reported by Schouten *et al.* (1998a) for the diatom *Rhizosolenia setigera*, whereas Massé *et al.* (2004) found similar carbon isotopic compositions of the C_{25} HBIs and phytol in *Haslea ostrearia*. This suggests an isotopic offset of ca. 6 ‰ for both phytane and C_{25} HBI. Results from culture experiments of the cyanobacterium species *Synechocystis* revealed an isotopic offset of 8.4 ‰ for bishomohopanol (Sakata *et al.*, 1997).

Values for δ_d can be obtained from the carbonate shells of planktonic foraminifera using the following equation:

$$\delta_d \approx \delta^{13}\text{C}_{\text{pr}} - 1 + (24.12 - 9866/T) \quad (\text{eq. 7.2})$$

The $\delta^{13}\text{C}$ of planktonic foraminifera ($\delta^{13}\text{C}_{\text{pf}}$) represents the $\delta^{13}\text{C}$ composition of the primary carbon in CaCO_3 . The term between brackets describes the isotopic effect associated with the equilibrium exchange reaction between $\text{CO}_{2\text{aq}}$ and HCO_3^- as reported by *Mook et al.* (1974), which only depends on temperature (T in degrees Kelvin).

Unfortunately, foraminiferal carbonate is absent in ACES sediments (*Shuijs et al.*, 2008, 2009). Instead, we used the $\delta^{13}\text{C}$ values of the surface-dwelling genus *Acarinina* reported for ETM2 at Walvis Ridge (*Lourens et al.*, 2005; *Stap et al.*, 2010). Although this induces one factor of uncertainty, the $\delta^{13}\text{C}_{\text{pf}}$ of $\sim 2\text{‰}$ for the period prior to ETM2 compares quite well with those of stacked carbonate isotope records, as well as with modeling studies for the Early Eocene (*Hayes et al.*, 1999; *Berner*, 2001, 2006), suggesting that this assumption is reasonable. We do not believe that in the semi-enclosed Arctic Basin additional effects, such as the input of recycled CO_2 from anoxic deep waters play a large role. *Van Breugel et al.* (2006) demonstrated that in an anoxic marine system the effect of recycling of respired CO_2 on the $\delta^{13}\text{C}$ of phytoplankton lipids is negligible. Sea surface temperatures (SSTs) used in Eq. 2 were obtained from the oxygen isotopes of the same foraminiferal records from Walvis Ridge and a TEX_{86} measurement during ETM2 (*Stap et al.*, 2010).

The calculated ϵ_p values for the pre-excursion interval show remarkably high carbon isotope fractionation factors of ca. 21–22 ‰ and ca. 14.5 ‰ for marine algae and (cyano)bacteria, respectively (**Table 7.3**). The lower value determined for (cyano)bacteria is consistent with the smaller carbon isotopic fractionation by cyanobacteria in comparison to algae (*Hayes*, 2001; *Popp et al.*, 1998b). During ETM2, ϵ_p values increase even further by 1–2 ‰. For all three biomarkers this results in ϵ_p values that lie close to the maximum fractionation of photoautotrophic organisms, i.e. 25–28 ‰ for the Rubisco enzyme of autotrophic eukaryotes (*Bidigare et al.*, 1997; *Goericke et al.*, 1994; *Popp et al.*, 1998b) and 16–22 ‰ for autotrophic cyanobacteria (*Sakata et al.*, 1997 and references cited therein).

The magnitude of ϵ_p is mainly determined by the carbon fixation enzyme and carbonate concentration mechanism, which in turn can be affected by factors such as the amount of available CO_2 in the water column ($[\text{CO}_{2\text{aq}}]$), growth rate, light intensity, and species-specific factors such as cell-geometry (e.g. *Jasper & Hayes*, 1990; *Laws et al.*, 1995; *Popp et al.*, 1998b; *Cassar et al.*, 2006). Thus, in principle, the observed increase in biomarker ϵ_p values during ETM2 can be caused by increased levels of $[\text{CO}_{2\text{aq}}]$, but there are several additional factors which may be potentially responsible for this. The most important ones are a decrease in specific growth rates, a change in cell geometry, a change in light intensity, and the carbon uptake mechanism (*Bidigare et al.*, 1997; *Laws et al.*, 1995; *Popp et al.*, 1998b; *Rau et al.*, 1997; *Burkhardt et al.*, 1999). It is unlikely that cell geometry has changed on this

Table 7.3 | Estimates for $p\text{CO}_2$ based on the $\delta^{13}\text{C}$ composition of S-bound phytane, C_{25} HBI, and C_{35} hopane

Biomarker	$\delta^{13}\text{C}^a$ (‰)	$\Delta\delta^b$ (‰)	δ_p^c (‰)	$\delta^{13}\text{C}_{\text{pl}}^d$ (‰)	SST-WR ^e (°C)	SST-AO ^f (°C)	δ_d^g (‰)	ϵ_p^h (‰)	ϵ_f^i (‰)	K_0 (mol L ⁻¹ atm ⁻¹)	$p\text{CO}_2^k$ (ppmv)			
											$b = 160$	$b = 200$	$b = 240$	
<i>pre-excursion interval (369.60-368.94 md)</i>														
S-bound phytane	-33.9 ± 0.4	6	-27.9	2	18.5	19	-8.7	19.7	25	0.03431	900	1100	1300	
S-bound phytane	-33.9 ± 0.4	6	-27.9	2	18.5	19	-8.7	19.7	27	0.03431	650	800	950	
S-bound C ₂₅ HBI	-33.3 ± 0.3	6	-27.3	2	18.5	19	-8.7	19.1	25	0.03431	800	1000	1200	
S-bound C ₂₅ HBI	-33.3 ± 0.3	6	-27.3	2	18.5	19	-8.7	19.1	27	0.03431	600	750	900	
S-bound C ₃₅ hopane	-31.5 ± 0.2	8.4	-23.1	2	18.5	19	-8.7	14.7	20	0.03431	900	1100	1350	
<i>Excursion interval (368.84-368.72 md)</i>														
S-bound phytane	-36.7 ± 0.4	6	-30.7	0	21.5	23	-10.4	21.0	25	0.0307	1300	1650	1950	
S-bound phytane	-36.7 ± 0.4	6	-30.7	0	21.5	23	-10.4	21.0	27	0.0307	850	1100	1300	
S-bound C ₂₅ HBI	-36.7 ± 0.2	6	-30.7	0	21.5	23	-10.4	20.9	25	0.0307	1300	1600	1900	
S-bound C ₂₅ HBI	-36.7 ± 0.2	6	-30.7	0	21.5	23	-10.4	20.9	27	0.0307	850	1100	1300	
S-bound C ₃₅ hopane	-35.1 ± 0.2	8.4	-26.7	0	21.5	23	-10.4	16.8	20	0.0307	1600	2000	2400	
<i>post-excursion interval (368.20-368.04 md)</i>														
S-bound phytane	-33.6 ± 0.2	6	-27.6	1.5	17.5	18	-9.3	18.8	25	0.0353	750	900	1100	
S-bound phytane	-33.6 ± 0.2	6	-27.6	1.5	17.5	18	-9.3	18.8	27	0.0353	550	700	850	
S-bound C ₂₅ HBI	-33.1 ± 0.2	6	-27.1	1.5	17.5	18	-9.3	18.2	25	0.0353	650	850	1000	
S-bound C ₂₅ HBI	-33.1 ± 0.2	6	-27.1	1.5	17.5	18	-9.3	18.2	27	0.0353	500	650	800	
S-bound C ₃₅ hopane	-32.5 ± 0.3	8.4	-24.1	1.5	17.5	18	-9.3	15.1	20	0.0353	900	1150	1400	

^aThe average $\delta^{13}\text{C}$ compositions of the indicated biomarkers^bThe isotopic offset between lipids and biomass for algae (Vehmanen *et al.*, 1998; Massé *et al.*, 2004; Oakes *et al.*, 2005) and for cyanobacteria (Sakata *et al.*, 1997)^cEstimated $\delta^{13}\text{C}$ composition of the primary photosynthate calculated from the $\delta^{13}\text{C}$ composition of the biomarkers and $\Delta\delta$ ^dAverage $\delta^{13}\text{C}$ composition of inorganic carbonate of the planktonic foraminifer *A. solidadensis* measured in sediments of Site 1263, 1265 and 1267 at Walvis Ridge (Laursen *et al.*, 2005; Sep *et al.*, 2010)^eAverage sea surface temperatures for Walvis Ridge obtained from the $\delta^{18}\text{O}$ composition of the planktonic foraminifer *A. solidadensis* (Sep *et al.*, 2010)^fAverage sea surface temperatures obtained from 'TEX' for the ACEX sediments at the Arctic Ocean (Mijic *et al.*, 2009)^gThe $\delta^{13}\text{C}$ composition of $\text{CO}_2(\text{aq})$ ^hThe calculated carbon isotopic fractionation associated with the photosynthetic fixation of carbonⁱThe maximum carbon isotopic fractionation associated with the photosynthetic fixation of carbon^jThe solubility constant K_h of Henry's Law from Weiss (1974)^kThe calculated atmospheric CO_2 concentrations for three different b -values

relative short time interval of the ETM2 for both the marine algae and (cyano) bacteria. Moreover, we also use S-bound phytane which is a biomarker not specific for only one group of organisms, but is contributed by many different species of marine algae and cyanobacteria. Furthermore, all available information indicates that productivity increased rather than decreased during ETM2 (see above), which theoretically should lead to a decrease of ϵ_p values. To avoid the imprint of growth rate changes on fractionation, we only used $\delta^{13}\text{C}$ values before, and directly after the interval where several lines of evidence, including elevated biomarker concentrations, indicated elevated productivity (see section 4.1).

Another important aspect to consider is the carbon uptake mechanism used by autotrophs during photosynthesis. Many photosynthetic organisms have evolved mechanisms to actively take up CO_2 or HCO_3^- (a so-called carbon concentrating mechanism or CCM) in order to overcome the deficiency of the enzyme Rubisco in low- CO_2 /high-alkaline environments and this mechanism will impact a reduced isotopic fractionation (Giordano *et al.*, 2005). In our case, however, the time of ETM2 most likely belonged to a high- CO_2 /low pH world, considering the large input of ^{13}C -depleted carbon, making it unlikely that they need a CCM. Furthermore, isotopic modeling which incorporates active transport show that ϵ_p is still a function of growth rate and CO_2 under nutrient limitation (though this function is different under light limitation (Cassar *et al.*, 2006). Finally, the very negative biomarker $\delta^{13}\text{C}$ values suggest that the organisms that made the lipids likely did not use a CCM, which has also been previously suggested for diatoms that biosynthesize HBI isomers (Schouten *et al.*, 2000a).

Growth experiments of aquatic algae indicate that light-limitation may also have a potential effect on isotopic fractionation (Burkhardt *et al.*, 1999; Cassar *et al.*, 2006). However, at this latitude it is likely that phytoplankton thrived only during summer in full light conditions, particularly with the absence of ice at this time. The only change in light conditions could appear when the water column is more stratified and fresher during ETM2, resulting in increasing light intensity and an increase in the magnitude of isotopic fractionation. However, the time of highest stratification, i.e. when isorenieratene derivatives are present, is some time after the CIE. In contrast, this interval is marked by slightly enriched ^{13}C values for the different biomarkers. This suggests that light limitation cannot explain the isotopic fractionation patterns we observe. We, therefore, mostly attribute the increase in ϵ_p to a substantial increase in $[\text{CO}_2(\text{aq})]$, in turn caused by elevated atmospheric $p\text{CO}_2$ levels during ETM2.

7.4.4 A first attempt to estimate $p\text{CO}_2$ for ETM2 using carbon isotopic fractionation factors

For alkenone-producing haptophytes the relationship between $[\text{CO}_2(\text{aq})]$ and ϵ_p is relatively well constrained (Pagani *et al.*, 2002a and references cited therein). There-

fore, stable carbon isotopic fractionation records using long-chain alkenones are frequently used for $p\text{CO}_2$ reconstructions (e.g. *Andersen et al.*, 1999; *Benthien et al.*, 1999; *Pagani et al.*, 1999, 2002a,b, 2005; *Bijl et al.*, 2010; *Palmer et al.*, 2010). However, *Popp et al.* (1998b) also reported a relation between $[\text{CO}_2(\text{aq})]$, growth rate and cell dimension for certain diatoms and cyanobacteria, although again other factors such as light intensity may play a role as well (*Burkhardt et al.*, 1999; *Cassar et al.*, 2006). This would imply that the carbon isotope composition of specific marine algal biomarkers, other than alkenones, may also be applicable for $p\text{CO}_2$ reconstructions. Indeed, ancient $p\text{CO}_2$ levels were determined by *Freeman & Hayes* (1992) using the carbon isotopic fractionations of sedimentary porphyrins (*Popp et al.*, 1989). Furthermore, variations in the offset between carbonate and organic matter isotopic composition have been applied as paleo- $p\text{CO}_2$ proxy to reconstruct the expected drawdown in atmospheric CO_2 during the late Cenomanian oceanic anoxic event (*Jarvis et al.*, 2011). Their trend in isotopic fractionation is remarkably consistent with previously estimated Cretaceous $p\text{CO}_2$ values using the $\delta^{13}\text{C}$ values of the specific marine biomarkers (S-bound) phytane and C_{35} hopane (*Bice et al.*, 2006; *Sinninghe Damsté et al.*, 2008).

Here we follow the approach of *Freeman & Hayes* (1992), *Bice et al.* (2006) and *Sinninghe Damsté et al.* (2008) to provide estimates of $p\text{CO}_2$ during the early Eocene ETM2 interval. Large uncertainties and assumptions which are associated with this approach will be discussed below. Our goal here is merely to present estimates of the atmospheric CO_2 concentrations and changes therein, which potentially can give insight in the changes of $p\text{CO}_2$ levels across an Eocene hyperthermal, and provide a method which can be used at other environmental settings where similar isotopic biomarker records can be obtained.

7.4.4.1 Calculation of $p\text{CO}_2$ estimates

In order to reconstruct the atmospheric CO_2 concentrations across ETM2 from carbon isotopic fractionation factors, we assume that the relationship between ϵ_p and $[\text{CO}_2(\text{aq})]$, based on the calibration of $\delta^{13}\text{C}$ composition of alkenones, is also applicable for $\delta^{13}\text{C}$ values of other biomarkers produced by photoautotrophic organisms, in this case S-bound phytane, C_{25} HBI and C_{35} hopane. If so, then the degree of isotopic fractionation (ϵ_p) in a cell can in theory be related to CO_2 concentrations using the following equation (*Bidigare et al.*, 1997):

$$\epsilon_p = \epsilon_f - b / [\text{CO}_2(\text{aq})] \quad (\text{eq. 7.3})$$

For haptophyte algae it has been shown that b displays a strong positive correlation with phosphate concentrations (*Andersen et al.*, 1999; *Benthien et al.*, 2002; *Bidigare et al.*, 1997; *Pagani*, 2002), and thus, if phosphate concentrations were known then b , and thereby $[\text{CO}_2(\text{aq})]$, could be estimated. A similar relation, with different b -values, is observed for other algae (*Popp et al.*, 1998b) and we assume here that

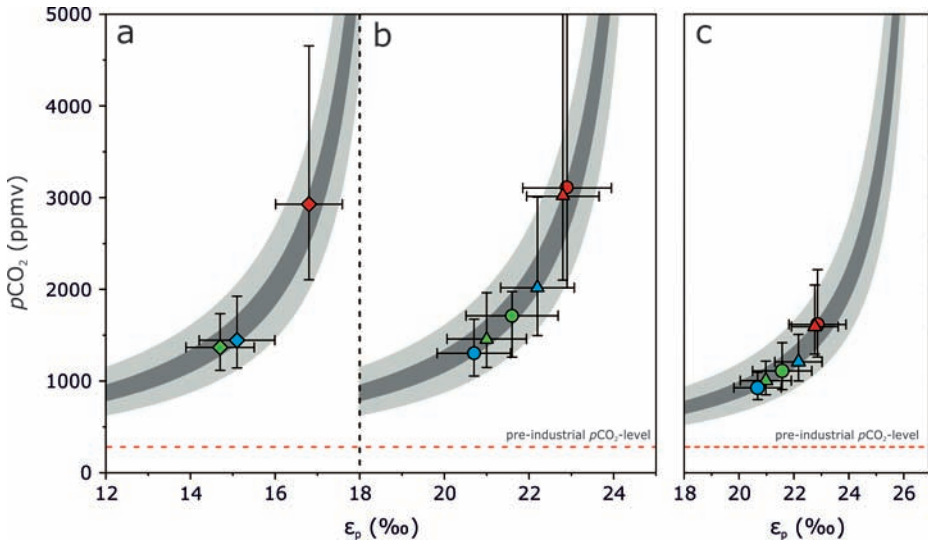


Figure 7.4 | Estimations of the atmospheric CO_2 concentrations for the pre-ETM2 interval (green symbols), CIE of ETM2 (red symbols) and the post-ETM2 interval (blue symbols) using: (a) the average $\delta^{13}\text{C}$ values of C_{35} hopane (diamonds) using a maximum fractionation level (ϵ_f) of 20 ‰; (b) the average $\delta^{13}\text{C}$ values of phytane (circles) and C_{25} HBI (triangles) with an ϵ_f of 25 ‰. (c) the average $\delta^{13}\text{C}$ values of phytane (circles) and C_{25} HBI (triangles) using an ϵ_f value of 27 ‰. Error bars include variations in SST and $\delta^{13}\text{C}_{\text{pr}}$ of 1 °C and 0.5 ‰, respectively, in addition to analytical errors. The grey shaded areas give the range of b (160-240) with $b=200$ as intermediate value. Note that the uncertainty of the $p\text{CO}_2$ estimates increases with higher ϵ_p values. Minimum $p\text{CO}_2$ values using this approach are 590, 860 and 520 ppmv for the pre-ETM2 interval, the CIE of ETM2 and the post-ETM2 interval, respectively. This is at least 2 to 3 times pre-industrial $p\text{CO}_2$ levels (blue dotted line).

b -values of these algae also depend on nutrients such as phosphate. However, it is difficult to predict the PO_4 concentrations of Arctic surface waters, especially considering the stratified conditions during ETM2. *Andersen et al.* (1999) reported an inverse relationship between the bulk nitrogen isotopes and phosphate concentrations in equatorial and south Atlantic core-top sediments. They used this relationship to reconstruct b and in turn the $p\text{CO}_2$ levels using their calibration of sedimentary $\delta^{13}\text{C}$ alkenones. As an approach to constrain the b -value for Eq. 7.3, we applied this relationship to the Early Eocene Arctic Ocean by using the nitrogen isotope values measured by *Knies et al.* (2008), leading to average phosphate concentrations of $1.25 \mu\text{mol L}^{-1}$ prior to ETM2 to $1.5 \mu\text{mol L}^{-1}$ just at the onset of ETM2. Depending on the calibration, this leads to a b -value ranging between 160 to 240. The $p\text{CO}_2$ estimates obtained using the approach outlined above are illustrated in **figure 7.4**. Here we plotted the $\epsilon_p - \text{CO}_2$ relationship of the algal biomarkers for the three time intervals at an intermediate b -value of 200. The error-bars include

uncertainties in SST ($\pm 1^\circ\text{C}$) and $\delta^{13}\text{C}_{\text{pf}}$ ($\pm 0.5\text{‰}$), in addition to the analytical errors. To illustrate the importance of b , we varied this parameter over a range of 160–240 (**Table 7.3** and **Fig. 7.4**). One has to bear in mind, though, that our $p\text{CO}_2$ estimates are based on the $\epsilon_{\text{p}} - [\text{CO}_2(\text{aq})]$ relationship originally calibrated for $\delta^{13}\text{C}$ alkenones (*Pagani et al.*, 2002a and references cited therein). In addition, we assume that the $\delta^{13}\text{C}_{\text{pf}}$ from Walvis Ridge is a representative of that in the Arctic Ocean during the ETM2. The propagated uncertainty stemming from these assumptions is difficult to quantify and is further discussed below.

For all three periods, the estimated $p\text{CO}_2$ values are practically similar using three independent biomarkers and all suggest that $p\text{CO}_2$ values were at least 2x pre-industrial values, i.e. the minimum $p\text{CO}_2$ estimates (considering all the uncertainties). Furthermore, when using the intermediate b -value, the estimated $p\text{CO}_2$ values are 800 to 1100 ppmv (3 to 4 x pre-industrial values) for the pre-excursion interval and 1100 to 2000 ppmv (4 to 7 x pre-industrial values) for the CIE of ETM2 (see **Table 7.3**). Thus, $p\text{CO}_2$ during ETM2 may have been 300 to 800 ppmv higher than prior to the ETM2.

7.4.4.2 Uncertainties, caveats and future outlook

Clearly, our estimated $p\text{CO}_2$ values are all associated with large uncertainties as indicated by the large error bars in **Fig. 7.4**, and we caution that they should not be taken at face value. As mentioned before these $p\text{CO}_2$ estimates are relying on a number of assumptions: (1) The $\delta^{13}\text{C}$ composition of the DIC ($\delta^{13}\text{C}_{\text{pf}}$ in Eq. 7.2) of the Arctic Ocean surface waters equals the surface water $\delta^{13}\text{C}$ of DIC of the subtropic SE Atlantic Ocean at Walvis Ridge during the Early Eocene; (2) The relationship between ϵ_{p} and $[\text{CO}_2(\text{aq})]$, based on the calibration of $\delta^{13}\text{C}$ composition of alkenones, is also applicable for $\delta^{13}\text{C}$ values of other biomarkers produced by photoautotrophic organisms, in this case S-bound phytane, C_{25} HBI and C_{35} hopane; (3) The b value of photoautotrophs other than haptophyte algae are also related to nitrogen isotopic compositions. Since these assumptions have not yet been tested, it is not possible to estimate potential errors they introduce in the $p\text{CO}_2$ estimates, but clearly they will have a large impact. Furthermore, there are a number of uncertainties associated with estimations of the isotopic fractionation factors as discussed in section 4.3. For example, an uncertainty in $\delta^{13}\text{C}_{\text{pf}}$ may arise due to diagenesis and vital effects, and may be in the order of 0.5 ‰. An uncertainty of that magnitude will result in an equal uncertainty of 0.5 ‰ in ϵ_{p} . In turn, this will result in a significant error of the $p\text{CO}_2$ estimations, which will be higher with higher ϵ_{p} values. The error caused by uncertainties in SST estimates is twofold. An increase of 1 °C causes ϵ_{p} to increase with $\sim 0.12\text{‰}$. The second uncertainty is in the sensitivity of the Arctic SST on the $p\text{CO}_2$ estimates as the solubility of CO_2 is higher under lower sea water temperatures. In comparison with uncertainties in $\delta^{13}\text{C}_{\text{pf}}$, an uncertainty in SST does not result in a large error in the $p\text{CO}_2$ estimates

Figure 7.4 | $p\text{CO}_2$ estimates inferred from diatom biomarkers from Holocene Arabian Sea sediments (Netherlands Indian Ocean Program) sampled at different sites (*Schouten et al.*, 2000).

Site	SST (°C)	$\delta^{13}\text{C}_{\text{pt}}$ (‰)	δ_a (‰)	Biomarker	$\delta^{13}\text{C}$ (‰)	ϵ_p (‰)	b (kg $\mu\text{mol}^{-1} \text{L}^{-1}$)	$[\text{CO}_2(\text{aq})]$ ($\mu\text{mol kg}^{-1}$)	$p\text{CO}_2$ (ppmv)
451	25	2	-8	$\text{C}_{25.0}$ HBI	-23.3	9.5	140	9.0	310
453	25	2	-8	$\text{C}_{25.0}$ HBI	-21.7	7.8	140	8.1	280
921	25	2	-8	$\text{C}_{25.3}$ HBI	-19.9	6.0	140	7.3	250
921	25	2	-8	$\text{C}_{25.3}$ HBI	-19.4	5.5	140	7.2	250
921	25	2	-8	$\text{C}_{25.4}$ HBI	-21.7	7.8	140	8.1	280

(10-100 ppmv per 1°C) and depends on the amount of $[\text{CO}_2(\text{aq})]$. Thus, uncertainties in SST cause a relatively minor effect on our $p\text{CO}_2$ estimates. Nevertheless, our ‘background’-ETM2 $p\text{CO}_2$ estimates are in agreement with other estimates using proxy data (*Demicco et al.*, 2003; *Lowenstein & Demicco*, 2006) and modeling (*Berner & Kothavala*, 2001; *Pagani et al.*, 2006a; *Zeebe et al.*, 2009) for the early/middle Eocene.

Clearly, further research constraining the viability of this approach is needed. Especially, a good calibration between biomarker $\delta^{13}\text{C}$, ϵ_p and $p\text{CO}_2$ based on modern microorganisms other than haptophytes, is essential to gain better insight in the factors that influence isotopic fractionation as discussed in the previous section. These calibrations are needed to test the assumptions that are at the base of our $p\text{CO}_2$ reconstructions. Another way to test the reliability of our fractionation model is to compare estimated $p\text{CO}_2$ using existing $\delta^{13}\text{C}$ records of organic biomarkers with better-constrained $p\text{CO}_2$ conditions during past intervals, such as the last glacial cycles. As a first step, we used the $\delta^{13}\text{C}$ of biomarkers of C_{25} HBIs in Holocene sediments of the Arabian Sea (*Schouten et al.*, 2000a) to estimate pre-industrial $p\text{CO}_2$ levels using our method. We arrive at values between 250 to 300 ppmv, which compares favourably well with pre-industrial $p\text{CO}_2$ values (**Table 7.4**).

7.5 CONCLUSION

We measured concentrations and the $\delta^{13}\text{C}$ composition of sulfur-bound biomarkers of marine algal and bacterial origin in sediments deposited in the Arctic Ocean during ETM2, which record environmental change and primary producer responses. Prior to ETM2, the depositional environment was eutrophic with anoxic bottom water conditions, evident from the high TOC content and the presence of sulfur-bound chemical fossils. The various biomarkers show a negative CIE of 3-4.5 ‰, synchronously with a CIE of 3.5 ‰ in $\delta^{13}\text{C}_{\text{TOC}}$, confirming a decrease in the $\delta^{13}\text{C}$ of the global exogenic carbon pool. Biomarker concentrations and carbon isotope records indicate that primary productivity increased during ETM2. This led to higher oxygen consumption and contributed to the develop-

ment of photic zone euxinia. The CIE of the biomarkers is larger than that recorded in marine carbonates, suggesting an increase in the isotopic fractionation of the marine primary producers, likely due to elevated $p\text{CO}_2$ levels. Using the carbon isotopic fractionation factors, we made a first attempt to reconstruct atmospheric CO_2 concentrations and yield a potential range in $p\text{CO}_2$ values of 800 to 1100 ppmv (3 to 4 x pre-industrial values) and 1100 to > 2000 ppmv (4 to >7 x pre-industrial values) for the pre-excursion and ETM2, respectively. However, these estimations are subjected to large limiting factors and uncertainties. Critically, to estimate carbon isotopic fractionation factors we adopted the surface water $\delta^{13}\text{C}_{\text{DIC}}$ values of Walvis Ridge as a representative of the Arctic Ocean surface waters during ETM2. In addition, our $p\text{CO}_2$ estimates are based on the assumption that the $\epsilon_p - [\text{CO}_2(\text{aq})]$ relationship, originally calibrated for the $\delta^{13}\text{C}$ composition of alkenones, is also applicable for other biomarkers. Therefore, our estimated $p\text{CO}_2$ values should be considered with care. Rather, they are meant to give an idea on what scale $p\text{CO}_2$ levels may have changed during an Eocene hyperthermal. A more thorough testing of the use of $\delta^{13}\text{C}$ composition of biomarkers derived from marine microorganisms for $p\text{CO}_2$ reconstructions is needed, before this method can be used as a tool for reconstructing $p\text{CO}_2$ conditions of past climate.

ACKNOWLEDGMENTS

This research used samples and data provided by the Integrated Ocean Drilling Program (IODP). This is publication number DW-2011-1007 of the Darwin Center for Biogeosciences, which partially funded this project. Appy Sluijs thanks the Netherlands Organization for Scientific Research (NWO) for funding (Veni grant 863.07.001) and the European Research Council under the European Community's Seventh Framework Program for ERC Starting Grant 259627. We thank Jerry Dickens, Mark Pagani, and two anonymous reviewers for their critical comments on the manuscript and M. Kienhuis, J. Ossebaar and A. Mets for their technical support.

REFERENCES

- Abdul Aziz**, H.A., Hilgen, F.J., van Luijk, G.M., Sluijs, A., Kraus, M.J., Pares, J.M., Gingerich, P.D., 2008. Astronomical climate control on paleosol stacking patterns in the upper Paleocene-lower Eocene Willwood Formation, Bighorn Basin, Wyoming. *Geology* 36, 531-534.
- Adrian**, R., O'Reilly, C.M., Zagarese, H., Baines, S.B., Hessen, D.O., Keller, W., Livingstone, D.M., Sommaruga, R., Straile, D., Van Donk, E., Weyhenmeyer, G.A., Windler, M., 2009. Lakes as sentinels of climate change. *Limnology and Oceanography* 54, 2283-2297.
- American Public Health Association (APHA)**, and Water Environment Federation (WEF), 1998. Standard Methods for the Examination of Water and Wastewater, 20th Edition. United Book Press, Inc., Baltimore, Maryland.
- Andersen**, N., Müller, P.J., Kirst, G., Schneider, R.R., 1999. Alkenone $\delta^{13}\text{C}$ as a proxy for past PCO_2 in surface waters: Results from the Late Quaternary Angola Current. In: Fischer, G.W., G. (Ed.), Use of Proxies in Paleooceanography: Examples from the South Atlantic. Springer, Berlin, pp. 469-488.
- Arar**, E.J., Collins, G.B., 1997. Method 445.0, *In Vitro* determination of chlorophyll *a* and pheophytin *a* in marine and freshwater algae by fluorescence, Methods for the Determination of Chemical Substances in Marine and Estuarine Environmental Matrices. National Exposure Research Laboratory, Office of research and development, USEPA., Cincinnati, Ohio (EPA/600/R-97/072, Sept. 1997).
- Arbuckle**, K.E., Downing, J.A., 2001. The influence of watershed land use on lake N:P in a predominantly agricultural landscape. *Limnology and Oceanography* 46, 970-975.
- Auguet**, J.C., Casamayor, E.O., 2008. A hotspot for cold crenarchaeota in the neuston of high mountain lakes. *Environmental Microbiology* 10, 1080-1086.
- Auguet**, J.C., Nomokonova, N., Camarero, L., Casamayor, E.O., 2011. Seasonal changes of freshwater ammonia-oxidizing archaeal assemblages and nitrogenspecies in oligo-trophic alpine lakes. *Applied and Environmental Microbiology* 77, 1937-1945.
- Backman**, J., Moran, K., McInroy, D.B., Mayer, L.A., scientists, E., 2006. Arctic Coring Expedition (ACEX), Proceedings of Integrated Ocean Drilling Program.
- Barnola**, J.M., Raynaud, D., Korotkevich, Y.S., Lorius, C., 1987. Vostok ice core provides 160,000-year record of atmospheric CO_2 . *Nature* 329, 408-414.
- Barnola**, J.M., Raynaud, D., Neftel, A., Oeschger, H., 1983. Comparison of CO_2 measurements by two laboratories on air from bubbles in polar ice. *Nature* 303, 410-413.
- Battin**, T.J., Kaplan, S., Findlay, S., Hopkinson, C.S., Marti, E., Packman, A.L., Newbold, J.D., Sabater, F., 2008. Biophysical controls on organic carbon fluxes in fluvial networks. *Nature Geoscience* 1, 95-100.
- Bauch**, D., Carstens, J., Wefer, G., Thiede, J., 2000. The imprint of anthropogenic CO_2 in the Arctic Ocean: evidence from planktic $\delta^{13}\text{C}$ data from watercolumn and sediment surfaces. *Deep-Sea Research Part II-Topical Studies in Oceanography* 47, 1791-1808.

- Bauersachs, T.**, Speelman, E.N., Hopmans, E.C., Reichart, G.-J., Schouten, S., Sinninghe Damsté, J.S., 2010. Fossilized glycolipids reveal past oceanic N₂ fixation by heterocystous cyanobacteria. *Proceedings of the National Academy of Sciences of the United States of America* 107, 19190-19194.
- Bauersachs, T.**, Hopmans, E.C., Compaoré, J., Stal, L.J., Schouten, S., Sinninghe Damsté, J.S., 2009a. Rapid analysis of long-chain glycolipids in heterocystous cyanobacteria using high-performance liquid chromatography coupled to electrospray ionization tandem mass spectrometry. *Rapid Communications in Mass Spectrometry* 23, 1387-1394.
- Bauersachs, T.**, Compaoré, J., Hopmans, E.C., Stal, L.J., Schouten, S., Sinninghe Damsté, J.S., 2009b. Distribution of heterocyst glycolipids in cyanobacteria. *Phytochemistry* 70, 2034-2039.
- Bechtel, A.**, Smittenberg, R.H., Bernasconi, S.M., Schubert, C.J., 2010. Distribution of branched and isoprenoid tetraether lipids in an oligotrophic and a eutrophic Swiss lake: Insights into sources and GDGT-based proxies. *Organic Geochemistry* 41, 822-832.
- Beman, J.M.**, Chow, C.E., King, A.L., Feng, Y.Y., Fuhrman, J.A., Andersson, A., Bates, N.R., Popp, B.N., and Hutchins, D.A., 2011. Global declines in oceanic nitrification rates as a consequence of ocean acidification. *Proceedings of the National Academy of Sciences of the United States of America* 108, 208-213.
- Benning, C.**, Huang, Z.H., Gage, D.A., 1995. Accumulation of a novel glycolipid and a betaine lipid in cells of *Rhodobacter sphaeroides* grown under phosphate limitation. *Archives of Biochemistry and Biophysics* 317, 103-111.
- Benthien, A.**, Andersen, N., Müller, P.J., Schneider, R.R., Wefer, G., 1999. Alkenone $\delta^{13}\text{C}$ -derived $p\text{CO}_2$ levels in surface waters of the southern Atlantic: Holocene vs. last glacial maximum, ASLO Aquatic Science Meeting. American Society of Limnology and Oceanography, Santa Fe.
- Benthien, A.**, Andersen, N., Schulte, S., Müller, P.J., Schneider, R.R., Wefer, G. 2002. Carbon isotopic composition of the C_{37:2} alkenone in core top sediments of the South Atlantic Ocean: Effects of CO₂ and nutrient concentrations. *Global Biogeochemical Cycles* 16.
- Benthien, A.**, Zondervan, I., Engel, A., Hefter, J., Terbruggen, A., and Riebesell, U., 2007. Carbon isotopic fractionation during a mesocosm bloom experiment dominated by *Emiliania huxleyi*: Effects of CO₂ concentration and primary production. *Geochimica Et Cosmochimica Acta* 71, 1528-1541.
- Berg, I.A.**, Kockelkorn, D., Buckel, W., Fuchs, G., 2007. A 3-hydroxypropionate/4-hydroxybutyrate autotrophic carbon dioxide assimilation pathway in archaea. *Science* 318, 1782-1786.
- Berner, R.A.**, 2006. GEOCARBSULF: A combined model for Phanerozoic atmospheric O₂ and CO₂. *Geochimica Et Cosmochimica Acta* 70, 5653-5664.
- Berner, R.A.**, Kothavala, Z., 2001. GEOCARB III: A revised model of atmospheric CO₂ over phanerozoic time. *American Journal of Science* 301, 182-204.

- Bi, X.H.**, Sheng, G.Y., Liu, X.H., Li, C., Fu, J.M., 2005. Molecular and carbon and hydrogen isotopic composition of *n*-alkanes in plant leaf waxes. *Organic Geochemistry* 36, 1405-1417.
- Bice, K.L.**, Birgel, D., Meyers, P.A., Dahl, K.A., Hinrichs, K.U., and Norris, R.D., 2006. A multiple proxy and model study of Cretaceous upper ocean temperatures and atmospheric CO₂ concentrations. *Paleoceanography* 21.
- Bice, K.L.**, Marotzke, J., 2002. Could changing ocean circulation have destabilized methane hydrates at the Paleocene/Eocene boundary? *Paleoceanography* 17, 81-89.
- Biddle, J.F.**, Lipp, J.S., Lever, M.A., Lloyd, K.G., Sørensen, K.B., Anderson, R., Fredricks, H.F., Elvert, M., Kelly, T.J., Schrag, D.P., Sogin, M.L., Brenchley, J.E., Teske, A., House, C.H., Hinrichs, K., 2006. Heterotrophic Archaea dominate sedimentary subsurface ecosystems off Peru. *Proceedings of the National Academy of Sciences of the United States of America* 103, 3846-3851.
- Bidigare, R.R.**, Fluegge, A., Freeman, K.H., Hanson, K.L., Hayes, J.M., Hollander, D., Jasper, J.P., King, L.L., Laws, E.A., Milder, J., Milerio, F.J., Pancost, R., Popp, B.N., Steinberg, P.A., and Wakeham, S.G., 1997. Consistent fractionation of ¹³C in nature and in the laboratory: Growth-rate effects in some haptophyte algae. *Global Biogeochemical Cycles* 11, 279-292.
- Bijl, P.K.**, Houben, A. J. P., Schouten, S., Bohaty, S.M., Sluijs, A., Reichart, G.-J., Sinninghe Damsté, J.S., Brinkhuis, H., 2010. Transient middle Eocene atmospheric CO₂ and temperature variations. *Science* 330, 819-821.
- Blaga, C.I.**, Reichart, G.J., Heiri, O., Sinninghe Damsté, J.S., 2009. Tetraether membrane lipid distributions in water-column particulate matter and sediments: a study of 47 European lakes along a north-south transect. *Journal of Paleolimnology* 41, 523-540.
- Blaga, C.I.**, Reichart, G.-J., Schouten, S., Lotter, A.F., Werne, J.P., Kosten, S., Mazzeo, N., Lacerot, G., Sinninghe Damsté, J.S., 2010. Branched glycerol dialkyl glycerol tetraethers in lake sediments: Can they be used as temperature and pH proxies? *Organic Geochemistry* 41, 1225-1234.
- Bligh, E.G.**, Dyer, W.J., 1959. A rapid method of total lipid extraction and purification. *Canadian Journal of Biochemistry and Physiology* 37, 911-917.
- Bøggild, O.B.**, 1918. Den vulkanske aske i moleret Danmarks Geologiske Undersøgelse II Række, no. 33, 1-159.
- Bolle, M.P.**, Pardo, A., Hinrichs, K.-U., Adatte, T., Von Salis, K., Keller, G., Muzylev, N., 2000. The Paleocene-Eocene transition in the marginal northeastern Tethys (Kazakhstan and Uzbekistan). *International Journal of Earth Sciences* 89, 390-414.
- Boller, A.J.**, Thomas, P.J., Cavanaugh, C.M., Scott, K.M., 2011. Low stable carbon isotope fractionation by coccolithophore *RubisCO*. *Geochimica Et Cosmochimica Acta* 75, 7200-7207.
- Booth, I.R.**, 1985. Regulation of cytoplasmic pH in Bacteria. *Microbiological Reviews* 49, 359-378.
- Borin, S.**, Ventura, S., Tambone, F., Mapelli, Schubotz, F., Brusetti, L., Scaglia, B., D'Acqui, L.P., Solheim, B., Turicchia, S., Marasco, R. ,

- Hinrichs, K.-U., Baldi, F., Adani, F., Daffonchio, D. 2010. Rock weathering creates oases of life in a High Arctic desert. *Environmental Microbiology* 12, 293-303.
- Bottjer, D.J.**, Droser, M.L., 1992. Paleoenvironmental patterns of biogenic sedimentary structures. In: Maples, C.G., West, R., R. (Eds.), Trace fossils, Paleontological Society Short Courses in Paleontology, University of Tennessee, Knoxville, pp. 130-144.
- Bowen, G.J.**, Beerling, D.J., Koch, P.L., Zachos, J.C., Quattlebaum, T., 2004. A humid climate state during the Palaeocene/Eocene thermal maximum. *Nature* 432, 495-499.
- Bowen, G.J.**, Koch, P.K., Gingerich, P.D., Norris, R.D., Bains, S., Corfield, R.M. 2001. Refined isotope stratigraphy across the continental Paleocene-Eocene boundary on Polecat Bench in the Northern Bighorn Basin In: Gingerich, P.D. (Ed.), Paleocene-Eocene stratigraphy and biotic change in the Bighorn and Clarks Fork Basins. Papers on Paleontology. University of Michigan, Wyoming.
- Bowen, G.J.**, Zachos, J.C., 2010. Rapid carbon sequestration at the termination of the Palaeocene-Eocene Thermal Maximum. *Nature Geoscience* 3, 866-869.
- Bradley, A.S.**, Fredricks, H., Hinrichs, K.U., Summons, R.E., 2009. Structural diversity of diether lipids in carbonate chimneys at the Lost City Hydrothermal Field. *Organic Geochemistry* 40, 1169-1178.
- Brandsma, J.**, Hopmans, E.C., Brussaard, C.P.D., Witte, H.J., Schouten, S., Sinninghe Damsté, J.S., 2012a. Spatial distribution of intact polar lipids in North Sea surface waters: Relationship with environmental conditions and microbial community composition. *Limnology and Oceanography* 57, 959-973.
- Brandsma, J.**, Hopmans, E.C., Philippart, C.J.M., Veldhuis, M.J.W., Schouten, S., Sinninghe Damsté, J.S., 2012b. Low temporal variation in the intact polar lipid composition of North Sea coastal marine water reveals limited chemotaxonomic value. *Biogeosciences* 9, 1073-1084.
- Brassell, S.C.**, Lewis, C.A., de Leeuw, J.W., de Lange, F., Sinninghe Damsté, J.S., 1986. Isoprenoid thiophenes: novel products of sediment diagenesis? *Nature* 320, 160-162.
- Bray, E.E.**, Evans, E.D., 1961. Distribution of *n*-paraffins as a clue to recognition of source beds. *Geochimica et Cosmochimica Acta* 22, 2-15.
- Bühning, S.I.**, Smittenberg, R.H., Sachse, D., Lipp, J.S., Golubic, S., Sachs, J.P., Hinrichs, K.U., Summons, R.E., 2009. A hypersaline microbial mat from the Pacific Atoll Kiritimati: insights into composition and carbon fixation using biomarker analyses and a ¹³C-labeling approach. *Geobiology* 7, 308-323.
- Burkhardt, S.**, Riebesell, U., Zondervan, I., 1999. Effects of growth rate, CO₂ concentration, and cell size on the stable carbon isotope fractionation in marine phytoplankton. *Geochimica et Cosmochimica Acta* 63, 3729-3741.
- Caldeira, K.**, Wickett, M.E., 2003. Anthropogenic carbon and ocean pH. *Nature* 425, 365-365.
- Cao, L.**, Caldeira, K., Jain, A.K., 2007. Effects of carbon dioxide and climate change on ocean acidification and carbonate mineral saturation.

- Geophysical Research Letters* 34, L05607.
- Cassar, N.**, Laws, E.A., Popp, B.N., 2006. Carbon isotopic fractionation by the marine diatom *Phaeodactylum tricornutum* under nutrient- and light-limited growth conditions. *Geochimica et Cosmochimica Acta* 70, 5323-5335.
- Castañeda, I.S.**, Schouten, S., 2011. A review of molecular organic proxies for examining modern and ancient lacustrine environments. *Quaternary Science Reviews* 30, 2851-2891.
- Cerling, T.E.**, 1991. Carbon dioxide in the atmosphere: Evidence from Cenozoic and Mesozoic paleosols. *American Journal of Science* 291,377-400.
- Chikaraishi, Y.**, Naraoka, H., 2003. Compound-specific δD - $\delta^{13}C$ analyses of *n*-alkanes extracted from terrestrial and aquatic plants. *Phytochemistry* 63, 361-371.
- Chun, C.O.J.**, Delaney, M.L., Zachos, J.C., 2010. Paleoredox changes across the Paleocene-Eocene thermal maximum, Walvis Ridge (ODP Sites 1262, 1263, and 1266): Evidence from Mn and U enrichment factors. *Paleoceanography* 25, PA4202.
- Cole, J.J.**, Prairie, Y.T., Caraco, N.F., McDowell, W.H., Tranvik, L.J., Striegl, R.G., Duarte, C.M., Kortelainen, P., Downing, J.A., Middelburg, J.J., Melack, J., 2007. Plumbing the global carbon cycle: Integrating inland waters into the terrestrial carbon budget. *Ecosystems* 10, 171-184.
- Collister, J.W.**, Rieley, G., Stern, B., Eglinton, G., Fry, B., 1994. Compound-specific $\delta^{13}C$ analyses of leaf lipids from plants with differing carbon-dioxide metabolisms. *Organic Geochemistry* 21, 619-627.
- Coolen, M.J.L.**, Abbas, B., van Bleijswijk, J., Hopmans, E.C., Kuypers, M.M.M., Wakeham, S.G., Sinninghe Damsté, J.S., 2007. Putative ammonia-oxidizing Crenarchaeota in suboxic waters of the Black Sea: a basin-wide ecological study using 16S ribosomal and functional genes and membrane lipids. *Environmental Microbiology* 9, 1001-1016.
- Cramer, B.S.**, Wright, J.D., Kent, D.V., Aubry, M.P., 2003. Orbital climate forcing of $\delta^{13}C$ excursions in the late Paleocene-early Eocene (chrons C24n-C25n). *Paleoceanography* 18, 1079.
- Crouch, E.M.**, Dickens, G.R., Brinkhuis, H., Aubry, M.P., Hollis, C.J., Rogers, K.M., Visscher, H., 2003. The *Apectodinium* acme and terrestrial discharge during the Paleocene-Eocene thermal maximum: new palynological, geochemical and calcareous nanno-plankton observations at Tawanui, New Zealand. *Paleogeography Palaeoclimatology Palaeoecology* 194, 387-403.
- Crumpton, W.G.**, Isenhardt, T.M., Mitchell, P.D., 1992. Nitrate and organic N analyses with second-derivative spectroscopy. *Limnology and Oceanography* 37, 907-913.
- de Kluijver, A.**, 2012. Carbon flows in natural plankton communities in the Anthropocene. PhD Thesis, Utrecht University.
- de Leeuw, J.W.**, Frewin, N.L., Van Bergen, P.F., Sinninghe Damsté, J.S., Collinson, M.E., 1995. Organic carbon as a palaeoenvironmental indicator in the marine realm. In: Bosence, D.W.J., Allison, P.A. (Eds.), *Marine Palaeoenvironmental Analysis from Fossils*. Geological Society Special Publication, pp. 43-71.

- Dean, W.E.**, Gorham, E., 1998. Magnitude and significance of carbon burial in lakes, reservoirs, and peatlands. *Geology* 26, 535-538.
- DeConto, R.M.**, Galeotti, S., Pagani, M., Tracy, D., Schaefer, K., Zhang, T., Pollard, D., Beerling, D.J., 2012. Past extreme warming events linked to massive carbon release from thawing permafrost. *Nature* 484, 87-91.
- Degens, E.T.**, Guillard, R.R., Sackett, W.M., Hellebus, J., 1968. Metabolic fractionation of carbon isotopes in marine plankton -I. Temperature and respiration experiments. *Deep-Sea Research* 15, 1-9.
- Dembitsky, V.M.**, 1996. Betaine ether-linked glycerolipids: chemistry and biology. *Progress in Lipid Research* 35, 1-51.
- Dickens, G.R.**, 2000. Methane oxidation during the Late Palaeocene Thermal Maximum. *Bulletin De La Societe Geologique De France* 171, 37-49.
- Dickens, G.R.**, 2003. Rethinking the global carbon cycle with a large, dynamic and microbially mediated gas hydrate capacitor. *Earth and Planetary Science Letters* 213, 169-183.
- Dickens, G.R.**, 2011. Down the Rabbit Hole: toward appropriate discussion of methane release from gas hydrate systems during the Paleocene-Eocene thermal maximum and other past hyperthermal events. *Climate of the Past* 7, 831-846.
- Dickens, G.R.**, Castillo, M.M., Walker, J.C.G., 1997. A blast of gas in the latest Paleocene: Simulating first-order effects of massive dissociation of oceanic methane hydrate. *Geology* 25, 259-262.
- Dickens, G.R.**, Oneil, J.R., Rea, D.K., Owen, R.M., 1995. Dissociation of oceanic methane hydrate as a cause of the carbon isotope excursion at the end of the Paleocene. *Paleoceanography* 10, 965-971.
- Dickson, A.B.**, Sabine, C.L., Christian, J.R., 2007. Guide to the best practices for ocean CO₂ measurements. PICES Special Publication, 3. North Pacific Marine Organization, Sidney, Canada.
- Dickson, A.G.**, Goyet, C., 1994. Handbook of methods for the analysis of the various parameters of the carbon dioxide system in sea water.
- Diefendorf, A.F.**, Freeman, K.H., Wing, S.L., Graham, H.V., 2011. Production of *n*-alkyl lipids in living plants and implications for the geologic past. *Geochimica et Cosmochimica Acta* 75, 7472-7485.
- Downing, J.A.**, Cole, J.J., Middelburg, J.J., Striegl, R.G., Duarte, C.M., Kortelainen, P., Prairie, Y.T., Laube, K.A., 2008. Sediment organic carbon burial in agriculturally eutrophic impoundments over the last century. *Global Biogeochemical Cycles* 22, GB1018.
- Downing, J.A.**, Prairie, Y.T., Cole, J.J., Duarte, C.M., Tranvik, L.J., Striegl, R.G., McDowell, W.H., Kortelainen, P., Caraco, N.F., Melack, J.M., Middelburg, J.J., 2006. The global abundance and size distribution of lakes, ponds, and impoundments. *Limnology and Oceanography* 51, 2388-2397.
- Downing, J.A.**, Watson, S.B., McCauley, E., 2001. Predicting Cyanobacteria dominance in lakes. *Canadian Journal of Fisheries and Aquatic Sciences* 58, 1905-1908.
- Eglinton, G.**, Hamilton, R.J., 1967. Leaf epicuticular waxes. *Science* 156, 1322-1335.

- E**kart, D.D., Cerling, T.E., Montañez, I.P., Tabor, N.J., 1999. A 400 million year carbon isotope record of pedogenic carbonate: Implications for paleoatmospheric carbon dioxide. *American Journal of Science* 299, 805-827.
- E**rtefai, T.F., Fisher, M.C., Fredricks, H.F., Lipp, J.S., Pearson, A., Birgel, D., Udert, K.M., Cavanaugh, C.M., Gschwend, P.M., Hinrichs, K.U., 2008. Vertical distribution of microbial lipids and functional genes in chemically distinct layers of a highly polluted meromictic lake. *Organic Geochemistry* 39, 1572-1588.
- F**abry, V.J., 2008. Marine calcifiers in a high-CO₂ ocean. *Science* 320, 1020-1022.
- F**ahy, E., Subramaniam, S., Brown, H.A., Glass, C.K., Merrill, A.H., Murphy, R.C., Raetz, C.R.H., Russell, D.W., Seyama, Y., Shaw, W., Shimizu, T., Spener, F., van Meer, G., VanNieuwenhze, M.S., White, S.H., Witztum, J.L., Dennis, E.A., 2005. A comprehensive classification system for lipids. *Journal of Lipid Research* 46, 839-861.
- F**ang, J.S., Barcelona, M.J., 1998. Structural determination and quantitative analysis of bacterial phospholipids using liquid chromatography/electrospray ionization/mass spectrometry. *Journal of Microbiological Methods* 33, 23-35.
- F**arquhar, G.D., O'Leary, M.H., Berry, J.A., 1982. On the relationship between carbon isotope discrimination and the intercellular carbon dioxide concentration in leaves. *Australian Journal of Plant Physiology* 9, 121-137.
- F**eely, R.A., Sabine, C.L., Lee, K., Berelson, W., Kleypas, J., Fabry, V.J., Millero, F.J., 2004. Impact of anthropogenic CO₂ on the CaCO₃ system in the oceans. *Science* 305, 362-6.
- F**erber, L.R., Levine, S.N., Lini, A., Livingston, G.P., 2004. Do cyanobacteria dominate in eutrophic lakes because they fix atmospheric nitrogen? *Freshwater Biology* 49, 690-708.
- F**ischer, W.W., Summons, R.E., Pearson, A., 2005. Targeted genomic detection of biosynthetic pathways: anaerobic production of hopanoid biomarkers by a common sedimentary microbe. *Geobiology* 3, 33-40.
- F**letcher, B.J., Beerling, D.J., Brentnall, S.J., Royer, D.L., 2005. Fossil bryophytes as recorders of ancient CO₂ levels: Experimental evidence and a Cretaceous case study. *Global Biogeochemical Cycles* 19, GB3012.
- F**rancois, R., Altabet, M.A., Goericke, R., McCorkle, D.C., Brunet, C., Poisson, A., 1993. Changes in the $\delta^{13}\text{C}$ of surface water particulate organic matter across the subtropical convergence in the SW Indian Ocean. *Global Biogeochemical Cycles* 7, 627-644.
- F**reeman, K.H., 2001. Isotopic biogeochemistry of marine organic carbon. In: Valley, J.W., Cole, D.R. (Eds.), *Stable Isotope Geochemistry*. Mineralogical Society of America, Washington, DC, pp. 579-605.
- F**reeman, K.H., Hayes, J.M., 1992. Fractionation of carbon isotopes by phytoplankton and estimates of ancient CO₂ levels. *Global Biogeochemical Cycles* 6, 185-98.
- F**reeman, K.H., Wakeham, S.G., 1992. Variations in the distributions and isotopic compositions of alkenones in Black Sea particles and sediments. *Organic Geochemistry* 19, 277-285.

- Frentzen, M.**, 2004. Phosphatidylglycerol and sulfoquinovosyldiacylglycerol: anionic membrane lipids and phosphate regulation. *Current Opinion in Plant Biology* 7, 270-276.
- Frömel, T.**, Knepper, T.P., 2008. Mass spectrometry as an indispensable tool for studies of biodegradation of surfactants. *Trac-Trends in Analytical Chemistry* 27, 1091-1106.
- Fry, B.**, Jannasch, H.W., Molyneux, S.J., Wirsén, C.O., Muramoto, J.A., King, S., 1991. Stable isotope studies of the carbon, nitrogen and sulfur cycles in the Black Sea and the Cariaco Trench. *Deep-Sea Research Part A. Oceanographic Research Papers* 38, S1003-S1019.
- Fuller, N.**, Rand, R.P., 2001. The influence of lysolipids on the spontaneous curvature and bending elasticity of phospholipid membranes. *Biophysical Journal* 81, 243-254.
- Giordano, M.**, Beardall, J., Raven, J.A., 2005. CO₂ concentrating mechanisms in algae: Mechanisms, environmental modulation, and evolution. *Annual Review of Plant Biology* 56, 99-131.
- Goerick, R.**, Montoya, J.P., Fry, B., 1994. Physiology of isotopic fractionation in algae and cyanobacteria. In: Lajtha, K., Michener, R. (Eds.), *Stable Isotopes in Ecology and Environmental Science*. Blackwell Science, London, pp. 187-221.
- Gorham, E.**, Dean, W.E., Sanger, J.E., 1983. The chemical composition of lakes in the north-central United States. *Limnology and Oceanography* 28, 287-301.
- Grasshoff, K.**, Ehrhardt, M., Kremling, K., 1983. *Methods of seawater analysis*. Wiley VCH, Weinheim.
- Greenwood, D.R.**, Wing, S.L., 1995. Eocene continental climates and latitudinal temperature gradients. *Geology* 23, 1044-1048.
- Haines, T.H.**, 2001. Do sterols reduce proton and sodium leaks through lipid bilayers? *Progress in Lipid Research* 40, 299-324.
- Hallam, S.J.**, Mincer, T.J., Schleper, C., Preston, C.M., Roberts, K., Richardson, P.M., DeLong, E.F., 2006. Pathways of carbon assimilation and ammonia oxidation suggested by environmental genomic analyses of marine *Crenarchaeota*. *Plos Biology* 4, 520-536.
- Hancock, H.J.L.**, Dickens, G.R., Thomas, E., Blake, K.L., 2007. Reappraisal of early Paleogene CCD curves: foraminiferal assemblages and stable carbon isotopes across the carbonate facies of Perth Abyssal Plain. *International Journal of Earth Sciences* 96, 925-946.
- Handley, L.**, Crouch, E.M., Pancost, R.D., 2011. A New Zealand record of sea level rise and environmental change during the Paleocene-Eocene Thermal Maximum. *Palaeogeography Palaeoclimatology Palaeoecology* 305, 185-200.
- Handley, L.**, Pearson, P.N., McMillan, I.K., Pancost, R.D., 2008. Large terrestrial and marine carbon and hydrogen isotope excursions in a new Paleocene/Eocene boundary section from Tanzania. *Earth and Planetary Science Letters* 275, 17-25.
- Harvey, H.R.**, Fallon, R.D., Patton, J.S., 1986. The effect of organic matter and oxygen on the degradation of bacterial membrane lipids in marine sediments. *Geochimica et Cosmochimica Acta* 50, 795-804.

- Hasle, G.R.**, Syvertsen, E.E., 1996. Marine diatoms. In: Tomas, C.R. (Ed.), *Identifying Marine Phytoplankton*. Academic Press, San Diego, pp. 5-385.
- Hayes, J.M.**, 1993. Factors controlling ^{13}C contents of sedimentary organic compounds: Principles and evidence. *Marine Geology* 113, 111-125.
- Hayes, J.M.**, 2001. Fractionation of carbon and hydrogen isotopes in biosynthetic processes. *Stable Isotope Geochemistry* 43, 225-277.
- Hayes, J.M.**, Strauss, H., Kaufman, A.J., 1999. The abundance of ^{13}C in marine organic matter and isotopic fractionation in the global biogeochemical cycle of carbon during the past 800 Ma. *Chemical Geology* 161, 103-125.
- Heilmann-Clausen, C.**, 1994. Review of Paleocene dinoflagellates from the North Sea region. *GFF* 116, 51-53.
- Heilmann-Clausen, C.**, 1995. Palæogene aflejring over Danskekalken. In: Nielsen, O.B. (Ed.), *Aarhus Geokompender No. 1, Danmarks geologi fra Kridt till i dag*, pp. 69-114.
- Heilmann-Clausen, C.**, 2006. Korallrev og lerhav (excl. Danian). In: Larsen, G. (Ed.), *Naturen i Danmark, Geologien*. Gyldendal, Copenhagen, pp. 181-186 & 191-226.
- Heilmann-Clausen, C.**, Nielsen, O.B., Gersner, F., 1985. Lithostratigraphy and depositional environments in the Upper Paleocene and Eocene of Denmark. *Bulletin of the Geological Society of Denmark* 33, 287-323.
- Heilmann-Clausen, C.**, Schmitz, B., 2000. The late Paleocene thermal maximum $\delta^{13}\text{C}$ excursion in Denmark? *GFF* 122, 70-70.
- Henderiks, J.**, Pagani, M., 2007. Refining ancient carbon dioxide estimates: Significance of coccolithophore cell size for alkenone-based $p\text{CO}_2$ records. *Paleoceanography* 22, PA3202.
- Herfort, L.**, Schouten, S., Boon, J.P., Sinninghe Damsté, J.S., 2006. Application of the TEX_{86} temperature proxy to the southern North Sea. *Organic Geochemistry* 37, 1715-1726.
- Herrmann, M.**, Saunders, A.M., Schramm, A., 2009. Effect of lake trophic status and rooted macrophytes on community composition and abundance of ammonia-oxidizing prokaryotes in freshwater sediments. *Applied and Environmental Microbiology* 75, 3127-3136.
- Hilgen, F.J.**, Kuiper, K.F., Lourens, L.J., 2010. Evaluation of the astronomical time scale for the Paleocene and earliest Eocene. *Earth and Planetary Science Letters* 300, 139-151.
- Hoefs, M.J.L.**, Schouten, S., de Leeuw, J.W., King, L.L., Wakeham, S.G., Sinninghe Damsté, J.S., 1997. Ether lipids of planktonic archaea in the marine water column. *Applied and Environmental Microbiology* 63, 3090-3095.
- Hönisch, B.**, Ridgwell, A., Schmidt, D.N., Thomas, E., Gibbs, S.J., Sluijs, A., Zeebe, R., Kump, L., Martindale, R.C., Greene, S.E., Kiessling, W., Ries, J., Zachos, J.C., Royer, D.L., Barker, S., Marchitto, T.M., Moyer, R., Pelejero, C., Ziveri, P., Foster, G.L., Williams, B., 2012. The geological record of ocean acidification. *Science* 335, 1058-1063.

- Hooigstraten, A.**, Timmermans, K.R., de Baar, H.J.W., 2012. Morphological and physiological effects in *Proboscidea alata* (Bacillariophyceae) grown under different light and CO₂ conditions of the modern Southern Ocean. *Journal of Phycology* 48, 559-568.
- Hopmans, E.C.**, Weijers, J.W.H., Schefuß, E., Herfort, L., Sinninghe Damsté, J.S., Schouten, S., 2004. A novel proxy for terrestrial organic matter in sediments based on branched and isoprenoid tetraether lipids. *Earth and Planetary Science Letters* 224, 107-116.
- Huber, M.**, Caballero, R., 2011. The early Eocene equable climate problem revisited. *Climate of the Past* 7, 603-633.
- Hughen, K.A.**, Eglinton, T.I., Xu, L., Makou, M., 2004. Abrupt tropical vegetation response to rapid climate changes. *Science* 304, 1955-1959.
- Huguet, C.**, Hopmans, E.C., Febo-Ayala, W., Thompson, D.H., Sinninghe Damsté, J.S., Schouten, S., 2006. An improved method to determine the absolute abundance of glycerol dibiphytanyl glycerol tetraether lipids. *Organic Geochemistry* 37, 1036-1041.
- Huguet, C.**, Kim, J.H., de Lange, G.J., Sinninghe Damsté, J.S., Schouten, S., 2009. Effects of long term oxic degradation on the U^K₃₇, TEX₈₆ and BIT organic proxies. *Organic Geochemistry* 40, 1188-1194.
- Huuse, M.**, Clausen, O.R., 2001. Morphology and origin of major Cenozoic sequence boundaries in the eastern North Sea Basin: top Eocene, near-top Oligocene and the mid-Miocene unconformity. *Basin Research* 13, 17-41.
- Iglesias-Rodriguez, M.D.**, Halloran, P.R., Rickaby, R.E.M., Hall, I.R., Colmenero-Hidalgo, E., Gittins, J.R., Green, D.R.H., Tyrrell, T., Gibbs, S.J., von Dassow, P., Rehm, E., Armbrust, E.V., Boessenkool, K.P., 2008. Phytoplankton calcification in a high-CO₂ world. *Science* 320, 336-340.
- Ingalls, A.E.**, Huguet, C., Truxal, L.T., 2012. Lipids of Archaeal Glycerol Dialkyl Glycerol Tetraethers among size-fractionated particulate organic matter in Hood Canal, Puget Sound. *Applied Environmental Microbiology* 78, 1480-1490.
- IPCC**, 2007. Climate Change 2007: The Physical Science Basis. Contribution of Working Group I to the fourth Assessment Report of the Intergovernmental Panel on Climate Change. Cambridge University Press, Cambridge, United Kingdom and New York, NY, USA, 996 pp.
- Ishii, I.**, Fukushima, N., Ye, X.Q., Chun, J., 2004. Lysophospholipid receptors: Signaling and biology. *Annual Review of Biochemistry* 73, 321-354.
- Jaramillo, C.**, Ochoa, D., Contreras, L., Pagani, M., Carvajal-Ortiz, H., Pratt, L.M., Krishnan, S., Cardona, A., Romero, M., Quiroz, L., Rodriguez, G., Rueda, M.J., de la Parra, F., Morón, S., Green, W., Bayona, G., Montes, C., Quintero, O., Ramirez, R., Mora, G., Schouten, S., Bermudez, H., Navarrete, R., Parra, F., Alvarán, M., Osorno, J., Crowley, J.L., Valencia, V., Vervoort, J., 2010. Effects of rapid global warming at the Paleocene-Eocene boundary on neotropical vegetation. *Science* 330, 957-961.
- Jarvis, I.**, Lignum, J.S., Gröcke, D.R., Jenkyns, H.C., Pearce, M.A., 2011.

- Black shale deposition, atmospheric CO₂ drawdown, and cooling during the Cenomanian-Turonian Oceanic Anoxic Event. *Paleoceanography* 26, PA3201.
- Jasper, J.P.**, Hayes, J.M., 1990. A carbon isotope record of CO₂ levels during the late Quaternary. *Nature* 347, 462-464.
- Jasper, J.P.**, Hayes, J.M., Mix, A.C., Prahl, F.G., 1994. Photosynthetic fractionation of ¹³C and concentrations of dissolved CO₂ in the central equatorial Pacific during the last 255,000 years. *Paleoceanography* 9, 781-798.
- Jeffrey, S.W.**, Mantoura, R.F.C., Wright, S.W., 1997. Phytoplankton pigments in oceanography: guidelines to modern methods. UNESCO.
- Jenkyns, H.C.**, 2010. Geochemistry of oceanic anoxic events. *Geochemistry Geophysics Geosystems* 11, Q03004.
- John, C.M.**, Bohaty, S.M., Zachos, J.C., Sluijs, A., Gibbs, S., Brinkhuis, H., Bralower, T.J., 2008. North American continental margin records of the Paleocene-Eocene thermal maximum: Implications for global carbon and hydrological cycling. *Paleoceanography* 23, PA2217.
- Jones, J.R.**, Bachmann, R.W., 1978. Trophic status of Iowa lakes in relation to origin and glacial geology. *Hydrobiologia* 57, 267-273.
- Jung, M.Y.**, Park, S.J., Min, D., Kim, J.S., Rijpstra, W.I.C., Sinninghe Damsté, J.S., Kim, G.J., Madsen, E.L., Rhee, S.K., 2011. Enrichment and characterization of an autotrophic ammonia-oxidizing archaeon of mesophilic crenarchaeal group I.1a from an agricultural soil. *Applied and Environmental Microbiology* 77, 8635-8647.
- Kalff, J.**, 2001. Limnology: inland water ecosystems. Prentice Hall, Inc., Upper Saddle River, New Jersey, USA.
- Kender, S.**, Stephenson, M.H., Riding, J.B., Leng, M.J., Knox, R.W.O.B., Peck, V.L., Kendrick, C.P., Ellis, M.A., Vane, C.H., Jamieson, R., 2012. Marine and terrestrial environmental changes in NW Europe preceding carbon release at the Paleocene-Eocene transition. *Earth and Planetary Science Letters* 353-354, 108-120.
- Kennett, J.P.**, Stott, L.D., 1991. Abrupt deep-sea warming, paleoceanographic changes and benthic extinctions at the end of the Paleocene. *Nature* 353, 225-229.
- Kim, J.H.**, van der Meer, J., Schouten, S., Helmke, P., Willmott, V., Sangiorgi, F., Koç, N., Hopmans, E.C., Sinninghe Damsté, J.S., 2010. New indices and calibrations derived from the distribution of crenarchaeal isoprenoid tetraether lipids: Implications for past sea surface temperature reconstructions. *Geochimica et Cosmochimica Acta* 74, 4639-4654.
- Kleypas, J.A.**, Buddemeier, R.W., Archer, D., Gattuso, J.P., Langdon, C., Opdyke, B.N., 1999. Geochemical consequences of increased atmospheric carbon dioxide on coral reefs. *Science* 284, 118-120.
- Knies, J.**, Mann, U., Popp, B.N., Stein, R., Brumsack, H.J., 2008. Surface water productivity and paleoceanographic implications in the Cenozoic Arctic Ocean. *Paleoceanography* 23, PA1S16.
- Knox, R.W.O.B.**, 1996a. Tectonic controls on sequence development in the Paleocene and earliest Eocene of SE England: implications for North Sea stratigraphy. In: Hesselbo,

- S.P., Parkinson, D.N. (Eds.), Sequence stratigraphy in British geology. Geological Society Special Publication, London, pp. 209-230.
- Knox, R.W.O.B.**, 1996b. Correlation of the Early Paleogene in Northwest Europe: an overview. In: Knox, R.W.O.B., Corfield, R.M., Dunay, R.E. (Eds.), Correlation of the Early Paleogene in Northwest Europe. Geological Society Special Publication, London, pp. 1-11.
- Knox, R.W.O.B.**, 1998. The tectonic and volcanic history of the North Atlantic region during the Paleocene-Eocene transition: implications for NW European and global biotic event. In: Aubry, A.-P., Lucas, S., Berggren, W.A. (Eds.), Late Paleocene-Early Eocene Climatic and Biotic Event in the Marine and Terrestrial Records. Columbia University Press, New York, pp. 91-102.
- Knox, R.W.O.B.** et al., 2010. Cenozoic. In: Dornenbaal, H., Stevenson, A. (Eds.), Petroleum Geological Atlas of the Southern Permian Basin Area. EAGE Publications b.v., Houten, pp. 211-223.
- Kohnen, M.E.L.**, Schouten, S., Sinninghe Damsté, J.S., de Leeuw, J.W., Merritt, D.A., Hayes, J.M., 1992. Recognition of paleobiochemicals by a combined molecular sulfur and isotope geochemical approach. *Science* 256, 358-362.
- Kohnen, M.E.L.**, Sinninghe Damsté, J.S., de Leeuw, J.W., 1991. Biases from natural sulfurization in paleoenvironmental reconstruction based on hydrocarbon biomarker distributions. *Nature* 349, 775-778.
- Kohnen, M.E.L.**, Sinninghe Damsté, J.S., Kock-van Dalen, A.C., ten Haven, H.L., Rullkötter, J., de Leeuw, J.W., 1990. Origin and diagenetic transformations of C₂₅ and C₃₀ highly branched isoprenoid sulphur compounds: Further evidence for the formation of organically bound sulphur during early diagenesis. *Geochimica et Cosmochimica Acta* 54, 3053-3063.
- Konings, W.N.**, 2006. Microbial transport: Adaptations to natural environments. *Antonie van Leeuwenhoek* 90, 325-342.
- Konings, W.N.**, Albers, S.V., Koning, S., Driessen, A.J.M., 2002. The cell membrane plays a crucial role in survival of bacteria and archaea in extreme environments. *Antonie van Leeuwenhoek* 81, 61-72.
- Könneke, M.**, Bernhard, A.E., de la Torre, J.R., Walker, C.B., Waterbury, J.B., Stahl, D.A., 2005. Isolation of an autotrophic ammonia-oxidizing marine archaeon. *Nature* 437, 543-546.
- Könneke, M.**, Lipp, J.S., Hinrichs, K.U., 2012. Carbon isotope fractionation by the marine ammonia-oxidizing archaeon *Nitrosopumilus maritimus*. *Organic Geochemistry* 48, 21-24.
- Koopmans, M.P.**, Köster, J., van Kaam-Peters, H.M.E., Kenig, F., Schouten, S., Hartgers, W.A., de Leeuw, J.W., Sinninghe Damsté, J.S., 1996. Diagenetic and catagenetic products of isorenieratene: Molecular indicators for photic zone anoxia. *Geochimica et Cosmochimica Acta* 60, 4467-4496.
- Koopmans, M.P.**, Rijpstra, W.I.C., Klapwijk, M.M., de Leeuw, J.W., Lewan, M.D., Sinninghe Damsté, J.S., 1999. A thermal and chemical degradation approach to decipher pristane and phytane precursors in

- sedimentary organic matter. *Organic Geochemistry* 30, 1089-1104.
- Kroopnick, P.M.**, 1985. The distribution of ^{13}C of SCO_2 in the world Oceans. *Deep Sea Research Part A. Oceanographic Research Papers* 32, 57-84.
- Kurtz, A.C.**, Kump, L.R., Arthur, M.A., Zachos, J.C., Paytan, A., 2003. Early Cenozoic decoupling of the global carbon and sulfur cycles. *Paleoceanography* 18, 1090.
- Kuypers, M.M.M.**, Blokker, P., Erbacher, J., Kinkel, H., Pancost, R. D., Schouten, S., Sinninghe Damsté, J.S., 2001. Massive expansion of marine archaea during a mid-Cretaceous oceanic anoxic event. *Science* 293, 92-94.
- Kvenvolden, K.A.**, 1993. Gas hydrates - Geological perspective and global change. *Reviews of Geophysics* 31, 173-187.
- Langer, G.**, Geisen, M., Baumann, K.H., Klas, J., Riebesell, U., Thoms, S., Young, J.R., 2006. Species-specific responses of calcifying algae to changing seawater carbonate chemistry. *Geochemistry Geophysics Geosystems* 7, Q09006.
- Laurson, G.V.**, King, C., 1999. Preliminary results of a foraminiferal analysis of a core from Østerrende, Denmark. In: Andreasson, F.P., Schmitz, B., Thompson, E.I. (Eds.), Early Paleogene warm climates and biosphere dynamics. Earth Science Centre Göteborg University, pp. C21.
- Laws, E.A.**, Bidigare, R.R., Popp, B.N., 1997. Effect of growth rate and CO_2 concentration on carbon isotopic fractionation by the marine diatom *Phaeodactylum tricornutum*. *Limnology and Oceanography* 42, 1552-1560.
- Laws, E.A.**, Popp, B.N., Bidigare, R.R., Kennicutt, M.C., Macko, S.A., 1995. Dependence of phytoplankton carbon isotopic composition on growth rate and $[\text{CO}_2]_{\text{aq}}$ - Theoretical considerations and experimental results. *Geochimica et Cosmochimica Acta* 59, 1131-1138.
- Laws, E.A.**, Popp, B.N., Cassar, N., Tanimoto, J., 2002. ^{13}C discrimination patterns in oceanic phytoplankton: likely influence of CO_2 concentrating mechanisms, and implications for palaeoreconstructions. *Functional Plant Biology* 29, 323-333.
- LeQuéré, C.**, Raupach, M.R., Canadell, J.G., Marland, G., Bopp, L., Ciais, P., Conway, T.J., Doney, S.C., Feely, R.A., Foster, P., Friedlingstein, P., Gurney, K., Houghton, R.A., House, J.I., Huntingford, C., Levy, P.E., Lomas, M.R., Majkut, J., Metzl, N., Ometto, J.P., Peters, G.P., Prentice, I.C., Randerson, J.T., Running, S.W., Sarmiento, J.L., Schuster, U., Sitch, S., Takahashi, T., Viovy, N., van der Werf, G.R., Woodward, F.I., 2009. Trends in the sources and sinks of carbon dioxide. *Nature Geoscience* 2, 831-836.
- Lechevalier, H.**, Lechevalier, M.P., 1989. Chemotaxonomic use of lipids - an overview. In: Ratledge, C., Wilkinson, S.G. (Eds.), Microbial lipids. Academic Limited, pp. 869-902.
- Leon-Rodriguez, L.**, Dickens, G.R., 2010. Constraints on ocean acidification associated with rapid and massive carbon injections: The early Paleogene record at ocean drilling program site 1215, equatorial Pacific Ocean. *Palaeogeography Palaeoclimatology Palaeoecology* 298, 409-420.
- Lewis, E.**, Wallace, D.W.R., 1998. Program Developed for CO_2 System

- Calculations ORNL/CDIAC-105., Carbon Dioxide Information Analysis Center, Oak Ridge National Laboratory, U.S. Department of Energy, Oak Ridge, Tennessee.
- Lipp, J.S.,** Hinrichs, K.U., 2009. Structural diversity and fate of intact polar lipids in marine sediments. *Geochimica et Cosmochimica Acta* 73, 6816-6833.
- Lipp, J.S.,** Morono, Y., Inagaki, F., Hinrichs, K.U., 2008. Significant contribution of Archaea to extant biomass in marine subsurface sediments. *Nature* 454, 991-994.
- Loomis, S.E.,** Russell, J.M., Sinninghe Damsté, J.S., 2011. Distributions of branched GDGTs in soils and lake sediments from western Uganda: Implications for a lacustrine paleothermometer. *Organic Geochemistry* 42, 739-751.
- Lotter, A.F.,** Birks, H.J.B., Hofmann, W., Marchetto, A., 1997. Modern diatom, cladocera, chironomid, and chrysophyte cyst assemblages as quantitative indicators for the reconstruction of past environmental conditions in the Alps. 1. Climate. *Journal of Paleolimnology* 18, 395-420.
- Lourens, L.J.,** Sluijs, A., Kroon, D., Zachos, J.C., Thomas, E., Röhl, U., Bowles, J., Raffi, I., 2005. Astronomical pacing of late Palaeocene to early Eocene global warming events. *Nature* 435, 1083-1087.
- Lowenstein, T.K.,** Demicco, R.V., 2006. Elevated eocene atmospheric CO₂ and its subsequent decline. *Science* 313, 1928-1928.
- Maberly, S.C.,** 1996. Diel, episodic and seasonal changes in pH and concentrations of inorganic carbon in a productive lake. *Freshwater Biology* 35, 579-598.
- Martens-Habbena, W.,** Berube, P.M., Urakawa, H., de la Torre, J.R., Stahl, D.A., 2009. Ammonia oxidation kinetics determine niche separation of nitrifying Archaea and Bacteria. *Nature* 461, 976-U234.
- Marzi, R.,** Torkelson, B.E., Olson, R.K., 1993. A revised carbon preference index. *Organic Geochemistry* 20, 1303-1306.
- Massé, G.,** Belt, S.T., Rowland, S.J., Rohmer, M., 2004. Isoprenoid biosynthesis in the diatoms *Rhizosolenia setigera* (Brightwell) and *Haslea ostrearia* (Simonsen). *Proceedings of the National Academy of Sciences of the United States of America* 101, 4413-4418.
- Mathot, S.,** Smith, W.O., Carlson, C.A., Garrison, D.L., Gowing, M.M., Vickers, C.L., 2000. Carbon partitioning within *Phaeocystis antarctica* (Prymnesiophyceae) colonies in the Ross Sea, Antarctica. *Journal of Phycology* 36, 1049-1056.
- McCarren, H.,** Thomas, E., Hasegawa, T., Röhl, U., Zachos, J.C., 2008. Depth dependency of the Paleocene-Eocene carbon isotope excursion: Paired benthic and terrestrial biomarker records (Ocean Drilling Program Leg 208, Walvis Ridge). *Geochemistry Geophysics Geosystems* 9, Q10008.
- McInerney, F.A.,** Wing, S.L., 2011. The Paleocene-Eocene Thermal Maximum: A perturbation of carbon cycle, climate, and biosphere with implications for the future. *Annual Review of Earth and Planetary Sciences* 39, 489-516.
- Meijer, H.J.G.,** Munnik, T., 2003. Phospholipid-based signaling in plants. *Annual Review of Plant Biology* 54, 265-306.

- Menzel, D.,** Hopmans, E.C., Schouten, S., Sinninghe Damsté, J.S., 2006. Membrane tetraether lipids of planktonic Crenarchaeota in Pliocene sapropels of the eastern Mediterranean Sea. *Palaeogeography Palaeoclimatology Palaeoecology* 239, 1-15.
- Meyers, P.A.,** 1997. Organic geochemical proxies of paleoceanographic, paleolimnologic, and paleoclimatic processes. *Organic Geochemistry* 27, 213-250.
- Meyers, P.A.,** Ishiwatari, R., 1993. Lacustrine organic geochemistry: An overview of indicators of organic matter sources and diagenesis in lake sediments. *Organic Geochemistry* 20, 867-900.
- Minnikin, D.E.,** Abdollah, H., Baddiley, J., 1974. Replacement of acidic phospholipids by acidic glycolipids in *Pseudomonas diminuta*. *Nature* 249, 268-269.
- Monnin, E.,** Indermühle, A., Dällenbach, A., Flückiger, J., Stauffer, B., Stocker, T.F., Raynaud, D., Barnola, J.M., 2001. Atmospheric CO₂ concentrations over the last glacial termination. *Science* 291, 112-114.
- Mook, W.G.,** Bommerson, J.C., Staverman, W.H., 1974. Carbon isotope fractionation between dissolved bicarbonate and gaseous carbon dioxide. *Earth and Planetary Science Letters* 22, 169-176.
- Mook, W.G.,** Tan, F.C., 1991. Stable carbon isotopes in rivers and estuaries. In: Degens, E.T., Kempe, S., Richey, J.E. (Eds.), *Biogeochemistry of major world rivers*. SCOPE.
- Mora, C.I.,** Driese, S.G., Seager, P.G., 1991. Carbon dioxide in the Paleozoic atmosphere: Evidence from carbon-isotope compositions of pedogenic carbonate. *Geology* 19, 1017-1020.
- Moran, K.,** Backman, J., Brinkhuis, H., Clemens, S.C., Cronin, T., Dickens, G.R., Eynaud, F., Gattacceca, J., Jakobsson, M., Jordan, R.W., Kaminski, M., King, J., Koç, N., Krylov, A., Martinez, N., Matthiessen, J., McInroy, D., Moore, T.C., Onodera, J., O'Regan, M., Pälke, H., Rea, B., Rio, D., Sakamoto, T., Smith, D.C., Stein, R., St John, K., Suto, I., Suzuki, N., Takahashi, K., Watanabe, M., Yamamoto, M., Farrell, J., Frank, M., Kubik, P., Jokat, W., Kristoffersen, Y., 2006. The Cenozoic palaeoenvironment of the Arctic Ocean. *Nature* 441, 601-605.
- Mulkidjanian, A.Y.,** Dibrov, P., Galperin, M.Y., 2008. The past and present of sodium energetics: May the sodium-motive force be with you. *Biochimica et Biophysica Acta - Bioenergetics* 1777, 985-992.
- Murphy, B.H.,** Farley, K.A., Zachos, J.C., 2010. An extraterrestrial ³He-based timescale for the Paleocene-Eocene thermal maximum (PETM) from Walvis Ridge, IODP Site 1266. *Geochimica et Cosmochimica Acta* 74, 5098-5108.
- Murry, M.A.,** Wolk, C.P., 1989. Evidence that the barrier to the penetration of oxygen into heterocysts depends upon two layers of the cell envelope. *Archives of Microbiology* 151, 469-474.
- Nicol, G.W.,** Leininger, S., Schleper, C., Prosser, J.I., 2008. The influence of soil pH on the diversity, abundance and transcriptional activity of ammonia oxidizing archaea and bacteria. *Environmental Microbiology* 10, 2966-2978.

- Nicolo, M.J.**, Dickens, G.R., Hollis, C.J., 2010. South Pacific intermediate water oxygen depletion at the onset of the Paleocene-Eocene thermal maximum as depicted in New Zealand margin sections. *Paleoceanography* 25, PA4210.
- Nicolo, M.J.**, Dickens, G.R., Hollis, C.J., Zachos, J.C., 2007. Multiple early Eocene hyperthermals: Their sedimentary expression on the New Zealand continental margin and in the deep sea. *Geology* 35, 699-702.
- Nielsen, O.B.**, Baumann, J., Zhang, D., Heilmann-Clausen, C., Larsen, G., 1986. Tertiary deposits in Store Bælt. In: Møller, J.T. (Ed.), Twenty five years of geology in Aarhus. Geoskrifter, pp. 235-253.
- Nomura, T.**, Cranfield, C.G., Deplazes, E., Owen, D.M., Macmillan, A., Battle, A.R., Constantine, M., Sokabe, M., Martinac, B., 2012. Differential effects of lipids and lyso-lipids on the mechanosensitivity of the mechanosensitive channels MscL and MscS. *Proceedings of the National Academy of Sciences of the United States of America* 109, 8770-8775.
- O'Regan, M.**, Moran, K., Backman, J., Jakobsson, M., Sangiorgi, F., Brinkhuis, H., Pockalny, R., Skelton, A., Stickley, C., Koç, N., Brumsack, H. J., Willard, D., 2008. Mid-Cenozoic tectonic and paleoenvironmental setting of the central Arctic Ocean. *Paleoceanography* 2, PA1S20.
- Oakes, J.M.**, Revill, A.T., Connolly, R.M., Blackburn, S.I., 2005. Measuring carbon isotope ratios of microphytobenthos using compound-specific stable isotope analysis of phytol. *Limnology and Oceanography-Methods* 3 511-519.
- Oba, M.**, Sakata, S., Tsunogai, U., 2006. Polar and neutral isoprenyl glycerol ether lipids as biomarkers of archaea in near-surface sediments from the Nankai Trough. *Organic Geochemistry* 37, 1643-1654.
- Ogawa, Y.**, Takahashi, K., Yamanaka, T., Onodera, J., 2009. Significance of euxinic condition in the middle Eocene paleo-Arctic basin: A geochemical study on the IODP Arctic Coring Expedition 302 sediments. *Earth and Planetary Science Letters* 285, 190-197.
- Or, J.C.**, Fabry, V.J., Aumont, O., Bopp, L., Doney, S.C., Feely, R.A., Gnanadesikan, A., Gruber, N., Ishida, A., Joos, F., Key, R.M., Lindsay, K., Maier-Reimer, E., Matear, R., Monfray, P., Mouchet, A., Najjar, R.G., Plattner, G.K., Rodgers, K.B., Sabine, C.L., Sarmiento, J.L., Schlitzer, R., Slater, R.D., Totterdell, I.J., Weirig, M.F., Yamanaka, Y., Yool, A., 2005. Anthropogenic ocean acidification over the twenty-first century and its impact on calcifying organisms. *Nature* 437, 681-686.
- Overmann, J.**, Cypionka, H., Pfennig, N., 1992. An extremely low-light-adapted phototrophic sulfur bacterium from the Black Sea. *Limnology and Oceanography* 37, 150-155.
- Pagani, M.**, 2002. The alkenone- CO_2 proxy and ancient atmospheric carbon dioxide. *Philosophical Transactions of the Royal Society of London Series* 360, 609-632.
- Pagani, M.**, Caldeira, K., Archer, D., Zachos, J.C., 2006a. An ancient carbon mystery. *Science* 314, 1556-1557.
- Pagani, M.**, Pedentchouk, N., Huber, M., Sluijs, A., Schouten, S., Brinkhuis, H., Sinninghe Damsté,

- J.S., Dickens, G.R., the Expedition 302 Scientists, 2006b. Arctic hydrology during global warming at the Palaeocene/Eocene thermal maximum. *Nature* 442, 671-675.
- Pagani, M.**, Lemarchand, D., Spivack, A., Gaillardet, J., 2005a. A critical evaluation of the boron isotope-pH proxy: The accuracy of ancient ocean pH estimates. *Geochimica et Cosmochimica Acta*, 69, 953-961.
- Pagani, M.**, Zachos, J.C., Freeman, K.H., Tipple, B., Bohaty, S., 2005b. Marked decline in atmospheric carbon dioxide concentrations during the Paleogene. *Science* 309, 600-603.
- Pagani, M.**, Freeman, K.H., Ohkouchi, N., Caldeira, K., 2002a. Comparison of water column $[\text{CO}_{2\text{aq}}]$ with sedimentary alkenone-based estimates: A test of the alkenone- CO_2 proxy. *Paleoceanography* 1, 1069.
- Pagani, M.**, Zachos, J.C., Freeman, K.H., 2002b. Eocene/Oligocene alkenone-based CO_2 estimates. *Geochimica et Cosmochimica Acta* 66, A578.
- Pagani, M.**, Arthur, M.A., Freeman, K.H., 1999. Miocene evolution of atmospheric carbon dioxide. *Paleoceanography* 14, 273-292.
- Palmer, M.R.**, Brummer, G.J., Cooper, M.J., Elderfield, H., Greaves, M.J., Reichert, G.J., Schouten, S., Yu, J.M., 2010. Multi-proxy reconstruction of surface water pCO_2 in the northern Arabian Sea since 29 ka. *Earth and Planetary Science Letters* 295, 49-57.
- Palmer, M.R.**, Pearson, P.N., 2003. A 23,000-year record of surface water pH and pCO_2 in the western equatorial Pacific Ocean. *Science* 300, 480-482.
- Panchuk, K.**, Ridgwell, A., Kump, L.R., 2008. Sedimentary response to Paleocene-Eocene Thermal Maximum carbon release: A model-data comparison. *Geology* 36, 315-318.
- Pancost, R.D.**, Pagani, M., 2006. Controls on the carbon isotopic compositions of lipids in marine environments. In: Volkman, J.K. (Ed.), *Marine Organic Matter: Biomarkers, Isotopes and DNA*, The Handbook of Environmental Chemistry. Springer-Verlag, Germany, pp. 209-249.
- Park, B.J.**, Park, S.J., Yoon, D.N., Schouten, S., Sinninghe Damsté, J.S., Rhee, S.K., 2010. Cultivation of autotrophic ammonia-oxidizing Archaea from marine sediments in coculture with sulfur-oxidizing bacteria. *Applied and Environmental Microbiology* 76, 7575-7587.
- Pearson, E.J.**, Juggins, S., Talbot, H.M., Weckstrom, J., Rosen, P., Ryves, D.B., Roberts, S.J., Schmidt, R., 2011. A lacustrine GDGT-temperature calibration from the Scandinavian Arctic to Antarctic: Renewed potential for the application of GDGT-paleothermometry in lakes. *Geochimica et Cosmochimica Acta* 75, 6225-6238.
- Pearson, A.**, McNichol, A.P., Benitez-Nelson, B.C., Hayes, J.M., Eglinton, T.I., 2001a. Origins of lipid biomarkers in Santa Monica Basin surface sediment: A case study using compound-specific $\delta^{14}\text{C}$ analysis. *Geochimica et Cosmochimica Acta* 65, 3123-3137.
- Pearson, P.N.**, Ditchfield, P.W., Singano, J., Harcourt-Brown, K.G., Nicholas, C.J., Olsson, R.K., Shackleton, N.J., Hall, M.A., 2001b. Warm tropical sea surface temperatures in the Late Cretaceous and Eocene epochs. *Nature* 413, 481-487.

- Pearson, P.N.**, Palmer, M.R., 2002. The boron isotope approach to paleo- $p\text{CO}_2$ estimation. *Geochimica et Cosmochimica Acta* 66, A586-A586.
- Pearson, P.N.**, Palmer, M.R., 2000a. Atmospheric carbon dioxide concentrations over the past 60 million years. *Nature* 406 695-699.
- Pearson, P.N.**, Palmer, M.R., 2000b. Estimating Paleogene atmospheric $p\text{CO}_2$ using boron isotope analysis of foraminifera. *Gff* 122, 127-128.
- Pedersen, G.K.**, 1981. Anoxic events during sedimentation of a Palaeogene diatomite in Denmark. *Sedimentology* 28, 487-504.
- Peterse, F.**, Nicol, G.W., Schouten, S., Sinninghe Damsté, J.S., 2010. Influence of soil pH on the abundance and distribution of core and intact polar lipid-derived branched GDGTs in soil. *Organic Geochemistry* 41, 1171-1175.
- Peterse, F.**, Kim, J.H., Schouten, S., Kristensen, D.K., Koç, N., Sinninghe Damsté, J.S., 2009a. Constraints on the application of the MBT/CBT palaeothermometer at high latitude environments (Svalbard, Norway). *Organic Geochemistry* 40, 692-699.
- Peterse, F.**, Schouten, S., van der Meer, J., van der Meer, M.T.J., Sinninghe Damsté, J.S., 2009b. Distribution of branched tetraether lipids in geothermally heated soils: Implications for the MBT/CBT temperature proxy. *Organic Geochemistry* 40, 201-205.
- Peterse, F.**, van der Meer, M.T.J., Schouten, S., Jia, G., Ossebaar, J., Blokker, J., Sinninghe Damsté, J.S., 2009c. Assessment of soil n -alkane δD and branched tetraether membrane lipid distributions as tools for paleoelevation reconstruction. *Biogeosciences* 6, 2799-2807.
- Petit, J.R.**, Jouzel, J., Raynaud, D., Barkov, N.I., Barnola, J.-M., Basile, I., Bender, M., Chappellaz, J., Davis, M., Delaygue, G., Delmotte, M., Kotlyakov, V.M., Legrand, M., Lipenkov, V.Y., Lorius, C., Pépin, L., Ritz, C., Saltzman, E., Stievenard, M., 1999. Climate and atmospheric history of the past 420,000 years from the Vostok ice core, Antarctica. *Nature* 399, 429-436.
- Pitcher, A.**, Hopmans, E.C., Mosier, A.C., Park, S.J., Rhee, S.K., Francis, C.A., Schouten, S., Sinninghe Damsté, J.S., 2011a. Core and intact polar glycerol dibiphytanyl glycerol tetraether lipids of ammonia-oxidizing Archaea enriched from marine and estuarine sediments. *Applied and Environmental Microbiology* 77, 3468-3477.
- Pitcher, A.**, Villanueva, L., Hopmans, E.C., Schouten, S., Reichart, G.J., Sinninghe Damsté, J.S., 2011b. Niche segregation of ammonia-oxidizing archaea and anammox bacteria in the Arabian Sea oxygen minimum zone. *ISME Journal* 5, 1896-1904.
- Pitcher, A.**, Hopmans, E.C., Schouten, S., Sinninghe Damsté, J.S., 2009. Separation of core and intact polar archaeal tetraether lipids using silica columns: Insights into living and fossil biomass contributions. *Organic Geochemistry* 40, 12-19.
- Popendorf, K.J.**, Lomas, M.W., van Mooy, B.A.S., 2011. Microbial sources of intact polar diacylglycerolipids in the Western North Atlantic Ocean. *Organic Geochemistry* 42, 803-811.
- Popp, B.N.**, Kenig, F., Wakeham, S.G., Laws, E.A., Bidigare, R.R., 1998a. Does growth rate affect ketone un-

- saturation and intracellular carbon isotopic variability in *Emiliania huxleyi*? *Paleoceanography* 13, 35-41.
- Popp, B.N.**, Laws, E.A., Bidigare, R.R., Dore, J.E., Hanson, K.L., Wakeham, S.G., 1998b. Effect of phytoplankton cell geometry on carbon isotopic fractionation. *Geochimica et Cosmochimica Acta* 62, 69-77.
- Popp, B.N.**, Takigiku, R., Hayes, J.M., Louda, J.W., Baker, E.W., 1989. The post-Paleozoic chronology and mechanism of ^{13}C depletion in primary marine organic matter. *American Journal of Science* 289, 436-454.
- Quandt, L.**, Gottschalk, G., Ziegler, H., Stichler, W., 1977. Isotope Discrimination by Photosynthetic Bacteria. *Fems Microbiology Letters* 1, 125-128.
- Rau, G.H.**, Riebesell, U., Wolf-Gladrow, D., 1996. A model of photosynthetic ^{13}C fractionation by marine phytoplankton based on diffusive molecular CO_2 uptake. *Marine Ecology Progress Series* 133, 275-285.
- Rau, G.H.**, Riebesell, U., Wolf-Gladrow, D., 1997. $\text{CO}_{2\text{aq}}$ -dependent photosynthetic ^{13}C fractionation in the ocean: A model versus measurements. *Global Biogeochemical Cycles* 11, 267-278.
- Rau, G.H.**, Takahashi, T., Desmarais, D.J., Repeta, D.J., Martin, J.H., 1992. The relationship between $\delta^{13}\text{C}$ of organic matter and $[\text{CO}_2(\text{aq})]$ in ocean surface water: Data from a JGOFS site in the northeast Atlantic Ocean and a model. *Geochimica et Cosmochimica Acta* 56, 1413-1419.
- Raven, J.**, Caldeira, K., Elderfield, H., Hoegh-Guldberg, O., Liss, P., Riebesell, U., Shepherd, J., Turley, C., Watson, A., 2005. Ocean Acidification due to Increasing Atmospheric Carbon Dioxide, Policy document 12/05. The Royal Society, London.
- Reinfelder, J.R.**, 2011. Carbon concentrating mechanisms in eukaryotic marine phytoplankton. *Annual Review of Marine Science* 3, 291-315.
- Retallack, G.J.**, 2001. A 300-million-year record of atmospheric carbon dioxide from fossil plant cuticles. *Nature* 411, 287-290.
- Riebesell, U.**, Zondervan, I., Rost, B., Tortell, P.D., Zeebe, R.E., Morel, F.M.M., 2000. Reduced calcification of marine plankton in response to increased atmospheric CO_2 . *Nature* 407, 364-367.
- Röhl, U.**, Westerhold, T., Bralower, T.J., Zachos, J.C., 2007. On the duration of the Paleocene-Eocene thermal maximum (PETM). *Geochemistry Geophysics Geosystems* 8, Q12002.
- Rohmer, M.**, Bisseret, P., Neunlist, S., 1992. The hopanoids, prokaryotic triterpenoids and precursors of ubiquitous molecular fossils. In: Moldowan, J.M., Albrecht, P., Philp, R.P. (Eds.), *Biological Markers in Sediments and Petroleum*. Prentice Hall, Englewood Cliffs, NJ, USA, pp. 1-17.
- Rost, B.**, Zondervan, I., Riebesell, U., 2002. Light-dependent carbon isotope fractionation in the coccolithophorid *Emiliania huxleyi*. *Limnology and Oceanography* 47, 120-128.
- Royer, D.L.**, 2001. Stomatal density and stomatal index as indicators of paleoatmospheric CO_2 concentration. *Review of Palaeobotany and Palynology* 114, 1-28.
- Royer, D.L.**, Berner, R.A., Beerling, D.J., 2001. Phanerozoic atmospheric CO_2 change: evaluating geochemical and paleobiological approaches. *Earth-Science Reviews* 54, 349-392.

- Royer, D.L.**, Osborne, C.P., Beerling, D.J., 2002. High CO₂ increases the freezing sensitivity of plants: Implications for paleoclimatic reconstructions from fossil floras. *Geology* 30, 963-966.
- Rudd, J.W.M.**, Kelly, C.A., Schindler, D.W., Turner, M.A., 1988. Disruption of the nitrogen cycle in acidified lakes. *Science* 240, 1515-1517.
- Rütters, H.**, Sass, H., Cypionka, H., Rullkötter, J., 2002. Phospholipid analysis as a tool to study complex microbial communities in marine sediments. *Journal of Microbiological Methods* 48, 149-160.
- Sabine, C.L.**, Feely, R.A., Gruber, N., Key, R.M., Lee, K., Bullister, J.L., Wanninkhof, R., Wong, C.S., Wallace, D.W., Tilbrook, B., Millero, F.J., Peng, T.H., Kozyr, A., Ono, T., Rios, A.F., 2004. The oceanic sink for anthropogenic CO₂. *Science* 305, 367-71.
- Sachse, D.**, Radke, J., Gleixner, G., 2006. δD values of individual *n*-alkanes from terrestrial plants along a climatic gradient - Implications for the sedimentary biomarker record. *Organic Geochemistry* 37, 469-483.
- Sakata, S.**, Hayes, J.M., McTaggart, A.R., Evans, R.A., Leckrone, K.J., Togasaki, R.K., 1997. Carbon isotopic fractionation associated with lipid biosynthesis by a cyanobacterium: Relevance for interpretation of biomarker records. *Geochimica et Cosmochimica Acta* 61, 5379-5389.
- Sanyal, A.**, Hemming, N.G., Hanson, G.N., Broecker, W.S., 1995. Evidence for a higher pH in the glacial ocean from boron isotopes in foraminifera. *Nature* 373, 234-236.
- Schefuß, E.**, Ratmeyer, V., Stuut, J.B.W., Jansen, J.H.F., Sinninghe Damsté, J.S., 2003. Carbon isotope analyses of *n*-alkanes in dust from the lower atmosphere over the central eastern Atlantic. *Geochimica et Cosmochimica Acta* 67, 1757-1767.
- Schidlowski, M.A.**, Aharon, P., 1992. Carbon cycle and carbon isotopic record: geochemical impact on life over 3.8 Ga of Earth history. In: Schidlowski, M. (Ed.), *Early Organic Evolution: Implications for Mineral and Energy Resources*. Springer-Verlag, Heidelberg, pp. 147-175.
- Schindler, D.W.**, 1977. Evolution of phosphorus limitation in lakes. *Science* 195, 260-262.
- Schmitz, B.**, Peucker-Ehrenbrink, B., Heilmann-Clausen, C., Åberg, G., Asaro, F., Lee, C.T.A., 2004. Basaltic explosive volcanism, but no comet impact, at the Paleocene-Eocene boundary: high-resolution chemical and isotopic records from Egypt, Spain and Denmark. *Earth and Planetary Science Letters* 225, 1-17.
- Schmitz, B.**, Pujalte, V., 2003. Sea-level, humidity, and land-erosion records across the initial Eocene thermal maximum from a continental-marine transect in northern Spain. *Geology* 31, 689-692.
- Schoell, M.**, Schouten, S., Sinninghe Damsté, J.S., de Leeuw, J.W., Summons, R.E., 1994. A molecular organic carbon isotope record of Miocene climate changes. *Science* 263, 1122-1125.
- Schoemann, V.**, Becquevort, S., Stefels, J., Rousseau, W., Lancelot, C., 2005. *Phaeocystis* blooms in the global ocean and their controlling mechanisms: a review. *Journal of Sea Research* 53, 43-66.

- Schoon, P.L.**, Heilmann-Clausen, C., Schultz, B.P., Sinninghe Damsté, J.S., Schouten, S., 2013. Extreme warming and environmental change of the North Sea Basin across the Palaeocene-Eocene boundary. *Organic Geochemistry*, in review.
- Schoon, P.L.**, Sluijs, A., Sinninghe Damsté, J.S., Schouten, S., 2011. Stable carbon isotope patterns of marine biomarker lipids in the Arctic Ocean during Eocene Thermal Maximum 2. *Paleoceanography* 26, PA3215.
- Schouten, S.**, Hopmans, E.C., Sinninghe Damsté, J.S., 2013. The organic geochemistry of glycerol dialkyl glycerol tetraether lipids: A review. *Organic Geochemistry* 54, 19-61.
- Schouten, S.**, Huguet, C., Hopmans, E.C., Kienhuis, M.V.M., Sinninghe Damsté, J.S., 2007a. Analytical methodology for TEX₈₆ paleothermometry by high-performance liquid chromatography/atmospheric pressure chemical ionization-mass spectrometry. *Analytical Chemistry* 79, 2940-2944.
- Schouten, S.**, Woltering, M., Rijpstra, W.I.C., Sluijs, A., Brinkhuis, H., Sinninghe Damsté, J.S., 2007b. The Paleocene-Eocene carbon isotope excursion in higher plant organic matter: Differential fractionation of angiosperms and conifers in the Arctic. *Earth and Planetary Science Letters* 258, 581-592.
- Schouten, S.**, Hopmans, E.C., Schefuß, E., Sinninghe Damsté, J.S., 2002. Distributional variations in marine crenarchaeotal membrane lipids: a new tool for reconstructing ancient sea water temperatures? *Earth and Planetary Science Letters* 204, 265-274.
- Schouten, S.**, Hoefs, M.J.L., Sinninghe Damsté, J.S., 2000a. A molecular and stable carbon isotopic study of lipids in late Quaternary sediments from the Arabian Sea. *Organic Geochemistry* 31, 509-521.
- Schouten, S.**, Hopmans, E.C., Pancost, R.D., Sinninghe Damsté, J.S., 2000b. Widespread occurrence of structurally diverse tetraether membrane lipids: Evidence for the ubiquitous presence of low-temperature relatives of hyperthermophiles. *Proceedings of the National Academy of Sciences of the United States of America*, 14421-14426.
- Schouten, S.**, van Kaam-Peters, H.M.E., Rijpstra, W.I.C., Schoell, M., Sinninghe Damsté, J.S., 2000c. Effects of an oceanic anoxic event on the stable carbon isotopic composition of Early Toarcian carbon. *American Journal of Science* 300, 1-22.
- Schouten, S.**, Breteler, W.C.M.K., Blokker, P., Schogt, N., Rijpstra, W.I.C., Grice, K., Baas, M., Sinninghe Damsté, J.S., 1998a. Biosynthetic effects on the stable carbon isotopic compositions of algal lipids: Implications for deciphering the carbon isotopic biomarker record. *Geochimica et Cosmochimica Acta* 62, 1397-1406.
- Schouten, S.**, Hoefs, M.J.L., Koopmans, M.P., Bosch, H.J., Sinninghe Damsté, J.S., 1998b. Structural characterization, occurrence and fate of archaeal ether-bound acyclic and cyclic biphytanes and corresponding diols in sediments. *Organic Geochemistry* 29, 1305-1319.
- Schrag, D.P.**, 1999. Effects of diagenesis on the isotopic record of late paleogene tropical sea surface

- temperatures. *Chemical Geology* 161, 215-224.
- Schubotz, F.**, Wakeham, S.G., Lipp, J.S., Fredricks, H.F., Hinrichs, K.U., 2009. Detection of microbial biomass by intact polar membrane lipid analysis in the water column and surface sediments of the Black Sea. *Environmental Microbiology* 11, 2720-2734.
- Shaw, N.**, 1974. Lipid composition as a guide to the classification of Bacteria. *Advances in Applied Microbiology* 17, 63-108.
- Siegenthaler, U.**, Monnin, E., Kawamura, K., Spahni, R., Schwander, J., Stauffer, B., Stocker, T.F., Barnola, J.M., Fischer, H., 2005. Supporting evidence from the EPICA Dronning Maud Land ice core for atmospheric CO₂ changes during the past millennium. *Tellus Series B-Chemical and Physical Meteorology* 57, 51-57.
- Sinninghe Damsté, J.S.**, Rijpstra, W.I.C., Hopmans, E.C., Weijers, J.W.H., Foesel, B.U., Overmann, J., Dedys, S.N., 2011. 13,16-dimethyl octacosanedioic acid (*iso*-diabolic acid), a common membrane-spanning lipid of *Acidobacteria* subdivisions 1 and 3. *Applied and Environmental Microbiology* 77, 4147-4154.
- Sinninghe Damsté, J.S.**, Ossebaar, J., Abbas, B., Schouten, S., Verschuren, D., 2009. Fluxes and distribution of tetraether lipids in an equatorial African lake: Constraints on the application of the TEX₈₆ palaeothermometer and BIT index in lacustrine settings. *Geochimica et Cosmochimica Acta* 73, 4232-4249.
- Sinninghe Damsté, J.S.**, Kuypers, M.M.M., Pancost, R.D., Schouten, S., 2008. The carbon isotopic response of algae, (cyano)bacteria, archaea and higher plants to the late Cenomanian perturbation of the global carbon cycle: Insights from biomarkers in black shales from the Cape Verde Basin (DSDP Site 367). *Organic Geochemistry* 39, 1703-1718.
- Sinninghe Damsté, J.S.**, Schouten, S., 2006. Biological markers for anoxia in the photic zone of the water column. In: Volkman, J.K. (Ed.), *Marine Organic Matter: Biomarkers, Isotopes and DNA*, The Handbook of Environmental Chemistry. Springer-Verlag, Berlin, Heidelberg, pp. 127-163.
- Sinninghe Damsté, J.S.**, Muyzer, G., Abbas, B., Rampen, S.W., Massé, G., Allard, W.G., Belt, S.T., Robert, J.M., Rowland, S.J., Moldowan, J.M., Barbanti, S.M., Fago, F.J., Denisevich, P., Dahl, J., Trindade, L.A.F., Schouten, S., 2004a. The rise of the rhizosolenid diatoms. *Science* 304, 584-587.
- Sinninghe Damsté, J.S.**, Rijpstra, W.I.C., Schouten, S., Fuerst, J.A., Jetten, M.S.M., Strous, M., 2004b. The occurrence of hopanoids in planctomycetes: implications for the sedimentary biomarker record. *Organic Geochemistry* 35, 561-566.
- Sinninghe Damsté, J.S.**, Schouten, S., Hopmans, E.C., van Duin, A.C.T., Geenevasen, J.A.J., 2002. Crenarchaeol: the characteristic core glycerol dibiphytanyl glycerol tetraether membrane lipid of cosmopolitan pelagic crenarchaeota. *Journal of Lipid Research* 43, 1641-1651.
- Sinninghe Damsté, J.S.**, Hopmans, E.C., Pancost, R.D., Schouten, S., Geenevasen, J.A.J., 2000. Newly discovered non-isoprenoid glycerol

- dialkyl glycerol tetraether lipids in sediments. *Chemical Communications* 17, 1683-1684.
- Sinninghe Damsté, J.S., Köster, J., 1998.** A euxinic southern North Atlantic Ocean during the Cenomanian/Turonian oceanic anoxic event. *Earth and Planetary Science Letters* 158, 165-173.
- Sinninghe Damsté, J.S., Wakeham, S.G., Kohnen, M.E.L., Hayes, J.M., de Leeuw, J.W., 1993.** A 6,000 year sedimentary molecular record of chemocline excursions in the Black Sea. *Nature* 362, 827-829.
- Sinninghe Damsté, J.S., de Leeuw, J.W., 1990.** Analysis, structure and geochemical significance of organically-bound sulfur in the geosphere: State of the art and future research. *Organic Geochemistry* 16, 1077-1101.
- Sinninghe Damsté, J.S., Rijpstra, W.I.C., de Leeuw, J.W., Schenck, P.A., 1988.** Origin of organic sulfur-compounds and sulfur-containing high molecular-weight substances in sediments and immature crude oils. *Organic Geochemistry* 13, 593-606.
- Sirevåg, R., Castenholz, R.W., 1979.** Aspects of carbon metabolism in *Chloroflexus*. *Archives of Microbiology* 120, 151-153.
- Sluijs, A., Dickens, G.R., 2012.** Assessing offsets between $\delta^{13}\text{C}$ of sedimentary components and the global exogenic carbon pool across Early Paleogene carbon cycle perturbations. *Global Biogeochemical Cycles* 26, 1-14.
- Sluijs, A., Bijl, P.K., Schouten, S., Röhl, U., Reichart, G.J., Brinkhuis, H., 2011.** Southern ocean warming, sea level and hydrological change during the Paleocene-Eocene thermal maximum. *Climate of the Past* 7, 47-61.
- Sluijs, A., Schouten, S., Donders, T.H., Schoon, P.L., Röhl, U., Reichart, G.J., Sangiorgi, F., Kim, J.H., Sinninghe Damsté, J.S., Brinkhuis, H., 2009.** Warm and wet conditions in the Arctic region during Eocene Thermal Maximum 2. *Nature Geoscience* 2, 777-780.
- Sluijs, A., Röhl, U., Schouten, S., Brumsack, H.J., Sangiorgi, F., Sinninghe Damsté, J.S., Brinkhuis, H., 2008.** Arctic late Paleocene-early Eocene paleoenvironments with special emphasis on the Paleocene-Eocene thermal maximum (Lomonosov Ridge, Integrated Ocean Drilling Program Expedition 302). *Paleoceanography* 23, PA1S11.
- Sluijs, A., Bowen, G.J., Brinkhuis, H., Lourens, L.J., Thomas, E., 2007a.** The Paleocene-Eocene Thermal Maximum super greenhouse: Biotic and geochemical signatures, age models and mechanisms of global change. In: Williams, M. (Ed.), *Deep-time perspectives on climate change: Marrying the signal from computer models and biological proxies*. geological Society, London, pp. 323-349.
- Sluijs, A., Brinkhuis, H., Schouten, S., Bohaty, S.M., John, C.M., Zachos, J.C., Reichart, G.J., Sinninghe Damsté, J.S., Crouch, E.M., Dickens, G.R., 2007b.** Environmental precursors to rapid light carbon injection at the Palaeocene/Eocene boundary. *Nature* 450, 1218-1222.
- Sluijs, A., Schouten, S., Pagani, M., Woltering, M., Brinkhuis, H., Sinninghe Damsté, J.S., Dickens, G.R., Huber, M., Reichart, G.J., Stein, R., Matthiessen, J., Lourens, L.J., Pedentchouk, N., Backman,**

- J., Moran, K., the Expedition 302 Scientists, 2006. Subtropical arctic ocean temperatures during the Palaeocene/Eocene thermal maximum. *Nature* 441, 610-613.
- Sluijs, A.**, Pross, J., Brinkhuis, H., 2005. From greenhouse to icehouse; organic-walled dinoflagellate cysts as paleoenvironmental indicators in the Paleogene. *Earth-Science Reviews* 68, 281-315.
- Smith, F.A.**, Wing, S.L., Freeman, K.H., 2007. Magnitude of the carbon isotope excursion at the Paleocene-Eocene thermal maximum: The role of plant community change. *Earth and Planetary Science Letters* 262, 50-65.
- Smith, V.H.**, 1983. Low nitrogen to phosphorus ratios favor dominance by blue-green algae in lake phytoplankton. *Science* 221, 669-671.
- Sohlenkamp, C.**, López-Lara, I.M., Geiger, O., 2003. Biosynthesis of phosphatidylcholine in bacteria. *Progress in Lipid Research* 42, 115-162.
- Speelmanns, G.**, Poolman, B., Konings, W.N., 1995. Na⁺ as coupling ion in energy transduction in extremophilic Bacteria and Archaea. *World Journal of Microbiology & Biotechnology* 11, 58-70.
- Stap, L.**, Lourens, L.J., Thomas, E., Sluijs, A., Bohaty, S., Zachos, J.C., 2010. High-resolution deep-sea carbon and oxygen isotope records of Eocene Thermal Maximum 2 and H2. *Geology* 38, 607-610.
- Stap, L.**, Sluijs, A., Thomas, E., Lourens, L., 2009. Patterns and magnitude of deep sea carbonate dissolution during Eocene Thermal Maximum 2 and H2, Walvis Ridge, southeastern Atlantic Ocean. *Paleoceanography* 24, PA1211.
- Stein, R.**, Boucsein, B., Meyer, H., 2006. Anoxia and high primary production in the Paleogene central Arctic Ocean: First detailed records from Lomonosov Ridge. *Geophysical Research Letters* 33, L18606.
- Storey, M.**, Duncan, R.A., Swisher, C.C., 2007. Paleocene-Eocene thermal maximum and the opening of the northeast Atlantic. *Science* 316, 587-589.
- Sturt, H.F.**, Summons, R.E., Smith, K., Elvert, M., Hinrichs, K.U., 2004. Intact polar membrane lipids in prokaryotes and sediments deciphered by high-performance liquid chromatography/electrospray ionization multistage mass spectrometry—new biomarkers for biogeochemistry and microbial ecology. *Rapid Communications in Mass Spectrometry* 18, 617-628.
- Summons, R.E.**, Franzmann, P.D., Nichols, P.D., 1998. Carbon isotopic fractionation associated with methylotrophic methanogenesis. *Organic Geochemistry* 28, 465-475.
- Summons, R.E.**, Jahnke, L.L., Hope, J.M., Logan, G.A., 1999. 2-Methylhopanoids as biomarkers for cyanobacterial oxygenic photosynthesis. *Nature* 400, 554-557.
- Summons, R.E.**, Powell, T.G., 1986. *Chlorobiaceae* in Paleozoic seas revealed by biological markers, isotopes and geology. *Nature* 319, 763-765.
- Sun, Q.**, Chu, G., Liu, M., Xie, M., Li, S., Ling, Y., Wang, X., Shi, L., Jia, G., Lü, H., 2011. Distributions and temperature dependence of branched glycerol dialkyl glycerol tetraethers in recent lacustrine sediments from China and Nepal. *Journal of Geophysical Research-Biogeosciences* 116, G01008.

- Svensen, H.**, Planke, S., Malthesørensen, A., Jamtveit, B., Myklebust, R., Eidem, T.R., Rey, S.S., 2004. Release of methane from a volcanic basin as a mechanism for initial Eocene global warming. *Nature* 429, 542-545.
- Talbot, H.M.**, Summons, R.E., Jahnke, L.L., Cockell, C.S., Rohmer, M., Farrimond, P., 2008. Cyanobacterial bacteriohopanepolyol signatures from cultures and natural environmental settings. *Organic Geochemistry* 39, 232-263.
- Thomas, D.J.**, Zachos, J.C., Bralower, T.J., Thomas, E., Bohaty, S., 2002. Warming the fuel for the fire: Evidence for the thermal dissociation of methane hydrate during the Paleocene-Eocene thermal maximum. *Geology* 30, 1067-1070.
- Thomas, E.**, Shackleton, N.J., 1996. The Paleocene-Eocene benthic foraminiferal extinction and stable isotope anomalies. In: Knox, R.W.O.B., Corfield, R.M., Dunay, R.E. (Eds.), *Correlation of the Early Paleogene in Northwest Europe*. Geological Society Special Publication, London, pp. 401-441.
- Tierney, J.E.**, Schouten, S., Pitcher, A., Hopmans, E.C., Sinninghe Damsté, J.S., 2012. Core and intact polar glycerol dialkyl glycerol tetraethers (GDGTs) in Sand Pond, Warwick, Rhode Island (USA): Insights into the origin of lacustrine GDGTs. *Geochimica et Cosmochimica Acta* 77, 561-581.
- Tierney, J.E.**, Russell, J.M., Eggermont, H., Hopmans, E.C., Verschuren, D., Sinninghe Damsté, J.S., 2010. Environmental controls on branched tetraether lipid distributions in tropical East African lake sediments. *Geochimica et Cosmochimica Acta* 74, 4902-4918.
- Tierney, J.E.**, Russell, J.M., 2009. Distributions of branched GDGTs in a tropical lake system: Implications for lacustrine application of the MBT/CBT paleoproxy. *Organic Geochemistry* 40, 1032-1036.
- Tranvik, L.J.**, Downing, J.A., Cotner, J.B., Loiselle, S.A., Striegl, R.G., Ballatore, T.J., Dillon, P., Finlay, K., Fortino, K., Knoll, L.B., Kortelainen, P.L., Kutser, T., Larsen, S., Laurion, I., Leech, D.M., McCallister, S.L., McKnight, D.M., Melack, J.M., Overholt, E., Porter, J.A., Prairie, Y., Renwick, W.H., Roland, F., Sherman, B.S., Schindler, D.W., Sobek, S., Tremblay, A., Vanni, M.J., Verschoor, A.M., von Wachenfeldt, E., Weyhenmeyer, G.A., 2009. Lakes and reservoirs as regulators of carbon cycling and climate. *Limnology and Oceanography* 54, 2298-2314.
- Tripathi, A.**, Elderfield, H., 2005. Deep-sea temperature and circulation changes at the Paleocene-Eocene thermal maximum. *Science* 308, 1894-1898.
- Tripathi, A.K.**, Elderfield, H., 2004. Abrupt hydrographic changes in the equatorial Pacific and subtropical Atlantic from foraminiferal Mg/Ca indicate greenhouse origin for the thermal maximum at the Paleocene-Eocene Boundary. *Geochemistry Geophysics Geosystems* 5, Q02006.
- Tyler, J.J.**, Nederbragt, A.J., Jones, V.J., Thurow, J.W., 2010. Assessing past temperature and soil pH estimates from bacterial tetraether membrane lipids: Evidence from the recent lake sediments of Lochnagar, Scotland. *Journal of Geophysical Research-Biogeosciences* 115, G01015.

- Uchikawa, J.**, Zeebe, R.E., 2010. Examining possible effects of seawater pH decline on foraminiferal stable isotopes during the Paleocene-Eocene Thermal Maximum. *Paleoceanography* 25, PA2216.
- Valisollalao, J.**, Perakis, N., Chappe, B., Albrecht, P., 1984. A Novel Sulfur-Containing C₃₅ Hopanoid in Sediments. *Tetrahedron Letters* 25, 1183-1186.
- Van Breugel, Y.**, Baas, M., Schouten, S., Mattioli, E., Sinninghe Damsté, J.S., 2006. Isorenieratane record in black shales from the Paris Basin, France: Constraints on recycling of respired CO₂ as a mechanism for negative carbon isotope shifts during the Toarcian oceanic anoxic event. *Paleoceanography* 21, PA4220.
- Van der Burgh, J.**, Visscher, H., Dilcher, D.L., Kürschner, W.M., 1993. Paleatmospheric signatures in Neogene fossil leaves. *Science* 260, 1788-1790.
- Van der Meer, M.T.J.**, Schouten, S., Sinninghe Damsté, J.S., 1998. The effect of the reversed tricarboxylic acid cycle on the ¹³C contents of bacterial lipids. *Organic Geochemistry* 28, 527-533.
- Van Mooy, B.A.S.**, Fredricks, H.F., 2010. Bacterial and eukaryotic intact polar lipids in the eastern subtropical South Pacific: Water-column distribution, planktonic sources, and fatty acid composition. *Geochimica et Cosmochimica Acta* 74, 6499-6516.
- Van Mooy, B.A.S.**, Fredricks, H.F., Pedler, B.E., Dyhrman, S.T., Karl, D.M., Koblížek, M., Lomas, M.W., Mincer, T.J., Moore, L.R., Moutin, T., Rappé, M.S., Webb, E.A., 2009. Phytoplankton in the ocean use non-phosphorus lipids in response to phosphorus scarcity. *Nature* 458, 69-72.
- Van Mooy, B.A.S.**, Rocap, G., Fredricks, H.F., Evans, C.T., Devol, A.H., 2006. Sulfolipids dramatically decrease phosphorus demand by picocyanobacteria in oligotrophic marine environments. *Proceedings of the National Academy of Sciences of the United States of America* 103, 8607-8612.
- Verschuren, D.**, Sinninghe Damsté, J.S., Moernaut, J., Kristen, I., Blaauw, M., Fagot, M., Haug, G.H., CHALLACEA Project Members, 2009. Half-precessional dynamics of monsoon rainfall near the East African Equator. *Nature* 462, 637-641.
- Volkman, J.K.**, Barrett, S.M., Dunstan, G.A., 1994. C₂₅ and C₃₀ highly branched isoprenoid alkenes in laboratory cultures of two marine diatoms. *Organic Geochemistry* 21, 407-413.
- Wagner, C.**, Adrian, R., 2009a. Cyanobacteria dominance: Quantifying the effects of climate change. *Limnology and Oceanography* 54, 2460-2468.
- Wagner, C.**, Adrian, R., 2009b. Exploring lake ecosystems: hierarchy responses to long-term change? *Global Change Biology* 15, 1104-1115.
- Walsby, A.E.**, 1985. The permeability of heterocysts to the gases nitrogen and oxygen. *Proceedings of the Royal Society B-Biological Sciences* 226, 345-366.
- Weijers, J.W.H.**, Schouten, S., Sluijs, A., Brinkhuis, H., Sinninghe Damsté, J.S., 2007a. Warm arctic continents during the Palaeocene-Eocene thermal maximum. *Earth and Planetary Science Letters* 261, 230-238.

- Weijers, J.W.H.,** Schouten, S., van den Donker, J.C., Hopmans, E.C., Sinninghe Damsté, J.S., 2007b. Environmental controls on bacterial tetraether membrane lipid distribution in soils. *Geochimica et Cosmochimica Acta* 71, 703-713.
- Weijers, J.W.H.,** Schouten, S., Hopmans, E.C., Geenevasen, J.A.J., David, O.R.P., Coleman, J.M., Pancost, R.D., Sinninghe Damsté, J.S., 2006a. Membrane lipids of mesophilic anaerobic bacteria thriving in peats have typical archaeal traits. *Environmental Microbiology* 8, 648-657.
- Weijers, J.W.H.,** Schouten, S., Spaargaren, O.C., Sinninghe Damsté, J.S., 2006b. Occurrence and distribution of tetraether membrane lipids in soils: Implications for the use of the TEX₈₆ proxy and the BIT index. *Organic Geochemistry* 37, 1680-1693.
- West, N.,** Alexander, R., Kagi, R.I., 1990. The use of silicalite for rapid isolation of branched and cyclic alkane fractions of petroleum. *Organic Geochemistry* 15, 499-501.
- Westerhold, T.,** Röhl, U., McCarren, H.K., Zachos, J.C., 2009. Latest on the absolute age of the Paleocene-Eocene Thermal Maximum (PETM): New insights from exact stratigraphic posituyion of key ash layers +19 and -17. *Earth and Planetary Science Letters* 287, 412-419.
- White, D.C.,** Davis, W.M., Nickels, J.S., King, J.D., Bobbie, R.J., 1979. Determination of the sedimentary microbial biomass by extractable lipid phosphate. *Oecologia* 40, 51-62.
- Wing, S.L.,** Harrington, G.J., Smith, F.A., Bloch, J.I., Boyer, D.M., Freeman, K.H., 2005. Transient floral change and rapid global warming at the Paleocene-Eocene boundary. *Science* 310, 993-996.
- Woltering, M.,** Werne, J.P., Kish, J.L., Hicks, R., Sinninghe Damsté, J.S., Schouten, S., 2012. Vertical and temporal variability in concentration and distribution of thaumarchaeotal tetraether lipids in Lake Superior and the implications for the application of the TEX₈₆ temperature proxy. *Geochimica et Cosmochimica Acta* 87, 136-153.
- Wörmer, L.,** Cirés, S., Velázquez, D., Quesada, A., Hinrichs, K.U., 2012. Cyanobacterial heterocyst glycolipids in cultures and environmental samples: Diversity and biomarker potential. *Limnology and Oceanography* 57, 1775-1788.
- Wu, Y.,** Xiang, Y., Wang, J., Zhong, J., He, J., Wu, Q.L., 2010. Heterogeneity of archaeal and bacterial ammonia-oxidizing communities in Lake Taihu, China. *Environmental Microbiology Reports* 2, 569-576.
- Wuchter, C.,** Abbas, B., Coolen, M.J.L., Herfort, L., van Bleijswijk, J., Timmers, P., Strous, M., Teira, E., Herndl, G.J., Middelburg, J.J., Schouten, S., Sinninghe Damsté, J.S., 2006. Archaeal nitrification in the ocean. *Proceedings of the National Academy of Sciences of the United States of America* 103, 12317-12322.
- Wuchter, C.,** Schouten, S., Boschker, H.T.S., Sinninghe Damsté, J.S., 2003. Bicarbonate uptake by marine Crenarchaeota. *FEMS Microbiology Letters* 219, 203-207.
- Yang, H.A.,** Ding, W.H., Zhang, C.L.L., Wu, X., Ma, X.F., He, G.Q., Huang, J.H., Xie, S.C., 2011. Occurrence of tetraether lipids in stalagmites: Implications for sources and

- GDGT-based proxies. *Organic Geochemistry* 42, 108-115.
- Yapp, C.J.**, 2004. Fe(CO₃)OH in goethite from a mid-latitude North American Oxisol: Estimate of atmospheric CO₂ concentration in the Early Eocene "climatic optimum". *Geochimica et Cosmochimica Acta* 68, 935-947.
- Yu, J.M.**, Elderfield, H., Hönisch, B., 2007. B/Ca in planktonic foraminifera as a proxy for surface seawater pH. *Paleoceanography* 22, PA2202.
- Zachos, J.C.**, McCarren, H., Murphy, B., Röhl, U., Westerhold, T., 2010. Tempo and scale of late Paleocene and early Eocene carbon isotope cycles: Implications for the origin of hyperthermals. *Earth and Planetary Science Letters* 299, 242-249.
- Zachos, J.C.**, Dickens, G.R., Zeebe, R.E., 2008. An early Cenozoic perspective on greenhouse warming and carbon-cycle dynamics. *Nature* 451, 279-283.
- Zachos, J.C.**, Schouten, S., Bohaty, S., Quattlebaum, T., Sluijs, A., Brinkhuis, H., Gibbs, S.J., Bralower, T.J., 2006. Extreme warming of mid-latitude coastal ocean during the Paleocene-Eocene Thermal Maximum: Inferences from TEX₈₆ and isotope data. *Geology* 34, 737-740.
- Zachos, J.C.**, Röhl, U., Schellenberg, S.A., Sluijs, A., Hodell, D.A., Kelly, D.C., Thomas, E., Nicolo, M., Raffi, I., Lourens, L.J., McCarren, H., Kroon, D., 2005. Rapid acidification of the ocean during the Paleocene-Eocene thermal maximum. *Science* 308, 1611-1615.
- Zachos, J.C.**, Wara, M.W., Bohaty, S., Delaney, M.L., Petrizzo, M.R., Brill, A., Bralower, T.J., Premoli-Silva, I., 2003. A transient rise in tropical sea surface temperature during the Paleocene-Eocene Thermal Maximum. *Science* 302, 1551-1554.
- Zachos, J.C.**, Pagani, M., Sloan, L., Thomas, E., Billups, K., 2001. Trends, rhythms, and aberrations in global climate 65 Ma to present. *Science* 292, 686-693.
- Zeebe, R.E.**, Zachos, J.C., 2007. Reversed deep-sea carbonate ion basin gradient during Paleocene-Eocene thermal maximum. *Paleoceanography* 22, PA3201.
- Zeebe, R.E.**, Zachos, J.C., Caldeira, K., Tyrrell, T., 2008. Carbon emissions and acidification. *Science* 321, 51-52.
- Zeebe, R.E.**, Zachos, J.C., Dickens, G.R., 2009. Carbon dioxide forcing alone insufficient to explain Paleocene-Eocene Thermal Maximum warming. *Nature Geoscience* 2, 576-580.
- Zink, K.G.**, Vandergoes, M.J., Mangelsdorf, K., Dieffenbacher-Krall, A.C., Schwark, L., 2010. Application of bacterial glycerol dialkyl glycerol tetraethers (GDGTs) to develop modern and past temperature estimates from New Zealand lakes. *Organic Geochemistry* 41, 1060-1066.
- Zink, K.G.**, Wilkes, H., Disko, U., Elvert, M., Horsfield, B., 2003. Intact phospholipids - microbial "life markers" in marine deep subsurface sediments. *Organic Geochemistry* 34, 755-769.

SUMMARY

In addition to the more acknowledged consequences of climate change, such as global warming, the current human-induced increase of CO_2 into the atmosphere is also responsible for a change in the chemical composition of seawater. Since 1750, the initiation of the industrial revolution, approximately 50% of the emitted anthropogenic CO_2 is taken up by the oceans. These enhanced concentrations of aquatic CO_2 is responsible for an increase of the seawater acidity and thus a decrease in pH, leading to ocean acidification, also known as “the other CO_2 -problem”. Research on the response of marine organisms to ocean acidification showed that especially calcifying organisms that build their skeletons from calcium carbonate, such as corals, can experience negative consequences. This is mainly due to the decrease in carbonate saturation state of the oceans. The consequences for non-calcifying organisms are less clear, and depend on physiological and environmental factors. Many micro-organisms (algae, bacteria and archaea) are important players within the marine food web and the global carbon cycle, and it is therefore crucial to understand their role in the future acidification process. One way to assess this issue is to look at past time periods of geologically rapid increases in atmospheric CO_2 and decreases in ocean pH and reconstruct the changes in microbial community dynamics.

In this thesis the response of micro-organisms to high CO_2 and low pH levels has been investigated by studying the distribution patterns and the stable carbon isotopic composition of specific biomarkers or “chemical fossils” in present day (part I) and past (part II) environments.

Part I: Contemporary Systems

The degree of carbon isotopic fractionation has been shown to depend on various factors, such as the stable carbon isotope ($\delta^{13}\text{C}$) value of the carbon as well as amount of available carbon. This last aspect has been used to develop a method to reconstruct atmospheric CO_2 concentrations using specific biomarkers of marine microorganisms. Other environmental and physiological factors, such as growth rate, light intensity, and cell morphology, are found to play a role as well in determining the magnitude of carbon isotopic fractionation. Through cultivation experiments with the marine algae *Phaeocystis antarctica* and *Proboscia alata*, both important primary producers, the combined effect of these factors were studied on the carbon isotopic fractionation of the organic matter of these two species. Although significant species-dependent variations in carbon isotopic fractionation were observed between the two culture studies, the results clearly suggest that the aquatic CO_2 concentration is the main factor controlling the magnitude of frac-

tionation for both *P. antarctica* and *P. alata*. This suggests that certain algal biomarkers are suitable for past $p\text{CO}_2$ reconstructions.

To assess the direct control of pH on certain membrane lipids, the distributional patterns of branched glycerol dialkyl glycerol tetraethers (GDGTs) and that of intact polar lipids (IPLs) were analysed in 23 lakes in Iowa and Minnesota, USA. These lakes exhibit a large variation in lake water pH, alkalinity and trophic state. Branched GDGTs are membrane lipids composed of branched alkyl chains, which may contain one or two cyclopentane moieties. The control of pH on the distribution of branched GDGTs, expressed by the Cyclisation of Branched Tetraether (CBT) index in soils has been well established, but in lakes this is less well understood. The strong negative relationships between the CBT index and lake water pH found in the USA lake dataset showed that the majority of these membrane lipids are produced within the water column, in accordance with previous studies. This implies that lake sediments can be used for lake-pH reconstructions, although caution is recommended for lakes with pH levels that exceed 8.5. Probably the bacteria that produce the branched GDGTs reached their limit in making adaptations to their cell membranes above this pH level. This may be related to the variation in ion composition of the lakes and this can perhaps also explain the even stronger correlation with lake water alkalinity than with the pH of the lake water. However, the exact underlying mechanisms that explain this relationship remains to be elucidated.

The Iowa and Minnesota lake surface water suspended particulate matter also contained a wide variety of IPLs. These are complex molecules that form the main building blocks of the membranes of cellular organisms and are ubiquitously present in all natural environments. Although most IPL classes were found in all of the lakes, some significant differences could be observed. These could mainly be explained on the basis of trophic level variability, rather than a direct effect of lake water pH on the IPL distribution and abundances. For instance, the eutrophic Iowa lakes all contained a high abundance of lyso-IPLs (IPLs that contain only one fatty acid chain), which were generally not detected in the oligotrophic Minnesota lakes and is most likely due to the high ion content in the Iowa lakes. Furthermore, the higher abundance of glycolipids in eutrophic compared to oligotrophic lakes could be related to an increased N_2 -fixation by heterocystous cyanobacteria to sustain primary productivity.

Part II: Past Systems

The Palaeocene-Eocene Thermal Maximum (PETM; ~56 Ma) and Eocene Thermal Maximum 2 (ETM2; ~54 Ma) are climate events, also known as hyperthermals, characterized by warming of the deep and surface oceans. They are associated with large perturbations of the global carbon cycle, which is expressed as negative carbon isotope excursions (CIEs) suggesting a massive injection of ^{13}C -

depleted carbon into the ocean-atmosphere system, most likely due to the release of methane hydrates. This led further to large decreases in ocean pH evidenced by severe carbonate dissolution. To gain more insights into the regional magnitude of the CIE, warming and environmental changes in Northern Europe during the PETM, the distribution and stable carbon isotopic composition of specific marine and terrestrial biomarker lipids from two sites from the North Sea Basin were analysed. Although similar as recorded at other sites, the CIE found in leaf-wax *n*-alkanes derived from higher plants is possibly affected by regional variability, such as a change in source area, vegetation and/or precipitation patterns. Palaeoenvironmental reconstructions showed a strong shift in the depositional palaeoenvironment of the North Sea Basin from well-oxygenated to euxinic (anoxic and sulfidic) at the onset of the PETM. This was evident by the presence of sulfur-bound isorenieratane, a diagenetic product of the specific biomarker isorenieratene and derived from anoxygenic photosynthetic green sulfur bacteria. Reconstructed sea surface water and continental air temperatures using the TEX₈₆^H and MBT'/CBT proxies indicate a warming of 8-10 °C and 5-8 °C, respectively. The magnitude of the SST warming is higher than recorded at most other locations and may be due to regional variability, amplifying the warming in the North Sea Basin.

The magnitude of the CIEs of the PETM and ETM2 vary widely per site and carbon reservoir studied. This greatly complicates the constraining of the actual CIE and thereby the amount of carbon that was involved during these hyperthermals. In order to constrain the CIEs a new approach was tested that potentially enables the reconstruction of $\delta^{13}\text{C}$ of dissolved inorganic carbon by analysing the stable carbon isotopes of biphytanes derived from Thaumarchaeotal GDGTs in sediments deposited during the PETM in the North Sea Basin and ETM2 in the Arctic Ocean. These biphytanes record a $\sim 3.6\text{‰}$ for the PETM and $\sim 2.5\text{‰}$ for ETM2. This is respectively similar and slightly higher than the CIE reconstructed from marine calcite, suggesting that the CIE recorded in Thaumarchaeotal GDGTs may represent the actual CIE of marine DIC during these Eocene hyperthermals.

To investigate the response of marine microorganisms to the climatic and environmental changes across ETM2 in the Arctic Ocean, the concentration and stable carbon isotope profiles of several sulfur-bound biomarkers, derived from marine photoautotrophs, were studied. The results show that the palaeoenvironment of the Arctic Ocean was highly productive with sub-oxic to anoxic bottom water conditions during the entire studied interval. Sometimes sulfur-bound isorenieratane was detected, suggesting that at some occasions anoxia even reached into the photic zone. Furthermore, the higher CIE recorded in the sulfur-bound biomarkers in comparison to that recorded in marine calcite at the Walvis Ridge in the Atlantic Ocean, suggests that the biomarkers were subjected to increased stable carbon isotopic fractionation due to elevated $p\text{CO}_2$ levels during ETM2. Using the $\delta^{13}\text{C}$ composition of three selected sulfur-bound biomarkers (i.e. phytane, C₃₅ hopane and a C₂₅ highly branched isopenoid) derived from different kinds of or-

ganisms, we reconstructed atmospheric CO₂ concentrations for intervals before, during and after ETM2. Although these reconstructions are subjected to some uncertainties, the three independent biomarkers did yield similar *p*CO₂ values, suggesting an increase towards at least 4 times pre-industrial levels.

The studies presented in this thesis give insight into the role of primary producers within the global carbon cycle and underlying feedback mechanisms during periods of enhanced atmospheric CO₂ concentrations and decreased ocean pH values and led to the development of a number of new and potentially promising proxies. The CBT index is now shown to record lake water pH and alkalinity and may therefore be suitable for reconstructing lake water chemistry. The strong dependence of stable carbon isotopic fractionation on aquatic CO₂ concentrations in several algal species as well as the application of algal biomarkers in reconstructions of past *p*CO₂ levels during the ETM2 suggests that specific biomarkers from various groups of important phytoplankton groups can be used for the reconstruction of past *p*CO₂ levels. Finally, the stable carbon isotopic composition of isoprenoid GDGTs derived from Thaumarchaeota show great potential as proxy for the reconstruction of stable carbon isotope values of dissolved inorganic carbon and may be used as a new approach to constrain the negative carbon isotope excursions during Eocene hyperthermals.

In all, the results in this thesis show that the distribution and stable carbon isotopic values of lipid biomarkers add great value in studying past and contemporary ocean acidification and to assess the consequences for future climate change.

SAMENVATTING

Naast de meer bekende gevolgen van klimaatverandering, zoals de opwarming van de aarde, zorgt de huidige toename van CO_2 in de atmosfeer door menselijk activiteiten ook voor een chemische verandering in de samenstelling van het zeewater. Sinds 1750, het begin van de industriële revolutie, is ongeveer 50% van het antropogeen geproduceerde CO_2 opgenomen door de oceanen. Deze verhoogde CO_2 -concentratie heeft geleid tot een toename van de zuurtegraad van het zeewater en dus een daling in de pH. Dit leidt uiteindelijk tot oceananverzuring, ook wel ‘het andere CO_2 -probleem’ genoemd. Onderzoek naar de reactie van mariene organismen op oceananverzuring heeft aangetoond dat vooral calcificerende (zoals bijvoorbeeld koralen) hiervan negatieve gevolgen zullen ondervinden doordat de kalkskeletjes makkelijker oplossen. De gevolgen voor organismen die geen kalkskeletten maken zijn minder bekend, en zijn afhankelijk van hun fysiologie en van tal van omgevingsfactoren. Veel micro-organismen (algen, bacteriën en archaea) vervullen een sleutelrol in het mariene voedselweb en de koolstofcyclus en een beter begrip van hun rol binnen de huidige en toekomstige oceananverzuring is daarom van cruciaal belang. Door het bestuderen en reconstrueren van de veranderingen veroorzaakt door oceananverzuring op micro-organismen in het geologische verleden, waarin een snelle stijging in atmosferische CO_2 concentraties en daarmee extreme vormen van oceananverzuring optraden, kan een beter begrip met betrekking tot deze problematiek verkregen worden.

In dit proefschrift is gekeken naar de respons van micro-organismen op een verhoogde CO_2 -concentratie dan wel verlaagde pH door het bestuderen van de distributiepatronen en de stabiele koolstofsotoopsamenstelling ($\delta^{13}\text{C}$) van specifieke biomarkers, ook wel “chemische fossielen” genoemd, in het heden (Deel I) en het geologisch verleden (Deel II).

Deel I: Moderne Systemen

De mate van koolstofsotoopfractionatie (KIF) hangt af van verscheidene factoren, zoals de $\delta^{13}\text{C}$ -waarde van de koolstof die door het organisme wordt opgenomen en de hoeveelheid koolstof die beschikbaar is. Deze laatste factor heeft geleid tot een methode om atmosferische CO_2 concentraties te reconstrueren. Hierbij wordt gebruik gemaakt van de KIF van specifieke biomarkers afkomstig van mariene micro-organismen. Andere omgevings- en fysiologische factoren, zoals groeisnelheid, lichtintensiteit en celmorfologie hebben echter ook een grote rol in het bepalen van de mate van KIF. In cultuurstudies met de mariene algen *Phaeocystis antarctica* en *Proboscia alata*, beide belangrijke primaire producenten, werd op experimentele basis het gecombineerde effect getest van bovengenoemde fac-

toren op de KIF van het organische materiaal van deze twee algensoorten. Alhoewel significante, soortafhankelijke verschillen in KIF zijn waargenomen met beide algen, laten de resultaten duidelijk zien dat de aquatische CO₂-concentratie de belangrijkste factor is voor het bepalen van de mate van KIF tijdens koolstofopname tijdens de fotosynthese voor zowel *P. antarctica* en *P. alata*. Hieruit blijkt dat bepaalde biomarkers afkomstig van algen een hoog potentieel hebben als toepassing voor pCO₂ reconstructies.

Voor het aantonen van de directe invloed van pH op bepaalde membraanlipiden, zijn de distributiepatronen van vertakte glycerol dialkyl glycerol tetraethers (GDGTs) en die van intacte polaire lipiden (IPLs) geanalyseerd in het oppervlaktewater van 23 meren in de Verenigde Staten (Iowa en Minnesota). Deze meren zijn geselecteerd op basis van hun grote variatie in pH, alkaliniteit en trofische staat. Vertakte GDGTs zijn membraanlipiden die opgebouwd zijn uit alkylketens met methylvertakkingen en kunnen ook één of twee cyclopentaanringen bevatten. Tussen de pH en de distributie van vertakte GDGTs in bodems is een goed verband gevonden en dit wordt uitgedrukt met behulp van de 'Cyclisation of Branched Tetraether'(CBT)-index. Dit verband wordt echter in meren minder goed begrepen. In deze studie werd een sterk negatieve correlatie gevonden tussen de CBT-index en de pH van de Amerikaanse meren. Dit laat zien dat deze membraanlipiden voornamelijk in het meer zelf worden geproduceerd en niet aangevoerd door bodemerositie, wat al was gesuggereerd in eerdere studies. Dit betekent dat meersedimenten mogelijk gebruikt kunnen worden voor reconstructie van de pH van het meer in het verleden. Er wordt echter aanbevolen om voorzichtig te zijn met meren die een pH hebben hoger dan 8.5. Waarschijnlijk bereiken de bacteriën die de vertakte GDGTs produceren op dat moment een limiet voor het maken van adaptaties aan hun celmembraan boven deze pH-waarden. Dit kan te maken hebben met de hoge ionenconcentraties in deze meren en kan wellicht ook het sterkere verband verklaren tussen de distributie van vertakte GDGTs en alkaliniteit in vergelijking met die met pH. Het onderliggende mechanisme moet echter nog worden opgehelderd.

Het gesuspenseerd particulier materiaal in de Amerikaanse meren bevat ook een gevarieerd spectrum aan IPLs. Deze complexe moleculen vormen de belangrijkste bouwstenen van de membranen in organismen en zijn wijdverspreid aanwezig in alle natuurlijke milieus. Alhoewel de belangrijkste IPL-structuren in alle meren zijn aangetroffen, zijn er toch significante verschillen gedetecteerd. Dit kan hoofdzakelijk worden verklaard op basis van de trofische variabiliteit, in plaats van een direct effect van pH op de IPL-distributie en -concentraties. Bijvoorbeeld, de eutrofe meren in Iowa bevatten allen een zeer hoge concentratie aan lyso-IPLs (IPLs die maar één vetzuurketen bevatten). Deze werden niet aangetroffen in de oligotrofe meren in Minnesota. Dit kan waarschijnlijk verklaard worden door hogere ionenconcentraties in de Iowa meren in vergelijking met de meren in Minnesota. Verder zijn ook hogere concentraties van glycolipiden aangetroffen in de

eutrofe meren ten opzichte van de oligotrofe meren. Dit wordt waarschijnlijk veroorzaakt door specifieke cyanobacteriën die stikstof (N_2) fixeren en zo de hoge primaire productie in de eutrofe meren in stand kunnen houden.

Deel II: Periodes uit het Geologisch Verleden

Het Paleoceen-Eoceen Thermaal Maximum (PETM; ~56 miljoen jaar geleden) en Eoceen Thermaal Maximum 2 (ETM2; ~53 miljoen jaar geleden) zijn episodes van snelle klimaatveranderingen, ook wel hyperthermalen genoemd. Zij worden gekenmerkt door opwarming van de diepzee en oppervlaktewateren. Ze worden verder geassocieerd met grote verstoringen van de mondiale koolstofcyclus, die zich uiten als negatieve koolstofsotoopexcursies (KIEs). Deze zijn veroorzaakt door massieve injecties van ^{13}C -arm koolstof in de atmosfeer en oceaan, waarschijnlijk in de vorm van methaan afkomstig van “smeltende” methaanhidraten. Dit heeft verder geleid tot grote daling van de pH van de oceaan met als gevolg oplossing van calciumcarbonaten. Om een beter inzicht te verkrijgen in de regionale omvang van de KIE, de opwarming en de milieuveranderingen gedurende de PETM, zijn de distributiepatronen en $\delta^{13}C$ waarden van specifieke mariene en terrestrische biomarker-lipiden in sedimenten van twee PETM secties in Denemarken bestudeerd. De KIE gevonden in de *n*-alkanen afkomstig van hogere plantenwassen komt overeen met KIEs gevonden op andere locaties, maar is waarschijnlijk beïnvloed door regionale variabiliteit, zoals een verandering van het gebied vanwaar de *n*-alkanen werden getransporteerd, en een verandering in vegetatie en/of precipitatiepatronen. Paleomilieureconstructies laten verder een sterke verschuiving zien in het paleomilieu van het Noordzeebekken van goed geventileerde naar euxinische (zuurstofloze en zwavelrijke) omstandigheden aan het begin van de PETM. Dit kan worden geconcludeerd aan de hand van de aanwezigheid van zwavelgebonden isorenierataan, een diagenetisch product van het specifieke pigment isorenierateen afkomstig van anoxygene fotosynthetiserende groene zwavelbacteriën. Reconstructies van de oppervlaktezeewatertemperatuur en de jaargemiddelde luchttemperatuur boven nabijgelegen landmassa's, gebruikmakende van de TEX^{H}_{86} en MBT'/CBT temperatuurproxies, laten een opwarming zien van respectievelijk 8-10°C en 5-8°C. De oppervlaktezeewatertemperatuur is hoger dan geregistreerd op de meeste andere PETM-locaties en is mogelijk veroorzaakt door regionale verschillen die de opwarming van het oppervlaktewater in de Noordzee vergrootten.

De grootte van de negatieve KIEs die optraden tijdens de PETM en ETM2 verschilt aanzienlijk per locatie en is tevens afhankelijk van welke vorm van koolstof gebruikt wordt voor de reconstructie. Dit compliceert de bepaling van de ware grootte van de atmosferische KIEs en daardoor de schatting van de hoeveelheid koolstof die tijdens deze hyperthermalen is vrijgekomen. In sedimenten afgezet in het Noordzeebekken tijdens de PETM en in de Arctische Oceaan tijdens

ETM2 is de stabiele koolstofsotoopsamenstelling van zogenaamde bifytanen, de ether-gebonden lipiden van Archaea, geanalyseerd. Er is specifiek gekeken naar bifytanen afkomstig van het GDGT crenarchaeol dat specifiek is voor (mariene) Thaumarchaeota. De analyse van de stabiele $\delta^{13}\text{C}$ -waarde van crenarchaeol is een potentieel nieuwe manier om de variaties in de stabiele $\delta^{13}\text{C}$ -waarde van opgelost anorganisch koolstof te kunnen bepalen. De resultaten laten een negatieve KIE in crenarchaeol zien van 3.6 ‰ voor de PETM en 2.5 ‰ voor ETM2, respectievelijk gelijk aan en hoger dan de KIE gereconstrueerd met behulp van calciumcarbonaat uit andere locaties. Het is dus zeer waarschijnlijk dat de gereconstrueerde KIE uit de GDGTs afkomstig van Thaumarchaeota de werkelijke KIE van opgelost anorganisch koolstof weergeeft.

In sedimenten afkomstig uit de Arctische Oceaan afgezet tijdens ETM2 is de reactie van mariene micro-organismen op klimaat- en milieuveranderingen bestudeerd. Dit is gedaan aan de hand van de distributiepatronen en $\delta^{13}\text{C}$ -waarden van zwavelgebonden biomarkers, afkomstig van mariene fotoautotrofen. Hiermee werd aangetoond dat het paleomilieu van de Arctische Oceaan gekenmerkt werd door een hoge productiviteit met bodemwatercondities variërend van zuurstofarm tot geheel zuurstofloos. In enkele intervallen werd de specifieke biomarker zwavelgebonden-isorenierataan gedetecteerd. Dit toont aan dat in sommige gevallen de zuurstofloze condities tot in de fotische zone reikten. Verder is een hogere negatieve KIE gevonden in de zwavelgebonden-biomarkers in vergelijking met de KIE in calciumcarbonaat in sedimenten afgezet op de Walvisrug in de Atlantische Oceaan. Dit impliceert dat een toegenomen KIF veroorzaakt door een verhoogde atmosferische en oceanische CO_2 -concentratie gedurende ETM2. Door gebruik te maken van de $\delta^{13}\text{C}$ -waardes van drie zwavelgebonden-biomarkers (fytan, C_{35} hopaan en een C_{25} hoogvertakte isoprenoïd), afkomstig van verschillende groepen organismen, zijn de atmosferische CO_2 -concentraties gereconstrueerd van voor, tijdens en na ETM2. Alhoewel deze reconstructies onderhevig zijn aan onzekerheden, kon wel worden vastgesteld dat de $\delta^{13}\text{C}$ -waarden van deze drie onafhankelijke biomarkers, atmosferische CO_2 -concentraties voorspellen tijdens de KIE van ETM2, van op z'n minst vier keer pre-industriële $p\text{CO}_2$ -waarden.

De studies gebundeld in dit proefschrift geven inzicht in de rol van primaire producenten binnen de koolstofcyclus en de onderliggende 'feedback'-mechanismen tijdens perioden van verhoogde CO_2 -concentraties en verlaagde pH-waarden van de oceanen en hebben geleid tot het ontwikkelen van nieuwe, veelbelovende proxies. Het is nu aangetoond dat de CBT-index als indicator voor de pH en alkaliniteit in het water van meren gebruikt kan worden en daardoor potentieel geschikt is voor de reconstructie van de waterchemie in meren. De sterke afhankelijkheid van de stabiele KIF van de aquatische CO_2 -concentratie in verscheidene mariene algensoorten, in combinatie met het succesvol toepassen van $\delta^{13}\text{C}$ -waarden van biomarkers voor de reconstructie van atmosferische CO_2

concentratie gedurende ETM2, rechtvaardigt het gebruik van $\delta^{13}\text{C}$ -waarden van specifieke biomarkers van verschillende belangrijke groepen fytoplankton voor het reconstrueren van atmosferische CO_2 -concentraties in het geologische verleden. Tot slot, het gebruik van de stabiele koolstofisotopsamenstelling van bifytanen afkomstig van de GDGTs van Thaumarchaeota laat een hoge potentie zien als nieuwe methode voor de reconstructie van de $\delta^{13}\text{C}$ waarde van opgelost anorganisch koolstof en kan dus mogelijk als nieuwe methode worden gebruikt om de ware negatieve KIEs van Eocene hyperthermalen, te kunnen bepalen.

Samenvattend tonen de resultaten in dit proefschrift aan dat de distributiepatronen en stabiele koolstofisotoopsamenstelling van specifieke biomarkerlipiden een sterke bijdrage kunnen leveren aan het beoordelen van de gevolgen van oceaanverzuring in het verleden, heden en de toekomst.

ACKNOWLEDGEMENTS / DANKWOORD

En dan opeens is dat magische moment aangebroken en dan is het klaar!

Mijn PhD ging met vallen en opstaan en ik heb ontzettend veel geleerd. Ik wil dan ook iedereen bedanken die hierin een bijdrage heeft geleverd. Ik heb een buitengewoon leuke tijd gehad op Texel en vind het nu jammer om van iedereen afscheid te moeten nemen.

Mijn avontuur in de Organische Geochemie begon met de hoorcollegeseries van Jan de Leeuw en Jaap Sinninghe Damsté die ik tijdens mijn Masterfase gevolgd heb. Alleen de titel (destijds) vond ik al geweldig: “From Big Bang to Baby Boom and Beyond”. Jan en Jaap, bedankt dat jullie me hebben enthousiasmeert voor dit mooie vakgebied.

Jaap en Stefan, jullie zijn de kapteins van het BGC-schip en zonder jullie zou het stuurloos zijn. Bedankt voor alle steun en commentaar. Ik bewonder jullie werkwijze en jullie snelle replek. Ik hoop dat ik daar in de toekomst een voorbeeld aan kan nemen. Stefan, dank je wel voor al je geduld en dat je kantoor altijd open stond. Je hebt me vaak kunnen opbeuren als ik het niet meer zag zitten en me de juiste weg op kunnen sturen wanneer ik in het PhD-doolhof dreigde te verdwalen.

Maar wat is een schip zonder machinisten om het te laten varen. Marianne, Irene, Anhelique, Ellen, Jort, Monique. Jullie zorgen voor een welgeoliede machine. Bedankt voor al jullie hulp in het lab. Jort, bedankt voor alles. Je hebt me de kneepjes van het laboratorium laten zien en kon altijd op je hulp vertrouwen. Maar ook jij Michiel, bedankt voor al je hulp met de IRM en de EA. Verder, je cynisme werd zeer gewaardeerd.

En dan alle andere BGC-matrozen / and then all the other BGC-sailors: Alina, Andrea, Angela, Antje, Arjan, Cecile, Cindy, Claudia, Cornelia, Darci, Denise, Daniela, Daniëlle, David, Dorien, Elda, Eli, Elisabeth, Els, Francien, Isla, Jaco, Joost, Jord, Kees, Kevin, Laura, Lisa, Loes, Luke, Marcel, Margot, Marta, Martina, Nicole, Kim, Raquel, Rob, Ronald, Sabine, Sandra, Sebastiaan, Sebastian, Thorsten, Veronica, Yvon. Thank you all for the fun times in the lab, during coffee breaks, occasional parties, conferences, etc.....

I have switched many times between offices and therefore had the pleasure to share offices with a great deal of people: Adam, Veronica, Darci, Sabine, Arjan & Elda (well almost then), Francien, Sandra, and Raquel.

Raquel, you have been such a good colleague and friend. You are a very serious

person and have a realistic view on the world, and I admire your strength and focus. Thank you for all the lunches and teas together. And of course for the time together in Italy, USA, Switzerland. Thank you so much for all the conversations (sometimes until dawn) and your support when I needed it!

Ook Margot bedankt voor de fijne tijd in Amerika. En ook voor de gezellige gesprekken, de yoga sessies in het begin en voor de slaappleaats toen ik opeens buiten stond zonder sleutel.

Elda, het was leuk om je “aquarium-maatje” te zijn, ook al was het water soms wel erg koud!

Claudia, I will really miss our music sessions together! We shared the same passion for music and our struggle with the pieces of Bach. It was fun, wherever we played; your tiny room, the NIOZ canteen with an untuned mouse-invested piano, at the music school (♫♫ boom-en-takken-blaadjes ♫) or at the nice house concerts of Marijn. And I also thank you that you and Merel joined me to see Apocalyptica in Amsterdam. It was fantastic! We further had a great time together in the Swiss alps, despite all the muscle pain after our tough hikes! But it was worth it!! ☺ But now you are going to be married, I have to ask: will you now grow up? ;-) In any case, I wish you all the best with Santi!!

Then it is time to thank the visiting crew: Marita, Kasia, Mariska, Corné, Lennart van Maldegem, Rodrigo, Melissa, Jess, Ariane, Lara, Amber, Willemijn, Laura Buckles, Luciane, Carmina, Frederike and all the others I don't remember the names anymore....

Kasia, you are a very nice person and it was a privilege to work with you. I would like to thank you and Mikkel for staying at your home in Aarhus and for introducing me into the world of zombie- and other hilarious movies! ☺

Then there are also the other NIOZ-people I would like to thank, who contributed to the fun time I had during my PhD: Craig & Julie and of course little Lauren, John, Thalia, Anna, Astrid, Marcel Bakker, Jan-Berend, Karel Bakker, Libby, Jenny, Leslie, Juliane, Viola, Sharyn, Pedro, Catarina, Sofia, Amanda, Paul, Santi, Claire, Cees, Lukas, Yvo, Richard, Lennart Groot, Jordi, Hélène, Valeska, Andjin, Merel, Maarten, and all the other people I forget to mention....

Astrid en Anna, als projectpartners, dank jullie wel voor de samenwerking. Anna, we hebben een hele leuke tijd gehad in Iowa en Minnesota, ik vond het heel fijn om met je samen te werken en met goede resultaten tot gevolg. We hebben veel lol gehad aan het Wabana Lake, ondanks het vroege opstaan, en natuurlijk tijdens onze tocht naar Chicago. Wat een fantastische stad!

John, you are an interesting person and your sadistic thoughts made lunch times much more interesting! ;-) Thank you very much for the fun time in Almere and for creating THE picture. It's beautiful!!!

Thalia, thank you too for your musical contribution. I wished we could have played more together!

Ik wil ook hier graag plaats vrij maken om de niet-academische staf te bedanken van de ICT-, financiële en technische afdelingen, voor al hun hulp en ondersteuning. Vooral bedankt: Bert Aggenbach, Joke Mulder, Hilde Kooijman en Siem Groot.

Vrienden en familie, ook jullie heel erg bedankt voor alle steun.

Marcel, Jolanda, Joeri en Vivian ik vond het erg leuk dat jullie me hebben opgezocht op Texel. Ik heb een super leuke dag gehad. Edwin, Iris, Max en Nina, dat geldt natuurlijk ook voor jullie. Jammer dat ik net op het punt stond om te gaan verhuizen, waardoor het wat chaotisch was.

Dikke knuffel voor Babet. We blijven elkaar trouw, zelfs als we elkaar heel lang niet zien of spreken. We kunnen alles tegen elkaar zeggen en dat waardeer ik enorm. Bedankt dat je mijn beste vriendin wilt zijn en blijven!

Frans, jou wil ik speciaal bedanken voor je hulp tijdens mijn zoektocht naar een promotieplaats. Jij hebt me in contact gebracht met de juiste mensen van het NWO. Dit heeft ervoor gezorgd dat ik de stoute schoenen aantrok en uiteindelijk op het NIOZ terechtkwam. En ook Petra natuurlijk hartelijk bedankt!

Als laatste wil ik mijn ouders bedanken. Zelfs als ik in het meest vervallen huis van Texel wil gaan wonen of met de gekste beesten aan kom zetten, jullie zijn er altijd voor mij en blijven mij steunen, waar ik ook ben, wat ik ook doe. Ik ben jullie heel erg dankbaar voor al de support, aandacht, liefde en geborgenheid die ik in al die jaren heb mogen ontvangen!

CURRICULUM VITÆ

Petra Larissa Schoon was born on 5 September 1980 in Rotterdam, the Netherlands. In 1998 she received her HAVO diploma at the Alberdingck Thym College in Hilversum. After being rejected to join the Koninklijke Marechaussee, she started with Office Management at Hoogeschool Schoevers in Utrecht. Though soon it became clear this was not the correct career choice and always fascinated by rocks she decided that she wanted to study geology. To be accepted at university, this however implied, that she needed an additional degree in physics and mathematics, which she received in the following two years. Meanwhile, she worked as a compounder at International Flavors and Fragrances (IFF) in Hilversum. In 2001 she finally could start studying Earth Sciences at Utrecht University and in June 2007 Petra received her Master's degree with a specialization in Biogeology. In March that following year she started her PhD in Organic Biogeochemistry at the Royal Netherlands Institute for Sea Research (NIOZ) on Texel, under the supervision of prof.dr.ir. Stefan Schouten and prof.dr.ir. Jaap Sinninghe Damsté, which resulted in this thesis. Since February 2013 Petra started as a postdoctoral researcher at the University of California in Riverside (UCR), to study ancient membrane lipids from Archaean rocks.



photo by Claudia Zell